Genetic determinants of the magnitude of type-I interferon responses in mice: α-protein kinase I as a novel candidate gene

Milena Stanković

University College London
and
The Francis Crick Institute
PhD Supervisor: Andreas Wack

A thesis submitted for the degree of
Doctor of Philosophy
University College London
January 2020

Declaration

I, Milena Stanković confirm that the work presented in this thesis is my own. Where information has been derived from other sources, I confirm that this has been indicated in the thesis.

Abstract

Flu disease is an important public health burden worldwide, caused by the influenza virus that rapidly mutates and can cause severe disease and even death. While host genetic factors can also contribute to disease severity and susceptibility, no precise genetic determinant has been elucidated yet.

Type-I IFNs, IFN-α/β, are hallmark molecules of the host innate immune responses, indispensable to the elimination of viruses. Previous work in our team directly correlated IFN-α/β levels in the lung to influenza susceptibility in a mouse model. Influenza-susceptible 129 mice exhibited higher IFN-α/β levels upon infection than resistant BL/6 mice, although all parameters of infection were similar. This PhD project was focused on uncovering the genetic determinants of excessive IFN-α/β production in mice.

In this thesis, I present the impact of a novel candidate Chromosome 3 region in IFN-α/β responses: the R17 locus. A homozygous congenic BL/6 allele of the R17 locus contributed to reducing IFN-α/β and cytokine levels and to rescuing the susceptibility to influenza of the otherwise susceptible 129 mice. I report increased susceptibility *in vivo* and IFN-α/β production *in vitro* of BL/6 mice deficient in a candidate gene from the R17 locus, the α-protein kinase 1: ALPK1. Finally, this work reports some progress on elucidating the role of ALPK1 in IFN-α/β production pathways. By means of global phospho-proteome assays, a novel putative phosphorylation target of ALPK1, WWC2, is reported. This finding suggests a role for a previously unreported interaction between IFN-α/β responses and the Hippo pathway in innate immunity.

Impact Statement

Influenza-caused respiratory disease is an important public health burden worldwide. As many as 650 thousand cases of influenza-related deaths are reported annually, with 3-5 million people developing severe disease. Antiviral treatments are increasingly losing efficiency against this rapidly mutating virus, and the available vaccine does not guarantee protection since it does not always match the circulating virus strain. Therefore, novel options for treatment of influenza disease are urgently needed, as influenza remains a pandemic threat.

The work presented in this PhD thesis contributes to identifying genetic factors that impact IFN production during influenza disease in mice, and thereby possibly the intensity and the pathogenic potential of the immune response. The findings reported here will hopefully set a base for novel candidate studies on genetic bases of IFN production during immune responses. Since IFN production is triggered in a wide range of situations, advancing the scientific knowledge on the molecular mechanisms governing it can help improve the understanding of not only influenza disease, but also autoimmune and autoinflammatory diseases including interferonopathies, as well as bacterial infections and even some neurological disorders and cancer.

Aside from the virus strain potency and pre-existing immunity, host genetic factors play a major role in determining the severity and outcome of flu disease in humans. The modulation of immune response intensity by IFN production is the crucial component of a healthy and efficient immune response to influenza virus. Uncovering novel factors that contribute to regulating IFN production could potentially help identify specific targets for host-directed disease treatment. Targeting host factors could be a more efficient and universal way of dealing with the infection, thus bypassing the ever-mutating influenza virus and improving treatment options.

Acknowledgement

I would like to thank the Francis Crick Institute and its funding bodies: the Wellcome Trust, Cancer Research UK, Medical Research Council and the associated charities, for their full sponsorship of my PhD.

I am thankful to my supervisor, Andreas Wack, for the opportunity to pursue this project and enjoy a PhD in one of the top Institutes and Universities in the world. I am thankful to him for his time and support, especially in the beginning, in learning about a field that was entirely new to me.

I would also like to thank my thesis committee: my secondary supervisor at UCL, Andrew Smith, and Crick group leaders Victor Tybulewicz and George Kassiotis. I am thankful to their generous sharing of knowledge, ideas, and new ways forward for my project. I would like to extend a special thanks to Andrew Smith, for his generous support in exploring new techniques and his critical view of my data. I am thankful to him for shaping his role as secondary supervisor into a true mentorship. I am also thankful to Juliet Foote (Cancer Research Center of Toulouse, previous member of Tony Segal lab at UCL) and Tomoko Kumagai from the Smith team, for their guidance and knowledge through our attempts at creating immortalized bone marrow progenitor cell lines.

I am also thankful to Cecilia Johansson (Imperial College London) and Mahdad Noursadeghi (University College London) for the time they have invested to read and assess this work.

Further, I would like to acknowledge colleagues from the Wack team. I am thankful to Sophia Davidson, who introduced me to the background of this project, for teaching me *in vivo* work and flow cytometry. I am thankful to Teresa McCabe, a past lab member, for being a great colleague and housemate. I am also grateful to my colleagues: Helena Aegerter, Jack Major, Justina Kulikauskaite, Ashleigh Howes and Stefania Crotta for their encouragement and the great scientific discussions, especially during some trying times this project has gone through. I would also like to thank them all for introducing a Mediterranean-born girl to the thrills (and terrors) of ice-skating during our lab Christmas outings!

Further, I am grateful to my colleague Katja Finsterbusch for her generous professional and personal support. I am also most grateful for her giggly voice that

illuminated busy lab mornings. I owe a special thanks to Konrad Bradley, a former Wack lab member, and a virology expert we could not have done without. He has been a pillar of support and a source of knowledge and has, unknowingly, transferred his passion for the influenza virus to the unsuspecting molecular biologist that I was. I am also thankful to him for his feedback on this thesis. I owe a great *merci* to my colleague and friend Julie Rappe. I am in awe of her curiosity and integrity that I learned a lot from. I am grateful for her steady support, her presence, and her companionship.

Most of the work presented here would have been impossible without the fantastic support from the Crick scientific technology platforms. I am grateful to Jamie Barrett and Ade Adekoya, to Tinashe Matambanadzo and Luis Valencia, and to the Senior Team of the Experimental 1 Unit, for their help with husbandry and mouse work. I am grateful to the Flow Cytometry STP for their rich knowledge and expertise, and to the Proteomics STP, Bram Snijders and Helen Flynn, for all the support they provided in the phospho-proteomics assays. I would also like to thank the High Throughput Sequencing facility, in particular Robert Goldstone and Nourdine Bah for their expertise in designing and analysing the RNA-seq assay presented in this thesis.

I also owe my gratitude to Fiona Powrie (Kennedy Institute of Rheumatology, Oxford) for the mouse strains 129.C3BR17 and (for the initial experiment) *Alpk1*$^{-/-}$ they shared.

My PhD life would not have been the same without the companionship of my PhD student colleagues (year 2015). I am grateful to my friends Tom Mercer and Dorita Tsourouktsoglou for their positive energy and the great times together. I owe a heartfelt *gracias* to the wonderful Mar Cabeza Cabrerizo and Anna Perdrix Rosell, my supportive, fun and inspirational friends. I am also very grateful to Alessia Caramello and Paloma Fernandez Calvo for their friendship, their unwavering support and great moments spent together in the past four years.

I am especially grateful to the extraordinary people whom I met in during my studies at ENS Paris, whose warmth and presence are thoroughly missed: Justine Schaeffer, Anne Grelat, Valentine Verzat, Coralie Trentesaux, Antonin Weckel, Xavier Audier, Aurélien Villedieu, Thomas Aubier and Pierre Quévreux. I am thrilled that my friendship with this adventurous, highly intelligent and witty little group crosses borders and withstands the test of time.

I am grateful to my friends back home, Jovana Lalić, Jelena Nenezić and Nikola Radonjić, for their unconditional support and love throughout the years, regardless of geographical distance. There is more to thank them for than could fit into these acknowledgments. I am also grateful to Jovana Vučević for her warmth, her presence and the second generation family friendship that we proudly maintain.

I am thankful to Hermione Armitage, the yoga teacher hero who provided a mental safe space for me even in situations of emotional turmoil.

I would especially like to thank my now fiancé, Simon Brunner. I am deeply thankful for his love, friendship, support and understanding that have been my strength through many challenges within and outside of this PhD. I admire his intelligence, integrity, his positive energy and unwavering optimism. I am also thankful to him for proof-reading this thesis. I also owe my gratitude to Simon's wonderful parents, Stefanie and Peter, for their warmth and their steady support in weathering through the challenges in the past years.

I am forever indebted to my wonderful parents, my mother Vesna and my late father Siniša, for providing a safe, supportive and warm home for myself and my brother Božidar. I can only hope that I can begin to justify the sacrifices, the investment and the faith that they bestowed upon us. I am extremely grateful to them and to my brother, for their unconditional love and encouragement, not least during this PhD. I am also deeply thankful to my inspirational late grandfather, Savo Mijović, MD. He, more than anyone else, would have wished to see this thesis.

Table of Contents

Table of figures

List of tables

Abbreviations

(c)DC – (conventional) dendritic cell

(G)M-CSF – (granulocyte) monocyte-colony stimulation factor

AKT – protein kinase B

Alpk1 - α-protein kinase

AM – alveolar macrophage

Amotl2 – angiomotin like 2

AP-1 – activator protein 1

Ap1ar – AP-1 complex associated protein

aPKC – atypical protein kinase C

ATF2/4 – activating transcription factor 2/4

BAL – bronchio-alveolar lavage

BM – bone marrow

BMDM – bone marrow-derived macrophages

CBP – CREB-binding protein

CCL2 – C-C motif chemokine 2 (also MCP-1)

CCR2 – CCL2 receptor

CD4/8/11b/c/103 – cluster of differentiation 4/8/11b/c/103

cGAMP – cyclic GMP-AMP

cGAS – cyclic GMP/AMP synthase

Chr/Ch – chromosome

CpG – cytosine-guanine dinucleotide islands in ssDNA

CREB – cAMP response element-binding protein

DR5 – death receptor 5

dsRNA/ssRNA – double-stranded RNA/single-stranded RNA

EIF(4E) – eukaryotic initiation factor (4E)

Elk – ETS like 1 protein

ERK1 – extracellular signal-regulated kinase

F4/80 – EGF-like module-containing mucin-like hormone receptor-like 1

Flt3(L) – FMS-like tyrosine kinase 3 (ligand)

FOS – Fos proto-oncogene (AP-1 subunit)

FSC – forward scatter (flow cytometry)

GAS – IFN γ-activated sites

GPCR – G-protein coupled receptor

GTPase – hydrolase enzyme of nucleotide guanosine triphosphate

GWAS - genome-wide association study

HA – hemagglutinin

HIV – human immunodeficiency virus

HMGA1 – high-mobility group protein 1

IκB - nuclear factor of κ-light polypeptide gene enhancer in B-cells

IAV- influenza A virus

IFITM1/2/3 - interferon-induced transmembrane protein 1/2/3

IFITM3 – interferon-induced transmembrane protein 3

IFN – interferon (type-I IFN)

IFNAR - IFNα/β receptor

IFNGR – IFN γ receptor

IgA/G/M – immunoglobulin A/G/M

IKK – inhibitor of NFκB kinase

IL-6/8/10/12 – interleukin 6/8/10/12

IP-10 – interferon γ-induced protein (also CXCL10 – C-X-C-motif chemokine 10)

IRAK1/2/4 – interleukin-1 receptor-associated kinase 1

IRF1/3/7/9 – interferon-transcription factor 1/3/7/9

ISG – interferon-stimulated gene

ISGF3 – interferon-stimulated gene factor 3

ISRE – IFN-stimulated response element

JAK1 – Janus-kinase 1

JNK – c-Jun N-terminal kinase

KO – knockout

Larp7 - la Ribonucleoprotein Domain Family Member 7

LATS1/2 – large tumor suppressor kinase 1/2

LPS – lipopolysaccharide

Ly6C/G – lymphocyte antigen 6C/G

M1/2 – matrix 1 / 2 protein (IAV)

mAb – monoclonal antibody

MAVS – mitochondrial antiviral signaling protein

MDA5 – melanoma differentiation-associated protein 5

MDCK – Madin-Darby Canine Kidney cells

MHC – major histocompatibility complex

MIP-1α - macrophage inflammatory protein 1α (also CCL4)

MoDCs – monocyte-derived DCs

MoMPhs – monocyte-derived Macrophages

MPhs – macrophages

MST1/2 – mammalian sterile-20-like kinase

MSU – monosodium urate

mTOR – mammalian target of rapamycin

Mx1/A – Mx dynamin-like GTPase 1/A

MyD88 - myeloid differentiation primary response gene 88

NA – neuraminidase

NAP-1 – nucleosome assembly protein

NEMO – (IKKγ) – NFκB essential modulator

Neurog2 – neurogenin 2

NFκB – nuclear factor kappa-light-chain-enhancer of activated B-cells

NP – nucleoprotein (IAV)

NS (NEP) – nuclear export protein (IAV)

p.i. – post-infection

p38 – MAPK (mitogen-activated protein kinase) of 38kDa

PAMPs – pathogen-associated molecular patterns

PB1/2 – polymerase basic 1 / 2 (IAV polymerase)

pDC – plasmacytoid dendritic cell

PI3K – phosphoinositide 3-kinase

PKR – protein kinase R

Poly(I:C) – polyinosinic:polycytidylic acid

PRD I/II/III/IV – PTS regulation domain I/II/III/IV

PRRs – pattern recognition receptors

QTL – quantitative trade locus

RANTES – regulated on activation, normal T-cell expressed and secreted (CCL5)

RIG-I – retinoic-acid inducible gene

RLR – RIG-I-like receptor

RNP – ribonucleoprotein (IAV)

SA – sialic acid

SFV – Semliki forest virus

Siglec-F/H – sialic acid-binding immunoglobulin-type lectins F/H

SINTBAD – (TBKBP1) – TBK-binding protein 1

SNP – single nucleotide polymorphism

SNP – single nucleotide polymorphism

SOCS1 – suppressor of cytokine signaling 1

SSC – side scatter (flow cytometry)

STAT1/2 - Signal Transducer and Activator of Transcription ½

STING – STimulator of Interferon Genes

TAK1 – (MAP3K7) - TGFβ-activated kinase 1

TAZ – transcriptional coactivator with PDZ-binding domain

TBK1 – TANK binding kinase 1

TF – transcription factor

TGFβ1 – transforming growth factor β

Tifa - TRAF-interacting protein with forkhead-associated domain

TIRAP – Toll/interleukin-1 receptor domain-containing adapter protein

TLR – Toll-like Receptor

TNFα - tumor necrosis factor α

TRAF3 – TNF receptor associated factor 3

TRAF6 - TNF Receptor Associated Factor 6

TRAIL – tumor necrosis factor ligand superfamily member

TRAM – TRIF-related adaptor molecule

TRIF - TIR-domain-containing adapter-inducing interferon-β

TRIM – tripartite motif protein

TSS – transcription start site

TYK2 – tyrosine kinase 2

VSV – vesicular stomatitis virus

WHO – World Health Organisation

WT – wild-type

WWC1/2 – WW domain coiled-coiled domain containing protein 2

YAP – Yes-associated protein

Chapter 1. Introduction

1.1 Influenza disease

1.1.1 Influenza disease as a public health burden

Flu disease is a term used for respiratory infections caused by the strain of RNA viruses called influenza viruses. Of the four genera in the RNA virus *Orthomyxoviridae* family, A,B,C and D (reviewed in (Palese P, 2013)), only influenza A and B viruses circulate and cause infections in humans. The influenza A virus causes almost yearly outbreaks of varying scopes, and has been at the origin of several pandemics, the deadliest of which, the “Spanish flu” pandemic in 1918, claimed 50 million lives (Johnson and Mueller, 2002).

Influenza is an important public health burden, with 2-5 million people estimated to develop severe influenza worldwide per year (WHO). In spite of this, it remains difficult to prevent, diagnose and treat. The symptoms resemble those of respiratory infections caused by other viruses, and can vary in severity depending on the host’s immune system and overall health, the point in infection, the viral strain, and previous influenza infections. The most vulnerable portions of the population are those with insufficient immune responses, including young children, the elderly and the immunosuppressed (pregnant women, HIV patients or those with chronic disease under immunosuppressants). Notably, people aged 65 or above have the highest death rate facing influenza (Thompson et al., 2009).

The remainder of the population, namely those 15-65 years of age, in good overall health and with a healthy immune system, can nevertheless show variability in their response to the influenza virus, to the point of hospitalisation and even death. The sources of this variation are numerous and their contributions often unclear, but there is agreement that host factors such as individual immune responses, the extent of inflammation, previous history of flu disease, and the genetic background all play a role in the final outcome of the infection.

1.1.2 Influenza virus

1.1.2.1 IAV particle: surface proteins and RNA genome

Virions of influenza A comprise a viral envelope made of the lipid bilayer membrane derived from the infected host cell, embedded into which stand the characteristic glycoprotein structures of hemagglutinin (HA) and neuraminidase (NA).

Hemagglutinin is critical in viral recognition of host cells upon infection. It binds specifically to sialic acid residues on the cell membrane, causing viral entry and infection in the upper or lower respiratory tract (Skehel and Wiley, 2000),(Wiley and Skehel, 1987). In the acidic pH of the endosome, HA undergoes a dramatic conformational change that triggers the fusion of the viral membrane with the endosomal membrane to initiate escape. Interestingly, adaptations in avian virus HA to function in the lower pH of the human endosome were linked to the capacity of the virus to trigger pandemic disease in humans and infect ferrets (Russier et al., 2016), (Shelton et al., 2013).

Neuraminidase is another key component of the IAV particle. Its most prominent role involves the cleavage of sialic acid residues on the cell surface and the surface of new influenza virions upon budding. This process prevents the virion reattachment to the host cell via the HA molecules to complete budding, and helps clear out the mucus in the epithelium to enhance viral spread. Thermo-sensitive mutants of NA showed accumulation of virions on the membrane of infected cells (Palese et al., 1974). Other described functions for NA include somewhat indirectly proven facilitation of viral entry (Matrosovich et al., 2004) and aiding late endosome trafficking to enhance viral replication (Suzuki et al., 2005). Similar to HA, low pH-stable NA mutants were found in pandemic human influenza viruses, proving that NA plays a role in the virulence of the viral strain (Takahashi and Suzuki, 2015).

Clinically, the different substrains of influenza A virus are distinguished by their surface HA and NA types. As of today, 18 different HA versions are known (H1 to H18), of which 16 are in circulation in avian species and 2 in bats (Fouchier et al., 2005), (Tong et al., 2013). Eleven NA subtypes have been described to date, all of them circulating in birds, and two in bats (N10 to N11) (Hussain et al., 2017). It is the combination of these subtypes and their numbers that gives rise to IAV strain names (eg H3N2, H5N1 etc). A subgroup of highly pathogenic IAV, H5Nx, and especially

H5N1, circulate in wild birds and occasionally transfer to domestic poultry. As they are at the origin of sporadic outbreaks that cause high mortality in humans, they are constantly monitored for novel mutations and reassortments (Nunez and Ross, 2019). H1N1 strain was at the origin of the Spanish flu pandemic of 1918, as well as another pandemic in 2009. H2N2 strain (Hong Kong IAV) caused a pandemic in 1957/58, whereas an H3N2 strain spread worldwide in 1968. Ultimately, the last deadly pandemic of flu in 2009 was caused by a novel reasserting H1N1 virus (Hussain et al., 2017). Moreover, H7N9 strains are emerging as novel outbreak and pandemic threats, appearing in 2013 in China and since then infecting 1625 people and causing 622 deaths (Imai et al., 2017), (Long et al., 2019).

The inside of the viral particle contains the IAV genome. As a member of the *Orthomyxoviridae* family of viruses (reviewed in (Bouvier and Palese, 2008), (Palese P, 2013)), IAV bears a single-stranded, negative-sense RNA genome comprising of 8 segments. The segments 1,3,4 and 5 only encode a single protein each: PB2, PA, HA and NP. Another viral polymerase subunit, PB1, is encoded by two genes on segment 2 (which in some strains also contains the gene encoding a small pro-apoptotic factor PB1-F2). Segment 6 of the IAV genome encodes solely the NA protein. Meanwhile, the M1 matrix protein is encoded by a gene on segment 7, and the interferon antagonist protein NS1 is encoded on segment 8 (Bouvier and Palese, 2008). The IAV RNA-dependent RNA polymerase, encoded by the segments PA, PB1 and PB2, exploits the cellular machinery to multiply the viral genomic material (Braam et al., 1983). The internal organisation of the assembled IAV particle is centered around viral ribonucleoproteins (RNPs), composed of the viral ss-RNA genome of IAV coated with NP, PB1, PB2 and PA proteins.

1.1.2.2 IAV replication cycle

As previously indicated, the initial step in IAV infection is the HA-mediated recognition and binding to the sialic-acid receptors on the host cell, followed by the escape from the endosome by membrane fusion. The uncoated viral ribonucleoprotein complexes are subsequently transported into the nucleus for replication of the viral genome and generation of mRNA. This process is, in molecular terms, relatively slow: a study by the inhibition of viral entry by ammonium chloride

found that viral entry took 25min to uncoating, and a further 10min for the viral RNPs to be found in the nucleus (Martin K., 1991).

In polarised epithelial cells, the viral assembly and budding occurs at the apical membrane of the cells (Rodriguez Boulan and Sabatini, 1978). Binding preferentially occurs at lipid rafts (Rossman and Lamb, 2011). Lipid rafts are detergent-resistant, cholesterol-rich, highly mobile portions of the cell membrane which are thought to be platforms for various types of signaling (Brown and Rose, 1992), (Simons and Ikonen, 1997). In fowl plague, influenza, VSV and SFV infections, HA and viral RNPs were shown to localise to lipid raft domains in the apical membrane (Takeda et al., 2003), (Scheiffele et al., 1999), (Carrasco et al., 2004). NA is thought to enhance the process of lipid raft binding and generally virus budding (Leser and Lamb, 2005), (Chen et al., 2007), (Ohkura et al., 2014).

In the nucleus, the viral RNA genome is transcribed and replicated from the starting RNA viral template by the IAV polymerase. The viral genome is replicated by the viral RNA-dependent RNA polymerase (RdRp), the three subunits of which are imported into the nucleus along with the genome. It uses the negative-sense viral RNA as a template for the synthesis of novel mRNA templates and complementary RNA intermediates, both positive-sense. The latter is subsequently used as a template for the production of more negative-sense viral RNA to replicate the viral genome (Bouvier and Palese, 2008). Once capped and poly-adenylated to resemble host mRNA, viral mRNA is exported into the cytoplasm where it is translated into proteins. Once produced, all the components of the IAV virion assemble at the cell membrane and begin the process of budding and cleavage, which allows them to further spread through the host organism (Bouvier and Palese, 2008).

1.1.3 IAV hosts, circulation and treatments

Although IAV can infect a broad range of host species, from birds to swine to bats, the animal reservoir is maintained in avian species. It is considered a zoonotic disease, periodically acquiring enough mutations to become able to infect humans, especially in settings where humans are in close contact with infected animals. It is relatively rare that IAV gains the capability to infect a human host, coming from an avian or swine reservoir. However, by antigenic shift, an invading IAV encountering other IAV genomes within the same host cell can readily reassort segments of the

genome (Schrauwen and Fouchier, 2014). In this way, IAV can not only gain the capability to transmit from animals to humans, but also between humans, resulting in devastating influenza epidemics and pandemics. Furthermore, while in circulation, IAV acquires further mutations due to its error-prone polymerase and lack of proof reading in a process called antigenic drift. By this process, a simple mutation in the genome, exposed to evolutionary pressures such as the host environment (Smith et al., 2004) or antiviral treatment (Ong and Hayden, 2007), can give rise to novel mutations in the viral genes. Ultimately, IAV continues to circulate in both human and animal reservoirs (Landolt and Olsen, 2007), (Taubenberger and Morens, 2008). Therefore, a new outbreak or epidemic of flu is always possible, and research in this area remains of fundamental importance to public health.

Influenza vaccines are widely used in an attempt to prevent infection in the vulnerable portions of the population. They are produced based on the IAV strains currently in circulation, but the virus is very mutation-prone. Moreover, given that large-scale vaccine production involves using chicken eggs to grow the virus, there are concerns about IAV acquiring mutations during egg adaptation as well (Kotey et al., 2019). The influenza vaccine remains, therefore, of varying efficiency.

In people who do contract the infection, the currently approved treatment options are based on M2 ion channel blockade (amantadine and rimantadine), neuraminidase inhibition (oseltamivir, zanamivir and peramivir), or IAV polymerase blockade (favipiravir) (McKimm-Breschkin, 2013). However, the majority of IAV strains, including H1N1 and H3N2 that are currently in circulation, are resistant to M2 ion channel blockers (Hussain et al., 2017). In addition, H1N1 subtypes are all resistant to oseltamivir (indeed, the 2009 H1N1 pandemic strain was shown to have mutations that rendered it resistant to the inhibitor). Due to these issues, options in host-based treatments for influenza are being considered (Yip et al., 2018), with compounds that block parts of the cellular machinery involved in antiviral responses, such as for example endosomal acidification inhibition or excessive host inflammation. While these potential therapies elicit slower emergence of resistant strains and offer longer administration windows, they also present a significant risk of host cytotoxicity. There is therefore no silver bullet-type treatment for influenza as of today.

1.2 Laboratory models of influenza infection

Since influenza A has a large host base, different animal models are used to study its transmission and infection mechanism. While pigs and chickens are used to study infection in these hosts, ferrets are considered as the gold standard model for influenza transmission in humans (Belser et al., 2011). They are 1) susceptible to the same strains of virus that infect humans, 2) susceptible to the same viral transmission routes via respiratory droplets, 3) mimic the human infection course most faithfully, and 4) their serum cross reactivity with different substrains closely mimics the human situation.

Wild mice, in turn, are not natural reservoirs of influenza. The reason for this is the expression of the gene *Mx1*, encoding a GTPase protein which interferes with the replication of IAV in the nucleus (Staeheli et al., 1988), (Pavlovic et al., 1992). Laboratory strains of mice possess a non-sense mutation in this gene or a deletion of three exons in its coding sequence, making it non-functional and allowing their infection. It is worth mentioning that Mx1 in other influenza hosts such as chickens and humans (human version: MxA) is not sufficient for influenza protection as most virus strains have evolved to evade it. Taking into account all of these findings, the pertinence of a mouse model of IAV infection is more questionable in terms of future application to humans (Pavlovic et al., 1992). Different mouse strains have been shown to differ in their influenza susceptibility. The most susceptible mouse strains were reported to be the 129 strain (Davidson et al., 2014) and the DBA/2 strain (Samet and Tompkins, 2017), while C57BL/6 mice are the least susceptible. They can survive influenza infection in doses lethal to the susceptible strains and clear out the virus successfully after about 7 days, while 129 mice show increased disease-associated morbidity and mortality.

The influenza virus strains used in this thesis for *in vivo* and *in vitro* infections are of the H3N2 (X31) and H1N1 (PR8) strains. PR8 is a mouse-adapted version of the human H1N1 strain A/Puerto Rico/8/1934, whereas X31 is a reassortant virus of the PR8 backbone with HA and NA genes of the H3N2 A/Hong Kong/1/1968 strain (Bouvier and Lowen, 2010). Since these influenza strains are used for mouse infections, they have been adapted to the mouse host through serial passaging, and are likely to carry significant mutations compared to their original human-adapted counterparts (Bouvier and Lowen, 2010). Therefore, studies of influenza infection in

mice are not entirely representative of human infections, but given the ease of genetic studies in mice and their rapid breeding, they remain a pertinent laboratory model. In this thesis, both of these two IAV strains are used for *in vitro* infections, and X31 for *in vivo* infections. It is worth noting that the virulence of the two virus strains differs, with laboratory mice being significantly more susceptible to the PR8 strain than to the X31 strain.

As previously mentioned, the susceptibility to influenza is not solely determined by the virus itself, but also by the host factors. In dealing with the influenza virus, the host's immune system response and genetic background contribute to the final outcome of the infection. The immune responses to influenza virus and other non-self pathogens, are addressed in the following chapter.

1.3 The immune system and influenza virus clearance

Regardless of their function, all cells of a multicellular organism carry a shared signature of surface markers. Pathogen-associated molecular patterns (PAMPs), the external antigens from bacteria, viruses, parasites or toxins, are readily recognised as "non-self" (foreign/danger), eliminated and memorised by the cells of *the immune system*, comprised of the innate and the adaptive immune facets (Murphy, 2012). The innate immune system is the first line of defense against perceived danger, relying on a system of germline-encoded danger receptors called pattern recognition receptors (PRRs) (Medzhitov, 2001), (Janeway, 1989). On the other hand, the adaptive immune system is comprised of an army of extremely specialised cells that provide antigen-specific clearance and immune memory (Murphy, 2012).

In mammals, almost all leukocytes (innate and adaptive immune cells) take origin from pluripotent hematopoietic stem cells in the bone marrow (Kondo et al., 2003). These progenitors give rise to oligopotent stem cells that are at the origin of almost all innate and adaptive immune cell lineages, as well as red blood cells: common myeloid (CMPs) and lymphoid cell progenitors (CLPs), granulocyte-monocyte progenitors (GMPs) and megakaryocyte-erythrocyte progenitors (Murphy, 2012). CMPs and GMPs are at the origin of innate immune cells, or myeloid cells, namely granulocytes (neutrophils, eosinophils, basophils, mast cells), some macrophages, monocytes and some dendritic cells, whereas CLPs give rise to cells

of both adaptive immune cells such as B and T-cells, and innate cells such as NK cells (Schraml and Reis e Sousa, 2015), (Geissmann et al., 2010), (Akashi et al., 2000), (Kondo et al., 1997). Each of these cell types has very specific roles in the recognition and clearance of influenza and other infections, which will be described more in detail in the following sections.

It is impossible to devise an *in vitro* system that can replicate the complexity of the immune responses and the interplay between cells that occurs in order for the infection to be cleared out. Therefore, cell models are used as a replacement in order to address specific facets of the immune response and the recognition pathways that are activated in different cells. The cell models used for this purpose in this thesis are described further in this chapter.

1.3.1 Immune responses to influenza virus *in vivo*

1.3.1.1 Infection of epithelial cells and the early response

The lung and the upper airways are in constant contact with the air and all the PAMPs found in the outside world: from dust to pollen particles to pathogens. Therefore, as an organ, the lung has a high tolerance threshold to external stimuli (Wack et al., 2015). This tolerance is due to the activity of the lung epithelial cells. Via the secretory cells and the ciliated apical membranes of epithelial cells, this tissue produces mucus that coats the inside of the respiratory pathways, and moves it unidirectionally towards the oesophagus to keep the respiratory organs clear of obstruction.

In the very first steps of infection, IAV binds the sialic acid molecules clustered on the apical membrane of the epithelial cells, and it is subsequently taken up via endosomes (Edinger et al., 2014). Once inside the cell, epithelial cells recognise viral PAMPs in the cytosol using a PRR from the RLR family called RIG-I, but also in the endosomal compartment using the PR transmembrane receptor called TLR3. RIG-I engagement in epithelial cells activates a signalling cascade that results in type-I IFN production, which ultimately leads to the establishment of an antiviral state and the recruitment of immune cells to the infection site (Denney and Ho, 2018) (more details in 1.4). Epithelial cells are the origin of the initial burst of type-I IFN upon infection. They are permissive to IAV replication and release virions upon the completion of the viral cycle. They can also specifically upregulate the production of type-III IFN, or

IFN-λ, which has been shown to have similar effects to type-I IFNs in terms of transcriptional inductions (Crotta et al., 2013). This is thought to be a good backup anti-viral mechanism to the hallmark type-I IFNs and to represent an interesting therapeutic target because of the lack of pathogenicity induced (Davidson et al., 2016).

1.3.1.2 Alveolar macrophages: the first innate immunity responders

Alveolar macrophages (AM) patrol the luminal lining of the lung epithelium scanning for pathogens and other insults. A subset of the macrophage immune cell population, they are terminally differentiated and specialised in engulfing pathogens and clearing out cell debris and surfactants (Divangahi et al., 2015), (Guilliams et al., 2013). Alveolar macrophages are easily distinguishable from other cell types in the lung, as they are large autofluorescent cells (FSC^{hi}, SSC^{hi}) that carry a set of specific surface markers that they are highly positive for, namely SIGLEC-F, F4/80 and CD11c.

In annual circulating strains of influenza, the virus is predominantly localised in the upper respiratory airways, where it remains until infection clearance. AMs are not very abundant in the upper airways so they rarely encounter the incoming viruses. However, IAV strains such as H5N1 and H1N1 can descend into the lung as the infection progresses (van Riel et al., 2006). In the alveolar space, AMs are vital in influenza infection because they are the first immune sensors of the incoming virus and of infected and damaged epithelial cells.

Both mouse and human AMs were shown to be susceptible to influenza virus infection and to express viral proteins ((Rodgers and Mims, 1981), (Rodgers and Mims, 1982), (van Riel et al., 2006), (Short et al., 2012), (Yu et al., 2011)). However, budding of virus particles off the cell membrane is virtually absent in AMs (Londrigan et al., 2015) and virus particle assembly defective in human monocyte-derived macrophages (Bedi et al., 2018), preventing virus shedding and spread in these cell types. In spite of this, some research has shown that the replication of highly pathogenic influenza virus strains such as H1N1 and H5N1 is active in the RAW264.7 cell model of murine macrophages (Marvin et al., 2017), (Cline et al., 2013). These two strains were shown to infect AMs, with H5N1 being successful at replication, while H1N1 is not (Yu et al., 2011).

Macrophages are capable of recognising the viral RNA genome using RIG-I and TLR3-mediated signalling, much like epithelial cells do (Wu et al., 2015). Moreover, they uptake cellular debris of infected cells and respond by triggering the production of pro-inflammatory cytokines and chemokines (Vangeti et al., 2018). In influenza infection, the most prominent pro-inflammatory cytokines produced by AMs and monocyte-derived macrophages include TNF-α, IL-12p40, IP-10, IL-6 and IL-8 (Hoeve et al., 2012), (Vangeti et al., 2018). Interestingly, while AMs are considered to dampen immune responses at first, they have been shown to exacerbate responses to influenza both through IFN and cytokine production (Tate et al., 2010).

1.3.1.3 Dendritic cells: the sentinels and antigen presenters

Dendritic cells are another sentinel cell type-In the lung. In steady state, they patrol along the basal membrane of the epithelial cells, monitoring the airways for pathogen infection.

Dendritic cells arise from common dendritic cell precursor cells in the bone marrow (reviewed by (Schraml and Reis e Sousa, 2015)). Stimulated by Flt3L, this cell subset gives rise to conventional dendritic cells and plasmacytoid dendritic cells (pDCs), both of crucial importance in influenza and pathogen clearance and IFN synthesis (Onai et al., 2006), (Onai et al., 2007) (more detail on pDCs in subsection 1.3.1.4). Flt3L is the ligand of Flt3, a receptor tyrosine kinase, and it is sufficient to induce differentiation of DC subsets. Flt3L is used both *in vivo* to stimulate DC production in mice (Karsunky et al., 2003), (Maraskovsky et al., 1996) and *in vitro* to favour DC lineage formation and ultimately pDC differentiation from bone marrow precursors (Naik et al., 2007). DCs (pDCs excluded) terminate their differentiation outside the bone marrow and ultimately give rise to two cDC populations, distinguished by their surface markers: CD103+ DCs, and CD11b+ DCs, both of which are present in the lung at steady state (Guilliams et al., 2013). Monocyte-derived DCs, a differentiated population of monocytes recruited to the lung as the lung-dwelling DCs leave during infection (Cao et al., 2012), have a distinct role in pro-inflammatory cytokine production, contributing to the overall inflammatory environment of a late-stage infected lung.

Human peripheral monocyte-derived DCs, an *in vitro* human model for their lung counterparts, were shown to uptake IAV into the endosomal compartment

(Baharom et al., 2017). Following this, cDCs are capable of producing cytokines as well as type-I IFN, but are not the major *in vivo* producer of either. Their main function is antigen presentation, i.e. the initiation of establishment of an antigen-specific adaptive immune response. 24h-48h following infection, cDCs migrate into the lymphatic system (usually the lymph node draining the lung, the mediastinal lymph node), where they present the encountered antigens to T-cell populations. Both DC cell types were shown to be efficient in antigen presentation to CD4+ T-cells (further for details on T-cells to follow), while the $CD103^{hi}$ DCs are more efficient at activating CD8+ T-cells (Kim and Braciale, 2009), (del Rio et al., 2007). This antigen presentation step is crucial, as it links the innate and the adaptive immune response and ensures antigen-specific clearance in the lung.

1.3.1.4 Plasmacytoid dendritic cells: the IFN producers

Plasmacytoid dendritic cells (pDCs) are small lymphocyte-like cells that terminally differentiate in the bone marrow. They can take origin from dendritic cell myeloid progenitors (shared with cDCs) or common lymphoid progenitors (reviewed in (Reizis, 2019)). While Flt3L is sufficient to stimulate pDC development from myeloid precursors (Karsunky et al., 2003), in lymphoid progenitors type-I IFN was shown to act synergistically with Flt3L in upregulating Flt3 and pDC differentiation (Chen et al., 2013). Flt3L is also used as a stimulant for *in vitro* derivation of pDC-like cells BM progenitors (Brasel et al., 2000). Following differentiation, pDCs migrate out of the bone marrow and into the peripheral lymphoid organs and blood, where they remain until recruitment cues are perceived during infection.

Surface markers on mouse-derived pDCs differ from those on human pDCs. Mouse pDCs have intermediate to high CD11c expression, whereas human pDCs are negative (rev. in (Hochrein et al., 2002)). Unlike cDCs, mouse pDCs are CD11b negative and express Siglec-H (sialic-acid binding immunoglobulin-like lectin H) (Zhang et al., 2006) and B-220 (a marker they share with mouse B-cells). Since some spleen-dwelling macrophages and B-cells share Siglec-H and B220 expression with pDCs, respectively, PDCA-1 (a tetherin described to prevent retroviral release in HIV infection (Neil et al., 2008)) is used in conjunction with these markers to distinguish pDCs *in vivo* (Medina et al., 2013). However, it is worth noting that PDCA-1 is also

upregulated on other innate immune cells during infection (AMs, monocytes, DCs, neutrophils).

pDCs (in their immature form) are highly specialised in type-I IFN production, and especially that of IFN-α (Nakano et al., 2001), (Asselin-Paturel et al., 2001). The pDC specialisation in production of IFN during infection is due to the inherently high expression of IRF7, a type-I IFN specific transcription factor, and to the rapid engagement of an IFN positive-feedback loop through its receptor IFNAR. More detail on IFNs and this cascade is discussed in sections 1.4.1.2 and 1.5.1.2 of this thesis. It is thought that thanks to this rapid IFN upregulation, pDCs are non-permissive to viral replication. Aside from high type-I IFN production, pDCs also secrete type-III IFN (IFN-λ), although its predominant producers are lung epithelial cells.

Though IAV was shown to enter pDCs, viral replication was abortive and did not induce viral protein translation and particle release (Thitithanyanont et al., 2007). The studies on viral entry into pDCs are few and far between, so it remains unclear whether the virus entry is mediated by a classical HA-SA binding or some other mechanism, such as viral exosome exchange between proximal cells as it was shown in hepatitis infection (Webster et al., 2016), (Dreux et al., 2012). One study, in porcine peripheral blood-derived pDCs, proved that both sialic acid residues on cell membranes as well as an intact HA on the virus were necessary to pDC-driven IFN-α production (Bel et al., 2011). Additionally, (Diebold et al., 2004) showed that IFN-α production in pDCs can also be induced by heat-inactivated influenza virus *in vitro*, indicating that IFN production can be stimulated by recognition of viral RNA upon entry. This was in concordance with another study (Bel et al., 2011) in that, upon virus heat inactivation at 65°C, where HA integrity is compromised, no IFN-α production was observed *in vitro.* Both these studies point to an entry of IAV into pDCs, which causes the viral ssRNA to be exposed in the endosomal compartment for PAMP recognition. This is not so difficult to imagine, as SA residues are ubiquitous in the host cells and are bound to galactose molecules on a multitude of different receptors (Skehel and Wiley, 2000). In this thesis, murine pDCs respond to *in vitro* incubation with live influenza X31 virus (see Results) with IFN-α and IFN-β production, but no effect on viral replication was addressed. *In vivo,* it is acknowledged that pDC-mediated IFN-α production is triggered by viral antigen

uptake either directly or through infected or lysed cells ((Lui et al., 2009), (Assil et al., 2015), (Webster et al., 2016)). This in turn triggers maturation of pDCs into antigen-presenting cells to CD4+ and CD8+ T-cells (Fonteneau et al., 2003) and is thought to accelerate viral clearance.

By virtue of their extreme potential to synthetise type-I IFN, pDCs also have a high potential to damage the lungs and other immune cells. One of the mechanisms by which this can happen is the action of IFN itself, especially in the cases where its production is too elevated (described in subsection 1.4.3).

1.3.1.5 Monocytes: the pro-inflammation mediators

Following pathogen infection or generally injury to the lung, the AM and cDC populations get depleted and can be replenished by incoming monocytes. Monocytes are incompletely differentiated CD11b+, Ly6C+ or negative cells that originate in the bone marrow from a monocyte-macrophage DC progenitor (Geissmann et al., 2010), (Hettinger et al., 2013). The Ly6C+ population, named inflammatory monocytes, contributes to cellular replenishment *in situ* and drives the pro-inflammatory cytokine responses in influenza and other infections. Ly6C+ bone marrow-dwelling immature monocytes express the CCL2 (MCP-1) ligand receptor CCR2, upregulated in IFN stimulation. Upon CCL2 binding, CCR2 initiates bone marrow egress of monocytes into the infected lung, where they give rise to monocyte-derived DCs and MPhs (Serbina and Pamer, 2006). These MoDCs and MoMPhs have a more pro-inflammatory phenotype than resident AMs and DC (Cao et al., 2012), and have been associated with IAV pathology (Lin et al., 2008).

Ly6C+ monocytes are known for their pro-inflammatory cytokine production capabilities, necessary for recruitment of other monocytes and neutrophils, and ultimately successful virus clearance. They drive the expression of TNFα, IL-12, IL-18, IL-1α/β and other critical cytokines and chemokines (Lauvau et al., 2014). This monocyte-driven cytokine production is upregulated in response to type-I IFN present in the lung upon influenza infection (Uccellini and Garcia-Sastre, 2018). However, accumulation and persistent recruitment of monocytes to the lung during influenza infection is often linked to poor outcomes owing to their contribution to the “cytokine storm” (Coates et al., 2018), (Lin et al., 2014).

In response to type-I IFN, monocytes also upregulate the expression of TRAIL, a ligand for DR5 receptor on epithelial cells inducing their apoptosis. Through this mechanism, they were shown to directly participate in influenza-induced morbidity and host susceptibility in the context of prolonged IFN exposure (Herold et al., 2008), (Ellis et al., 2015), (Davidson et al., 2014), (Davidson et al., 2015).

1.3.1.6 Neutrophils, eosinophils and the adaptive immune response roles in influenza infection

Neutrophils and eosinophils are members of the granulocyte family of immune cells (which also includes basophils) (Amulic et al., 2012). Easily distinguishable by their murine surface markers, neutrophils are CD11b+ Ly6G+ (Amulic et al., 2012), (Daley et al., 2008) and eosinophils Siglec-F+ CD11c-. The main roles of these cells during infection is to contribute to the synthesis of pro-inflammatory cytokines and cellular recruitment into the lung, which is necessary for the smooth resolution of infection.

Neutrophils are recruited early on in infection (starting day 2-3) (Tate et al., 2008) thanks to IFN cues from the lung resident cells (Seo et al., 2011). They were also shown to phagocytose apoptotic influenza-infected cells *in vivo* in the mouse lung, in what is possibly a virus-replication controlling process (Hashimoto et al., 2007). Increased neutrophil presence was shown in the early stages of infection with the highly virulent H1N1 and H5N1 influenza viruses (Perrone et al., 2008). Reports correlated increased neutrophil recruitment with severity of respiratory disease in general (rev. in (Camp and Jonsson, 2017)). However, other data suggested a protective effect of neutrophils in respiratory infections, especially in the case of high pathogenicity virus strains (Tate et al., 2008, Tate et al., 2009, Tate et al., 2011). Meanwhile, eosinophils were shown to help resolve influenza infection in mice by initiating T-cell recruitment and aiding antigen presentation (Samarasinghe et al., 2017).

1.3.1.7 Adaptive immune response to influenza virus

Cells of the adaptive immune system have multiple roles in IAV infection. Most prominent effectors for IAV clearance and anti-IAV memory are CD4+ and CD8+ T-cells and B-cells. Like all other lymphocytes, these cells take origin from the common

lymphoid progenitor in the bone marrow. In steady state, they recirculate and populate the lymphoid organs such as spleen and lymph nodes.

The adaptive immune system ensures the restriction, clearance and memory of influenza infection (Chen et al., 2018). CD8+ T-cells perceive antigens presented by the dendritic cells in draining lymph nodes and, prompted by IFN-$\alpha/\beta/\gamma$ and IL-2/IL-12 cytokines, differentiate into cytotoxic T-cells capable of restricting infection by killing virus-infected cells (Kreijtz JH, 2011), (A. W. S. Ho, 2011). CD8+ "cytotoxic" T-cells eliminate infected cells by inducing their apoptosis (Grant et al., 2016). Meanwhile, CD4+ T-cells differentiate into subtypes of helper T-cells in response to antigen presentation, and also participate in inducing apoptosis of infected cells (Soghoian D.Z., 2010).

B-cells provide specific long-term memory of perceived antigens thanks to their specificity for class-switched antibody formation. This response usually occurs between 7 and 14 days post-infection. The main antibody types produced in influenza infection are IgA and IgG (Arulanandam et al., 2001), (Rangel-Moreno et al., 2008), though IgM is also synthetised by the resident memory B-cells in the lung at the very beginning of the infection, and was shown to contribute to viral clearance (Lam and Baumgarth, 2019). Following successful IAV infection resolution, memory B-cells will continue to reside in the lung, lymph nodes near the lungs, or bone marrow and spleen, providing rapid induction of antibody production in future homotypic infections.

1.3.2 BM-derived *in vitro* cell models for infection and stimulation

In this subsection, I will describe the *in vitro* cell models used in this thesis to study IAV infection and PAMP recognition and how they compare to their *in vivo* counterparts. The rationale behind using these cells was to exploit a more simple and controllable system than that of the extremely complex and multi-faceted immune responses *in vivo*. Both of the cell types that will be described are derived from whole bone marrow, and differentiated using well known cytokines and growth factors.

1.3.2.1 Bone marrow-derived macrophages

BMDMs are a long-standing cell model in immunology. They have been used to model bacterial and viral infections and cell receptor stimulation alike. BMDM overall morphology of large autofluorescent cells (FSC^{hi}, SSC^{hi}) closely mimics that of *in vivo* macrophages. They also express F4/80, a marker which was described as specific to *in vivo* macrophage populations as well.

Derivation of BMDM-rich cultures in this thesis relied on M-CSF stimulation. This cytokine, along with GM-CSF, is a driver of development for macrophage populations from bone marrow cell precursors *in vivo.* However, cell populations generated *in vitro* with these two differentiation factors are not identical. GM-CSF can induce differentiation of DC-like cells, monocytes and macrophages (Inaba et al., 1992). The cell subtypes defined as macrophage-like were shown to upregulate their antigen-presenting capacity (Fischer et al., 1988), and their pro-inflammatory cytokine production upon transient GM-CSF challenge (Fleetwood et al., 2007), making them functionally more similar to monocytes and DCs overall. In accordance with these findings, a recent study demonstrated that GM-CSF-differentiated cell populations *in vitro* are in fact a mix of DCs and F4/80+ CD11b+ macrophages (Helft et al., 2015). Therefore, while GM-CSF is solicited *in vivo* during macrophage differentiation, its employment *in vitro* on whole bone marrow precursors yields a mixed population that was not suitable for this thesis *in vitro* models.

In contrast, using M-CSF for *in vitro* derivation of BMDMs yields more pure and reliable cells with macrophage phenotypes, and it is the currently widely used methodology for BMDM *in vitro* derivation (Murray et al., 2014). The current most widely used protocol involves the use of L-cell supernatants, since they contain M-CSF in certain amounts. For cost and practical purposes, this differentiation media was also employed for BMDM generation this thesis. However, *stricto sensu,* it is more desirable to use recombinant M-CSF rather than L-cell supernatant for obvious reasons of possible presence of cell-stimulating contaminants in the media (Warren and Vogel, 1985).

M-CSF-derived BMDMs show similar cytokine response patterns to those of alveolar macrophages upon IAV infection, namely upregulation of transcription and translation of IL-6, IFNβ and TNFα (Maelfait et al., 2012). Similarly, in Rift Valley

fever virus infection *in vitro* BMDMs responded with IFNβ, TNFα, and IL-1α synthesis, reminiscent of macrophage responses *in vivo* (Roberts et al., 2015).

1.3.2.2 Bone marrow-derived plasmacytoid dendritic cell-enriched populations

Deriving pDCs for usage *in vitro* is more challenging than in the BMDM case, since Flt3L is a known inducer of DC populations *in vivo*, as was described earlier. Two different ways to obtaining pDC-like cells *in vitro* have been reported: 1. inoculating mice with FLT3L intra-peritoneally and purifying pDCs from the spleen or 2. extracting whole bone marrow and subjecting the progenitors to FLT3L *in vitro* (Bjorck, 2001). In either case, FLT3L yields a mixed culture of DCs and pDCs, which always requires specific antigen-driven purification in order to isolate pDC-like cells. Generally, mouse pDCs *in vitro* carry similar markers to their *in vivo* counterparts: CD11c, Siglec-H, B220 cells and PDCA-1. In this thesis, the stimulation of pDC production was achieved from bone marrow precursors followed by purification using B220 surface markers. A purification with the more specific Siglec-H markers was attempted but yielded very low final numbers (though it was highly pure in pDC-like cells). Because of the *in vitro* culture heterogeneity, the FLT3L-stimulated bone marrow cultures are referred to as “pDC-enriched” cultures.

1.4 Interferons and cytokines in health and disease

As seen previously, cytokines, and especially interferons, are produced by virtually all immune cells in response to infection, and they have paramount roles in pathogen clearance and host recovery. In this subchapter, I will elaborate on the role of interferons and cytokines in influenza and other infections, as well as their contributions to immunopathology.

1.4.1 The interferon system

The interferon family of cytokines was first described as early as 1957, in seminal work by Isaacs and Lindenmann (Isaacs, 1957a, Isaacs, 1957b). They were named “interferons” because they were shown to “interfere” with the replication of IAV, as well as Newcastle disease, Sendai and vaccinia viruses. Interestingly, the IFN-inducing stimulus in these experiments was a 56°C inactivated influenza virus.

As has been shown several times, heat-inactivated viruses do not induce IFN synthesis, and therefore, it is likely that some viral particles used in this experiment were not completely degraded, making initial particle recognition by RIG-I possible. Further, it is possible that this low-level viral infection activated the reported production of interferons.

Interferons are crucial antivirals and immune modulators in different contexts. In the following three subsections, they are described in more detail and their roles in influenza infection and other host challenges addressed more in depth.

1.4.1.1 Type-II and type-III IFNs – roles in influenza and other infections

The interferons form a large family of immune modulators composed of three different types: type-I (IFN-α, IFN-β and others), type-II (IFN-γ) and type-III (IFN-λ).

Type-II IFN (IFN-γ) is produced by lymphocytes, typically NK cells, activated T-cells and macrophages, and it is a marker of enhanced antigen presentation and T-cell maturation activity (reviewed in (Schoenborn and Wilson, 2007), (Saha et al., 2010)). It induces transcription, via the IFNGR JAK/STAT cascade, from GAS-sequence-containing promoters, of genes such as IRF1 and IRF9 transcription factors and SOCS1, a negative regulator of innate immune responses. Indeed, an analysis of GAS sequences content unveiled the presence of these sequences in a multitude of factors from STAT1 to TLR receptors to all IRF TFs (Saha et al., 2010). Increased susceptibility to mycobacterial infection was linked to deficiencies in the IFNγ signaling, in IFNγ itself as well as in IFNGR subunits (Bell and Noursadeghi, 2018), (Wu et al., 2019), (Al-Muhsen and Casanova, 2008).

The IFNλ family includes IFN-λ1 (IL29A, pseudogene in mice), IFN-λ2 (IL-28A), IFN-λ3 (IL-28B), and the human IFN-λ4 (Wack et al., 2015). In mice, all of these genes (and pseudogenes) are located on chromosome 7. IFN-λ is produced largely by the lung epithelial cells, but pDCs and DCs were also shown to express it, albeit in more modest quantities than type-I IFN (Coccia et al., 2004), (Wack et al., 2015). IFN-λ signaling occurs through a receptor complex composed of IL-28R1 and IL-10R2, the former only being expressed on lung and gut epithelial cells (Kotenko et al., 2003), (Blazek et al., 2015). IFN-λ expression seems to be governed through IRF3, IRF7, NFκB and AP-1, much like that of IFN-α/β (Osterlund et al., 2007).

IFN-λ have similar effects to type-I IFNs in terms of establishment of an antiviral state and the induction of effector gene transcription in the airway epithelia (Crotta et al., 2013), but without the pathology caused to the host (Davidson et al., 2016). It is possible that IFN-λ is a backup antiviral mechanism, as mice lacking type-I IFN receptor are able to survive and eliminate influenza (Mordstein et al., 2008), (Davidson et al., 2014). IFN-λ had been successful in a clinical trial for the treatment of hepatitis C in humans (Muir et al., 2014), and treatment of mice during IAV infection improved overall outcomes (Davidson et al., 2016).

1.4.1.2 Type-I IFNs: genes, transcription and translation and receptor

Type-I IFNs are the hallmark innate immune defense molecules. They are not influenza-specific, but the first responders in any virus infection, and even in some forms of sterile inflammation and autoimmunity. They can theoretically be produced by any cell type challenged by non-self PAMP molecules. As they are the focus of this thesis, it is to be assumed from this point onwards that "IFN" stands for type-I IFN, unless otherwise indicated. The type-I IFN family is composed of five sub-types in humans: IFN-α, IFN-β, IFN-ε, IFN-κ, and IFN-ω (Platanias, 2005). Given that this thesis was based on studying the production and the effects of IFNα/β, these will be addressed in more detail in the subsequent section.

IFNβ is encoded by a single gene, IFN-β1, located on chromosome 4 in mice (9 in humans). IFN-β transcription initiation depends largely on the stimulus, the PRR pathway engaged, and on the cell type. However, these various cellular pathways converge towards two biggest acknowledged IFN-β transcription factors: NFκB and IRFs (Schmitz et al., 2014), (Chen et al., 2017), (Panne et al., 2007), (Makris et al., 2017), (Stetson and Medzhitov, 2006), (Wang et al., 2016a). Namely, IRF3 and IRF7 are known as central virus-activated TFs of IFN-β1 (and IFN-αs). The IFN-β1 promoter contains binding sequences for both NFκB and the IRF3/CBP-p300 transcription factor complex (the PRD domains II and IV, and I and III, respectively). PRD domains are also recognised by IRF7 and are contained, in a modified form (PRD-LE) in the IFN-α promoter sequence as well (reviewed in (Taniguchi and Takaoka, 2002), (Honda et al., 2006)). IAV, following the viral genome recognition in the cytoplasm, activates phosphorylation and nuclear translocation of IRF3 and thus transcription of IFN-β1. In an evolutionarily pertinent confirmation of the importance

of IRF3 in IFN-β1 induction, IAV has evolved immune evasion mechanisms to interfere with IRF3 to stop IFN-β production (Yi et al., 2017) (as shown in an *in vitro* model).

Aside from these TFs alone, an *Ifn*-β "enhanceosome", a complex of proteins that is able to rapidly increase its transcription by binding to specific enhancer sequences upstream of its TSS, controls *Ifn*-β1 expression. The enhanceosome was shown to consist of major transcription factors: NFκB (p50:p65(RelA)), ATF-2/c-Jun, IRF3 and IRF7 and the scaffold protein HMGA1 (previously HMGI(Y)) (reviewed in (Panne et al., 2007), (Honda et al., 2006)). Interestingly, the binding of IRF3 to the *Ifn-β* promoter was shown to be less stable alone than in the assembled enhanceosome *in vitro* upon Sendai virus infection (Wathelet et al., 1998). The enhanceosome is responsive to viral infection, upon which it docks onto the nucleotide region -102 to -47bp relative to the *Ifn*-β TSS (Panne et al., 2007) to trigger *Ifn-β* transcription. Moreover, it was shown that the activity of this enhanceosome allows for more rapid recruitment of CBP-Pol II to the promoter of *Ifn-β1* to allow for increased transcription rates (Yie et al., 1999). IRF3 is generally more potent at activating *Ifn-β1* transcription, whereas IRF7 is efficient at activating both *Ifn-β* and *Ifn-α* expression (Marie et al., 1998).

IFN-α proteins are encoded by 14 different intron-lacking genes (*Ifn*-α1-14) in mice and 13 in humans (*Ifn*-α1-13), arranged in a cluster near the *Ifn*-β1 genes. They have antiviral, anti-proliferative and immune modulatory properties (Lavoie et al., 2011), (Gibbert et al., 2013). While most if not all virus-infected cells produce type-I IFNs, the largest IFN-α producing and secreting cells, as was previously mentioned, are pDCs, but both *in vivo* and *in vitro* other cell types have been shown to express different IFN-α proteins (Gibbert et al., 2013).

There is some discord concerning the mechanism which allows pDCs to respond with rapid and robust IFN-α synthesis to different stimuli. On the one hand, it is proposed that high IFN-α levels in pDCs are due to a mechanism involving an auto-amplification loop via the type-I IFN receptor IFNAR, and the transcription factor IRF7 (Sato et al., 1998), (Marie et al., 1998). Other studies had proposed that pDCs have a steady-state high expression of IRF7 compared to other immune cells, which allows for rapid and high induction of IFNα transcription. Indeed, a study detected a higher level of IRF7 expression in splenocyte CD11b- CD11c+ pDC subsets

compared to other tissues upon infection, while IRF3 expression remained similar across tissues (Prakash et al., 2005). This however, was not due to the increased stability of the IRF7 protein itself. IRF7 was shown to have a short half-life with fresh protein production assured by IFN in steady state at low levels, or by the activation of IFN synthesis during virus infection (Prakash and Levy, 2006). Interestingly, in both spleen and thymus it was shown that both at steady-state and in viral challenge, IRF3 half-life was higher than that of IRF7, indicating that IRF3 is a more stable protein *in vivo* (Prakash and Levy, 2006). A suitable mechanism to take all these findings into account was proposed in an *in vitro* model of MEFs (Sato et al., 2000). It proposed a steady-state IRF3-mediated *Ifn*-β production, which could initiate a first burst of IFN-α4 and IRF7 synthesis upon stimulation, followed by an intense, IRF7-mediated production of IFN-α1,2,4 and 5 to ensure clearance (in this case) of Newcastle Disease Virus. Given the fact that IRF7 is in fact an ISG, its transcription is mediated via the IFNAR cascade and ISGF3-mediated transcription. Overall, IRF7 basal expression in pDCs is probably a good primer for IFN-α/β induction, but insufficient to explain their specialisation as the host's most potent IFN producers (Reizis et al., 2011).

The ubiquitous effect of IFNs is mirrored in their receptor IFNAR, composed of two subunits, IFNAR1 and IFNAR2. IFNAR is ubiquitously expressed on all cells in the body, including all immune system cells, rendering the IFN effects systemic. While both IFN-α and IFN-β can recognise and bind to IFNAR, IFN-β was shown to have higher affinity of binding than the IFN-α subtypes (Jaks et al., 2007) (reviewed in (Gibbert et al., 2013)). Moreover, some studies have proposed a separate, independent signaling pathway initiated by the binding of IFN-β to IFNAR1 subunit, even without the presence of IFNAR2 (Kaur and Platanias, 2013), (de Weerd et al., 2013). The result of IFNAR-mediated signaling is the transcription of more than 200 genes called interferon-stimulated genes (ISGs).

1.4.1.3 The interferon-stimulated genes (ISGs) and their cell-specific production and effects

ISG-encoded proteins have systemic cell-dependent effects in the host immune defenses. They are effectively the translator of the IFN message into anti-pathogen and immunomodulatory effects, and differ depending on the cell type

perceiving IFN. A number of different factors in immune defenses are in fact ISGs: from PRRs, IRFs and other transcription factors, to negative regulators of immune responses. Some examples of ISGs pertinent in IAV infection resolution will be briefly addressed here.

A big subset of ISGs are directed against pathogens specifically. In the case of IAV, multiple factors can interfere with the viral life cycle or upregulate host's immune responses (reviewed in (Schoggins and Rice, 2011), (Iwasaki and Pillai, 2014)). Typically, murine Mx1 protein has proven antiviral effects in interfering with the virus replication. In humans, IFITM3 is a susceptibility factor to influenza (Everitt et al., 2012). IFITM3 is also an ISG, and alongside IFITM1 and IFITM2 it was shown to block the fusion of the viral and host membranes upon virus entry in IAV, dengue and West Nile virus infections (Brass et al., 2009). The TRIM family of proteins (especially TRIM22 and TRIM25) help regulate the immune system response for successful elimination of IAV (Di Pietro et al., 2013) and other viruses (Munir, 2010). Viperin protein is another ISG, shown to interfere with the formation of lipid rafts that IAV uses for budding off infected cells (Wang et al., 2007). PKR was shown to interfere with protein translation by phosphorylating EIF2α activating the NFκB pathway and stabilising IFN-α and IFN-β proteins (Balachandran et al., 2000).

Some proteins that negatively regulate inflammation signaling are also ISGs. SOCS proteins are negative regulators of IFN-α/β, IFN-γ, IL-2, IL-6, and many others, doing so by a negative feedback mechanism of IFNAR degradation (Alexander, 2002).

A big sub-family of ISGs are host factors directed at increasing inflammation, recruiting innate and adaptive immune cells to the infection site, and activating the adaptive immune responses. The expression of IRF7, TLR3/7/9, as well as RIG-I and cGAS, is inducible by IFNAR signaling.

Ultimately, some ISGs are pro-apoptotic, directed at limiting excessive immune responses and at eliminating infected cells. Combinations of ISGs were shown to be effective in inducing apoptosis of lung epithelial cells. Namely, TRAIL is an ISG that is specifically expressed by circulating inflammatory monocytes. It is a ligand that can bind death receptors (DR5 typically) expressed on epithelial cells during infection, to induce epithelial cell apoptosis, a process proven potentially pathogenic to the murine IAV host (Davidson et al., 2014, Ellis et al., 2015).

1.4.2 Cytokines that participate in influenza infection defense

Aside from IFN, a whole plethora of cytokines are produced during influenza infection, whether in response to IFN presence or in NFκB-led pathways running in parallel or indirectly stimulated by IFN. For example, basal or IFN-dependent induction of RIG-I and TLR7 expression can trigger NFκB signaling and cytokine production since this TF is downstream of both of these receptors (Fukuyama and Kawaoka, 2011).

IFN-dependent signaling to the immune system cells can result in the upregulation IL-6, IL-18, MIP-1α, IL-1β, RANTES and TNF-α in monocytes and macrophages (Hervas-Stubbs et al., 2011), (Perrone et al., 2008). Of these, TNF-α, IL-6 and IL-1β are hallmark cytokines in influenza infection that drive disease severity (Garcia-Ramirez et al., 2015), (Fukuyama and Kawaoka, 2011). IL-12p70 and IL-18 are produced by DCs and macrophages in response to bacterial and virus stimuli to induce IFN-γ secretion by NK cells and T-cells (Gautier et al., 2005, Dienz et al., 2012), (Chen et al., 2018), (Monteiro et al., 1998). These cytokines act as chemoattractants and systemic pro-inflammation molecules to recruit immune cells to the site of infection. IFNs also elicit the upregulation of MHC molecules on DCs, and stimulate their antigen-presenting properties. CXCL10 production in the lung during RSV infection was shown to be dependent on the IFNAR cascade (however, this control could be a direct or an indirect effect of IFN) (Goritzka et al., 2014). In BMDMs, IFN-β was shown to induce CCL2 expression, with the IFN autocrine loop maintaining the production of this chemokine that was shown to cause monocyte recruitment *in vivo* (Pattison et al., 2013).

Another important molecule synthetised during acute influenza infection is IL-10. It is an anti-inflammatory cytokine produced by incoming virus-specific CD4+ and predominantly CD8+ T-cells to fine-tune antiviral responses and dampen inflammation (Sun et al., 2009).

Generally, the effective immune response to influenza (and to any other pathogen) requires a balanced immune response from the host. If the induced inflammation is too weak, the viral replication gets out of hand with damaging or fatal outcomes. On the other hand, overstimulation of the immune response in the form of intense IFN production or a “cytokine storm” can be detrimental to the host through

immune-mediated tissue damage (Liu et al., 2016), (Davidson et al., 2014), (Li et al., 2018).

1.4.3 Pathogenic potential of type-I IFN

By virtue of their ubiquitous action and the intensity of responses they elicit, IFN effects present a significant pathogenic threat to the host. This was found for both acute and chronic diseases. In the case of IAV infection, host-driven pathology can be independent of the virulence of the IAV strain. Moreover, IFNs are major drivers in autoimmune disease pathology (Davidson et al., 2015), (McNab et al., 2015).

In chronic infections, such as those with HIV, excessive IFN signaling in innate immunity has been linked with disease progression (Rajasuriar et al., 2013), (McNab et al., 2015). Moreover, TRAIL expression on pDCs (via the IFNα/β cascade activation) was shown to induce CD4+ T-cell apoptosis (Stary et al., 2009), (Hughes et al., 2012). Inversely, lower ISG responses were linked to more favourable outcomes and non-progressive disease. In LCMV infection amelioration was achieved upon blockade of the IFN cascade (Teijaro et al., 2013), (Wilson et al., 2013). In acute RSV infection, IFN-α/β were shown to promote pro-inflammatory cytokine production in the lungs (Goritzka et al., 2014), an effect expectedly abolished in *Ifnar-/-* mice.

1.4.3.1 IFN-α/β host pathology: a study of influenza infection in mice

A very clear pathogenic effect of IFN-α/β in influenza infection was demonstrated in a mouse study published in 2014 by our group (Davidson et al., 2014). This section will describe this study more in detail, as it laid the ground for the PhD project presented in this thesis.

(Davidson et al., 2014) demonstrated a contrast between the efficient viral clearance of IAV in C57BL/6 mice and the high IFN-α/β synthesis, lung damage, lung epithelial apoptosis, and a high pro-inflammatory cytokine secretion in 129 mice (a “cytokine storm”). Consequently, the morbidity and mortality in 129 mice was notably higher than in the C57BL/6 strain in IAV infection. The fact that the two mouse strains showed similar viral load in the lungs, and that the same virus strains (X31 or PR8) were used to infect them, led to the conclusion that the observed phenotype was due

to host-derived factors. Indeed, this study had shown that 129 morbidity and mortality were due to heightened IFN-α/β production compared to that in BL/6 mice. Direct proof came from comparing *Ifnar1-/-* 129 and BL/6 mice, in which the IFN-dependent ISG production cascade is abolished. Indeed, the 129 *Ifnar1-/-* mice survived influenza infection better than their WT counterparts, and *Ifnar1-/-* BL/6 mice were slightly more susceptible than their WT counterparts, but could still clear the infection. It is worth noting here that the effect of IFN-α distribution in BL/6 mice in another study showed to be time-dependent: if distributed during the infection, it was damaging, and if given prior to infection it had clear protective effects (Davidson et al., 2016). The question of timing of IFN-α/β responses was in concordance with the findings from (Davidson et al., 2014). Namely, 129 mice not only had increased IFN-α/β production compared to BL/6 mice, but also had a sustained increased IFN response and another peak of production of IFN later on in infection. The initial peak of production occurred at days 2-3 post-infection in both strains, similar in timing but not in intensity to BL/6 controls. It is possible that the pathogenic effects of IFN come from its prolonged production, but the sources and the mechanism behind this remain unclear.

It could be speculated that a lack of IFN production in both *Ifnar1-/-* strains might be lethal in influenza, due to lack of virus control. Since influenza virus infects productively only epithelial cells which both express and respond to type-I and type-III IFNs, it was shown that in absence of IFN-α/β, IFN-λ serves as antiviral effector substitute, as its mechanism of action induces similar transcriptional loops as that of IFN-α/β (Crotta et al., 2013). IFN-λ in influenza infection was reported to be protective without the associated pathology, and is considered as a therapeutic for severe influenza (Davidson et al., 2016). It lacks the effects of a “cytokine storm” that are characteristic of IFN-α/β and thus preserves the host from immune-mediated damage to the epithelium.

The ultimate consequence of increased and sustained IFN-α/β signaling in 129 mice was the expression of TRAIL on monocytes and DR5 in the lung epithelium, the association of which led to increased apoptosis of lung epithelial cells (Davidson et al., 2014). In *Ifnar1-/-* mice this effect was abolished, and WT 129 mice were rescued by treatment with mAbs blocking TRAIL-DR5 interaction.

As pDCs are the biggest (but not the only) IFN producers, and as they are PDCA-1 positive, systemic distribution of an α-PDCA-1 antibody was used to deplete them *in vivo* with the aim to bring down IFN production. This reduced IFN levels in 129 mice and their associated morbidity and mortality. However, this treatment poses some interpretation problems. Monocytes and alveolar macrophages have both been reported as important sources of IFN-α/β in influenza and other infections (Kumagai et al., 2007), (Barbalat et al., 2009), and they both upregulate PDCA-1 expression during infection. It is therefore impossible to determine with certainty the source of the increased IFN-α/β levels in these mice. It is in fact possible that all three cell types contribute to this phenotype, which could be imagined giving that pDCs produce a lot of it but only early on in infection, and that monocytes come in later and can differentiate into other potential sources of IFN. A study using a congenic mouse strain IFN-α6$^{gfp/+}$, where the GFP expression is controlled by the IFN-α6 promoter, addressed the source of IFN in another infection model: the respiratory syncytial virus (Goritzka et al., 2015). Using flow cytometry, high GFP (therefore IFN-α6) production was predominantly found not in pDCs, but in alveolar macrophages in the early stages of infection.

Ultimately, given that even *Ifnar1-/-* 129 mice are still slightly more susceptible than their *Ifnar1-/-* BL/6 controls, it is possible that not all the pathology is to be attributed to the mere excess of IFN, but also to cytokines, negative regulators, inflammation, TRAIL upregulation, or an entirely different factor. There could be another source of IFN production preceding the IFNAR cascade that is differentially regulated in the two mouse strains. A genetic difference between BL/6 and 129 mice could exist that could be at the origin of the dysregulation of IFN production, but possibly other mutations could explain the pathological inflammation signatures of this mouse strain. This hypothesis is explored as a central one in this thesis, and the progress in the quest for candidate genes is reported in the results chapters.

Studying excessive and prolonged IFN synthesis is clinically relevant, as IAV mutates rapidly past host defenses and current anti-viral treatments, and the currently available vaccines are not universal. It is therefore tempting to imagine a host-specific factor that could be targeted with a more stable treatment. Moreover, high IFN-α/β synthesis has been linked in humans to autoimmune disease, most importantly systemic lupus erythematosus. Uncovering the genetic origins of this

phenotype could be useful in treating this and other diseases where IFN was shown to have a potent pathological potential.

1.5 Innate immune recognition of PAMPs: events leading to IFN and cytokine synthesis

In this sub-chapter, the molecular mechanisms of signal transduction leading to IFN and cytokine production during different PAMP recognition events are addressed. While many protein factors participate in them, all of them seem to converge towards two distinct (albeit not independent) TF families: the IRF family (typically IRF3/7/9), or the NFκB family (a p50/p65 heterodimer or p65/p65 homodimer). IRFs are rather specialised in IFN transcription, whereas NFκB activates the transcription of many different cytokines and participate in IFN transcription as part of the IFN-β enhanceosome. These two transcription factor families differ in the DNA sequences they recognise and bind to. IRF transcription factors recognise PRDI and PRDIII domains within promoter sequences, whereas NFκB bind to PRDII and PRDIV (Honda et al., 2006).

NFκB is a family of proteins which, depending on the stimulus perceived, induce the expression of different sets of cytokines by differential assembly of subunit proteins to induce “canonical” or “non-canonical” NFκB signaling. The proteins that take part in the canonical NFκB signaling are p50 and p65 (also called RelA), which can form p50:p65 heterodimers, or p65:p65 homodimers (Li and Verma, 2002). Of the two proteins, p65 is the one with DNA-binding properties and it is the one that acts as a transcription factor upon activation after IκB ubiquitination and degradation (Kanarek and Ben-Neriah, 2012), (Li and Verma, 2002). In fact, REL-A (p65) has been shown to sustain a constitutive low-level expression of IFNβ1 in murine embryonic fibroblasts (Basagoudanavar et al., 2011). Meanwhile, non-canonical signaling is mediated mostly by the p52:RelB association. Given the variety of the signals transduced towards NFκB activation, different mechanisms have been proposed to be at the origin of stimulus-specific cytokine production. A study demonstrated that in spite of different TLR stimulations, REL-A DNA binding sites remained conserved (Borghini et al., 2018), but the modulation of IKK negative

regulation of NFκB was proposed to explain the differences in temporal transcriptional control (Werner et al., 2005), (Hoffmann et al., 2002).

1.5.1 Membrane-bound receptors in mice: TLRs

Toll like receptor family includes membrane-bound receptors localised at the plasma membrane or at the endosomal inner membranes. They detect bacterial and viral PAMPs and induce signaling cascades downstream of them leading to interferon (via IRFs/NFκB) and cytokine (NFκB-mediated) production.

1.5.1.1 Plasma membrane-bound TLR4 and TLR2

TLR4 is a PRR specialised in detecting PAMPs in the form of lipopolysaccharides (LPS) on the membrane of Gram-negative bacteria or RSV fusion protein on the viral envelope (Akira et al., 2006). LPS is also used in a purified form as an *in vitro* and *in vivo* agonist, to induce macrophage-mediated production of IFN-β and pro-inflammatory cytokines such as IL-1β, IL-6 and TNF-α. TLR4-mediated signaling has two branches: one mediated by the nearly ubiquitous MyD88 adapter leading to the production of pro-inflammatory cytokines, and another via TRIF/TRAF3 and TRAM, leading to IFN-β production (Akira et al., 2006), (Kagan et al., 2008).

In the molecular events leading up to NFκB activation, the binding of LPS to TLR4 recruits MyD88 and TIRAP adaptors to the TLR4 at the membrane (Figure 1.1). Following Myd88 recruitment, a complex is formed between IRAK1/2, IRAK4 and TRAF6 proteins, whereupon TRAF6, an E3 ubiquitin-ligase, can auto-ubiquitinate, resulting in the activation of TAB2, TAB3 and TAK1. This leads to the phosphorylation of NEMO and the recruitment and activation of an IKK protein complex (-γ, -α, -β), followed by the phosphorylation and degradation of IκB. This is a central signaling event that dissociates the NFκB complex, leading to the phosphorylation of p65 NFκB subunit and its translocation into the nucleus along with its adaptor protein p50. In human primary macrophage responses to LPS TLR4 stimulation (as well as TLR2 agonist Pam_3CSK), NFκB RelA (p65) subunit translocation into the nucleus was demonstrated by imaging assays (Noursadeghi et al., 2008). Parallel to the NEMO-regulated branch, TAK1 can also activate MAP-

kinases, including p38 and JNK, for sustained pro-inflammatory cytokine production via the AP-1 transcription factor (Akira et al., 2006), (Takeuchi and Akira, 2010).

On the other hand, LPS binding to TLR4 can also induce its translocation to the endosome along with the adaptor TRAM (Kawai et al., 2001), (Takeuchi and Akira, 2010). Following TRAM recruitment, and via TRIF, activation of TRAF3 leads to the NAP-1 and SINTBAD-mediated activation of TBK1 and IKK-ε. The two regulate the phosphorylation of the Ct domain of IRF3, which then forms homodimers and translocates into the nucleus to induce IFN transcription (Kawai and Akira, 2007). Aside from this part of the pathway, a recruitment of TRAF6/RIP-1 marks a branching-out of TRAM-mediated signaling which joins the TAK1-mediated cascade of NFκB activation.

TLR2 is a cell membrane surface TLR, specialising in the recognition of Gram positive bacteria-associated PAMPs (Figure 1.1). Its downstream signaling is largely shared with a TLR4 branch of MyD88/TIRAP-mediated signaling via IRAK and TRAF6 (Takeuchi and Akira, 2010). Ultimately, the resulting NFκB activation induces the production of pro-inflammatory cytokines.

1.5.1.2 TLRs at the endosomal membranes: TLR3, TLR7, TLR9

TLR3 is specialised in recognizing double-stranded viral RNA specifically in the endosome, and is the only TLR that does not rely on the MyD88 adaptor. It has been implicated in IAV recognition in epithelial cells and IAV-induced pneumonia via the activation of pro-inflammatory cytokine production (Wu et al., 2015), (Le Goffic et al., 2006), (Le Goffic et al., 2007). The classical agonist of TLR3 is a dsRNA molecule called poly(I:C) (Zhou et al., 2013). The TLR3 pathway shares the TRIF/TRAF3 and TRAF6-RIP-1 signaling branches with the TLR4 pathway. Respectively, these result in IRF3 phosphorylation and *Ifn*-β transcription (Doyle et al., 2002), and NFκB-mediated pro-inflammatory cytokine production (Kawai and Akira, 2007) (Figure 1.1).

TLR7 is expressed mainly by pDCs, detecting ssRNA genomes of IAV and other viruses in the endosome (Lee et al., 2003). However, even a simple poly:U molecule (TLR7 agonist) (Diebold et al., 2004), or even cellular mRNA or siRNA (Hornung et al., 2005) can trigger TLR7 activation and *Ifn*-α production in pDCs. Generally, presence of uridine ribonucleotides in the RNA stimulus of TLR7 seems

to trigger the signaling downstream of this receptor (Diebold et al., 2006). Unlike for TLR3, MyD88 is crucial in the TLR7-mediated IFN production, binding IRAK1, IRAK4, IKKα and TRAF6 into a complex recognised along with IRF7 (Kawai et al., 2004), (Uematsu et al., 2005), (Hoshino et al., 2006), (Kawai and Akira, 2007). IRF7 is phosphorylated by IKKα and IRAK1, upon which it dimerises, translocates to the nucleus, and initiates *Ifn*-α/β transcription. While IRF3 is also an *Ifn* TF, it is entirely dispensable in pDC-mediated recognition of PAMPs, and pDCs are crucially dependent on IRF7 for TLR7/9 mediated IFN production. Moreover, in an overlapping pathway with TLR4 and late-phase TLR3 signaling, TRAF6 can recruit TAK1, resulting in the phosphorylation of MAPK such as JNK and p38 downstream, activating AP-1 mediated transcription of inflammatory cytokines. Alternatively, TAK1 also activates NEMO/IKKα/IKKβ proteins to lead to p50:p65-mediated cytokine production (Figure 1.1).

TLR9, expressed by pDCs and cDCs, mediates viral and bacterial DNA recognition in the endosomal compartment. Its hallmark agonist are synthetic oligodeoxynucleotides (ODNs) bearing unmethylated CpG motifs, recognised as PAMPs by the host cell. The most widely used ODN classes are CpG-A and CpG-B, both able to bind to TLR9 and induce signaling downstream. However, it was shown that CpG-A induces higher IFN-α production in pDCs compared to CpG-B because it is maintained in the endosomal vesicles bound to TLR9 for a longer time, activating MyD88-IRF7-mediated IFN production (Sasai et al., 2010), (Honda et al., 2005). CpG-B stimulated pDCs upregulate production of IL-8, IL-6 and IL12p40, indicating differences in the nature of the pathways induced (Kerkmann et al., 2003), (Engel and Barton, 2010). Cytokine production from TLR9 stimulation can be triggered via MAPK stimulation like in TLR7 or via the NFκB stimulation axis as previously described in the case of TLR7 (Figure 1.1).

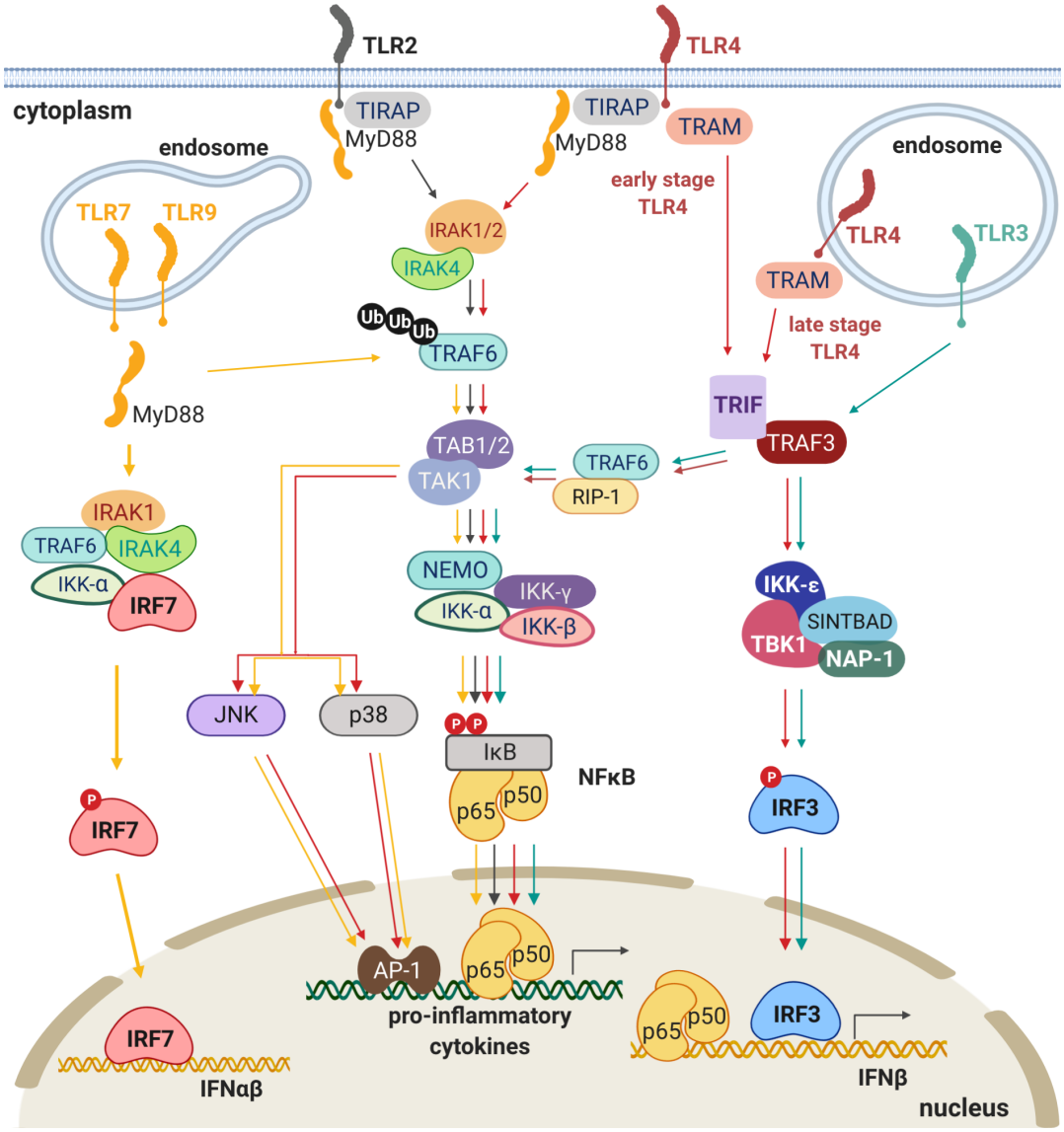

Figure 1.1 Intracellular pathways of Toll-like receptor activation in response to stimuli. TLR2 and TLR4 pathways (MyD88-dependent) from the cell membrane induce the activation of IRAK1/2/4 and TRAF6-mediated pathway, and via NEMO/IKKα/β/γ the activation of NFκB-mediated production of pro-inflammatory cytokines. Late-stage TLR4 signalling involves shuttling TLR4/TRAM complex to the endosome and TRIF/TRAF3-mediated TRAF6/NFκB or IKKε/TBK1/IRF3 signalling. TLR3 endosomal receptor activates a TRIF/TRAF3 cascade that induces the activation of TBK1/SINTBAD/NAP-1, in order to induce phosphorylation and nuclear translocation of the *Ifn*-β master TF, IRF3. Ultimately, TLR7 and TLR9 share the pathways of TRAF6/IRAK1/4-mediated IRF7 phosphorylation and *Ifn*-αβ production, and TRAF6/TAB/TABK1-mediated NFκB activation of pro-inflammatory cytokine production. Along with the TLR4 pathway, TLR7/9 signalling can lead to MAPK JNK and p38 activation from TAB1/2/TAK1 activation, and towards AP-1-mediated transcription. Red circles marked with "P" indicate phosphorylation events, and the arrows on the represented DNA represent transcriptional activation. The blue double line on the top of the figure is a simplified representation of the cell membrane. Created with Biorender.com, and exported under on a free trial on a premium plan.

1.5.2 Cytoplasmic receptors: RIG-I and the cGAS/STING system

1.5.2.1 Retinoic acid-inducible gene-I: RIG-I

RIG-I is a cytosolic sensor of RNA-related PAMPs. RIG-I recognises viral ssRNA genome in the cytosol, but it can also recognise other viral genome-related PAMPs (reviewed in (Goubau et al., 2013)). In the specific case of IAV, different patterns of its ssRNA genome can trigger RIG-I activation. RIG-I can recognise 5'ppp modifications on the IAV RNA (even 5'pp modifications, as shown by (Goubau et al., 2014)), whose substitution with hydroxyl groups was shown to abrogate RIG-I binding (Hornung et al., 2006), (Pichlmair et al., 2006), (Rehwinkel et al., 2010). Also, dsRNA was ultimately shown to be necessary for RIG-I recognition. In the case of IAV, the viral "panhandle" structure, a double-stranded blunt extremity formed by a 3'-5' end hybridisation in the RNA, is a RIG-I PAMP. This structure was shown to be indispensable for RIG-I recognition and signalling (Vela et al., 2012), (Schlee et al., 2009), (Schmidt et al., 2009), (Liu et al., 2015). In accordance with this, double-stranded synthetic RNA lacking any 5' modifications, poly(I:C), was shown to activate RIG-I signalling as well (Zeng et al., 2010). The most widely used RIG-I-specific synthetic agonist is 5'ppp dsRNA, which exploits both of the possible PAMPs recognised by the receptor and is a potent inducer of IFN-α/β *in vitro.*

During the virus replication cycle, its genome is exposed to the cytosol (albeit coated by NPs) at two occasions: immediately upon viral entry and membrane fusion, and after virus replication and cytoplasmic export. A study by (Killip et al., 2014) showed that viral RNA synthesis and nuclear export were both necessary for IRF3-mediated *Ifn*-β production in IAV recognition. Another study offered conclusive evidence that the IAV genome is recognised after viral replication. (Rehwinkel et al., 2010) demonstrated strong RIG-I-mediated IFN production upon recognition of viral genomes bound to the NS1 protein. NS1 is a non-structural viral protein produced only after a replication cycle of IAV, that serves to block IFN production in host cells (Garcia-Sastre et al., 1998), (Garcia-Sastre, 2011). IAV lacking NS1 are incapable of virus replication in presence of IFN (Garcia-Sastre et al., 1998). Therefore, because of the NS1 role and its binding to RIG-I, it has been suggested that initial recognition of incoming viral genomes was not the biggest contributor to IFN production (Rehwinkel et al., 2010). Moreover, as replication progresses, the shorter

viral RNA sequences that get exported into the cytosol were shown to be a good RIG-I agonist as well (Baum et al., 2010), (Rehwinkel et al., 2010). However, there is evidence to say that the initial recognition by RIG-I of incoming viruses has a role to play in innate immune IFN production as well, and that even nucleocapsid association to the viral genome can be a RIG-I PAMP (Collins et al., 2004), (Weber et al., 2013). In an interesting aside, it was proposed by (Rehwinkel et al., 2010) that to an extent, the latter findings could explain the initial discovery of IFN in 1957 by Isaacs and Lindenmann (Isaacs, 1957a). In this seminal article, IFN induction was reported in a setting of cell infection with heat-inactivated virus, which has lost its ability to replicate. This could mean that the interfering molecule that was published came from RIG-I recognition of nucleocapsid-associated genome of the incoming virus.

The signalling cascade downstream of RIG-I (similarly to MDA5, its homologue, which recognises viruses other than IAV) begins with the activation and oligomerisation of the mitochondria-bound adaptor MAVS. Next TRAF3, TBK1 and IKKε kinases are activated (Takeuchi and Akira, 2010), (Goubau et al., 2013), (Kell and Gale, 2015). TBK1 activation by phosphorylation is a signal for its retention in the cytoplasm, which liberates IRF3 from the complex and allows its phosphorylation, nuclear translocation and induction of IFNs in cooperation with phosphorylated IRF7. In addition, the NFκB pathway is activated during RIG-I stimulation, via the IKKα/IKKβ axis, resulting in p50:RelA activation and cytokine production (Figure 1.2).

1.5.2.2 cGAS/STING receptor cascade

Another surveillance system in the cytoplasm, distinct from the RIG-I receptor family, is the cGAS/STING second messenger-driven signaling pathway. Employed by DCs and macrophages in recognising dsDNA in the cytosol, it results in the initiation of IFN-α/β and cytokine production. Aside from double-stranded bacterial/viral DNA, it is also capable of recognising self-DNA exposed from damaged mitochondria or the engulfed dead cells. It is also a key receptor for retrovirus recognition, HIV included (Gao et al., 2013). cGAS (cyclic GMP-AMP synthase) catalyses the synthesis, from ATP and GTP, of the second messenger cyclic GMP-AMP (cGAMP for short) (Cai et al., 2014). This is done in a DNA-dependent manner, as shown by DNAse-I treatment in purified cGAS extracts in the

presence of DNA (Sun et al., 2013). The cGAMP that is synthetised contains two phospho-diester bonds: one between 2'OH on GMP and 5'phosphate on AMP, and the second between 3'OH on AMP and 5'phosphate on GMP. Thus, the resulting cGAMP isomer is called 2'3' cGAMP (Figure 1.2). The synthetic version 2'3' cGAMP can be exogenously transfected into cells as a direct means of activating this pathway. 2'3' cGAMP binds to the STING receptor on the ER and induces its activation and translocation to the Golgi (Ishikawa and Barber, 2008). During this process, activated STING recruits TBK1 and IKK kinases, which phosphorylate IRF3 and IκB (the inhibitor of NFκB proteins), respectively (Fang et al., 2017). The released NFκB proteins on the one side, and the phosphorylated IRF3 dimers on the other, translocate to the nucleus and cooperate in initiating the transcription of *Ifn*-β, *Il*-6, *Il*-1β, *Tnf* and other cytokines (Chen et al., 2016).

An IRF3-dependent transcription of a subset antiviral ISGs against different DNA viruses was demonstrated in the absence of IFNAR cascade in *Stat1-/-* fibroblasts (Schoggins et al., 2014). The same study demonstrated that cGAS/STING-lacking mice were susceptible to infection with RNA viruses, indicating possibly that STING is involved in recognising DNA from damaged cells *in vivo.*

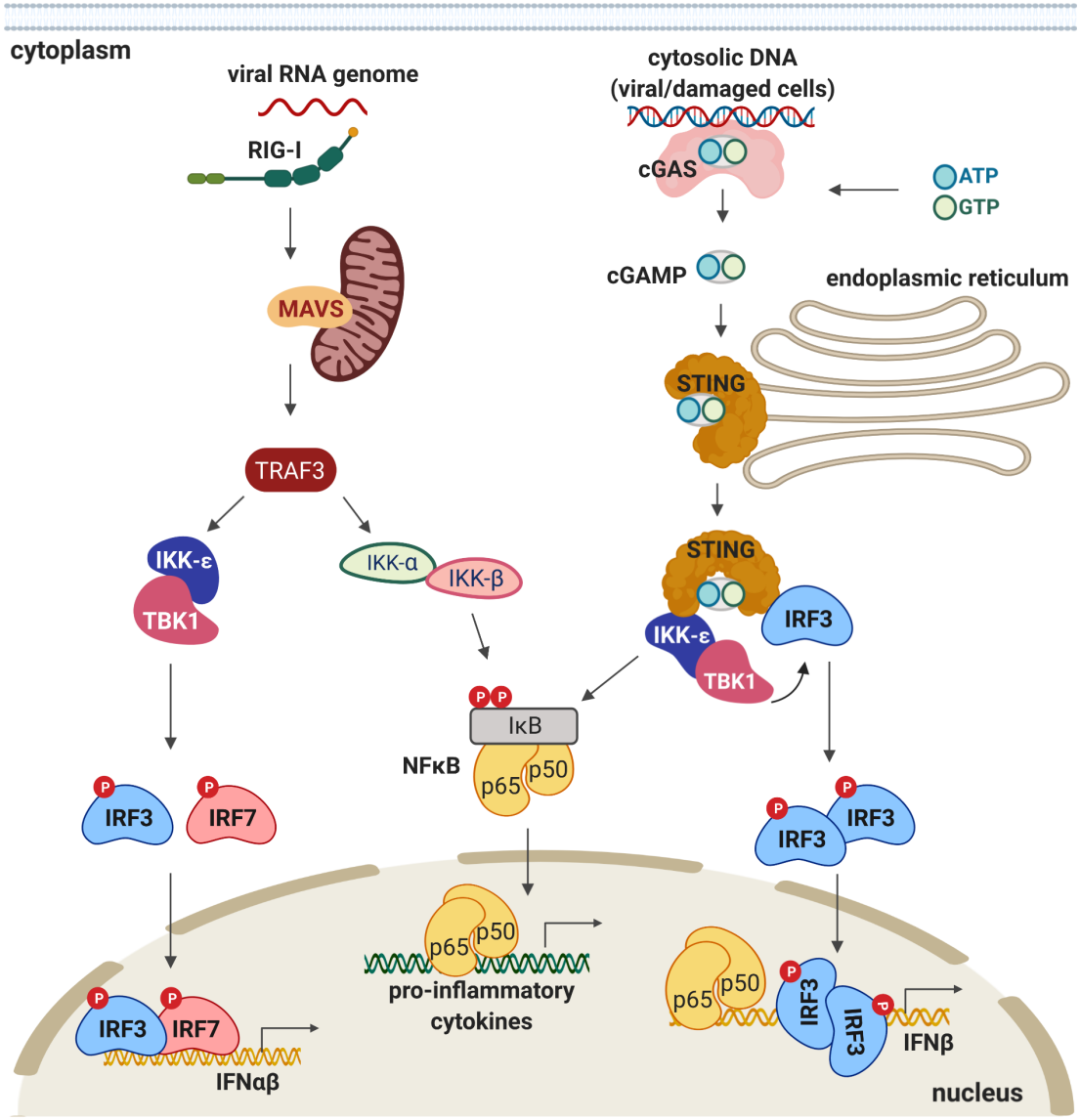

Figure 1.2 Cytosolic PAMP recognition RIG-I and STING/cGAS cascades. RIG-I activation induces activation of MAVs on mitochondria, and TRAF3-mediated activation of two separate signalling branches. One, via TBK1 and IKKε, mediates the IRF3 and IRF7 phosphorylation and *Ifn*-α/β transcription, whereas the other, IKKα/β-mediated branch induces the phosphorylation of IκB, dissociation from NFκB p50:p65 subunits, and the translocation of NFκB to the nucleus to induce the production of pro-inflammatory cytokines. STING is a receptor on the endoplasmic reticulum, activated by the second messenger cGAMP produced by cGAS from ATP and GTP. STING binds both IKKε/TBK1 and IRF3, the latter of which is phosphorylated as a result, and dimerises to translocate to the nucleus and induce *Ifn*-β transcription. IKKε/TBK1 activation in this cascade induce the NFκB activation and pro-inflammatory cytokine production as well. Red circles marked with "P" indicate phosphorylation events, and the arrows on the represented DNA represent transcriptional activation. The blue double line on the top of the figure is a simplified representation of the cell membrane. Created with Biorender.com, and exported under on a free trial on a premium plan.

1.5.3 The IFNAR cascade

One of the main effects of the aforementioned TLR and RLR pathway activation is mediated through the signaling of IFN-α/β. The main explanation for such far-reaching impact of IFN-α/β is that their corresponding dimeric receptor IFNAR (IFNAR1 and IFNAR2 subunits) is expressed on almost all cells in the organism, who respond to IFN cues in different ways.

Different signaling pathways can be triggered downstream of IFNAR upon IFN-α/β binding. On the cytoplasmic side of the IFNAR transmembrane receptor, the Ct tails of IFNAR1 and IFNAR2 subunits are bound to TYK2 and JAK1, respectively. IFN-α/β binding to the receptor induces tyrosine phosphorylation of both protein adaptors and triggers different signaling cascades downstream, composed mainly of proteins of the STAT family (Figure 1.3).

In the most classical IFNAR pathway, JAK1 phosphorylation induces the formation of the ISGF3 transcription factor complex, composed of p-STAT1, p-STAT2 and IRF9, which translocates to the nucleus and binds ISRE motifs in target gene promoters to induce their transcription (Makris et al., 2017). Typical targets containing ISRE motifs are *Ifn*-α/β themselves and a big subset of ISGs including but not limited to *Isg-15*, *Irf7* and *Ip-10*. Different STAT proteins can form different combinations of homodimers or heterodimers and translocate to the nucleus to bind IFN-γ-activated sites (GAS) on the DNA. Depending on which homo/heterodimer started the transcription, different ISGs gene expression can be induced (including *Irf1*, *Irf2*, *Irf8/9* and others) (Platanias, 2005). Generally speaking, ISG promoters contain ISRE or GAS sequences or both, allowing for a great plasticity in terms of responses downstream of IFNAR (Schoggins and Rice, 2011). IFNAR receptors can also signal via MAPKs such as p38 and JNK, by activating different transcription factors like FOS and ELK1 and JUN and ATF2 respectively (Figure 1.3). They in turn promote the production of GAS sequence containing-targets including inflammatory cytokines, pro-apoptotic effectors and generally anti-viral proteins. Ultimately, the IFNAR signaling can also activate the PI3K-dependent pathway via phosphorylation of AKT1 and CREB to mediate production of SMAD-binding element (SBE)-containing genes which modulate inflammatory responses and survival. Finally, an mTOR pathway can also be activated downstream of PI3K, via the mTOR-mediated phosphorylation of the eukaryotic translation initiation factor 4E-binding protein 1

(4EBP1) and its release of EIF4E, which allows cap-dependent mRNA translation in target cells (Platanias, 2005), (Hervas-Stubbs et al., 2011).

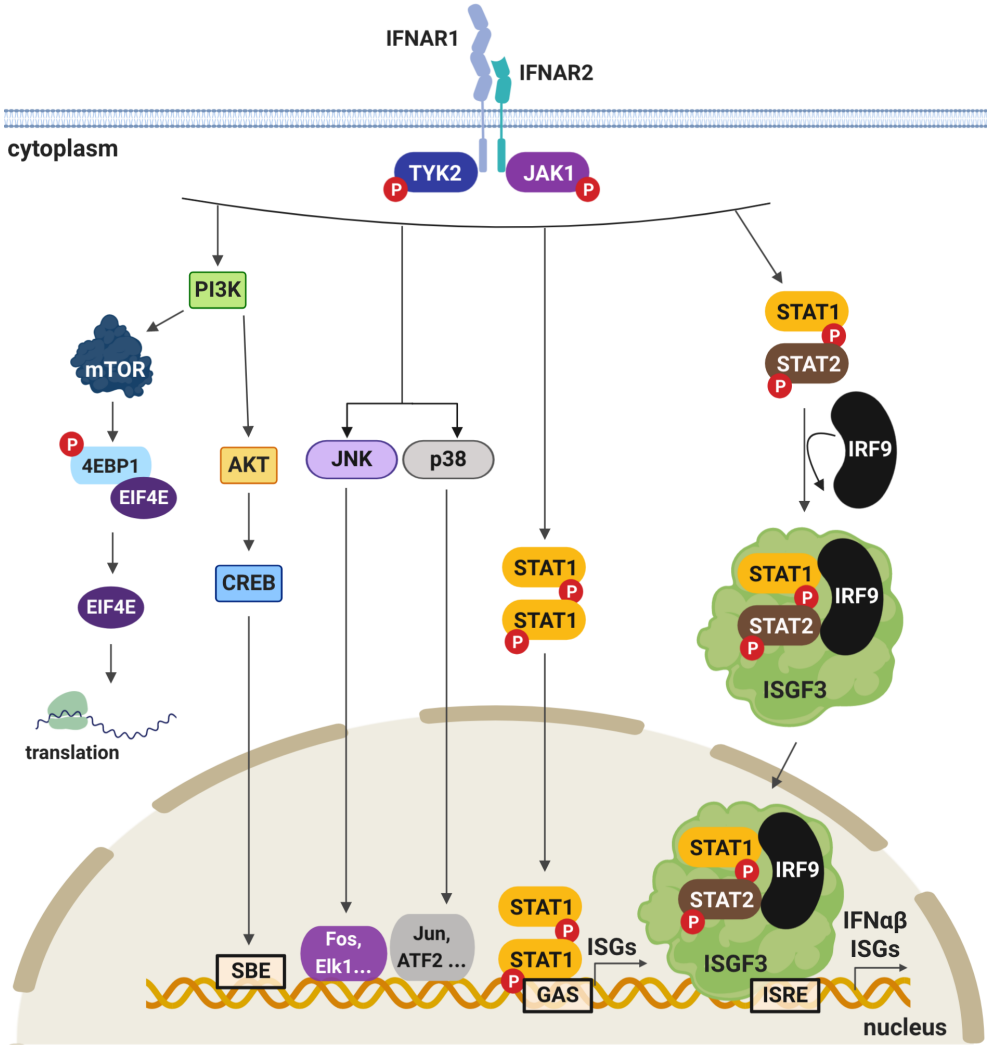

Figure 1.3 IFNAR-dependent pathways. Binding of IFN to the IFNAR receptor subunits leads to the activation of different sets of pathways downstream, all dependent on the phosphorylation of TYK2 and JAK1. The canonical pathway: phosphorylation and dimerisation of STAT1 and STAT2, binding to IRF9 and formation of the TF complex ISGF3 that binds to ISRE-element containing promoter sequences of ISGs, IFNs and other genes. Another pathway involves homodimerization of phosphorylated STAT1 and its binding in the nucleus of GAS-sequence containing promoter sequences of some ISGs. Thirdly, IFNAR activation can activate a MAPK pathway involving JNK and p38 activation for FOS/ELK1 or JUN/ATF2 – mediated transcription, respectively. More TFs are involved in the outcome of this pathway branch but they are not detailed in this work. Ultimately, IFNAR1/2 can also activate a PI3K-dependent pathway involving mTOR-mediated activation of translation via EIF4E, or AKT and CREB-mediated transcription of SBE-motif containing targets. Red circles marked with "P" indicate phosphorylation events, and the arrows on the represented DNA represent transcriptional activation. The blue double line on the top of the figure is a simplified representation of the cell

membrane. Created with Biorender.com, and exported under on a free trial on a premium plan.

1.6 Genetic determinants of influenza susceptibility

Studying host determinants of influenza outcome in humans is a complex task, not least so because influenza is such a common seasonal disease and that influenza symptoms are often confused with those of other respiratory diseases. Only very severe cases ever reach hospitalization stages, and at that point it is usually already quite late in infection to investigate the root of the problem. Humans as a population are much more genetically variable than inbred mice, and are constantly exposed to other microbes and different influenza strains that can, by means of pre-existing immunity, influence their susceptibility to a certain influenza strain. For these reasons, clean-environment-housed and inbred laboratory mice are not the best model for determining genetic bases of susceptibility to human disease. This is also why QTL studies are considerably more informative in humans. However, in infections, the molecular determinants of immune defenses are often induced by infection itself, and the factors that can influence the outcome are tightly interwoven in their functions, which renders QTL-type studies more complex. Nevertheless, some genetic factors that influence IAV susceptibility in humans and in mice have been uncovered.

1.6.1 Humans

While the *MxA* human homologue gene of the murine *Mx1* has not been shown to replicate *Mx1* efficiency *in vivo* (Pavlovic et al., 1995), the ISG IFITM3 has been associated with influenza clearance in humans (Everitt et al., 2012). A SNP had been identified in humans linking the *rs12252* allele of the gene to increased susceptibility to severe influenza in Chinese individuals (Ciancanelli et al., 2016), (Zhang et al., 2013), (Yang et al., 2015), but was refuted by a study involving more than 5000 controls with mild influenza that found no association with severe, but only with mild disease (Mills et al., 2014). Generally, GWAS studies in humans identified no reproducible single factor for influenza susceptibility, however they are often inherently flawed due to sample size, virus strain variability and reproducibility (Horby et al., 2013), (Ciancanelli et al., 2016). In an anecdotal study, a child with life-

threatening influenza was found to have an inborn IRF7 deficiency failing to upregulate type-I and type-III IFN responses (Ciancanelli et al., 2015).

In an effort to counteract the issues posed by the system of finding QTL determinants of disease, two very elegant and thorough, complementary *in vitro* studies identified *cis*- and *trans*- acting QTLs in responses to infections and stimuli. Firstly, a study by (Lee et al., 2014) carried out on 560 individuals used monocyte-derived DCs stimulated with LPS or IFN-β *in vitro* to unpick gene x environment interactions affecting QTL identification. By using the stimulation results in the form of mRNA expression and by leveraging large human datasets such as ENCODE and 1000 genomes project, they identified 121 loci, of which 35 were previously associated with autoimmune or infectious diseases in GWAS studies. Among the most important cis-QTLs, they uncovered polymorphisms in IFNAR1/2, as well as IRF7. Interestingly, they found that IRF7 acted as both a cis- and trans- eQTL in their system due to the IFNAR-mediated action of its target IFN-α/β. These findings clearly underlined the complexity of thorough genetic studies in infection models. The second work, published by (Fairfax et al., 2014), resorted to a similar approach in analysing primary human monocytes exposed to LPS or IFN-γ *in vitro* from 228 individuals. While identifying eQTLs in inducible and cis acting factors including *Il6, Traf6 and Socs1,* this study also uncovered that cis-QTLs in *Ifn-β* and *Irf2* rapidly acquire trans-acting network effects in stimulation. Firstly, both these studies confirmed the impact of the IFN network on responses to infection and stimulations in immune cell systems *in vitro.* Moreover, they pointed to the importance of addressing effectors upstream of major immune response regulators such as IFNs and IRFs, in order to uncover the genetic drivers of the observed variation.

1.6.2 Mice

As mentioned previously in this thesis, mice are not natural hosts to influenza due to the expression of the ISG *Mx1* gene that limits viral replication in the nucleus (Tumpey et al., 2007). While the inbred laboratory strains are susceptible to influenza disease due to the ablation of Mx1, susceptibility of different mouse strains can differ. DBA mice are known to be high responders in influenza infection, with a higher production of CCL2 and TNFα pro-inflammatory cytokines than the widely used BL/6 mice (Boon et al., 2009). The 129 mouse strain was identified as more susceptible

to H3N2 and H5N1 mouse-adapted influenza disease in a study by (Davidson et al., 2014). This phenotype was linked to increased IFN-α/β production and a cytokine storm occurring in these mice, as previously described in this thesis.

However, as laboratory mouse strains are highly inbred, in order to address possible genetic variability in the face of infections and in other disease models, a collaborative cross of mice was created (Collaborative Cross, 2012). Namely, 8 parental strains (A/J, C57BL/6J, 129S1/SvImJ, NOD/ShiLtJ, NZO/HiLtJ, CAST/EiJ, PWK/PhJ and WSB/EiJ) were crossed two by two for two generations and then the F2 offspring interbred and backcrossed to produce and stabilize genetic variability after 23 generations. This model is now widely used for studies of QTLs affecting disease outcomes.

In influenza infection, collaborative cross studies pointed to a set of genes connected to disease susceptibility: *Grap2, Nox4 and Il16,* which were not previously found in the context of influenza infection (Ferris et al., 2013). It is worth noting that *Mx1* was also identified in the same study. More importantly, concordant studies of the collaborative cross found, instead of a single association genotype-phenotype, a gradient of susceptibility clearly indicating that the susceptibility to H5N1 (Boon et al., 2009), H1N1 (Bottomly et al., 2012) and H3N2 (Boivin et al., 2012) in mice is not a single-gene locus but a mixed effect of multiple genes or loci (reviewed in (Horby et al., 2013)). The ensuing validation studies of H5N1 infection in the collaborative cross found differential viral load in the infected mice as well (Boon et al., 2011). Ultimately, using the collaborative cross, a genetic locus comprising of genes *Samd9l, Ica1* and *Slc25a13* was linked to CCL2, IFN-α and TNF-α production *in vivo*, but a KO mouse model of *Slc25a13* did not validate these findings (Boon et al., 2014). Along with the demonstration that cytokine production in the 66 analysed mouse strains is a phenotypic continuum, it further confirmed that multiple genes are involved in the influenza susceptibility phenotype, but brought no conclusive solution. It is possible that the lack of differences in CCL2 production in the *Slc25a13*$^{-/-}$ mice was due to the absence of the compound effect brought by other genes.

Importantly, three genetic loci governing pDC numbers *in vivo* were uncovered in murine chromosome 7, with the dominant one containing the gene *Flt3l,* encoding Flt3L protein crucial in pDC development and differentiation (Pelletier et al., 2012). Importantly, it was shown in the same study that IFN-α production capacities of pDCs were not influenced by this locus. In light of the (Davidson et al.,

2014) study, where the influenza susceptible 129 mice showed increased pDC numbers in the lung throughout the infection, and given that (Wolf et al., 2009) and others suggested that pDCs are dispensable during IAV infection, it is imaginable that IFN-dependent pathogenic potential is due to an increased numbers of pDCs in the lung. However, (Davidson et al., 2014) showed that per pDC IFN-α/β production was also higher in the susceptible mice, indicating that the origin of high IFN responses is to be sought in signaling pathways upstream of IFN production.

1.7 Origins of increased IFN-α/β production and genetic susceptibility to influenza in mice: the working hypothesis of this thesis

Based on the findings from (Davidson et al., 2014), a hypothesis about 129 strain-specific genetic determinants governing high IFN-α/β production and hence IAV susceptibility was developed. Moreover, unpublished work from S. Davidson indicated an intermediate IFN-α/β production in F1 mice from C57BL/6 and 129S8 crosses, with F2 offspring showing a distribution of IFN-α/β levels between the two extremes. Based on these findings, we hypothesised that the quantitative phenotype of high IFN-α/β responses in 129 mice could be governed by a multigenic genetic trait. More precisely, these genotype-phenotype signatures indicated a possible QTL-driven IFN-α/β phenotype in 129 mice.

Laboratory models of mice are highly inbred and laboratory crosses produce offspring that offers low genetic mapping resolution, rendering classical QTL and GWAS studies challenging (Hunter and Crawford, 2008). In order to tackle a high-resolution genotype-phenotype linkage analysis on a quantitative phenotype such as IFN-α/β levels in infection, high numbers of mice would be necessary (Ishikawa, 2017), limiting processing speed and comparability between samples.

To avoid this problem, a literature search was carried out to identify possible candidate genetic regions that could reduce the search scope for the genetic origins of high IFN-α/β production in influenza infection. A candidate genetic region was identified on Chromosome 3 based on the findings of Fiona Powrie and her team in a model of *H.hepaticus*-induced colitis disease (Boulard et al., 2012). In this model, much like in influenza infection, the 129S6 mouse strain exhibited high disease

morbidity and inflammation compared to the BL/6 control strain. Interestingly, this susceptibility could be rescued by introducing a congenic Chromosome 3 BL/6 locus of 1.7Mb into the 129S6 background (Boulard et al., 2012). This locus, named *Hiccs* (or R17), as part of the congenic 129 mouse strain (129.C3BR17), was examined for its impact on IFN-α/β production and influenza susceptibility in this thesis. More details on the *Hiccs* locus and its components are cited in the Introduction to Chapter 4 of this thesis.

Based on the work from (Boulard et al., 2012) and the results from this thesis, *Alpk1* was chosen as a candidate gene from the R17 locus to examine its role on influenza susceptibility and the intensity of the IFN-α/β response. *Alpk1* encodes an α-protein kinase with a role in gout inflammation and innate immune responses to bacteria (Zimmermann et al., 2017), (Garcia-Weber et al., 2018, Milivojevic et al., 2017, Ryzhakov et al., 2018), but no recognised role in influenza infection. In this thesis, the role of ALPK1 was examined in influenza innate immune responses, and one of its putative phosphorylation targets, the protein WWC2, investigated in the context of infection. The R17 locus, as well as ALPK1 and WWC2 proteins will be described more in detail in Chapters 4, 5 and 6 of this thesis, respectively.

Chapter 2. Materials & Methods

2.1 Mice and infections

All in vivo experiments were performed using mice of 8-12 weeks of age, of both genders, with keeping sex ratios and age as close as possible between genotypes. Mice used in this thesis (C57BL/6, 129S6, 129S7, 129S8, C57BL/6$^{Ifnar1-/-}$, 129S7$^{Ifnar1-/-}$) were bred at the MRC-National Institute for Medical Research (NIMR) in Mill Hill (2015-2016), and in the Francis Crick Institute (2016-2019) in specific pathogen free conditions. All mouse experiments were carried out under the project licence 70/7643 (NIMR) and P9C468066 (Francis Crick Institute). The congenic 129.C3BR17 mouse line, a kind gift from Dr Fiona Powrie (The Kennedy Institute of Rheumatology, Oxford, UK), was created on the 129S7 background and maintained as a homozygous line (Boulard et al., 2012). The *Alpk1* homozygous knock-out line was created by exon 10 deletion on a C57BL/6 background and was obtained from the Sanger Institute.

Light anaesthesia (3% isoflurane by inhalation) was administered to mice to be infected with the egg-derived influenza X31 virus (see preparation below). The virus was diluted in PBS (phosphate buffered saline), and given as 30μl intranasally. Mice were infected at 10-12 weeks of age with the indicated doses of X31 (in the morning between 9am and 12pm).

2.2 Influenza virus preparation

2.2.1 Egg-derived X31 influenza virus

The virus strain used for all the in vivo infections in this thesis was X31 (H3N2 A/Hong Kong/X31/68). X31 virus is a reassorted virus of the A/PR/8/34 backbone (H1N1, in short PR8, also used in this thesis), with HA and NA from the H3N2 strain. It was kindly gifted to our team by Dr John Skehel and Dr John McCauley (The Francis Crick Institute). X31 virus used for in vivo infections was grown in the allantoic cavity of 10-day embryonated hen's eggs. The final viral titer, expressed as 50% tissue culture infective dose ($TCID_{50}$), was calculated using the Spearman-Karber method by titration on confluent monolayers of Madin-Darby Canine Kidney (MDCK) cells. Cellular lysis was observed after 3 days. After confirming that the viral preparation was free of bacterial, mycoplasma and endotoxin contamination, it was aliquoted and stored at -80°C.

2.2.2 MDCK-derived X31 influenza virus

MDCK cells were grown to 80% confluence and their growth media replaced in the moment of infection with MEM/1% PSG/TPCK-trypsin (1:4000). The cells were infected with the egg-derived X31 virus at multiplicity of infection (MOI) of 1. At 24, 48 and 72h the supernatant was collected, and virus concentrated by ultracentrifugation (Beckman centrifuge, SW40 tubes) at 28000 rpm for 4 hours at 4°C through a cushion of 20%(w/v) sucrose solution. The viral pellet was resuspended in complete cell growth medium and virus titrated in the $TCID_{50}$ dose.

2.2.3 Monitoring of infection and clinical endpoints

The starting weights of the mice were recorded, and their weight loss monitored daily at 24h intervals after the infection time. The pre-defined clinical endpoint for this protocol was set at 80% of the starting weight unless otherwise indicated.

2.3 Collecting BAL and processing lungs into single-cell suspensions

Mice were sacrificed at 2,4,6, or 7 days post-infection by intra-peritoneal lethal injection of 600mg/kg Pentobarbital + 16mg/kg Mepivacaine, followed by confirmation by exsanguination by severing the femoral artery. The lungs were flushed with 500µl PBS. BAL was centrifuged at 1400rpm for 5min at 4°C, and the supernatants collected and stored at -80°C. The supernatants were analysed by ELISA for cytokines using established protocols (see below).

Whole lungs were collected in gentleMACS (Miltenyi) C-tubes in 5ml AB IMDM and homogenised according to manufacturer's instructions. Lungs were digested with 20µg/ml Liberase TL (Roche) and 50µg/ml DNAse-1 (Sigma) for 30min at 37°C, then homogenised further in the gentleMACS tubes and strained through a 70µm filter. Red blood cells were lysed using 5ml of 0.83% ammonium chloride, and the remaining cells washed with PBS prior to FACS staining.

Spleens were collected in 5ml AB-IMDM and homogenised by straining through a 70µm filter. Red blood cells were lysed in 5ml 0.83% ammonium chloride, and the remaining cells washed with PBS.

2.4 Staining cells for flow cytometry

Lung cells were stained in a mix of PBS anti-FCγRIII/II (FC block) and the relevant antibodies (cited in Table 1) for 1h at 4°C. After a wash in PBS, the cells were fixed using a 4% paraformaldehyde (PFA, Fisher Scientific) solution in PBS for 40min at room temperature, then washed twice with PBS. All flow cytometry experiments were carried out on an LSR Fortessa (BD) and the subsequent analyses performed on the FlowJo software (Treestar).

2.5 Determination of viral titers in the infected lungs and RT-qPCR

Whole lung fragments were harvested in 2.5mL RNAlater® (Applied Biosystems), incubated overnight at 4°C and then kept at -80°C prior to processing. Lung fragments were transferred into 3ml of RLT buffer (RNAeasy MiniKit, Qiagen) with β-mercaptoethanol (Sigma) and homogenized in a Kinematica Polytron 10-35 homogeniser. 600µl of lung homogenate was used for RNA extraction using the RNeasy MiniKit (Qiagen) according to manufacturer's protocol, and included an on-column DNA digestion. RNA quantification was performed on a ND-1000 Spectrophotometer (NanoDrop Technologies) and levels of RNA normalized prior to cDNA synthesis. cDNA was generated using the PCRBIO RT-PCR kit (PCR Biosystems) according to manufacturer's instructions. Quantification of cDNA targets was performed on an Applied Biosystems Quantstudio 3 RT-qPCR machine with 1x qPCRBIO Probe Mix LO-ROX (PCR Biosystems) and 1x Taqman primers (list in Table 3). Results are represented as ΔCt and represent values relative to the expression of the housekeeping gene HPRT.

2.6 Quantification of cytokines

To quantify proteins in the airways, BAL was harvested as previously cited and 50µl of supernatant used for cytokine analyses by ELISA. The concentration of IL-6 was measured using enzyme-linked immunosorbent assay (ELISA) mouse eBioscience Ready-Set-Go® kits, following manufacturer's protocol. The results were read at 450nm (signal) and 540nm (noise) wavelengths on a Safire II plate reader (Tecan). The IFN-α/β 2-Plex Mouse ProcartaPlex® Panel kit (eBioscience) was used to determine levels of type-I IFN in the BAL according to manufacturer's instructions, and results read on a Luminex 100 machine (BioRad). Similarly, the Cytokine and Chemokine 36-plex Mouse ProcartaPlex® Panel kit (eBioscience) was used to determine the concentrations of 36 different cytokines in the BAL (GM-CSF, IFN-λ, IL-1β, IL-12p70, IL-13, IL-18, IL-2, IL-4, IL-5, IL-6, TNFα, ENA-78, G-CSF, IFN-α, IL-1α, IL-15/IL15R, IL-28, IL-3, IL-31, LIF, M-CSF, IL-10, IL-17A, IL-22, IL-23, IL-27, IL-

9, Eotaxin, GROα, IP-10, MCP-1, MCP-3, MIP-1α, MIP-1β, MIP-2, RANTES) and the results were read using a Luminex 100 machine (BioRad).

2.7 Generation and stimulation of bone-marrow derived cells

Male mice of the indicated genotypes were sacrificed at 6-12 weeks of age and their femurs and tibiae were collected into AB-IMDM. Bones were cleaned of muscle and tissue and bone marrow was collected by centrifugation. Cell suspensions were strained through a 70µm filter and resuspended in 6ml cell culture media (RPMI Lonza, 10% FCS, Penicillin, Streptomycin, L-Glutamine, β-mercaptoethanol 50µM, HEPES 10mM (Gibco), Sodium pyruvate 1mM (Sigma Aldrich)) supplemented with 20% L-cell media containing M-CSF. 1ml of the cell suspension was added to 20ml of the same culture media in a 15cm Petri dish, and 6 dishes per mouse were kept in culture for 7 days. Cultures were replenished with 20ml fresh complete cell media with 20% L-cell medium at day 4. Adherent cells were washed with PBS and incubated in PBS 2% FCS and 2mM EDTA for 10min at 4°C to detach them from the dish. Differentiation was verified by preparing the suspension of adherent cells for flow cytometry staining as per previously described protocol and using antibodies in Table 1. This culture fraction was found to contain 90% BMDMs, defined as FSC high, SSC high, F4/80+ CD11b+. The remaining adherent cells were then plated, in complete RPMI medium without L-cell supplement at $2*10^5$ cells/well for ELISA, $4*10^5$ cells/well for RT-qPCR and RNA-seq, $2*10^6$ cells/well for WB or $9*10^6$ cells/Petri dish for phospho-proteomics assays. All cells that were subsequently used for analyses of phosphorylated proteins (by WB or phospho-proteomics) were incubated in starvation medium with only 1% FCS overnight and during the assays, to minimise background phosphorylation.

Plasmacytoid dendritic cell-enriched cultures were obtained by differentiating bone marrow progenitors in complete RPMI media (RPMI Lonza, 10% FCS, Penicillin, Streptomycin, L-Glutamine, β-mercaptoethanol 15µM) supplemented with 150ng/ml Flt3-ligand (PeproTech) for 7 days. Cultures were replenished with fresh media on day 4 as previously described. On day 7, floating and loosely adherent cells were harvested, incubated with B220-biotin (1:200) and coupled with streptavidin magnetic beads (Miltenyi). pDCs were positively selected using a LS-column on a QuadroMACS separator, as per manufacturer's instructions (Miltenyi

Biotech). A fraction of the B220-positive cultures was taken for flow cytometry staining as per described protocol and using antibodies in Table 1. The B220-positive enriched cell cultures were plated at $2*10^5$ cells/well in complete media without Flt3-ligand. The plated cells were stimulated as described in individual experiments and responses measured by IFN-α/β and IL-6 ELISA of the cell supernatants (as described above).

Unless stated otherwise, the concentrations and manufacturers of each stimulus used on BMDMs and pDC-enriched cultures are stated in Table 2. Stimulation times and optimization conditions are cited for each experiment and Figure in Results.

2.8 RNA extraction and quantification of mRNA transcripts

Stimulated BMDMs were rinsed with PBS and lysed in 350µl RLT buffer (RNAeasy MicroKit, Qiagen) with β-mercaptoethanol (Sigma). Lysed cells were processed to extract RNA using the RNAeasy MicroKit (Qiagen), according to manufacturer's instructions and including an on-column DNA digestion. RNA was quantified using a ND-1000 Spectrophotometer (NanoDrop Technologies). cDNA synthesis by retro-transcription was carried out as described in sub-chapter 2.5. Further quantification of cDNA targets was performed on an Applied Biosystems Quantstudio 3 RT-qPCR machine with 1x qPCRBIO Probe Mix LO-ROX (PCR Biosystems) and 1x Taqman primers (list in Table 2.2). Obtained raw results were in form of Ct (cycle threshold) values, indicating the number of cycles of replication required for the fluorescent signal to cross the threshold of background level. Ct values are proportional to the negative of the $\log_2$ of the initial amount (or concentration) of the amplicon. Therefore, higher Ct values reflect lower DNA amounts. To obtain the ΔCt (target/HPRT) values represented in the Results chapters of this work, the logged fluorescence signal was first normalised to that of the housekeeping gene HPRT by subtracting its log.

$$\Delta Ct = -(log_2(target) - log_2(HPRT))$$

The final quantification of cDNA targets was represented on the x-axes as "target/HPRT" to reflect the ΔCt value from the equation above, by employing the following equation:

$$target/HPRT = 2^{\Delta Ct}$$

2.9 Western Blotting

10^6 differentiated BMDMs were plated and incubated overnight in 1%FCS medium to reduce background phosphorylation. The next day, the cells were stimulated as indicated in Results, and lysed in 100μl 1x RIPA buffer (components listed in Table 4). Cell lysates were centrifuged at max speed for 10min and total protein measured in the supernatants using the Pierce Microplate BCA Protein Assay Kit (ThermoScientific), according to manufacturer's instructions. Equal amounts of total protein were taken for each sample and additioned with 50mM DTT and 4x Loading Buffer (Biorad). The samples were run on Criterion XT Bis-Tris 10% gels (BioRad) at 120V for 1.5hrs along with Precision Plus Protein Dual Color Standards (Biorad). Total protein was transferred onto PROTRAN® nitrocellulose membranes (PerkinEmler) using semi-dry transfer on a NovaBlot (GE) for 1.5hrs. Non-specific binding was blocked using 5% BSA (Sigma) in PBS 0.05% Triton (PBS-T). Membranes were incubated with the corresponding primary antibodies against mouse protein in 1% BSA PBS-T overnight (list of antibodies in Table 5). Membranes were washed with PBS-T and subsequently incubated with corresponding secondary antibodies coupled with HRP (goat anti-rabbit-HRP, Biorad and goat anti-mouse HRP). Chemiluminescence was revealed using Amersham™ ECL™ Western Blotting Detection Reagent (GE) and recorded on autoradiography films Amersham™ (Fisher Scientific).

2.10 Immunoprecipitation assays

$9*10^6$ BMDMs (differentiated according to the protocol above) were seeded in Corning® culture dishes (Thermo Fisher) and incubated overnight in complete media with 1% FCS. Cells were then washed with PBS and lysed in 1ml RIPA 1x lysis buffer supplemented with 0.3% Triton TX100, 1mM PMSF and 1x Protease inhibitor cocktail (Roche). Lysates were centrifuged at max speed for 15min and supernatants taken for further analysis. A portion of total supernatant was taken to serve as "IP" sample, and the remaining volume incubated with 5μg of corresponding antibody overnight (see Results): anti-PKCζ (Abcam PLC) or anti-WWC2 (Insight Biotechnology Limited). The negative control was achieved by incubating the same antibody with the lysis buffer only. The enrichment for target proteins was achieved

by purification using Magnetic Protein G beads (Thermo Fisher Scientific). Following immune-precipitation using an anti-aPKCζ antibody, samples were run on a gel as described previously, and membranes used for blotting with anti-WWC2 or anti-aPKCζ antibody (details on antibodies in Table 5).

2.11 Phospho-proteomics assays

Analyses of the global phospho-proteome in our stimulated samples were performed using TMT labelling. In preparation for the experiment, $9*10^6$ BMDMs were plated in tissue culture 10cm dishes (ThermoFisher) and incubated in 1% FCS BMDM media overnight. After stimulation (as indicated in Results, details in Table 2), cells were washed with PBS, and lysed in detergent-free urea lysis buffer (ingredients indicated in Table 4). The lysates were centrifuged at max speed for 10min, and supernatants kept at -80°C. Total protein dosage was performed using the Pierce Coomassie (Bradford) Protein Assay Kit (Thermofisher), and 200μg of total protein for each sample used for further proteomics workflow and analyses. The following workflow was established by the Proteomics Facility at the Francis Crick Institute (with thanks to Helen Flynn and Bram Snijders). Samples were reduced with DTT and alkylated with iodoacetamide overnight, and digested with rLysC (Wateo) and trypsin (V5280 Promega). This was followed by a C_{18} MacroSpin column clean-up of proteolytic digests and labelling of digested peptides using the TMT10plex Isobaric Label Reagent Set kit (ThermoScientific). The samples were checked for labelling efficiency (unmodified peptides as a percentage of total peptides for each labelling reaction) before proceeding with two phosphopeptide sequential enrichment steps by metal oxide affinity chromatography. TiO_2 enrichment was performed using the ThermoScientific High-Select TiO_2 kit according to manufacturer's instructions, followed by Fe-NTA enrichment with the ThermoScientific High-Select Fe-NTA enrichment kit. The peptides were fractionated by their pH using the Pierce™ High pH reversed-phase Peptide Fractionation kit (ThermoFisher), according to manufacturer's protocol. All peptides were analysed by mass spectrometry using an Orbitrap Fusion Lumos analyser. The obtained raw data was initially processed in MaxQuant. The Uniprot KB database of Mus musculus sequences was used for peptide identification. A protein, peptide and phosphosite estimated false discovery rate (FDR) of 1% was applied for generation of tables with

protein and phosphopeptide identifications and quantifications. Subsequently, reporter ion intensity values for different confirmed phosphosites were uploaded into Perseus software for further statistical analysis and data visualisation.

2.12 RNA sequencing

BMDMs were seeded at $4*10^5$/well and stimulated as indicated in the table below. Cells were lysed and RNA extracted as per previously described protocol (MicroKit® QIAGEN columns with an on-column DNA digestion). The RNA was quantified in each sample using Nanodrop, and a minimum of 489 ng of total RNA submitted for RNA-seq analysis. The number of reads per sample was 25 million for the submitted mRNA library. The libraries were prepared using the KAPA mRNA (poly:A) HyperPrep kit according to the manufacturer's instructions. The sequencing was completed on the HiSeq 4000 Instrument, with single end 100bp reads. The samples had an average of 29.5 million reads. Read quality was assessed using the FastQC quality control tool for high-throughput sequencing data. Adaptor sequences were removed from the reads by using Cutadapt-1.9.1. Each sample read library had passed all the quality control steps (using FastQC, RSeQC, RNA-SeQC), including, but not limited to, per sequence GC content, sequence length distribution, sequence duplication levels and gene body coverage, after being aligned and quantified to the mouse genome (Ensembl GRCm38 release 86) using the combination Star (v 2.5.2)/RSem (v.1.3.1) packages. A minimum of 97% of reads was aligned to the reference genome and the minimum number of identified genes was $15*10^3$. Differential expression analysis was performed in R-3.6.0. (R Core Team, 2018) using the DESeq2 package (version 1.24.0) as explained in the Results chapter. Differential genes were selected by applying a 0.05 false-discovery rate (FDR) threshold. Heatmaps were made using R-3.6.0 ComplexHeatmap package (v 2.0.0). Volcano plots were created using EnhancedVolcano package (v 1.2.0).

2.13 Statistical testing

Statistical testing was carried out in the Prism software. For comparison of two groups, a t-test comparison of means with no assumption of normal distribution of samples, Mann-Whitney test, was performed and statistical significance assigned for $p<0.05$. For comparison of three groups' means, the Kruskal-Wallis one-way

ANOVA test (without assumption of normal distribution) was performed (significance marked as * p<0.05; ** p<0.01; *** p<0.001). For weight loss curves, as well as comparisons of genotypes within multiple stimulation conditions (ex. Mock and X31), a two-way ANOVA was used, with a Dunett correction for multiple testing included, and significance reported for padj<0.05. For weight loss curves, the two-way ANOVA was used without sphericity assumption (i.e. using the Geisser-Greenhouse correction), with a mixed-effects model substituting the ANOVA where missing values were detected (ex. due to mice reaching clinical end points). Survival assays were statistically assessed using a log-rank Mantel-Cox test, with significance admitted where p<0.05. The statistical testing in the phospho-proteomics assays was a t-test Welch test comparing two means, including the multiple testing correction (significance admitted in padj<0.05). For the RNA-seq assay, the statistical analysis was carried out by using DESeq2 package version 1.24.0. with variance stabilising transformation (VST) applied to raw count data before PCA and Euclidian distance-based clustering.

2.14 Antibodies, primers and buffers used

Table 2.1 Antibodies used for flow cytometry

Antibody	Clone	Manufacturer	Dilution
B220	RA3-6B2	eBioscience	1:200
CD3	17A2	BioLegend	1:100
CD4	RM4-5/GK1.5	BioLegend	1:400
CD8	53-67	BioLegend/eBioscience	1:400
CD19	6D5/1D3	BioLegend/BD Pharmigen	1:400
CD11b	M1/70	BioLegend	1:4000
CD11c	N418	BioLegend	1:400
F4/80	BM8	BioLegend	1:100
IFNAR1	MAR1-5A3	BioLegend	1:200
Ly6C	HK1.4	BioLegend	1:400
Ly6G	1A8	BioLegend	1:200
MHC II	M5/114.15.2	BioLegend	1:600
NK1.1	PK136	BioLegend	1:400

PDCA-1	927	Biolegend	1:400
Siglec-H	551	BioLegend	1:200
Siglec-F	E50-2440	BD Pharmigen	1:600
Sca-1	D7	eBioscience	1:200
ZombieAqua		BioLegend	1:500

Table 2.2 Primers used for qPCR

Target gene	ThermoFisher Sci assay ID or 5'-3' Sequence
Hprt	Mm00446968_m1
Ifn-β1	Mm00439552_s1
Il-6	Mm00446190_m1
Irf3	Mm00516784_m1
Irf7	Mm00516791_g1
Stat1	Mm00439531_m1
Alpk1	Mm01320377_m1
Ap1ar	Mm01318187_m1
Tifa	Mm00455038_m1
573Rik	Custom (based on Boulard et al, 2012) (ThermoFisher Scientific; Taqman primer) sense GGCGAGCAGGATATTGAAGA antisense ATCCTTGTGAAGCCCATGTT Probe FAM-ATGGGTTCGCCAGAGTGGTT-TAMRA
Larp7	Mm01319419_m1
Wwc2	Mm00519373_m1
Amotl2	Mm00502287_m1

(all primers were Taqman primers)

Table 2.3 Composition of 1X RIPA buffer in water

Component	Final concentration
Tris-HCl pH=8	50 mM
Sodium chloride	150 mM
EDTA	1 mM
EGTA	1 mM
Sodium pyrophosphate	2.5 mM
Beta-glycerophosphate	1 mM
Sodium vanadate	1 mM
Triton Tx-100 (Biorad)	1%
Sodium dodecyl-sulphate	1%
Protease inhibitor cocktail (Roche)	1x

(unless stated otherwise, all components are from Sigma)

Table 2.4 Composition of 1X lysis buffer for phospho-proteomics assays in water

Component	Final concentration
Urea	8 M
HEPES pH=8.2	50 mM
Glycerol-2-phosphate	10 mM
Sodium-fluoride (NaF)	50 mM
Sodium Pyrophosphate	5 mM
EDTA	1 mM
Sodium vanadate *	1 mM
DTT *	1 mM
PMSF *	1 mM
Aprotinin *	1 µg/ml
Leupeptin *	1 µg/ml
Okadaic acid *	100 nM

* – added on the day of lysis. All components were from Sigma Aldrich.

Table 2.5 Primary antibodies used for WB

Target	Modified residue / ref	Manufacturer	Host and clonality	Dilution
β-actin	13E5	Cell Signaling	Rabbit monoclonal	1:5000
Phospho-TBK1/NAK	Ser172 / D52C2	Cell Signaling	Rabbit monoclonal	1:1000
Phospho-NF-0954B p65	Ser536 / 93H1	Cell Signaling	Rabbit monoclonal	1:1000
P65 (RelA)		Millipore	Mouse monoclonal	1:1000
Phospho-p38	T180,Y182 / 3D7	Cell Signaling	Rabbit monoclonal	1:1000
P38		Cell Signaling	Rabbit	1:1000
WWC2		ProteinTech Europe	Rabbit polyclonal	1:500
PKCζ	H-1	Insight Biotechnology	Rabbit monoclonal	1:1000

Table 2.6 Stimuli manufacturers and way of incubation

Stimulus	Cat n.	Manufacturer	Concentration
X31 (egg-der.)*		F. Crick Inst	*In vivo* (see Results) *In vitro* pDC - 10^5 $TCID_{50}$/ml BMDM – 10^6 $TCID_{50}$/ml
X31 (MDCK-der.)*		F. Crick Inst	pDC - 10^5 $TCID_{50}$/ml BMDM – 10^6 $TCID_{50}$/ml
PR8 (MDCK-der.)*		F. Crick Inst	pDC - 10^5 $TCID_{50}$/ml BMDM – 10^6 $TCID_{50}$/ml
LPS*	581-008-L0002	Enzo Life Science	0.5 μg/ml
Poly(I:C) HMW*	tlrl-pic	Invivogen	25 μg/ml
CpG-A (ODN2216)*	IAX-200-005-3001	Innaxon	6 μg/ml

CpG-B (ODN1668)*	ALX-746-051-M001	Enzo Life Science	1 μg/ml
LyoVec**	Lyec-2	Invivogen	1/20 final dilution / well
Poly:U**	tlrl-sspu	Invivogen	1/50 dilution in LyoVec; $1/10^3$ final
Lipofectamine**	11668019	ThermoFisher	10^{-3}μl lipofectamine / μl culture
2'3' cGAMP***	tlrl-nacga23-1	Invivogen	10 μg/ml
5'ppp dsRNA***	tlrl-3prna	Invivogen	50 ng/μl

* **Supernatant:** stimuli were dissolved in cell culture media and additioned onto cells in culture directly

** **Transfection:** stimuli were incubated with LyoVec reagent for 5min at RT and the complexes added onto cells in culture medium

*** **Transfection:** stimuli were mixed with OPTIMem media separately from Lipofectamine in OPTIMem, the two pooled in 1:1 ratio and incubated for 15min at room temperature, and the mix added to cells in OPTIMem medium

Chapter 3. Results 1: IFN-α/β production and influenza susceptibility phenotype confirmation in C57BL/6 and 129 mice

3.1 Introduction

The two experimental objectives of the results presented in this chapter were as follows: 1. to confirm the 129 *in vivo* phenotype of influenza susceptibility and high IFN-α/β and cytokine production compared to BL/6 mice (Davidson et al., 2014) and 2. to extend the studies to an *in vitro* model to start elucidating the origins of high IFN production.

The 129 phenotype of increased morbidity and mortality in influenza infection compared to BL/6 controls was initially described in the 129S7 mice (Davidson et al., 2014), and additional unpublished work carried out in the 129S8 strain. However, in this thesis 129S6/SvEv mice are used as the default 129 strain. 129S6/SvEv and 129S8 mouse lineages originate from breedings on different site of the same parental strain of 129/SvEv *Steel* mice (Simpson et al., 1997), so it was necessary to confirm that they presented similar phenotypes in the context of influenza infection. In this chapter, I investigate the susceptibility to influenza of 129S6/SvEv mice (morbidity and mortality compared to BL/6 controls) and their *in vivo* IFN-α/β and cytokine production.

While *in vivo* models of infection are essential, cell-to-cell interactions and tissue environment make the study of IFN-α/β production more difficult. Since this project is focused on genetic factors encoding excessive IFN-α/β production in 129S6/SvEv mice, *in vitro* models allow to isolate mouse strain-specific genetic factors from environmental cues and thus simplify the system. For these reasons, a large portion of the work presented in this chapter relies on *in vitro* assays using BMDMs and pDC-enriched cultures. These cells respond to influenza virus infection and a variety of different TLR/RLR/STING stimuli (see Introduction) by engaging the production of cytokines and IFN-α/β, which makes them a versatile tool for studying different signaling pathways.

After the initial recognition of IAV in the lungs, the secreted IFN-α/β bind to the ubiquitously expressed IFNAR receptor and induce different downstream effects

depending on the cell type and the activated cascade (Hervas-Stubbs et al., 2011). IFNAR activation also results in a positive feedback loop of IFN-α/β expression in certain cell types (see Introduction for details). Thus, it is more difficult to pinpoint the origin of IFN overproduction relative to the IFNAR cascade and the cell type. Using IFNAR1-/- mice, it was possible to study the signaling upstream of IFNAR only, as in these mice IFNAR-mediated signaling is abrogated. In this chapter, I present results of *in vitro* stimulations of BMDMs and pDCs from IFNAR1-/- BL/6 and IFNAR1-/- 129 genotypes. The role of newly synthetised proteins in IFN-α/β production is also investigated (in the presence or absence of the IFNAR cascade) by exposing cells to cycloheximide before stimulation.

3.2 Results

3.2.1 In vivo responses to influenza infection in 129 mice

3.2.1.1 IAV susceptibility and cytokine signatures of 129 strains of mice

Firstly, BL/6 and 129S6/SvEv or 129S8 mice were infected with the X31 influenza virus and their survival and weight loss followed over two weeks. The results (Figure 3.1a) indicate that both 129S6/SvEv and 129S8 strains have similar increased susceptibility to the virus compared to BL/6 controls. Their weight loss is significantly higher and survival significantly lower than that of BL/6 mice. Ultimately, all 129 mice of both strains succumbed to the infection. In concordance with previous published results, 129S8 mice show significantly increased levels of secreted IFN-α/β protein in the BAL fluid compared to BL/6 controls at day 2 post-infection (Figure 3.1b, magenta). It is worth noting that day 2 post-infection was chosen as a timepoint based on type-I IFN peaking times in infection (see Introduction). Encouragingly, the phenotype of 129S6/SvEv mice was comparable to that of 129S8, with significantly higher type-I IFN production in the BAL fluid compared to BL/6 mice. The reasons for large absolute value differences (in pg/ml) between the two experiments are currently unclear, but it is possible that they stem from switching from one ELISA assay to another, and the reduced assay sensitivity. These experiments demonstrated that 129S6/SvEv and 129S8 strains are similar in their influenza susceptibility and type-I IFN responses and that they could be used in a comparable

manner for future experiments. Further experiments were pursued with the 129S6/SvEv strain.

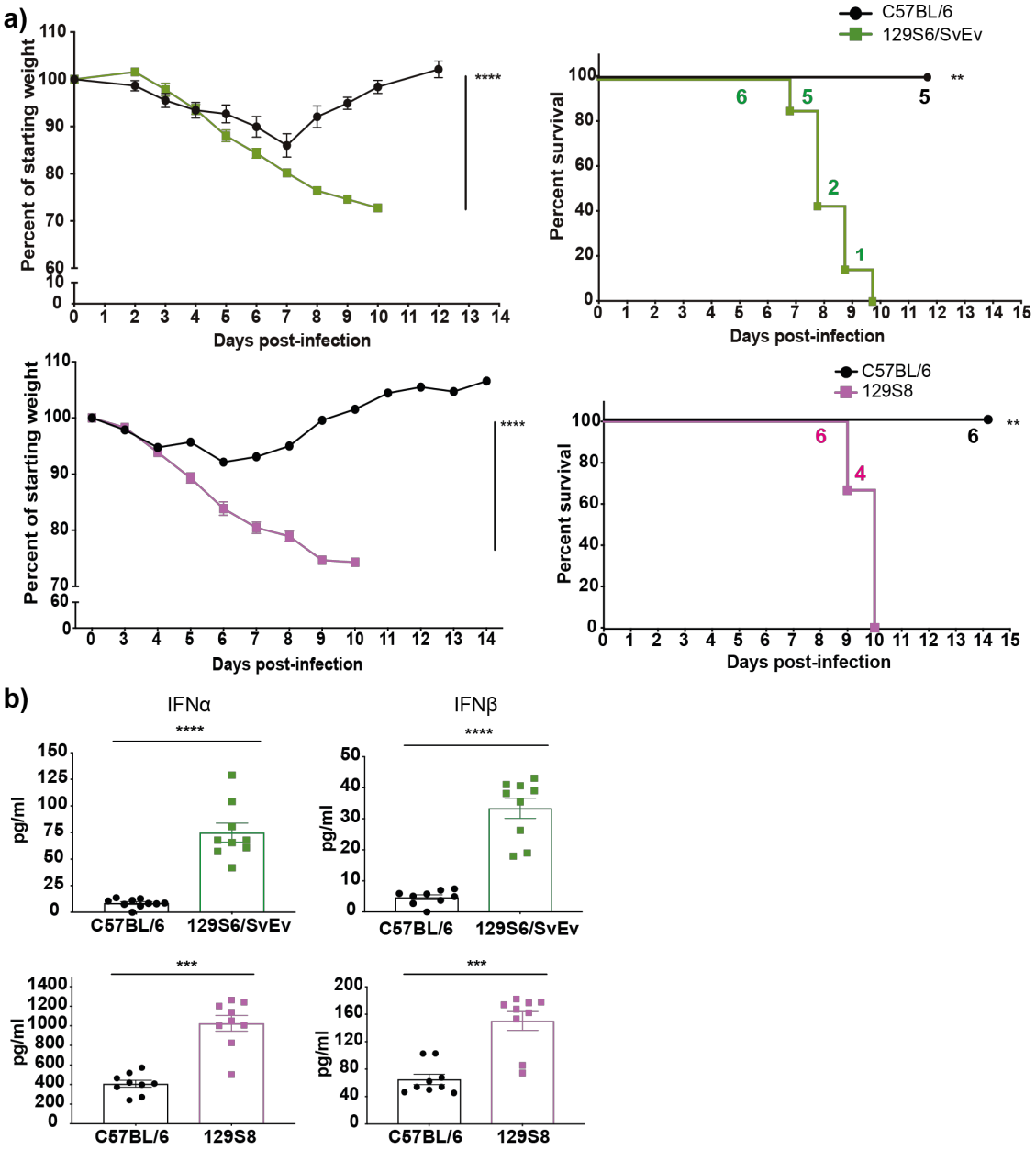

Figure 3.1 129S8 and 129S6/SvEv strains of mice show similar high susceptibility to X31 influenza virus compared to C57BL/6 controls, as well as increased type-I IFN production in the BAL two days post-infection. Mice of indicated genotypes were infected in separate experiments with 800 $TCID_{50}$ X31 per mouse. **A.** Weight loss and survival were recorded over two weeks following infection. Number of mice in exp1b at d0: C57BL/6 n=5 and 129S6 n=7, and in exp2: C57BL/6 n=6 and 129S8 n=6. Coloured numbers in the survival curves indicate number of surviving mice at a given timepoint in infection. Weight loss curves statistical tests 2-way ANOVA (significance $p<0.05$). Survival tests log-rank (Mantel-Cox, significance $p<0.05$). **B.**

48h post-infection, amounts of type-I IFN protein in the BAL were measured by ELISA (each symbol represents one mouse). Statistical test: Mann-Whitney t-test (no assumed normal distribution of data; * $p<0.05$; ** $p<0.01$; *** $p<0.001$; **** $p<0.0001$; non-significant comparisons are not shown). Data represented as mean±SEM. Data representative of four different experiments, carried out at least three times each.

Subsequently, levels of cytokines and chemokines at day 2 post-infection were analysed in the BAL fluid of 129S6/SvEv mice (Figure 3.2). Pro-inflammatory cytokine expression, such as IL-6, IL-1β, TNF-α, MIP-1β, MCP-1 and GRO-α, was found to be significantly increased in 129S6/SvEv mice compared to the BL/6 controls. This was true for most other cytokines and chemokines of detectable levels in the lung, as well as IFN-λ. Interestingly, levels of IL-10 were found to be comparable between the two genotypes. Overall, the first experiments had reproduced the observed 129S7 phenotype-In the 129S6/SvEv substrain, showing high mortality and cytokine production in these mice upon influenza infection.

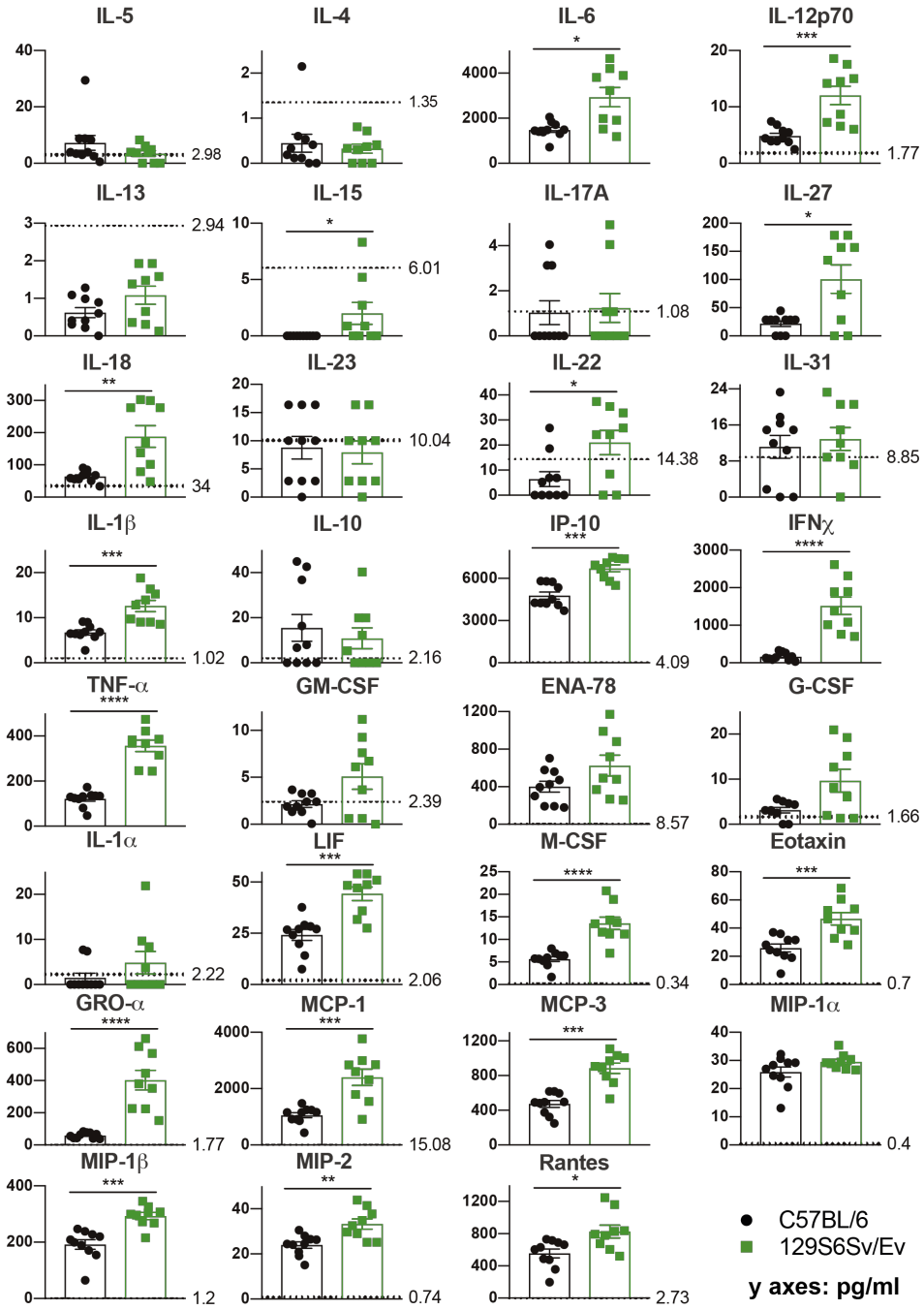

Figure 3.2 129S6/SvEv mice exhibit signs of a "cytokine storm" at 48h post-infection, with increased levels of pro-inflammatory cytokine secretion in the lung compared to BL/6 controls. After infection with X31, quantities of different cytokines were measured in the BAL using an ELISA multiplex assay. Statistical comparison was performed using a Mann-Whitney t-test (* $p<0.05$; ** $p<0.01$; *** $p<0.001$; **** $p<0.0001$; non-significant comparisons are not shown). Each symbol represents one mouse. All graphs originate from the same experiment and were measured as part of the same assay. Where relevant, lower detection limit lines are represented as dashed lines with a number indicating the lowest detected concentration (in pg/ml) of represented targets. Data represents one experiment.

3.2.1.2 Lung cell composition and mRNA responses of 129S6/SvEv mice in influenza infection

To test for immune cell recruitment during influenza infection, BL/6 and 129S6/SvEv mice were challenged with the X31 virus, and lung composition examined at 2 days post-infection by flow cytometry (Figure 3.3). Both pDC and DC proportions were increased in the 129S6 lungs compared to BL/6 controls (Figure 3.3a). Moreover, 129S6 mice showed proportionally significantly more neutrophil presence in the lung, as well as a tendency towards increased inflammatory monocyte recruitment. As these cells are recruited into the lung following IFN signals, this result confirmed our previous findings. This was less the case for alveolar macrophages, where a lower proportion of these cells was observed in the 129S6 compared to the BL/6 mice. Although it was slightly early in infection to observe a surge in adaptive immune cell recruitment, an increased proportion of CD4+ T-cells was noted in the lung of 129S6 mice. Interestingly, 129 mice showed significantly lower proportions of B-cells in the lung. Also, expression of PDCA-1, a cell surface marker ISG upregulated on activated immune cells upon IFN exposure infection, was compared between BL/6 and 129 immune cells. Given the observed differences in IFN-α/β levels and innate immune cell recruitment in the lungs of BL/6 and 129 mice, the expression of PDCA-1 as a marker of IFN-dependent cell activation was therefore interesting to address. The analysis of PDCA-1 MFIs on different immune cells (Figure 3.3b) showed that alveolar macrophages, dendritic cells and inflammatory monocytes all expressed significantly higher levels of PDCA-1 in 129 mice than in BL/6 controls.

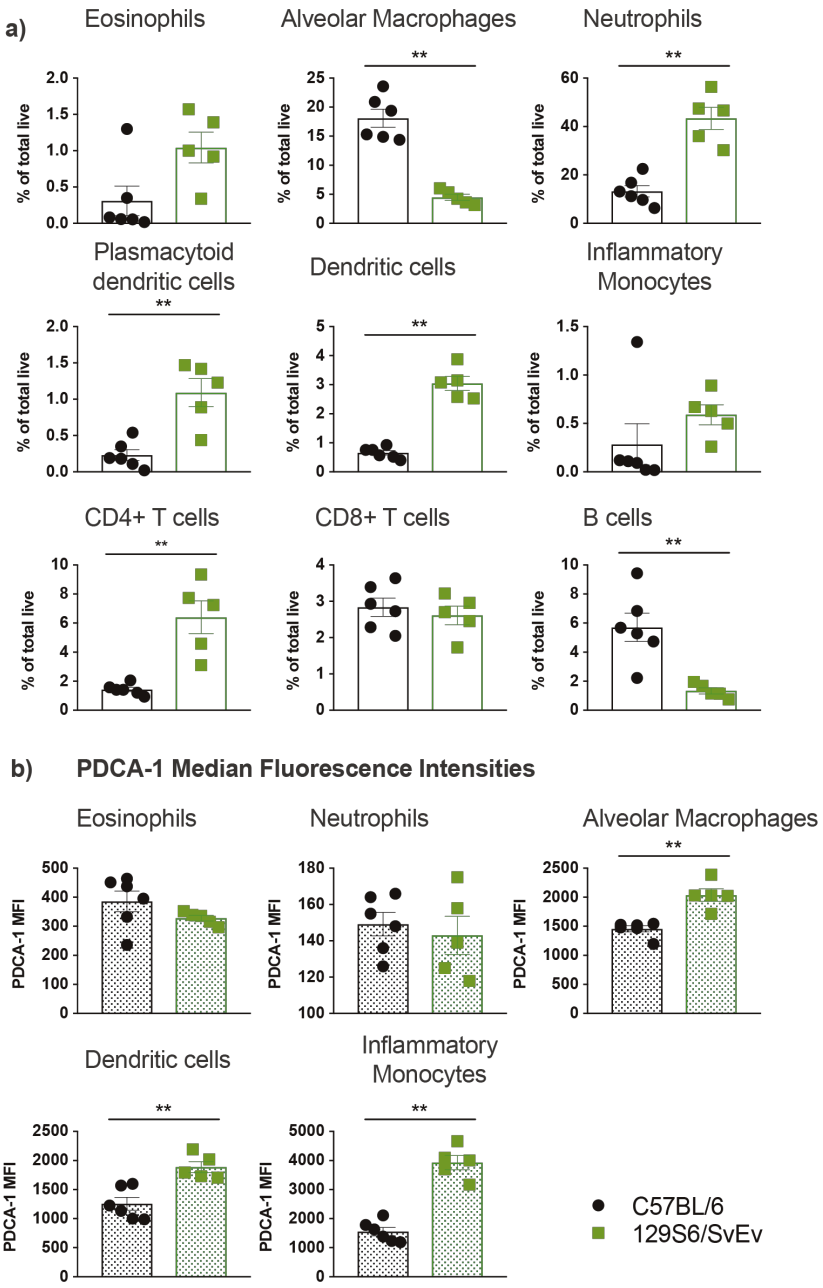

Figure 3.3. Recruitment of some immune cells to the lung at day 2 p.i. is significantly increased in 129S6/SvEv mice compared to BL/6 controls; PDCA-1 expression is increased on some immune cells in the 129S6 mice. A. At day 2 post-infection, lungs of mice infected with X31 were taken and processed for flow cytometry staining. The gating strategy used to obtain the displayed graphs is described in Material and Methods and Appendix Figure 8.1 and Figure 8.2 of this thesis. **B.** Median Fluorescence Intensity of PDCA-1 was recorded on the indicated cell types (same samples as a)). Each symbol represents a single mouse. Significance (* $p<0.05$; ** $p<0.01$; *** $p<0.001$; **** $p<0.0001$; non-significant comparisons are not shown) according to a Mann-Whitney t-test. Representative of five independent experiments.

Production and secretion of IFN is a complex process involving various cell types, different signaling pathways and protein exocytosis. In response to TLR/RLR recognition, mRNA synthesis responses occur in the stimulated cells. In the first wave of transcriptomic activation, the mRNA synthesis of *Ifn-β1* and *Il-6* and other NFκB-dependent cytokines occurs, followed by the IFNAR-dependent ISG production of *Stat1* and other target genes. Therefore, mRNA levels of *Ifn-β*, *Il-6* and *Stat1* were measured in the whole lung (without separation of epithelial and non-epithelial cells) of 129S6 and BL/6 mice at 48h post-X31 virus infection. Results of two independent experiments, represented in Figure 4a are representative of the observed variability while trying to investigate mRNA levels of the mentioned targets. In one experiment, both *Ifn-β1* and *Il-6* mRNA levels were lower in the 129S6 mice than in the BL/6 controls, contrary to all the previous protein-based experimental findings. However, this result was not reproducible: in one of the experiments that followed (Figure 3.4a), the mRNA levels in 129S6 lungs were higher than those in BL/6 lungs. *Stat1* mRNA levels were reproducibly stable between genotypes, whereas *Irf7* showed a trend for increased levels in 129S6 mice. Given the conflicting results in the lung, mRNA from cells recovered from the BAL fluid was quantified in a separate experiment (Figure 3.4b). A slight trend for increase in mRNA levels of all three targets analysed in these cells was observed.

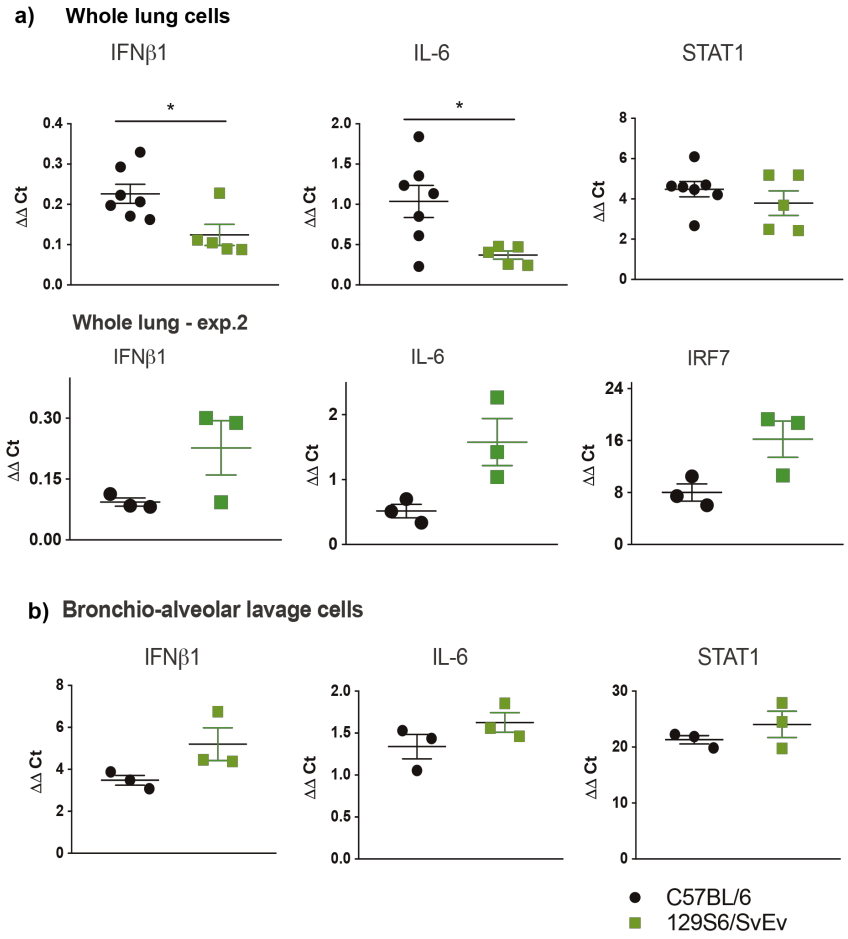

Figure 3.4 mRNA expression of *Ifn-β1*, *Il-6*, *Irf7* and *Stat1* in the lung shows inter-experimental variability, and no significant difference in the BAL. Samples were processed and mRNA levels quantified by QPCR. Results are represented as the fold increase relative to the expression of the housekeeping gene *Hprt*. Each symbol represents one mouse in the following samples, 48h post-X31 infection: **A.** whole lung samples; two rows represent results from two independent experiments; **B.** cells harvested from the BAL fluid. Statistical test: t-test without assumption of normal distribution: Mann-Whitney (* p<0.05; ** p<0.01; *** p<0.001; **** p<0.0001; non-significant comparisons are not shown). Data representative of at least three independent experiments (data in B. one experiment).

3.2.2 *In vitro* infection and stimulation of 129S6/SvEv BM-derived cells

Further, it was necessary to investigate the observed *in vivo* phenotype-In a more controlled and isolated system *in vitro*. For this purpose, we used bone marrow-derived cultures of BMDMs, or pDC-enriched cultures, of 129S6 and BL/6 mice, obtained as described in Material and Methods. I infected these cells with the X31 and PR8 strains of virus, or stimulated them with different TLR/RLR stimuli in order to check their IFN-α/β and IL-6 expression responses.

Stimulation of BMDMs with CpG-A (ODN-22165), through activation of TLR9 signaling, resulted in the induction of IFN-α/β and IL-6 (Figure 3.5a). Expression of IL-6 was comparably more intense than that of type-I IFN and was significantly higher in 129S6 BMDMs than in the BL/6 controls. This was also the case for IFN-β expression, while IFN-α levels were similar. Stimulation of TLR3 with poly(I:C) resulted in more intense upregulation of IL-6 and IFN-α production in the 129S6 background. Similar results were observed after activation of cGAS/STING and RIG-I pathways by 2'3'cGAMP and 5'ppp dsRNA (respectively).

Ultimately, when infected with X31 (MDCK-derived strain used for cell culture-grade stimulation), BMDMs of both genotypes responded with strong IFN-α/β production and secretion (Figure 3.5b). Once again, 129S6 BMDMs exhibited significantly higher levels of both proteins compared to BL/6 controls. Infection with the egg-derived X31 virus (the same strain as the one used for *in vivo* infections), yielded lower levels of type-I IFN than other viruses used, but resulted in the same increase in the IFN-α/β production in 129S6 cells. Finally, in the infection with the PR8 strain of influenza, no significant difference was observed between genotypes. Results of an independent experiment are shown in Figure 3.5c, and represent IL-6 expression upon challenge with the three different viruses mentioned. IL-6 expression is significantly higher in 129S6 BMDMs in all three virus strain scenarios. The pattern of these responses indicated that the *in vivo* phenotype of high type-I IFN responsiveness in 129S6 mice is reproducible at the *in vitro* level.

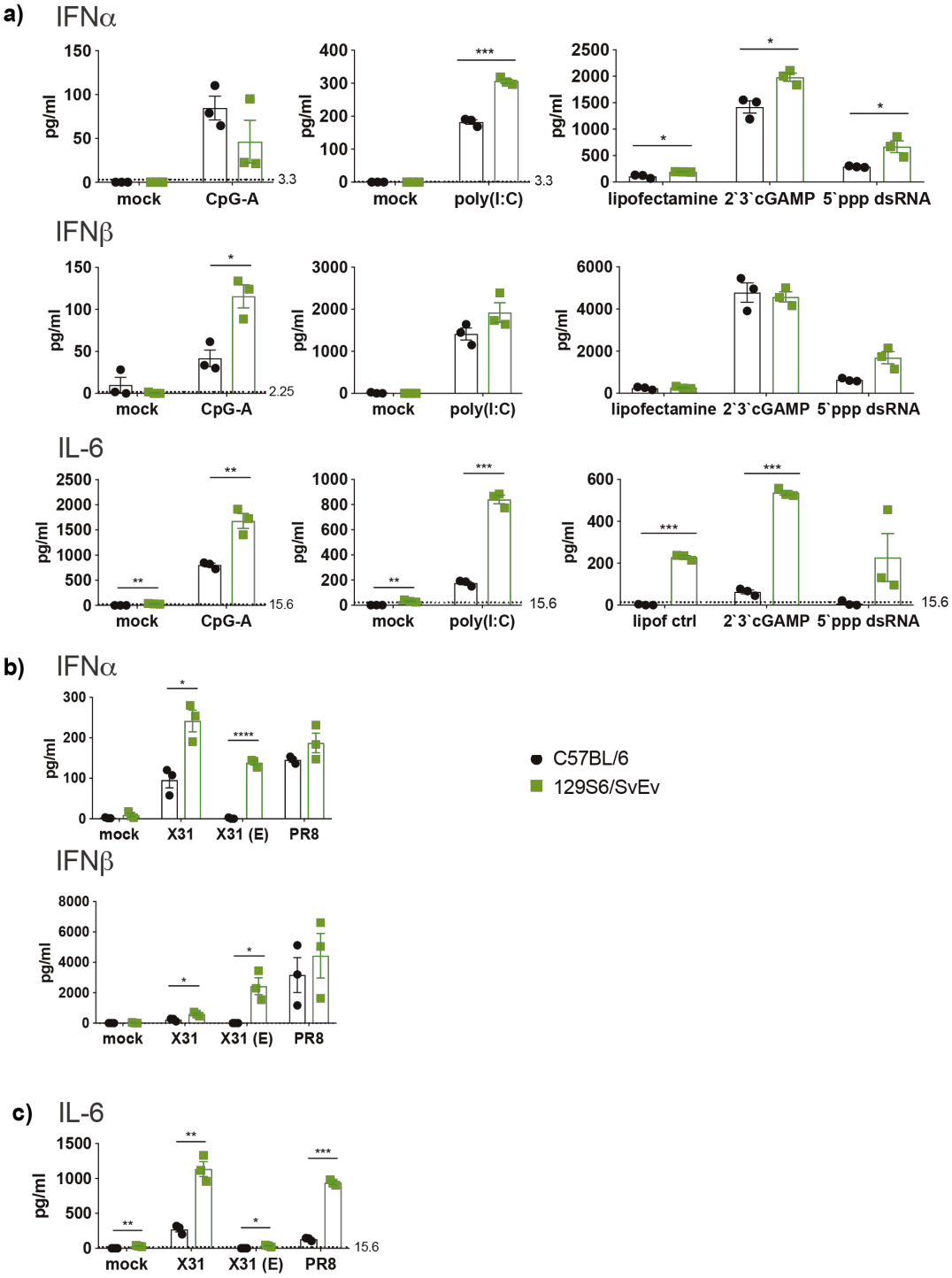

Figure 3.5. 129S6/SvEv BMDMs stimulated in vitro respond to TLR/RLR/STING stimulation and IAV infection with significantly higher secretion of IFN-α/β and IL-6 protein compared to the BL/6 controls. A. BMDMs were incubated with TLR9 and TLR3 agonists CpG-A (ODN1668) and poly(I:C) respectively, or transfected with STING agonist 2'3'cGAMP or the RIG-I specific stimulus 5'ppp dsRNA, and the levels of secreted IFN-α/β and IL-6 measured in the supernatants 24h post-stimulation by ELISA. For concentrations used for each stimulus, and detailed

protocols refer to Material and Methods. The dashed line represents the lower detection limit of the assay (number on the side indicates the lowest detected target concentration). **B.** BMDMs were infected with X31 (MDCK-derived unless otherwise indicated), egg-derived X31 (the strain used for in vivo infections), or PR8 viruses at 10^6 $TCID_{50}$/ml. Supernatants were collected 24h after infection and type-I IFN content analysed by ELISA. **C.** Result for IL-6 protein secretion recorded from a separate experiment in the same conditions and same stimulants used as in B. Each symbol is a separate mouse (biological replicates), and statistical significance was concluded where * $p<0.05$; ** $p<0.01$; *** $p<0.001$; **** $p<0.0001$ in a Mann-Whitney t-test with no assumption of normal distribution of data. Non-significant comparisons are not shown). Represented data is from three different assays and is representative of nine independent experiments.

Given the conflicting results on mRNA levels *in vivo* in the infected lung, I probed for genotype differences in IFN production in a more controlled setting in BMDMs. I also wanted to test whether mRNA production showed the same pattern of inter-genotype differences as the secreted proteins. For this purpose, BMDMs were stimulated with TLR/RLR agonists, or infected with X31 influenza virus (MDCK-derived strain only), and mRNA levels compared between 129S6 and BL/6 cells after 6h of stimulation (Figure 3.6). The most striking differences in *Ifn-β1* transcription between 129S6 and BL/6 BMDMs were observed in TLR9, STING and RIG-I specific stimulations (with CpG-A, 2'3'cGAMP and 5'ppp dsRNA, respectively). 129S6 cells showed significantly stronger responses compared to BL/6 controls. It is worth noting that the represented results are compounded from different independent experiments – each row represents the same analysed target, but the separate graphs are representative of different assays. Transfection with lipofectamine did not incur differences in *Ifn-β1* levels as a rule. Differences in *Il-6* mRNA quantity also seem to be stimulus-dependent, but the trend for stronger responses in the 129S6 BMDMs is more noticeable. In TLR4 stimulation with LPS, a classic activator of NFκB-dependent transcription, *Il-6* mRNA levels were significantly higher in 129S6 BMDMs. Similar results were observed upon STING and RIG-I specific stimulations. *Stat1* mRNA transcription seems similar between 129S6 and BL/6 BMDMs, except in 2'3'cGAMP stimulation, where, in opposition to the *Ifn-β1* result interpretation, the levels of this ISGs are significantly lower in the 129S6 BMDMs. It is important to stress that these stimulations, especially in the case of X31 infection, also showed considerable variations in terms of BL/6 vs 129S6 responses between experiments.

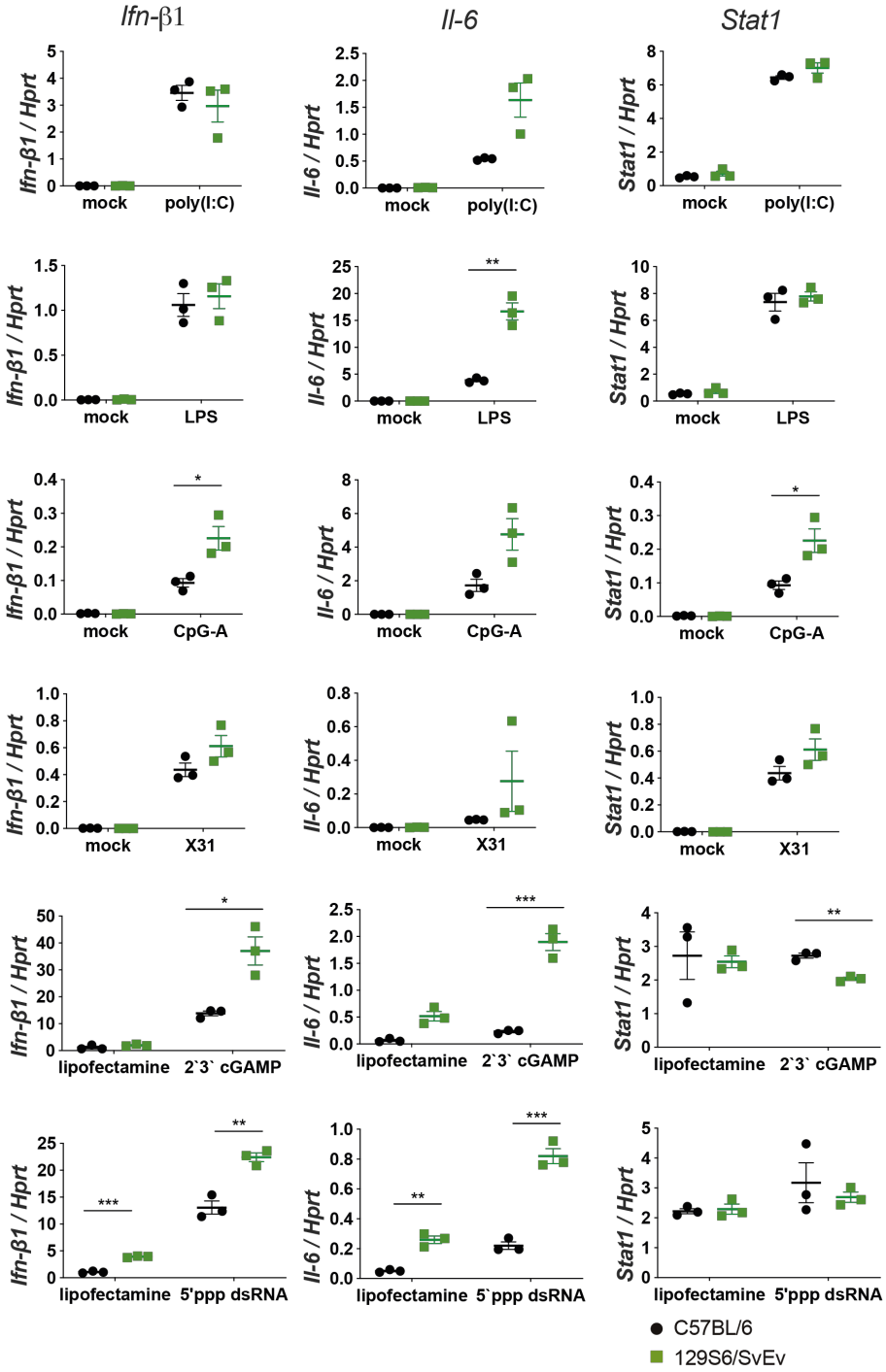

Figure 3.6 *Ifn-β1* transcription after RIG-I/STING activation, and Il6 transcription after TLR4/RIG-I/STING stimulation is reliably and significantly higher in 129S6/SvEv BMDMs than in BL/6 controls. BMDMs were incubated with the indicated stimuli (poly(I:C) for TLR3 stimulation, LPS for TLR2, CpG-A for TLR9, transfected 2'3'cGAMP for STING and transfected 5'ppp dsRNA for RIG-I specific activation, or infected with X31 at 10^6 $TCID_{50}$/ml. 6h after stimulation or infection, cells were harvested and processed for mRNA quantification by QPCR. Each symbol is a biological replicate, ie cells derived from 1 bone marrow. The values are plotted

as a mean ± SEM and are representative of a fold increase in expression relative to the housekeeping gene HPRT. Statistical significance (* p<0.05; ** p<0.01; *** p<0.001; **** p<0.0001; non-significant comparisons not shown) assessed by a t-test without assumption of normal distribution of data: a Mann-Whitney t-test. Represented data is pooled from three experiments but representative of six independent assays.

After BMDMs, pDC-enriched cultures were tested for responses to TLR9 (through CpG-A and CpG-B) and TLR7 stimulation (transfected poly:U) (Figure 3.7a), as well as TLR7/RIG-I activation through X31 viral infection (Figure 3.7b). The results strongly indicate that 129S6 pDCs show stronger IFN-α/β responses than their BL/6 counterparts. This was more noticeable in the case of IFN-β than IFN-α. However, in opposition to BMDMs, the most striking responses were observed upon PR8 infection, whereas MDCK-derived X31 virus generally yielded lower responses but still significantly higher IFN-β in 129S6 cells.

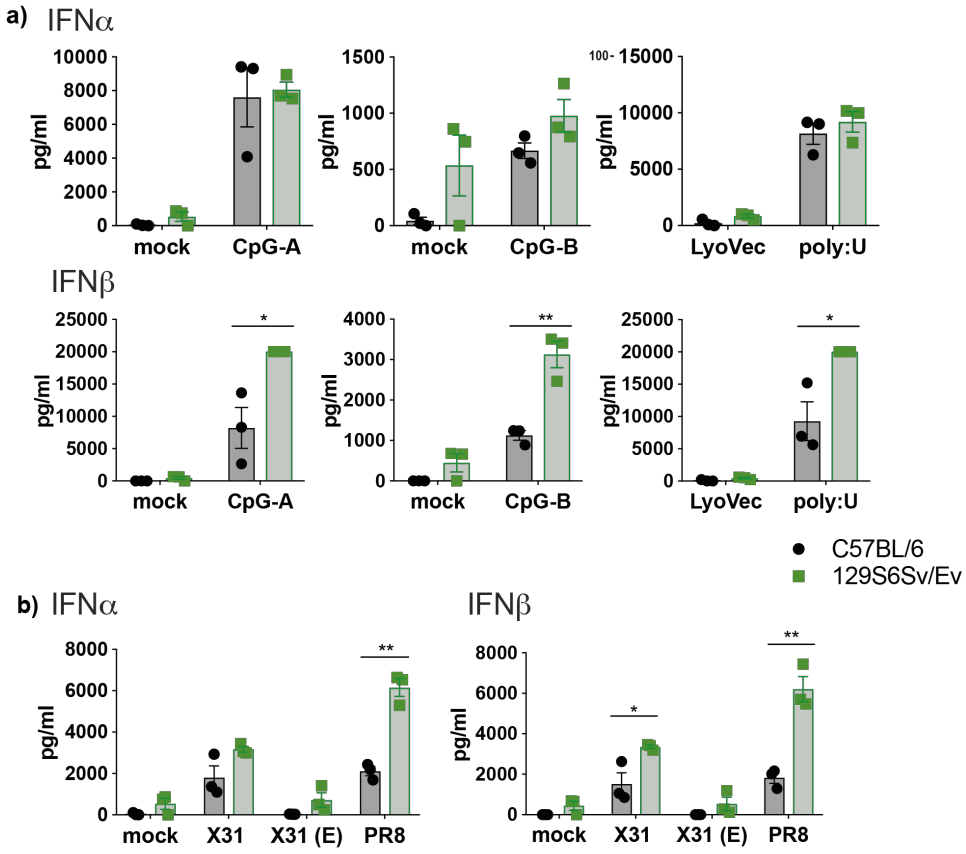

Figure 3.7 Flt3L-induced pDC-enriched cultures respond with significantly higher IFN-α/β protein secretion in the 129S6/SvEv background upon viral infection and TLR stimulation. A. pDC-enriched cultures were incubated for 24h with the indicated stimuli (CpG-A and CpG-B (ODN6618) for TLR9, LyoVec® transfected poly:U for TLR7 stimulation) and IFN-α/β secretion in the supernatant assessed by ELISA. **B.**

Similar to the BMDM experiment, pDC-enriched cell cultures were infected with X31 (MDCK- or egg-derived) or PR8 and IFN-α/β protein quantified by ELISA. Each symbol represents a technical replicate of a pooled bone marrow culture differentiated with Flt3L. Significance as per Mann-Whitney t-test * p<0.05; ** p<0.01; *** p<0.001; **** p<0.0001; non-significant comparisons are not shown. Data representative of six experiments.

3.2.3 IFN responses in absence of the IFNAR1-dependent IFN-α/β feedback loop

3.2.3.1 Ifnar-/- mouse susceptibility to IAV in vivo

Ifnar1-/- mice of the 129S7 and C57BL/6 backgrounds were infected with X31, and their weight loss and survival monitored for two weeks (Figure 3.8). 129S8 and C57BL/6 mice were used as WT controls. While *Ifnar1*-/- mice of both genotypes lost comparable amounts of weight, 129S7$^{Ifnar-/-}$ mice showed improved survival compared to the 129S8 controls (although remaining at 50% mortality). The survival curves of the two genotypes looked fairly similar during the first 10 days of the experiment, after which some of the 129S7$^{Ifnar-/-}$ mice started to recover and regain weight, whereas all the 129S8 mice succumbed to the infection. This was in concordance with previously published data which stated that blocking the IFNAR1 cascade can rescue 129 susceptibility to influenza (Davidson et al., 2014). Although the differences in weight loss between the two *Ifnar1-/-* genotypes were not noticeable, the survival of C57BL/6$^{Ifnar-/-}$ mice remained better than that of the 129S7$^{Ifnar-/-}$. This finding is discussed more in detail in the Discussion part of this chapter. However, as in other weight loss assays, mice that reached clinical endpoints were removed from the groups used for statistical analyses, so the resulting curves may appear more similar than they are in reality.

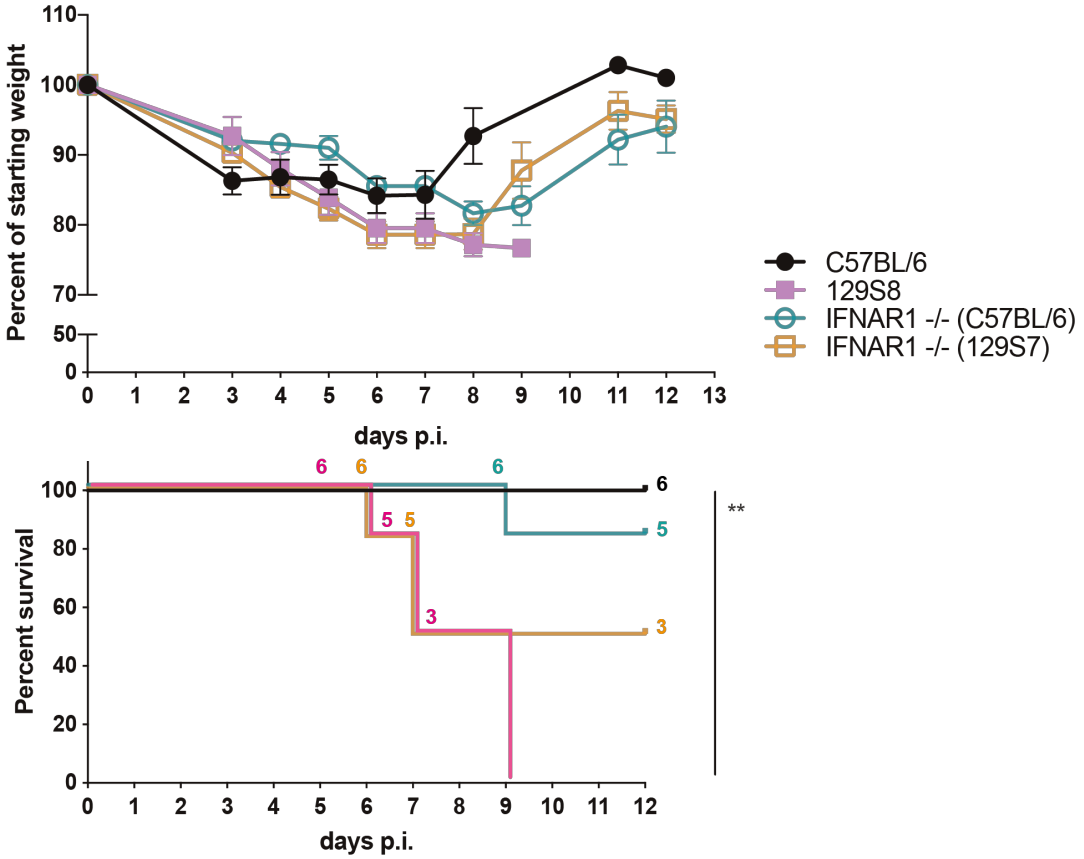

Figure 3.8 In absence of the IFNAR1 cascade, 129 mouse strain survival and weight loss are improved compared to the WT 129 mice – but survival is still lower than that of the C57BL/6$^{Ifnar1-/-}$ controls. 129S7$^{Ifnar1-/-}$ (n=6), C57BL/6$^{Ifnar1-/-}$ (n=5), 129S8 (n=5) and C57BL/6 (n=3) mice were infected with 800 $TCID_{50}$ X31 influenza virus per mouse, and their weight and survival were monitored. Coloured numbers in the survival curves indicate number of surviving mice at a given timepoint in infection. Weight loss curves statistical test: 2-way ANOVA, and survival curves: Mantel-Cox log-rank survival test (* $p<0.05$; ** $p<0.01$; *** $p<0.001$; **** $p<0.0001$; non-significant comparisons are not shown). Data representative of two independent assays.

3.2.3.2 Ifnar1-/- BM-derived cell responses in vitro

The increased *in vivo* susceptibility of the 129 background mice even in absence of the IFNAR cascade indicated a possible cause of increased IFN independent of the IFNAR receptor. However, it was unclear whether this increased susceptibility correlated with increased IFN *in vitro,* as sources of IFN production upstream of IFNAR can differ between cells and stimuli. Therefore, the *in vitro* responses of primary mouse cells were assessed *in vitro* in order to compare the IFN production of 129S7$^{Ifnar1-/-}$ and C57BL/6$^{Ifnar1-/-}$ mice.

Subsequently, responses to TLR/RLR stimuli and influenza virus of IFNAR1-/- cells were assessed *in vitro* in BMDMs and pDC-enriched cultures (respectively Figure 3.9a and Figure 3.9b). When stimulated with LPS (TLR4 recognition) or the influenza virus (RIG-I recognition), 129S7$^{Ifnar1-/-}$ BMDMs responded with significantly higher levels of IFN-β protein secreted compared to the C57BL/6$^{Ifnar1-/-}$. This difference in response was not observed in the case of stimulation with CpG-B (TLR9) but it is worth noting that the overall detected levels of IFN-β protein were extremely low, and close to the lower detection limit of the assay.

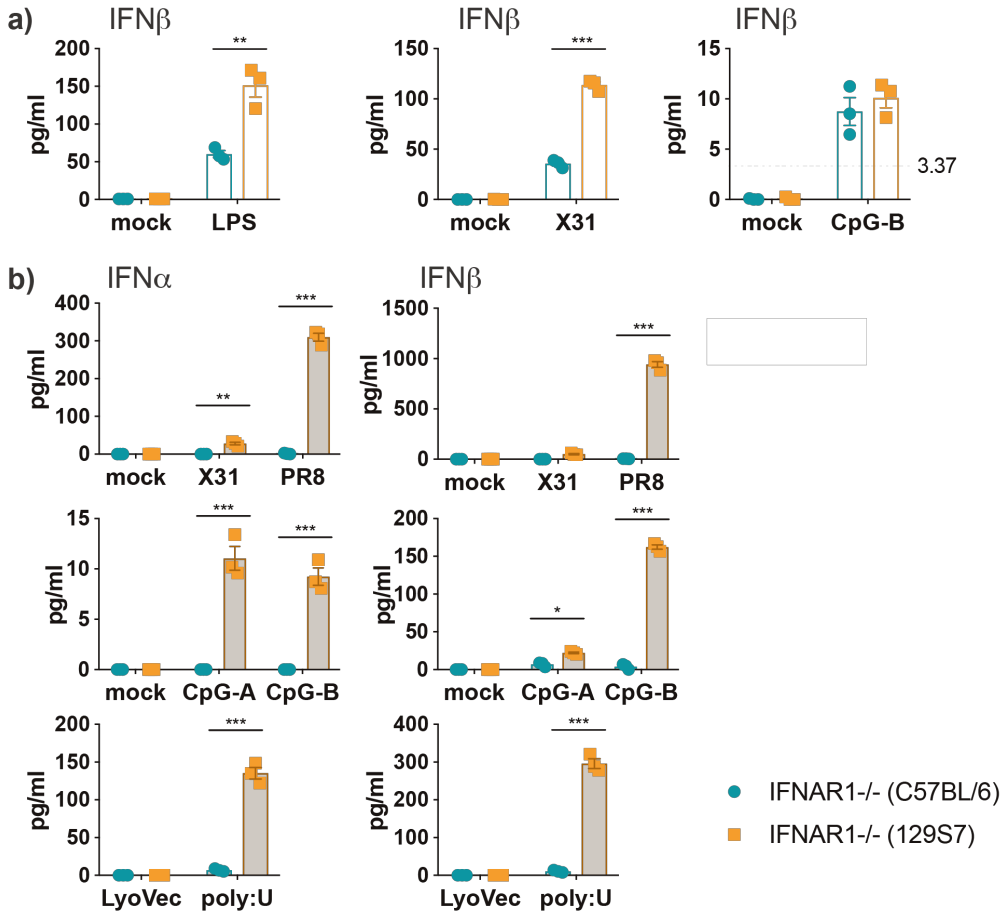

Figure 3.9 Even in the absence of IFNAR1 signalling, BMDMs and pDC-enriched cultures of the 129 background respond to TLR stimuli and influenza infection with higher IFN-α/β protein levels than the BL/6 controls.. A. 129S7$^{Ifnar1-/-}$ and C57BL/6$^{Ifnar1-/-}$ BMDMs were challenged with LPS, CpG-B or X31 influenza virus, and 24h later supernatants were collected and protein levels assessed by ELISA. Each symbol is a biological replicate, where cells originate from 1 mouse. The bars represent mean ± SEM. **B.** pDC-enriched cultures were challenged with influenza infection (X31 or PR8, both at 10^5 $TCID_{50}$/ml) or TLR stimuli (CpG-A, CpG-B and transfected poly:U) and supernatant IFN-α/β protein dosed by ELISA. Each symbol represents a technical replicate of a pooled bone marrow culture cultured as

indicated in Material and Methods. Statistical test: Mann-Whitney t-test: * p<0.05; ** p<0.01; *** p<0.001; **** p<0.0001; non-significant comparisons are not shown. Represented data is pooled from different assays (A. and B.) and representative of at least three independent experiments.

Since considerable amounts of produced type-I IFN in pDCs originate from the activation of a positive feedback loop via the IFNAR cascade, the overall levels of type-I IFN (Figure 3.9b) were considerably lower than in the WT BL/6 and 129 cells from previous results. However, it seems like IFNAR1-/- 129S7 pDCs still produce significantly higher amounts of IFN-α and IFN-β proteins than IFNAR1-/- C57BL/6 pDCs. This could be observed across different types of TLR stimuli tested, as well as during infection with X31 and PR8. In the case of IFN-β production in X31 infection, the protein levels recorded were very low and no significant difference was observed.

Finally, mRNA synthesis activation was also tested in IFNAR1-/- BMDMs, in order to compare the results with the previous data obtained in WT-cells. Similar to the WT scenario, very little differences between IFNAR1-/- 129S7 and IFNAR1-/- BL/6 BMDMs could be observed. Only in the case of IL-6 production in LPS and CpG-B stimulations did the 129 background show higher activation of transcription than the BL/6 (Figure 3.10a). CpG-A-induced *Ifnβ1* transcription was also addressed in slightly earlier stages of stimulation in a separate experiment (Figure 3.10b). Up until 8h of stimulation, a tendency for higher *Ifnβ1* expression was observed in the 129S7$^{Ifnar1-/-}$ BMDMs. The slight difference in CpG-A 3h stimulation time point between Figure 3.10a and Figure 3.10b is also indicative of inter-experimental variation in these assays. Also, the mRNA expression of IRF3, the master regulator of *Ifnβ1* transcription, was unchanged across all conditions and similar between the two genotypes.

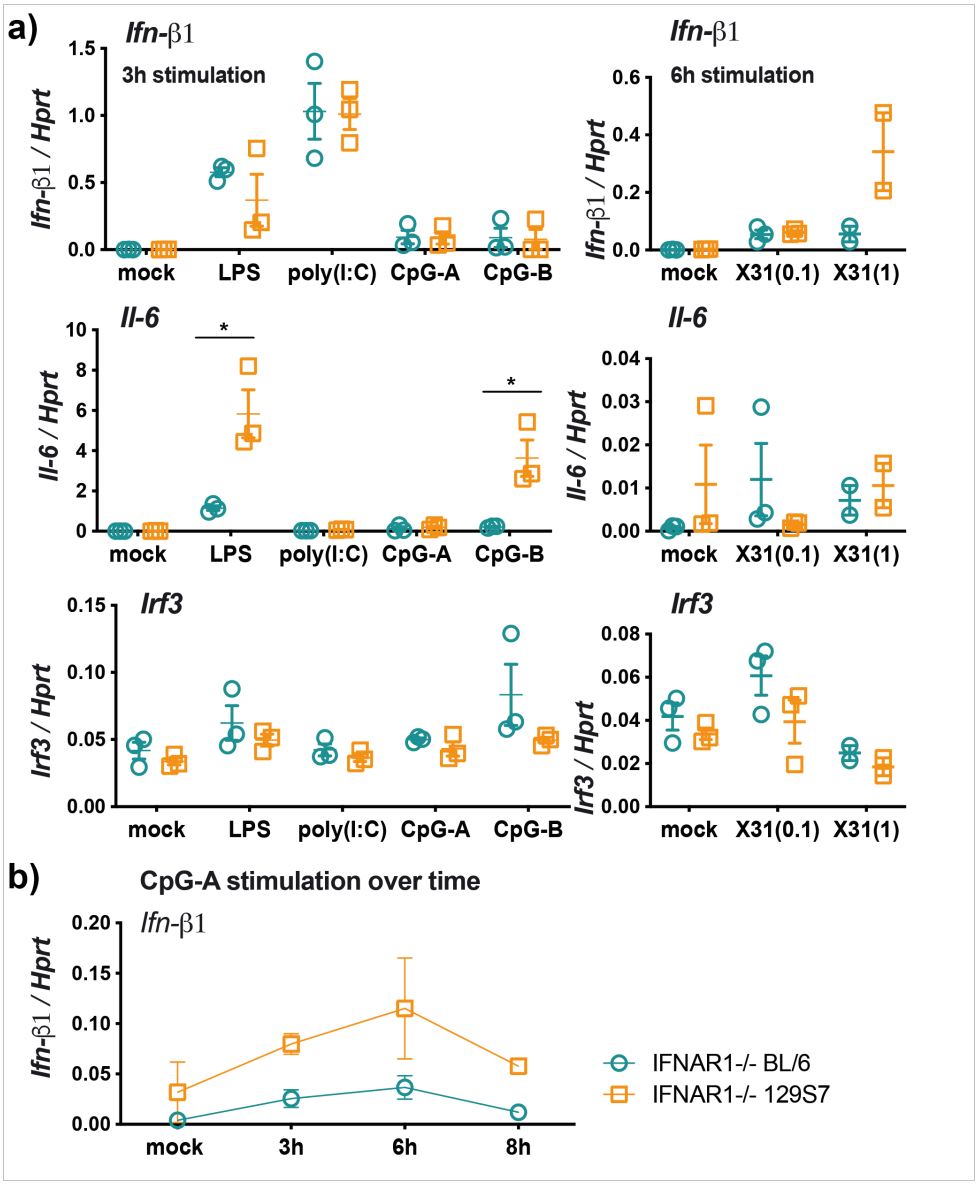

Figure 3.10 mRNA synthesis 6h following stimulation is similar between the 129 and BL/6 backgrounds in absence of the IFNAR cascade; *Ifn-β1* mRNA production 3h after CpG-A induction is slightly increased compared to the BL/6 background.

A. BMDMs from IFNAR1-/- 129S7 and IFNAR1-/- BL/6 mice were incubated for 6h in vitro with the indicated stimuli, after which levels of *Ifn-β1*, *Il-6* and *Irf3* mRNA were quantified by QPCR. ***B.*** BMDMs were stimulated with CpG-A and the expression of *Ifn-β1* mRNA quantified by QPCR in time. Each symbol represents a technical replicate of a pooled bone marrow culture cultured as indicated in Material and Methods. Mann-Whitney t-test * p<0.05; ** p<0.01; *** p<0.001; **** p<0.0001; non-significant comparisons are not shown. Data in A. and B. representative of two independent assays.

3.2.4 Dependence of the type-I IFN high-responder phenotype-I*n vitro* on newly synthetized proteins

Given that data seemingly indicated that the origin of high IFN production in infection could be upstream of IFNAR, it was next verified whether it depended on newly synthetized proteins. To this end, a reliable blocker of *de novo* protein synthesis, cycloheximide, was used. BMDMs were incubated with cycloheximide prior to and during a challenge with LPS. The early responses, mirrored by the triggering of mRNA synthesis, were recorded over a short period of time (to minimise cycloheximide toxicity) in C57BL/6$^{Ifnar1-/-}$ and 129S7$^{Ifnar1-/-}$ BMDMs (Figure 3.11). DMSO treatment was used as a control because cycloheximide is dissolved in this solvent.

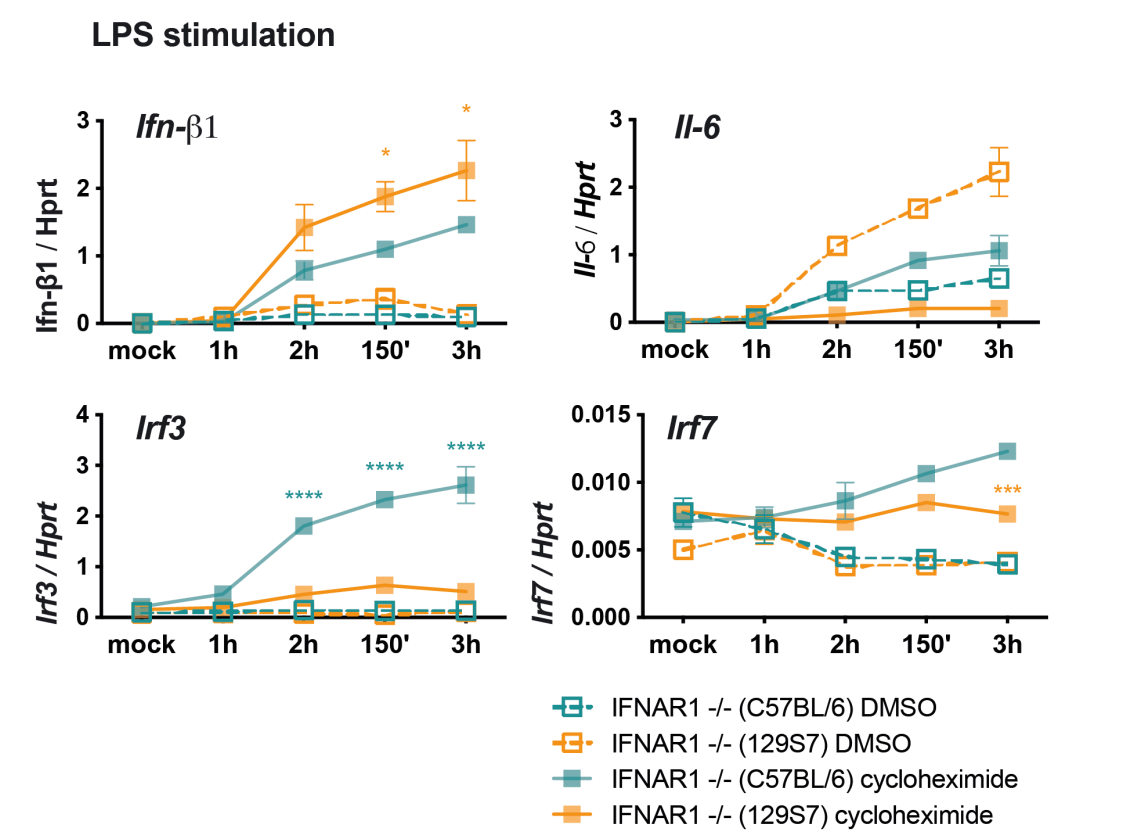

Figure 3.11 Blockade of de novo protein synthesis by cycloheximide provokes a surge in *Ifn-β1* transcription after LPS stimulation, significantly higher in 129S7$^{Ifnar1-/-}$ BMDMs. BMDMs from C57BL/6$^{Ifnar1-/-}$ and 129S7$^{Ifnar1-/-}$ mice were incubated with cycloheximide or DMSO for 1h prior and during stimulation with LPS for the indicated times. Dashed lines and empty symbols represent conditions pre-treated with DMSO, and full lines and symbols cycloheximide-treated cells. Each symbol is a mean±SEM representation of 3 biological replicates (3 mice) and is represented as fold increase relative to the expression of the housekeeping gene

Hprt. Statistical significance was assessed by a 2-way ANOVA with multiple comparisons correction for genotype-driven differences in the corresponding conditions (* $p<0.05$; ** $p<0.01$; *** $p<0.001$; **** $p<0.0001$; non-significant comparisons are not shown). Results representative of two independent experiments.

The observed *Ifn-β1* mRNA levels were significantly higher in both genotypes when cells were exposed to cycloheximide. Moreover, IFNAR1-/- 129S7 BMDMs responded with higher levels of *Ifn-β1* mRNA than their IFNAR1-/- BL/6 counterparts. The inverse was observed for *Il-6* mRNA, where cells treated with cycloheximide exhibited overall lower activation of *Il-6* transcription in the case of IFNAR1-/- 129 cells. The levels of *Irf7*, an ISG, were found to be very low and overall similar in time between genotypes, although they were marginally higher during cycloheximide exposure. Somewhat unexpectedly, higher *Irf3* mRNA levels were observed in the IFNAR1-/- BL6 BMDMs than in the 129 background (Figure 3.11), although this was only the case when cells were treated with cycloheximide. Without cycloheximide exposure, the overall transcription of *Irf3* was fairly low and similar between the two genotypes.

Further, a similar experiment was performed in WT BMDMs, with LPS stimulation, poly(I:C) stimulation or X31 infection. As in IFNAR1-/- BMDMs, cycloheximide treatment in WT-cells resulted in an increase in mRNA synthesis of *Ifn-β1* (Figure 3.12a), and this in both LPS and poly(I:C) stimulation settings. However, in neither of the cases was there a significant difference in *Ifn-β1* mRNA between BL/6 and 129 backgrounds. *Il-6* transcription was abrogated in presence of cycloheximide upon LPS stimulation, confirming the IFNAR1-/- observations. However, treatment with poly(I:C) in the absence of newly synthetized proteins induced a slight increase of *Il-6* mRNA production in the 129 background in time. As expected, *Stat1* mRNA production was abrogated soon after the beginning of stimulation, as *Stat1* transcription is the result of IFNAR cascade activation and new protein synthesis. There was also no observable difference between the 129 and BL/6 backgrounds.

As with TLR stimulation, RIG-I activation by X31 infection of BMDMs resulted, in time, in a strong increase in *Ifn-β1* transcription in presence of cycloheximide (Figure 3.12b). It seems like there is a beginning of a trend for high response in the 129 background, which might continue to become significant at a later timepoint not

investigated in this experiment. Similar results with a slightly more noticeable difference between 129 and BL/6 backgrounds, were observed for *Il-6* mRNA. Ultimately, *Stat1* transcription patterns in X31 infection followed those of LPS and poly(I:C). It seems from this experiment that a common negative regulator produced *de novo* upon stimulation could be restraining *Ifn-β1* and *Il-6* responses. It is also possible that the stress endured by the cells upon exposure to cycloheximide is modifying their responses, which would render the results uninterpretable.

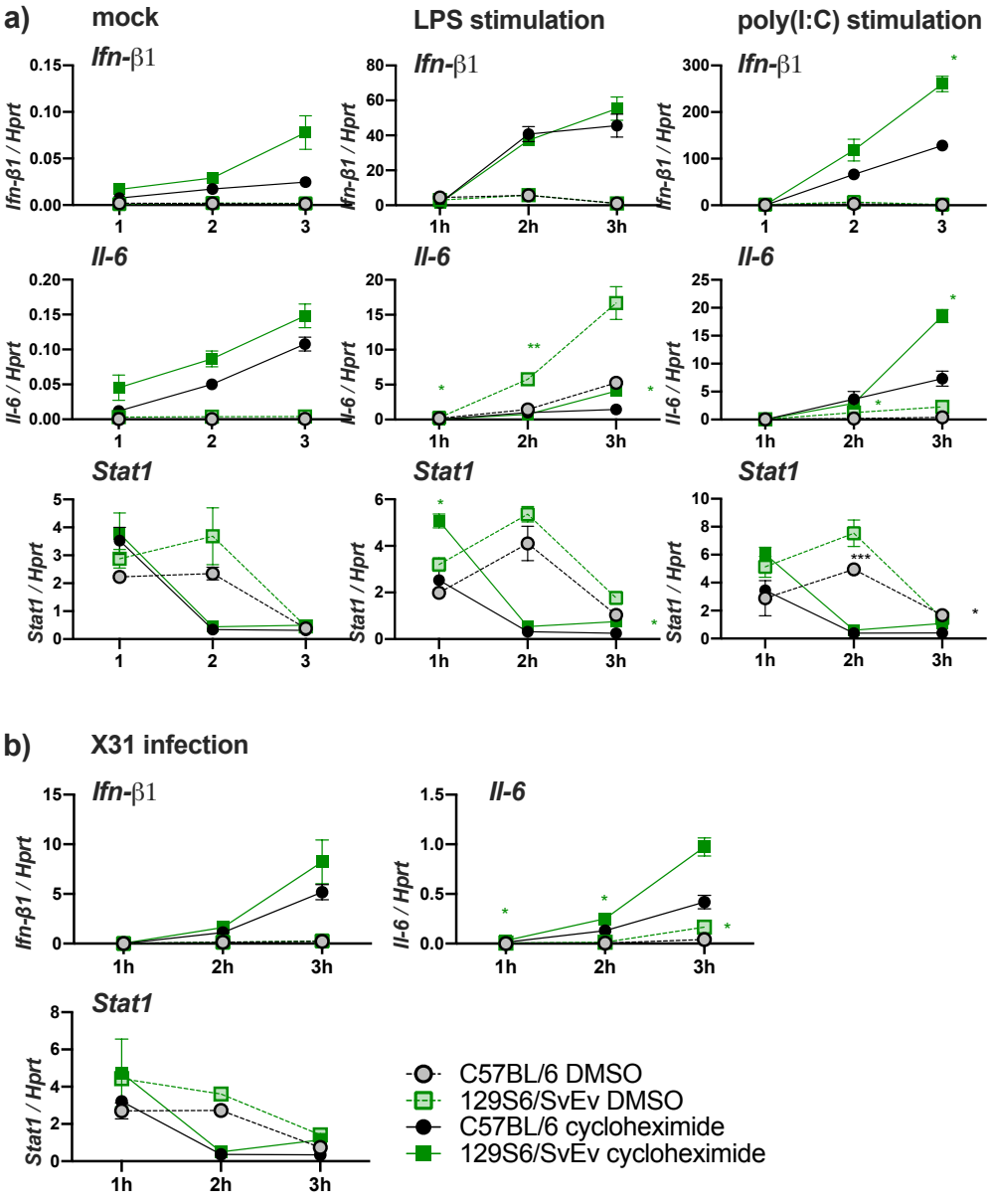

Figure 3.12 Blockade of de novo protein synthesis by cycloheximide provokes a surge in *Ifn-β1* transcription with stimulus-dependent differences between BL/6 and 129S6/SvEv genotypes. WT BL/6 and 129S6 BMDMs were exposed to

cycloheximide or DMSO for 1h prior and during **A.** stimulation with LPS or poly(I:C) or **B.** infection with X31, for the indicated times. Dashed lines and empty symbols represent cells pre-treated with DMSO, and full lines and symbols cycloheximide-treated cells. Each symbol is a mean±SEM representation of 3 biological replicates and is plotted as fold increase relative to the expression of the housekeeping gene *Hprt*. Statistical significance was tested in a 2-way ANOVA with multiple comparisons correction (* $p<0.05$; ** $p<0.01$; *** $p<0.001$; **** $p<0.0001$; non-significant comparisons are not shown) in the corresponding DMSO or cycloheximide conditions between the two genotype backgrounds, and are therefore testing for genotype-dependent differences. Data representative of two independent experiments.

3.3 Discussion

3.3.1 *In vivo* susceptibility of 129S6/SvEv mouse strain compared to previous findings

The presented results in WT mice *in vivo* have indicated that the 129S6 susceptibility phenotype-Is similar to that of the 129S7 and 129S8 strains, with higher mortality and stronger IFN-α/β *in vivo* responses in the lung of these mice compared to BL/6 controls.

It is however important to note that the results presented in this chapter point to another possible source of increased susceptibility to influenza in the 129 background. The weight loss and survival assays in *Ifnar-/-* mice showed that the BL/6 strain had a clear survival advantage regardless of the IFNAR cascade. Suppressing this signaling pathway would isolate the IFNAR-upstream relative effects as the only source of IFN and cytokine production in these mice. The results observed pointed to a possible inherent, IFNAR cascade-independent differences at the origin of the difference in susceptibility between BL/6 and 129 mice. This is however contradictory to the findings from (Davidson et al., 2014) which determined the interaction of TRAIL/DR5 as a downstream effect of IFN-α/β on survival. Given that both TRAIL and DR5 are ISGs, suppressing the IFNAR cascade would have resulted in similar phenotypes between *Ifnar1-/-* mice regardless of their background, but this is not observed in this work. Another possibility is that the phenotype differences observed in this case are not due to IFN-α/β at all, but rather to cytokine production. Effectively, 129 strain of mice was shown in the work from (Davidson et al., 2014) to exhibit a cytokine storm during influenza infection. Namely, 129 mice

showed higher production of pro-inflammatory cytokines compared to the BL/6 strain. It is therefore possible that the susceptibility phenotype of the 129 mice is due, at least in part, to high pro-inflammatory cytokine production.

Also, a surge of pro-inflammatory cytokines and pDC and cDC recruitment was observed as early as 2 days post-infection in the 129S6 mice compared to BL/6 controls, in concordance with susceptibility data. However, while it is known that AM numbers plummet after infection, I currently have no good explanation for significantly lower proportions of AMs in 129 mice observed at day 2 post-infection. It is worth noting that in other experiments this difference was not striking, therefore it is possible that the represented result is due to experimental variability or other conditions during infection. Namely, recent unpublished findings from our team have indicated that microbiome can affect influenza infection susceptibility in the 129S6 strain. Our team has been probing different 129S6 mice for presence of segmented filamentous bacteria, and found that some mice were positive and others not. This could partly explain the variations in results that I have observed. The SFB-positivity will therefore be considered in future experiments. Ultimately, the *in vivo* phenotype of the 129 mice was previously addressed in detail in work from (Davidson et al., 2014), and the goal of this introductory chapter of this thesis was to reproduce this phenotype-In a subtype of 129 mice. Since this was achieved with success, more focus was brought upon elucidating the molecular signaling pathways that cause the observed phenotype-In different *in vitro* assays.

As previously indicated, PDCA-1 is an ISG whose expression is upregulated on activated immune cells upon detection of IFN. Since a pan-α-PDCA1 antibody was used *in vivo* in 129S8 mice to block pDC-driven IFN production (Davidson et al., 2014), it was interesting to observe that in this system PDCA-1 is significantly more present on 129S6 inflammatory monocytes, cDCs and alveolar macrophages. This result indicated a higher activation of ISG production *in vivo* in innate immune cells in the 129 compared to the BL/6 background. Moreover, this result could also indicate that, while the increased IFN production in the 129 background could originate from upstream of IFNAR, it could be further amplified by the increased activity of the Jak/Stat pathway. The expression of PDCA-1 on pDCs was not represented because positivity for this marker was used as a gating criterion (see Appendix Figure 8.1 and Figure 8.2). This result indicates that the *in vivo* reduction of IFN-α/β levels could not be attributed solely to pDCs, as monocytes, DCs and

alveolar macrophages are also important sources of *in vivo* IFN-α/β (Swiecki and Colonna, 2011).

3.3.2 *In vitro* stimulation of 129S6/SvEv BMDMs and pDCs

In both BMDM and pDC stimulations *in vitro,* the phenotype of stronger 129S6 responses was generally observed with different stimuli. I will address the separate stimuli results more in detail in the general discussion, as their analysis will be more informative by comparing them with results still to follow. Interestingly, both *in vivo* and *in vitro* I was unable, through multiple different experiments, to observe robust and reproducibly significant differences in mRNA expression of *Ifn-β1* between the two genotypes. It is essential to note that experimental variability was observed in these assays and that the results should be interpreted with some caution. However, this result (and the variability) could also be indicative of post-transcriptional or post-translational differences between genotypes. It is imaginable that the IFN and cytokine mRNA, although initially expressed at the same level as in the BL/6 cells, is more stable in the 129 background due to an absence of quality control or degradation mechanisms, which could result in an ultimate increase in protein synthesis. Alternatively, the protein synthesis or export could be differentially regulated in the two backgrounds. This will be further developed in the Discussion chapter of this thesis.

Ultimately, it seems like the 129 phenotype originates upstream of the IFNAR1 cascade, as globally IFNAR1-/- mice *in vivo* and *in vitro* mirror the WT counterpart phenotypes. The subtle indication of this result points towards a pathway deregulation upstream of the IFNAR receptor, or to an inherent property of the 129 genotype that primes it for stronger responses in infection. However, based on these results, it cannot be excluded that a difference in regulation dependent the IFNAR cascade amplifies the initial high responses in 129 mice.

Cycloheximide-driven blockade of newly synthetized proteins yielded few differences between the two genotypes. While the behaviour of the whole system tends to change with cycloheximide introduction (molecular brakes of *Ifn-β1* transcription are lifted, for example, indicating a possible SOCS1 blockade), the differences between genotypes were observed only in some cases, namely in WT setting in TLR3 stimulation with poly(I:C), or in IFNAR1-/- cells in stimulation with

LPS (not reliably reproduced in the WT-cells). However, an interesting pattern in IL-6 expression regulation was observed, where newly synthetised proteins were necessary for IL-6 expression in TLR4 stimulation, but not in TLR3 activation or in absence of stimulus. The same findings in LPS stimulation were found in IFNAR1-/- cells. In both cases, the effect of cycloheximide on IL-6 expression was largely genotype-Independent, with transcription abrogation noted in both BL/6 and 129S6 backgrounds. TLR4 signaling relies on MyD88-dependent branch for NFκB activation, but also shares a TRAF3/TRIF MyD88-independent branch with the TLR3 signaling cascade, resulting in NFκB activation. MyD88 is a known ISG, so it is imaginable that cycloheximide could specifically affect the signaling cascade downstream of MyD88. The *Ifn-β1* expression seems unaffected by cycloheximide treatment in BMDMs, indicating a dependence on a non-ISG transcription factor. This finding is in concordance with the fact that IRF3 is the master regulator of IFN expression in macrophages, and that it was shown in this chapter that the *Irf3* expression is unhindered (and even stimulated) by cycloheximide in IFNAR1-/- cells.

3.3.3 Overall conclusion

Generally, while some experimental variation was observed and reported in this chapter, a reproducible positive correlation between high IFN-α/β production and influenza susceptibility was observed in comparisons of BL/6 and 129S6 mice *in vivo*. Overall, higher IFN and cytokine productions were observed *in vitro* in 129 cells as well, although the intensity of the differences depended strongly on the cell type and the stimulus and was prone to variation. While variations were observed in IFN-β protein expression to *in vitro* stimulations, IFN-α responses were more reproducibly higher in the 129 background. This could possibly indicate a synergy between cascades upstream and downstream of IFNAR to produce such a signature high response in 129 mice. However, the results from this chapter have proven that signaling cascades preceding IFNAR signaling are sufficient to generate significant differences both *in vivo* and *in vitro* between BL/6 and 129S6 mice in IFN production and ultimately influenza susceptibility. A candidate locus possibly involved in generating these disparities is addressed in the following Results chapter.

Chapter 4. Results 2 : Susceptibility to influenza and the *in vitro* responses of a congenic 129S6 mouse strain, 129.C3BR17

4.1 Introduction

Previous experiments have shown that the causes of elevated IFN-α/β production could originate from upstream of the IFNAR-mediated autocrine loop. However, no candidate genetic region or candidate gene causing high IFN production had been investigated in detail.

As mentioned in the Introduction of this thesis, a congenic mouse model of 129S6 origin was created by the team of Fiona Powrie in 2012 (Boulard et al., 2012). The study showed that the high susceptibility to *H.hepaticus*-induced colitis in 129S6 mice is rescued in the congenic model. The congenic mice, carrying a 1.7Mb locus named R17 (or *Hiccs*) of BL/6 origin on Chromosome 3 in the place of the endogenous 129S6 one, had lowered morbidity and mortality in infection with *H.hepaticus* compared to 129S6 controls (Boulard et al., 2012).

Compared to the colitis-resistant C57BL/6 strain, 129S6 mice showed increased intestinal inflammation and, in consequence to long term *H.hepaticus* infection, development of neoplastic lesions and cancer (Boulard et al., 2012). By inserting the congenic *Hiccs* (R17) locus of BL/6 origin into the susceptible mice, a decrease in production of pro-inflammatory cytokines (IL-17, IL-22, MIP-1α, TNF-α) was observed in the intestine (Boulard et al., 2012). Moreover, congenic mice were less likely to develop neoplasia and colon cancer on the long term.

The *Hiccs* (R17) locus is a telomeric region containing three hypothetical and five identified genes, as well as five miRNAs. Amongst known protein-coding genes are *Larp7*, *Neurog2*, *Alpk1*, *Tifa* and *Ap1ar*. *Larp7* was shown to participate in telomere maintenance (Holohan et al., 2016), while *Neurog2* mediates neuronal reprogramming (Smith et al., 2016). *Tifa* encodes a binding partner protein of TRAF6 (Takatsuna et al., 2003) and, interestingly, *Alpk1* as well (Milivojevic et al., 2017). The roles of *Alpk1* were less well described at the beginning of this work, but the encoded protein has now been implicated in innate immune responses to bacteria (see Chatper 5 for more detail) (Zhou et al., 2018). Meanwhile, *Ap1ar* was implicated

in endosomal transport and linked to pro-inflammatory responses through a binding partner protein in TLR4 signalling (Mertins et al., 2017).

In the same study, (Boulard et al., 2012) examined the R17 locus and its components by sequencing and expression analyses to compare the 129S6 and C57BL/6 strains. The mRNA expression of different genes in the colon was compared between congenic mice with the R17 locus of BL/6 origin (129.C3BR17 mice), and the susceptible negative controls bearing a different BL/6 congenic locus. *Ap1ar* was found to be more highly expressed in resistant 129.C3BR17 mice, whereas *Alpk1* expression was lower compared to susceptible strains. Amongst protein-encoding genes in the locus, only *Alpk1* and *Larp7* exonic sequences contained missense variants between BL/6 and 129S6 genomes, respectively 17 and 2. The total number of exonic polymorphisms between BL/6 and 129S6 sequences reported for these two genes was respectively 31 and 8 (Boulard et al., 2012).

Given these findings and clear parallels to our influenza model, the R17 locus was interesting to study as a candidate locus for high IFN-α/β production and increased influenza susceptibility (Davidson et al., 2014). In this chapter, I show results of *in vivo* and *in vitro* experiments aimed at comparing this congenic mouse strain with 129S6 and BL/6 controls. The assays performed *in vivo* probed for susceptibility to influenza infection in congenic mice, as well as IFN-α/β and cytokine production and immune cell recruitment in the lung.

To study whether the origin of the R17 locus (BL/6 or 129S6) could modulate the pathways leading to IFN production, *in vitro* experiments on previously described BMDM and pDC-enriched cultures were performed. In this chapter, I show comparisons of mRNA synthesis and protein secretion upon influenza infection or receptor pathway activation in BL/6, 129S6 and 129.C3BR17 cells. In addition, early pathway activation events are studied by assessing phosphorylation levels of some key factors leading to IFN and cytokine production. Notably, phosphorylation of TBK1 and NFκB p65 subunit in Toll-like receptor pathways (Kawai and Akira, 2011), (Gilliet et al., 2008), influenza recognition via RIG-I (Goraya et al., 2015) and cGAS/STING activation (Chen et al., 2016), are compared in BL/6, 129S6 and 129.C3BR17 BMDMs.

All the genes contained within the R17 locus (see Introduction) had been sequenced in the 129 background by Powrie and her team (Boulard et al., 2012).

One of them, *Alpk1*, was found to have 17 non-synonymous mutations in the 129 background compared to BL/6. In this chapter, I show the mRNA expression of different genes from this locus in BMDMs of BL/6, 129S6 and congenic mice. This was done with the goal to assess whether the transcription of any of these genes is controlled locally (from within the R17 locus), and whether it was influenced by influenza infection or receptor pathway stimulation.

4.2 Results

4.2.1 *In vivo* studies of the congenic 129.C3BR17 strain: susceptibility and *in vivo* IFN-α/β and cytokine production in response to influenza

The susceptibility to influenza of 129.C3BR17 mice was tested by following their weight loss and survival for two weeks post-infection and comparing it to the 129S6 and BL/6 controls (Figure 4.1).

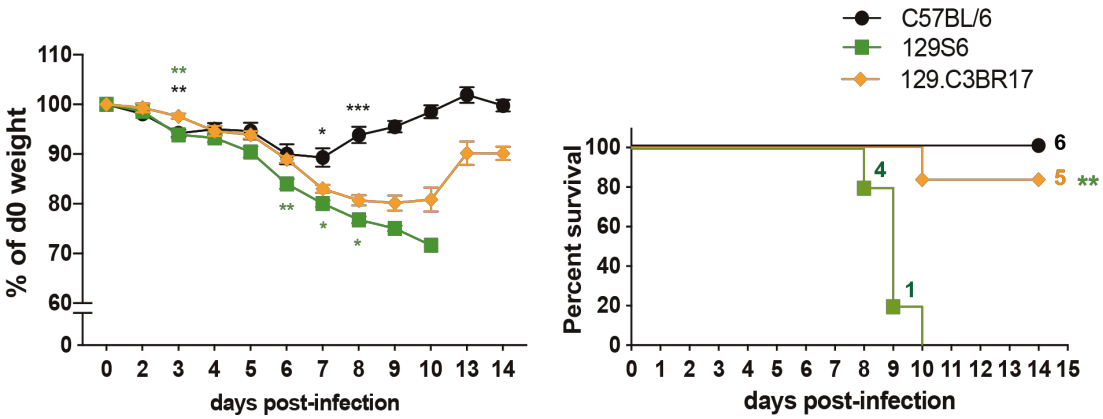

Figure 4.1 Weight loss patterns of 129.C3BR17 and 129S6 mice are similar up to day 10 post-infection, but the overall survival of infected 129.C3BR17 mice is significantly improved. C57BL/6 mice (n=6), 129S6 mice (n=5) and 129.C3BR17 mice (n=6) were infected with the X31 influenza virus at 3500 $TCID_{50}$ / mouse. Numbers in corresponding colours indicate the number of mice at an indicated day post-infection (survival curves). Their weight loss and survival were monitored for 14 days. Weight loss curves statistical tests 2-way ANOVA, compared BL/6 and 129S6 survival curves separately to the 129.C3BR17 one. Indicated significance in green indicates significant differences 129S6 vs 129.C3BR17 and in black BL/6 vs 129.C3BR17 (significance * $p<0.05$; ** $p<0.01$; $p<0.001$). Survival tests log-rank (Mantel-Cox, significance ** $p=0.0024$). Where no stars are indicated, no statistical significance was found during testing. Data representative of five independent experiments.

Interestingly, the 129.C3BR17 congenic mice showed improved survival compared to the 129S6 mice (which had 100% mortality). This result demonstrated that substituting the endogenous R17 locus for its BL/6 allele is sufficient to improve the survival of the 129 strain in influenza infection. It is therefore possible that one or more gene(s) within this locus, when in a 129 copy, contribute to the increased susceptibility to influenza of 129 mice. However, the result represented here is the most striking of all that were obtained when repeating this experiment. The survival of R17 mice ranged from 50% to 100%, whereas the weight loss patterns were reproducibly similar to those of 129S6 mice up to day 10 of infection. This could be due to varying infection conditions or perhaps some other environmental factor.

As increased IFN-α/β and cytokine levels in 129S6 mice are associated with poor survival in influenza, 129.C3BR17 BAL was probed for these proteins at different times post-infection (Figure 4.2). At the peak time of IFN synthesis (day 2 post-infection, Figure 4.2a), significantly less of IFN-α/β was detected in the BAL of congenic mice than in 129S6 mice. A similar trend was observed for IL-28 (IFN-λ) as well. Overall, at later points of infection, less type-I IFN is present in the lungs of infected mice, and IL-6 expression remains induced throughout the infection. Therefore, at day 4, and especially at day 7 post-infection (Figure 4.2b), the differences in IFN synthesis between 129S6 and congenic mice are less pronounced. Interestingly, the expression of IL-6 in the lung of congenic mice was not significantly different to that of the 129S6 control, in all three analysed timepoints post-infection.

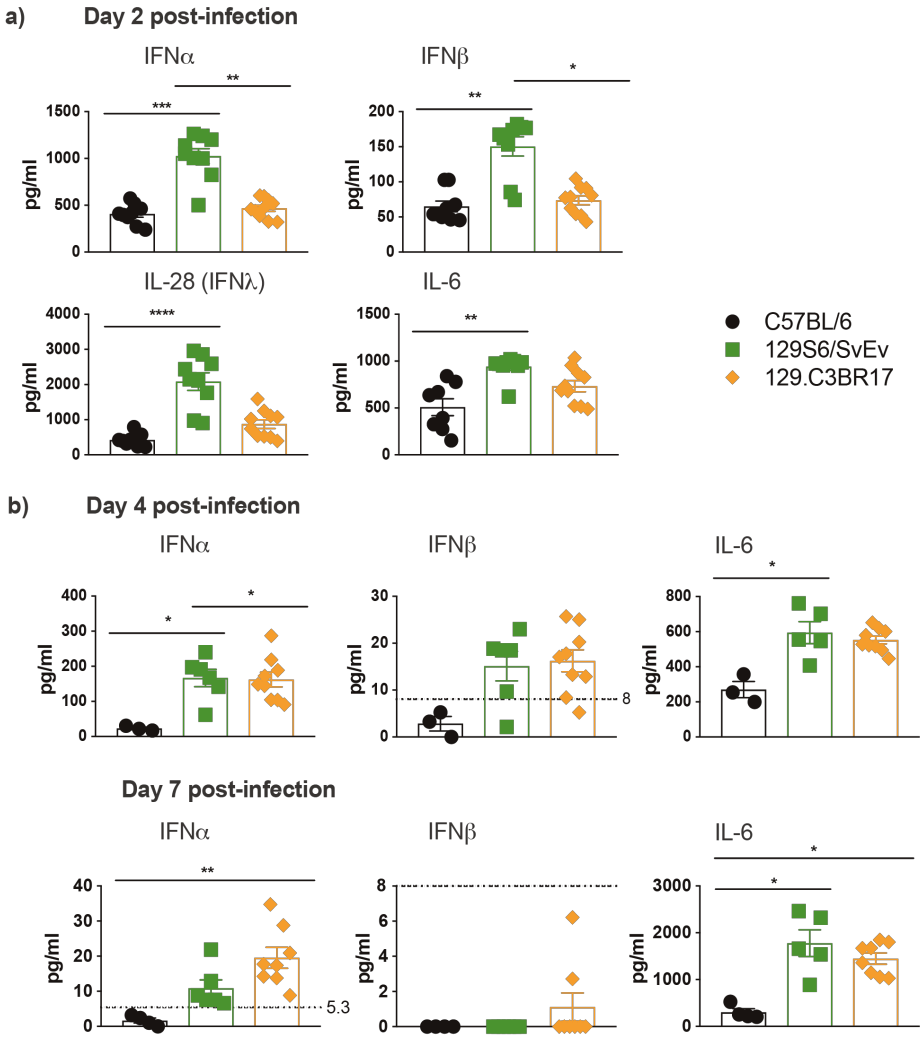

Figure 4.2 Type-I IFN responses in the BAL of infected congenic mice are reduced in amplitude compared to the 129S6 controls, while IL-6 levels are similar between the two genotypes. Mice were infected with X31 at 3500 $TCID_{50}$ / mouse and IFN-α,-β,-λ and IL-6 protein levels assessed in the BAL fluid by ELISA at the indicated times post-infection. **A.** 2 days, **B.** 4 days and 7 days. Each symbol represents one mouse and experiments in a) and b) are independent. Statistical test: Kruskal-Wallis ANOVA test with no assumption of normal distribution of data. * $p<0.05$; ** $p<0.01$; *** $p<0.001$; **** $p<0.0001$; non-significant comparisons are not shown. Data in A. representative of three experiments, and data in B. and C. of one experiment each.

As part of the influenza-induced morbidity phenotype-In 129S6 mice, a cytokine storm (a surge in pro-inflammatory cytokine production), was described in this background. In Chapter 1 it is demonstrated that levels of different cytokines and chemokines are higher in 129S6 lungs than in the BL/6 controls. Since type-I IFN production is lowered in congenic mice compared to 129S6 mice, the next step was to assess the levels of cytokines and chemokines in the lung of congenic mice two

days after infection (Figure 4.3). While the IL-6 levels showed a trend for reduction in the 129.C3BR17 mice, this was not significant, thus confirming previous findings. Similar trends were observed for IL-12p70, IL-1β, TNF-α and GM-CSF. In the case of IL-27, MCP-1 and MIP-1α and β, a statistically significant reduction compared to 129S6 levels was observed in congenic mice. These molecules are pro-inflammatory cytokines and chemokines and participate in the recruitment of monocytes and other immune cells to the infected lung. This result, in light of other findings in this chapter, will be analysed more in detail in the Discussion of this chapter.

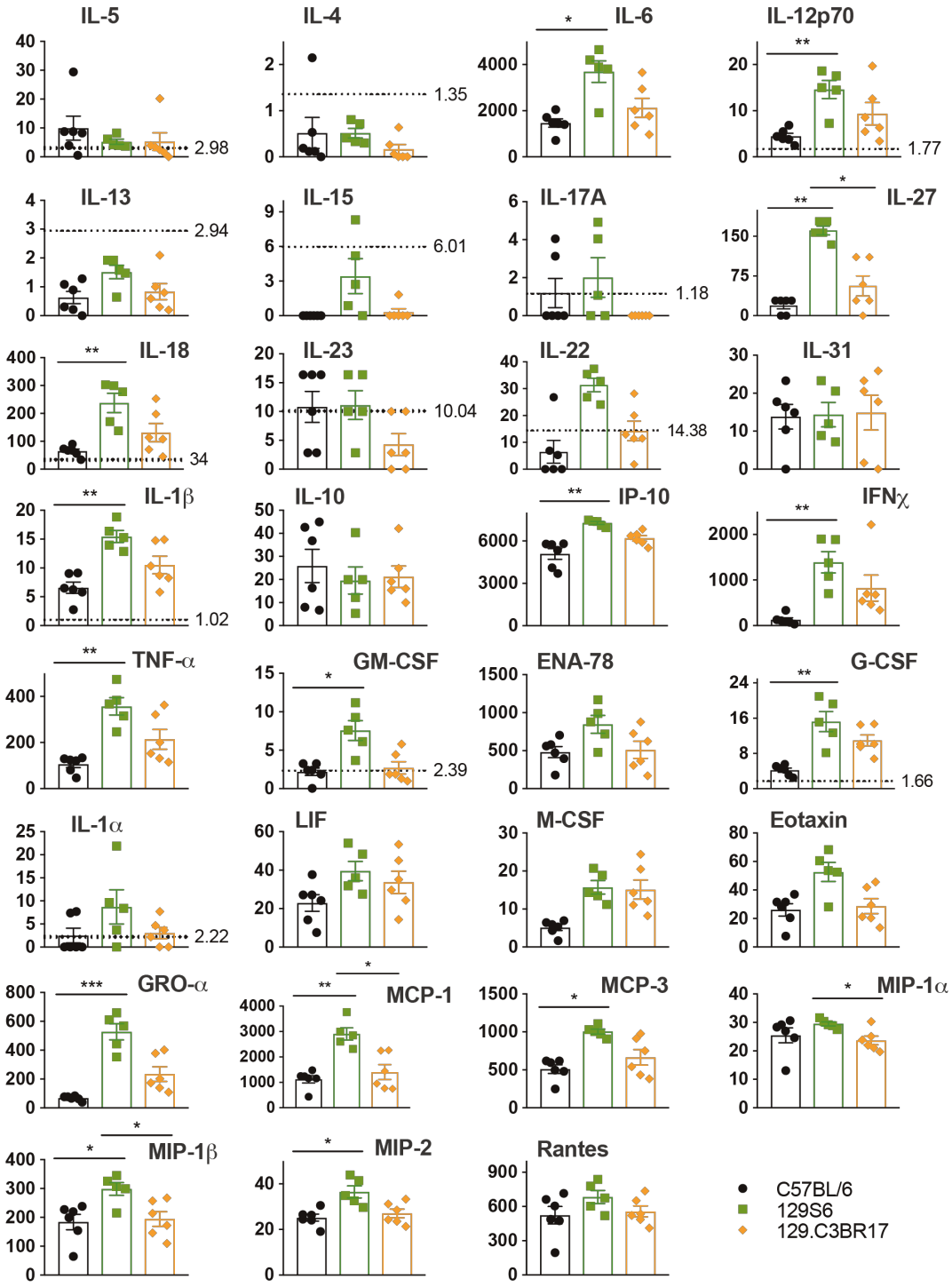

Figure 4.3 The lung of 129.C3BR17 mice at day 2 post-infection contains less IL-27, MCP-1, MIP-1α and MIP-1β, whereas multiple other pro-inflammatory cytokines are at the same level as in 129S6 mice. BL/6, 129S6 and 129.C3BR17 mice were infected with X31, and at day 2 post-infection, different cytokines and chemokines were quantified in the BAL by a multiplex ELISA assay. Each symbol represents one mouse. All values on y axes are represented as protein quantities in pg/ml. Dashed lines represent the lower detection limit where relevant (the exact limit in pg/ml being

denoted by the number on the right). Statistical test: Kruskal-Wallis ANOVA (no assumption of normal distribution of data) * $p<0.05$; ** $p<0.01$; *** $p<0.001$; **** $p<0.0001$; non-significant comparisons are not shown. Data from one experiment.

Given the multiplex results, it was interesting to compare the recruitment of immune cells to the lung at day 2 post-infection between congenic mice and the BL/6 and 129S6 controls (Figure 4.4a). Proportions of eosinophils, neutrophils and dendritic cells remained higher than in the BL/6 mice, following the 129S6 trend. CD4+ T-cell proportions early in infection were also slightly higher in the congenic mice than in the BL/6 mice. Like 129S6 mice, congenic mice also had highly reduced proportions of B-cells in the lung, significantly lower than in the BL/6 controls. Inversely, pDC proportions showed a clear trend of reduction compared to 129S6 mice, which was in concordance with the previous observation that IFN-α/β levels in the lungs of congenic mice were lowered compared to 129S6 mice. Significant reduction in PDCA-1 expression on 129.C3BR17 lung-dwelling immune cells compared to 129S6 one was detected only on dendritic cells, indicating a possible lower activation of these cells in the congenic background (Figure 4.4b).

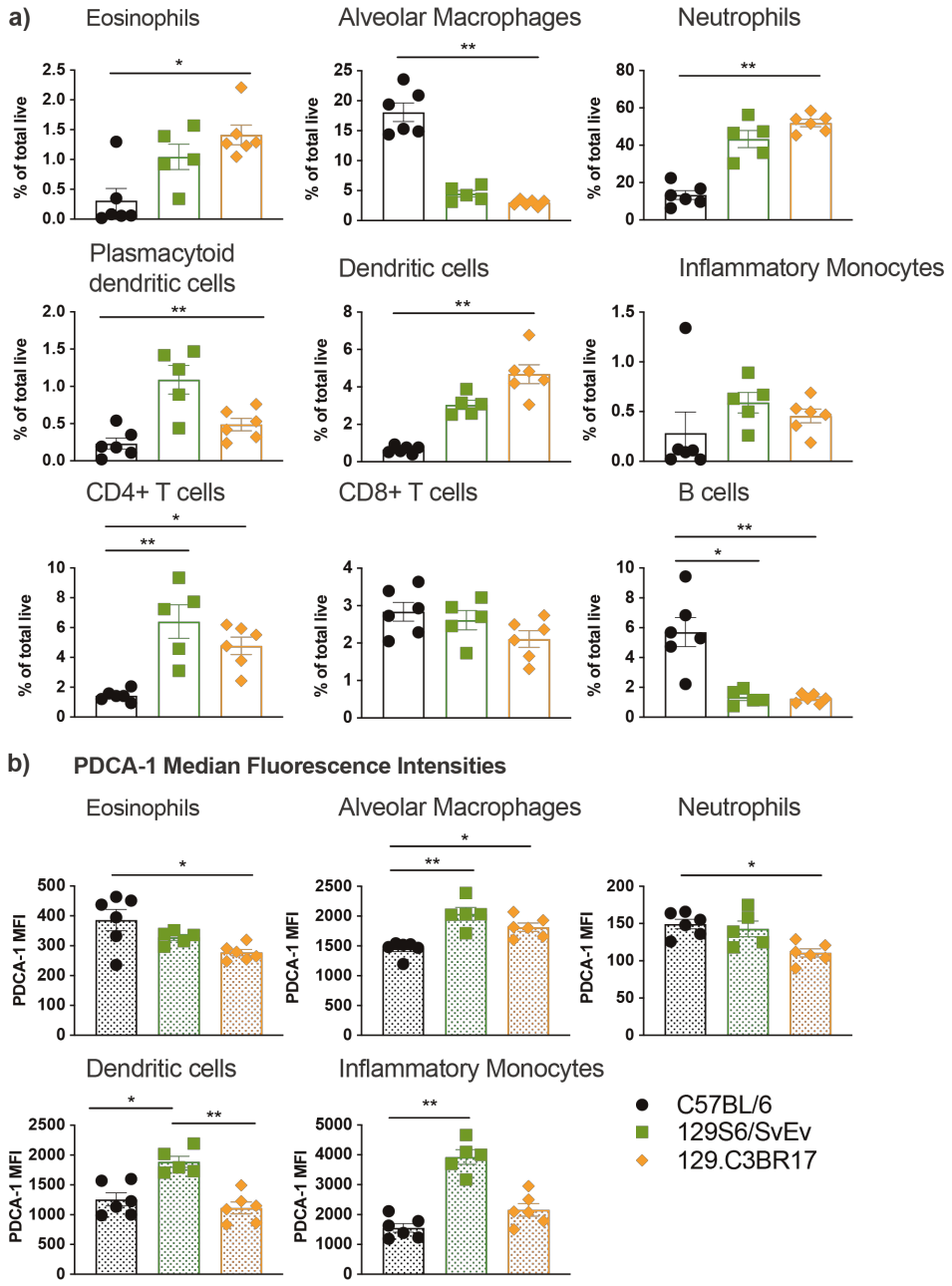

Figure 4.4 A reduction in pDC recruitment is observed in 129.C3BR17 mice compared to 129S6 controls at day 2 p.i ; the PDCA-1 expression in DCs and monocytes show a reduction in congenic mice compared to 129S6. Mice were infected with 3500 $TCID_{50}$ / mouse of X31 virus, and at day 2 post-infection the composition of the lung **A.** and PDCA-1 expression on immune cell subtypes **B.** were assessed by flow cytometry. NB this experiment is the same as in Figure 3.3of this thesis, with the addition of R17 mice here. Each symbol represents one mouse. Statistical test – Kruskal-Wallis ANOVA without assumption of normal distribution of data (* $p<0.05$; ** $p<0.01$; *** $p<0.001$; **** $p<0.0001$). Where no * indicates a pairwise comparison, no statistical significance was detected. Data representative of three experiments.

The mRNA expression of *Ifn-β1*, *Il-6* and *Irf7* was assessed in the lungs of infected congenic mice and BL/6 and 129S6 controls, as a means to verify whether it mirrored the observed differences in protein expression levels. At 24h post-infection, the mRNA expression of all three targets in 129.C3BR17 lungs was similar to the one in BL/6 controls (Figure 4.5). At 48h post-infection, 129S6 mice seemed to show a trend for high mRNA synthesis, whereas in congenic mice these levels stayed comparable to BL/6 controls. For comparison, in Figure 3.4 of this thesis, the differences between BL/6 and 129S6 mice in mRNA expression in the lung at 48h post-infection were significant, whereas here only a trend is observed. This is more evidence of the variability observed in the QPCR assays in the whole lung in this project.

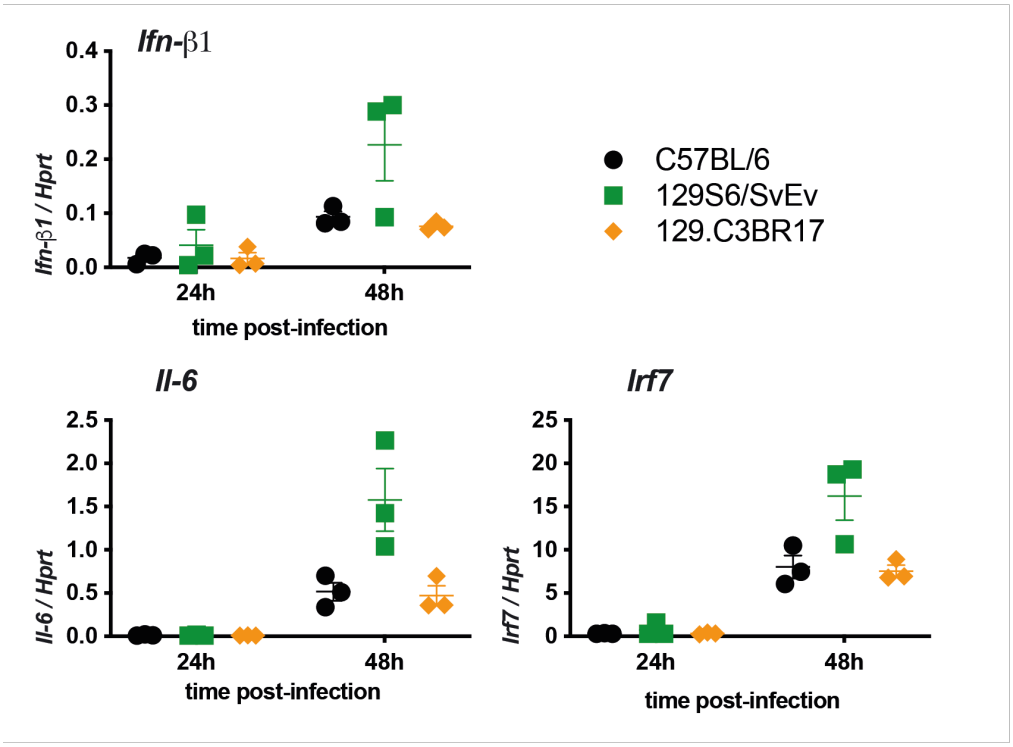

Figure 4.5 mRNA expression of *Ifn-β1*, *Il-6* and *Irf7* in the lung of infected congenic mice corresponds to that of the BL/6 controls and remains lower than the one of 129S6 mice. Mice of three genotypes were infected with 3500 $TCID_{50}$/mouse of X31 and whole lungs taken at 24h or 48h post-infection. mRNA was quantified by QPCR and the values represent the fold increase in expression relative to that of the housekeeping gene *Hprt*. Each symbol represents one mouse. Statistical test Kruskal-Wallis ANOVA was non-significant for all pairwise comparisons. 24h data representative of one experiment, and 48h data representative of two experiments.

4.2.2 BMDM and pDC assays to test responses to stimuli and infection *in vitro* in 129.C3BR17 cells

In vitro assays were performed to assess IFN-α/β and IL-6 production in 129.C3BR17 cells in response to stimuli and compare it to BL/6 and 129S6 cells. Firstly, BMDMs were stimulated with CpG-A (TLR9), poly(I:C) (TLR3), 2'3'cGAMP (cGAS/STING), 5'ppp dsRNA (RIG-I), LPS (TLR4), or infected with different strains of influenza virus (Figure 4.6). In response to a set of stimuli (Figure 4.6a), no significant reduction in IFN-α production compared to 129S6 levels was observed in the congenic BMDMs. There was a tendency for reduction in IFN-α production during TLR3 signaling (activated by poly(I:C)) but this was not significant. However, IFN-β protein levels were reduced in 129.C3BR17 compared to 129S6 cells, indicating that IRF3-mediated transcription could possibly be reduced by the introduction of the BL/6 allele of the R17 locus into the 129S6 genome. On the other hand, and in concordance with the *in vivo* data, IL-6 expression by congenic BMDMs was comparable to that in the 129S6 mice, and significantly higher than in BL/6 ones. This was observed across different stimulation conditions. Two different infection experiments are represented in Figure 4.6b as a demonstration of the observed inter-experimental variability. However, the common finding was that the IFN-α/β protein levels in 129.C3BR17 BMDMs were not significantly reduced compared to the 129S6 ones. Just like in the case of TLR stimulations, influenza infection resulted in high IL-6 levels in congenic cells, comparable to or higher than those recorded in the 129S6 cells. It is therefore possible that NFκB target expression is independent of the R17 locus origin. Stimulation through LPS (Figure 4.6c) resulted in similar patterns as other TLR stimuli, except in the case of IFN-α where a significant decrease compared to 129S6 levels was observed. An important reservation to have when considering the results of this figure is that BMDMs are not primary producers of IFN-α and that they are rather "specialised" in IFN-β production controlled by IRF3. These results will be further discussed in this chapter's and the general discussion.

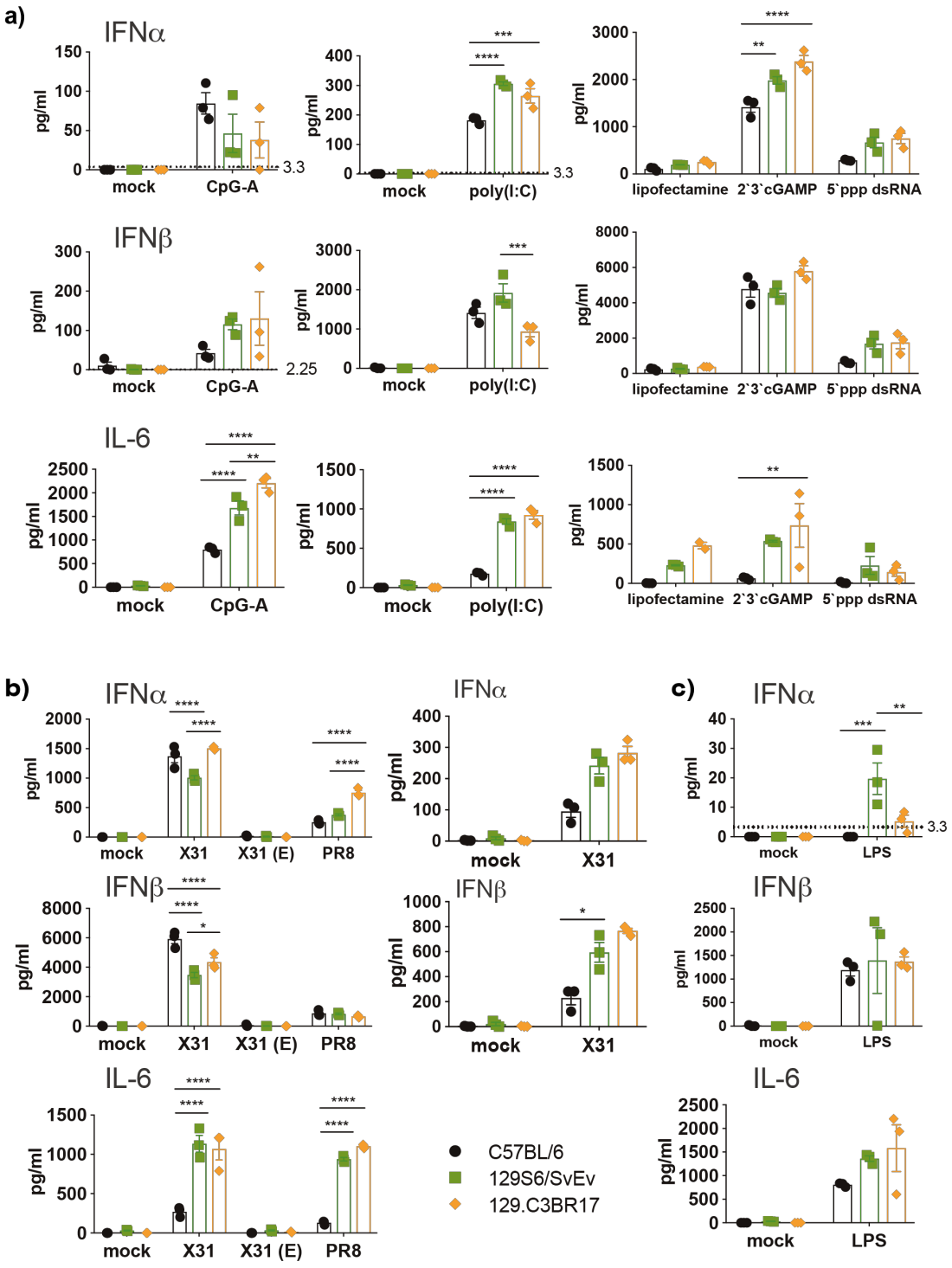

Figure 4.6 There is variability in IFN-α/β production responses from in vitro stimulated BMDMs; the TLR3 pathway could be affected by the R17 locus, but NFκB target IL-6 expression is unchanged. BMDMs were derived from BL/6, 129S6 and 129.C3BR17 mice as previously described. Cells were stimulated with indicated stimuli (see Material and Methods for concentrations) **A., C.** or infected with different strains of influenza virus (10^6 $TCID_{50}$/ml) for 24h **B.**, and supernatants analysed for IFN-α/β and IL-6 expression by ELISA. Each symbol represents one mouse. NB

These results are from the same experiment as Figure 3.5. Statistical testing – Kruskal-Wallis ANOVA test; * $p<0.05$; ** $p<0.01$; *** $p<0.001$; **** $p<0.0001$. Where no * indicates a pairwise comparison, no statistical significance was detected. Data in A. and C. is representative of seven independent experiments and represents data pooled from three different assays; data in B. is representative of two experiments.

Early responses to receptor-mediated pathway stimuli and to influenza virus were assessed by measuring mRNA transcription activity. *Ifn-β1*, *Il-6* and *Stat-1* transcription was quantified in BL/6, 129S6 and 129.C3BR17 BMDMs in order to compare it to protein expression patterns. Similar to previous findings comparing BL/6 and 129S6 only, mRNA levels were overall similar across genotypes and stimuli (Figure 4.7a). Only during STING activation by 2'3'cGAMP, a pathway that results exclusively in IFN production, was a reduction of *Ifn-β1* mRNA synthesis in congenic BMDMs in comparison to 129S6 controls observable. However, in infection with X31 (Figure 4.7b) a trend for reduction in *Ifn-β1* and *Il-6* mRNA levels was observed in the congenic mice. Interestingly, in all of the stimulations tested in different pathways, *Stat1* mRNA synthesis was comparable between genotypes, as was *Irf7* mRNA in influenza infection. Overall, these results indicate that the genotype of the R17 locus has limited influence on mRNA levels of *Ifn-β1*, *Il-6* and the two tested ISGs *Stat1* and *Irf7*. It is possible that this effect is either exerted later during stimulation or directly at the protein level instead.

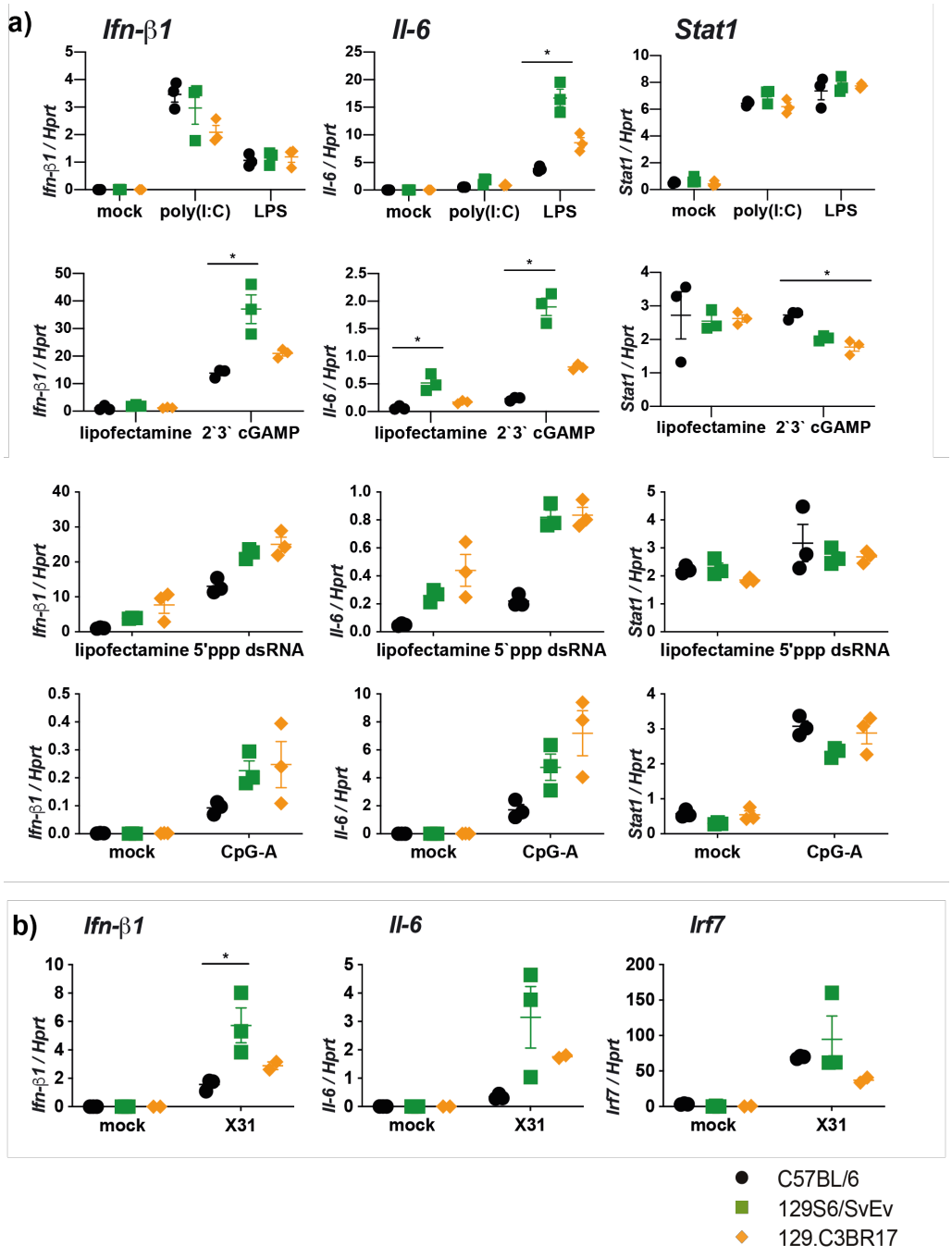

Figure 4.7 The origin of the R17 locus affects induction of *Ifn-β1* and *Il-6* mRNA in infection and STING stimulation in vitro. BMDMs from BL/6, 129S6 and 129.C3BR17 mice were stimulated with the indicated pathway stimuli **A.** or infected with the X31 virus **B.** mRNA was quantified after 6h of stimulation by QPCR. Each symbol represents a single mouse. Results are represented as mean ± SEM. Statistical test: Kruskal-Wallis (* p<0.05; ** p<0.01; *** p<0.001; **** p<0.0001; non-significant comparisons are not shown). NB: the represented data is from the same experiment as Figure 3.6. Data representative of four independent experiments.

As pDCs are biggest IFN producers *in vivo* and their type-I IFN levels were reduced early on in infection, responses of the 129.C3BR17 pDC-enriched cultures were also tested *in vitro* (Figure 4.8). In response to influenza infection, regardless of the virus strain used, a significant reduction in IFN-α/β protein production was detected in 129.C3BR17 pDCs compared to 129S6 controls. In fact, the expression of type-I IFN was reduced to levels comparable to those of BL/6 cells. In the case of TLR9 stimulations (CpG-A, CpG-B) or TLR7 stimulation (poly:U), IFN-β protein levels were significantly reduced in congenic cells compared to 129S6 ones. Therefore, the R17 locus origin is seemingly pertinent in pDC-driven IFN-α/β production in response to stimuli and infection. This result was interesting because influenza virus recognition happens through different pathways in BMDMs and pDCs. These results will be discussed further in this chapter.

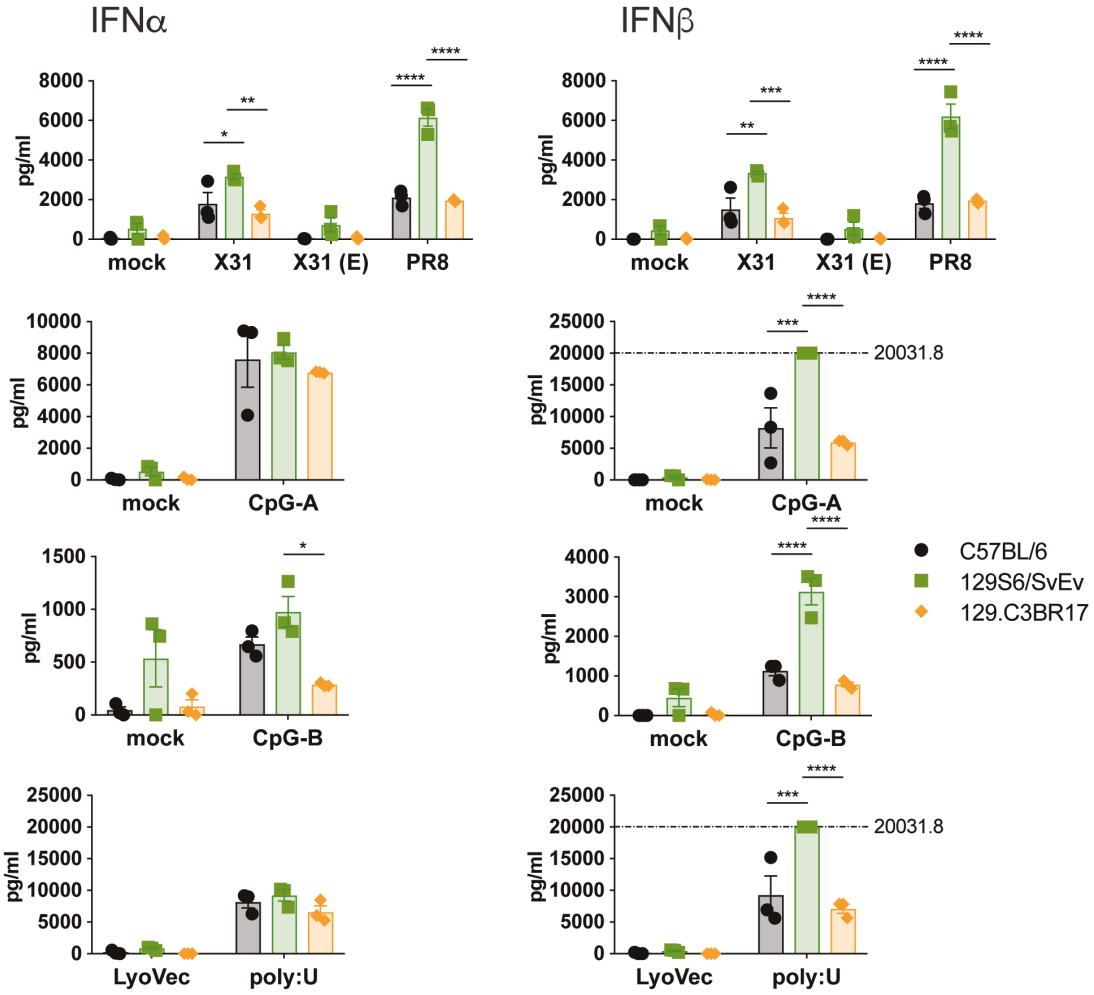

Figure 4.8 The BL/6 allele of the R17 locus contributes to the reduction of IFN-α/β secretion in pDC-enriched cultures. pDC-enriched cultures were derived from BL/6, 129S6 and 129.C3BR17 mice and infected with different strains of influenza (10^5 $TCID_{50}$/ml) or stimulated with TLR stimuli (CpG-A, CpG-B, poly:U) for 24h. Supernatants were harvested for protein quantification by ELISA. Each symbol represents one mouse (biological replicates). Statistical test: Kruskal-Wallis ANOVA, * $p<0.05$; ** $p<0.01$; *** $p<0.001$; **** $p<0.0001$; non-significant comparisons are not shown. Data representative of three independent experiments.

4.2.3 Impact of *de novo* synthetised proteins on the *in vitro* responses of 129.C3BR17 BMDMs

At this point in time it was not clear where exactly the R17 locus could be having an impact on IFN and cytokine production, in order to explain how it was affecting the survival of mice in influenza infection. Therefore, mRNA synthesis in response to X31 infection, and LPS and poly(I:C) stimulations was recorded in

BMDMs exposed to cycloheximide (a blocker of *de novo* protein synthesis) (Figure 4.9). Overall, the patterns of mRNA production in the congenic strain were comparable to those in BL/6 and 129S6 BMDMs, regardless of target studied (*Ifn-β1*, *Il-6*, *Stat1*) or stimulus used. In case of *Ifn-β1*, an increase in mRNA quantity upon cycloheximide treatment over time was observed. This was the case both in steady state and in all stimulations, although it was not significantly disparate between genotypes. *Il-6* expression was increased in cells exposed to cycloheximide in absence of stimuli. Similarly, in X31 infection and TLR3 stimulation with poly(I:C), *Il-6* transcription was increased in BMDMs of all three genotypes. Transcription of *Il-6* was only abrogated in presence of cycloheximide upon LPS stimulation, indicating a possible *de novo* synthetised factor connected to the TLR4 pathway that impacts *Il-6* production negatively. Once again, *Stat1* expression was unaffected by the genetic background, and abrogated upon cycloheximide exposure. It is clear from this experiment that regardless of the stimulus or cycloheximide treatment, the responses of 129.C3BR17 BMDMs were comparable to those of 129S6 controls.

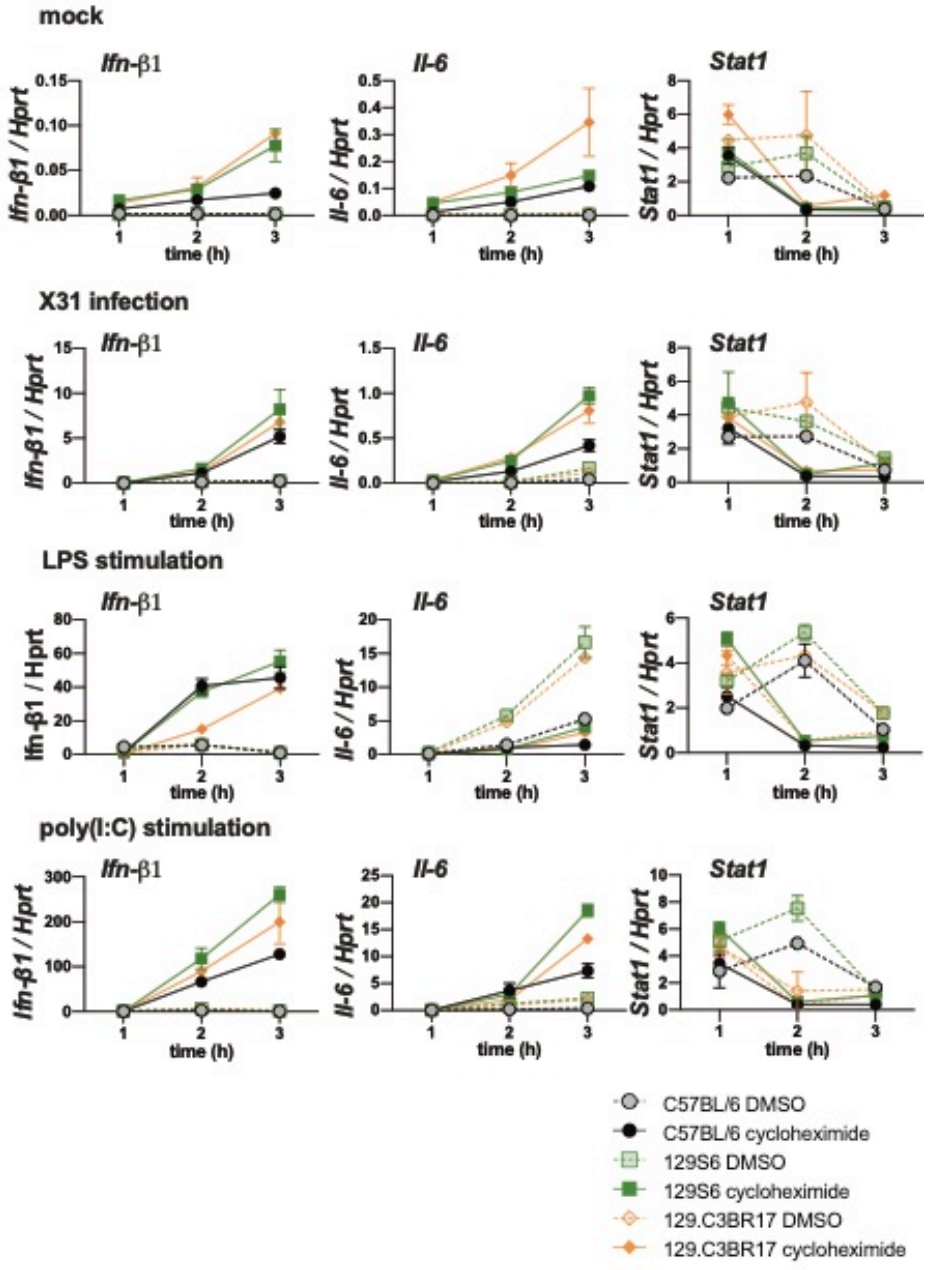

Figure 4.9 R17 locus origin does not encode differences in responses to cycloheximide treatment compared to BL/6 or 129S6 controls in BMDMs. Cells were infected with X31 (10^6 $TCID_{50}$/ml) or stimulated with LPS or poly(I:C) for the indicated times and *Ifn-β1*, *Il-6* and *Stat1* mRNA levels quantified by QPCR. Cells were incubated with DMSO or cycloheximide for 1h before and during the stimulation. DMSO was used a treatment control. Results are represented as mean ± SEM of three biological replicate samples. NB: results represented here are from the same experiment as in Figure 3.12. Statistical test: two-way ANOVA (Kruskal-Wallis test) * p<0.05; ** p<0.01; *** p<0.001; **** p<0.0001; non-significant comparisons are not shown. Only the pairwise comparisons between DMSO conditions for three genotypes, or cycloheximide conditions for three genotypes were examined. No statistical significance was found amongst these groups, and other

comparisons are not shown for clarity. Data representative of two independent experiments.

4.2.4 Activation of cascades leading to IFNα/β or cytokine production in 129.C3BR17 BMDMs

The signalling events leading up to *Ifn* and *Il-6* transcription involve the phosphorylation of components of signalling pathways. Typically, *Il-6* transcription is triggered by NFκB activation, which happens through phosphorylation of its subunit p65. *Ifn-α/β* transcription can be triggered by both IRF3 phosphorylation and NFκB activation and their translocation to the nucleus. Upstream, activation of TBK1 or p38 by phosphorylation are important steps in signal transduction of many different cascades. In order to address phosphorylation patterns of different factors within the RIG-I, STING and TLR4 cascades, BMDMs were stimulated for short times (1h, Figure 4.10a) or longer times (7h,Figure 4.10b) before investigating phosphorylation patterns of TBK1, p38 and p65. Total protein levels were also compared between genotypes. In short stimulations with LPS and 2'3'cGAMP there was no discernible difference in phosphorylation of p65, p38 or TBK1. However, 1h after influenza infection, a slight increase in p65 and p38 phosphorylation was observed in the 129S6 and 129.C3BR17 BMDMs compared to BL/6 mice. Phosphorylation of TBK1 was not detected at this timepoint in infection. It is worth noting however, that 7h post-infection (Figure 4.10b), there was no discernible difference in either p65 or p38 phosphorylation between the three genotypes, although both targets were notably more phosphorylated than in the control condition. Overall, these results indicate a possible higher phosphorylation and activation of NFκB p65-mediated transcription in the 129 background. No significant impact of the R17 locus genotype was observed in this assay, regardless of the timepoint of stimulation or the stimulus analysed.

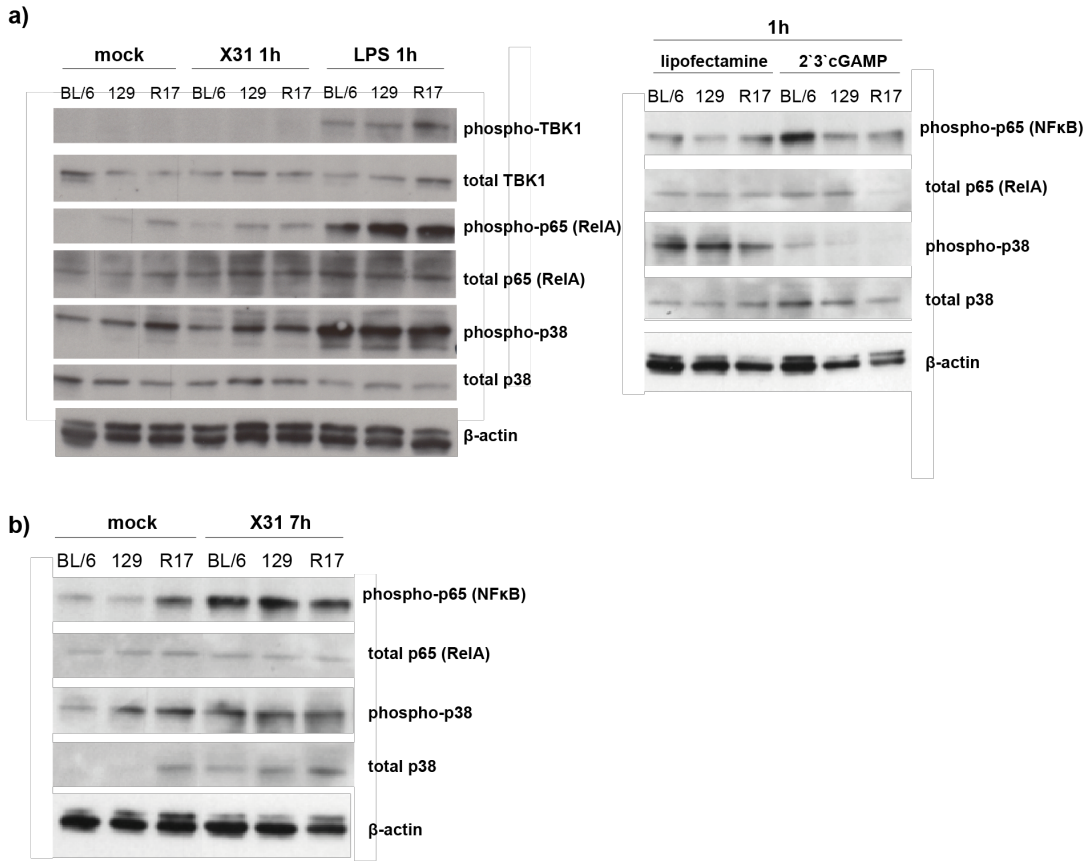

Figure 4.10 At early timepoints of infection and LPS stimulation, increased phosphorylation of p65 (NFκB) and p38 are detected in the 129S6 background, regardless of the R17 locus genotype. BL/6, 129S6 and 129.C3BR17 BMDMs were incubated in 1% FCS media overnight to reduce background phosphorylation before stimulation in vitro with X31 (10^6 $TCID_{50}$/ml), 2'3'cGAMP or LPS for the indicated times. Total protein from cell lysates was quantified using the Bradford dosage assay and separated by size on a 10% Bis-Tris Gel (as described in Material and Methods). Protein extracts were probed for expression of targets indicated in the middle and on the right using anti-mouse primary antibodies coupled to HRP-coupled secondary antibodies. Shorter time points of 1h **A.** or longer stimulation of 7h **B.** were examined by WB. Results represent three independent experiments.

4.2.5 Expression of genes in the R17 locus in BMDMs *in vitro*

The R17 locus, the only portion of BL/6 genome in congenic mice in an otherwise 129 genome, contains 7 genes and miRNAs. The function of these sequences in influenza infection, as well as expression patterns of the genes within this locus are unknown. Therefore, mRNA levels of *Ap1ar*, *Larp7*, *Tifa*, *Alpk1* and the pseudogene *573Rik* were quantified in stimulated BL/6, 129S6 and 129.C3BR17 BMDMs (Figure 4.11). The stimulants used were influenza infection (RIG-I), poly(I:C) (TLR3) and LPS (TLR4) stimulations. This assay was also a means to verify if the

expression of genes from the R17 locus was inducible by stimulation of the mentioned pathways. Tifa was the gene with the highest mRNA expression of all targets, but no discernible difference in expression was noted between genotypes. *Ap1ar*, *573Rik* and *Larp7* showed overall lower transcription levels and similar expression across genotypes. While *Alpk1* expression levels were generally low, the differences between genotypes were the most striking. The highest *Alpk1* mRNA expression was detected in 129S6 BMDMs in both unstimulated and stimulated cells, whereas BL/6 and 129.C3BR17 cells had similar levels of expression significantly lower than in 129s. Moreover, it seems like *Alpk1* expression in 129S6 cells was induced by all three stimuli to different extents. Overall, this result indicated that *Alpk1* was the only gene within the R17 locus whose expression was different in 129 and BL/6 backgrounds, and seemingly controlled from within the R17 locus.

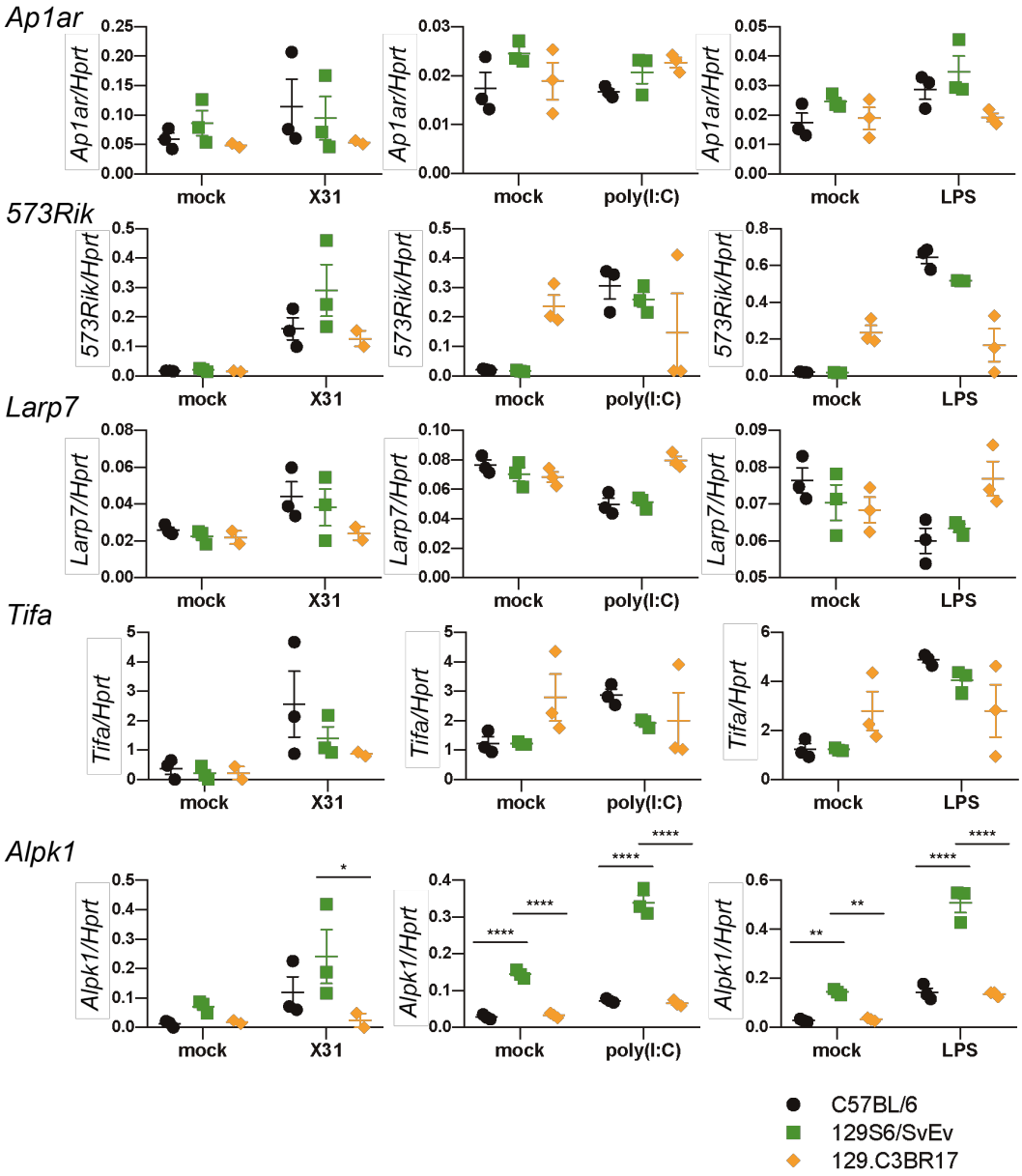

Figure 4.11 Of all genes inside the R17 locus, only the transcription of *Alpk1* is modulated from within the locus itself. BL/6, 129S6 and 129.C3BR17 BMDMs were stimulated with poly(I:C), LPS, or infected with X31 (10^6 $TCID_{50}$/ml) for 24h, and the mRNA quantified by QPCR. Each symbol represents a BMDM culture derived from one mouse. Represented values of expression are relative to the expression of the housekeeping gene HPRT. Statistical test: 2-way ANOVA; significance * p<0.05; ** p<0.01; *** p<0.001; **** p<0.0001, non-significant comparisons not shown. Data representative of two independent experiments.

Alpk1 is the gene with most non-synonymous SNPs in exons detected between C57BL/6 and 129S6 mice (as reported by (Boulard et al., 2012)). Also, the mRNA expression of *Alpk1* seems affected by the genotype of the R17 locus and stimulation. Therefore, patterns of *Alpk1* expression were further analysed to

determine the transcription levels of ALPK1 in stimulation, its dependence on the R17 locus origin, newly synthetised proteins, and the IFNAR cascade (Figure 4.12 a, b, c and d, respectively). It is worth noting that, in the effort to analyse the expression of ALPK1 further, protein quantification by WB was attempted multiple times using different commercially available antibodies. Unfortunately, none of the antibodies tested were able to detect ALPK1 protein in BMDMs. Therefore, all studies of *Alpk1* expression presented in this thesis are relative to its mRNA expression, with all the reservations the discussion of these results entails.

Just like in previous analyses, *Alpk1* expression after 6h of TLR9 stimulation with CpG-A was the highest in the 129S6 background, while 129.C3BR17 BMDMs showed similar expression patterns as C57BL/6 controls (Figure 4.12a). This was also true in the case of STING pathway activation with 2'3'cGAMP and RIG-I specific stimulation with 5'ppp dsRNA. Given that the transcription of *Alpk1* is seemingly controlled from within the R17 locus, mRNA levels of *Alpk1* were assessed in congenic F1(129.C3BR17x129wt) BMDMs where one R17 allele was of BL/6 and the other of 129S6 origin (Figure 4.12b). In the case of LPS stimulation especially, there was a step-wise reduction in *Alpk1* mRNA quantity in the 129 background with every introduced BL/6 copy of the R17 locus. At steady state and in TLR9 activation by CpG-B, similar expression of *Alpk1* mRNA was detected in the 129S6 BMDMs with both or one 129S6 copy of the R17 locus. It is therefore possible that the BL/6 copy of the transcription entity affecting *Alpk1* transcription is dominant and less active than its 129S6 counterpart. Further, in eliminating *de novo* protein synthesis using cycloheximide (Figure 4.12c), *Alpk1* expression was not affected in the early stages of X31 infection or TLR3 and TLR4 stimulations (poly(I:C) and LPS, respectively) in the BL/6 or congenic BMDMs. However, in the 129S6 background there was a clear reduction in expression in cells exposed to cycloheximide, starting at 2h post-stimulation. This indicates another peculiarity of *Alpk1* transcription in the 129S6 background, which seems to be at least partially affected by newly synthetised proteins. It is however worth noting that the unstimulated cells exposed to cycloheximide or DMSO showed similar patterns of *Alpk1* expression as the stimulated ones. There was no notable induction of *Alpk1* mRNA expression in the early stages of stimulation. Ultimately, the dependence of *Alpk1* mRNA synthesis on the IFNAR cascade was also addressed in X31 infection and LPS stimulation (Figure 4.12d). While overall levels of *Alpk1* mRNA were notably lower than in the WT-cells,

there was a trend for higher expression in 129S7$^{Ifnar1-/-}$ BMDMs compared to *Ifnar1*$^{-/-}$ BL/6 controls. This possibly indicates a mechanism of transcription control in the 129 genome that is independent of the IFNAR1-mediated cascade.

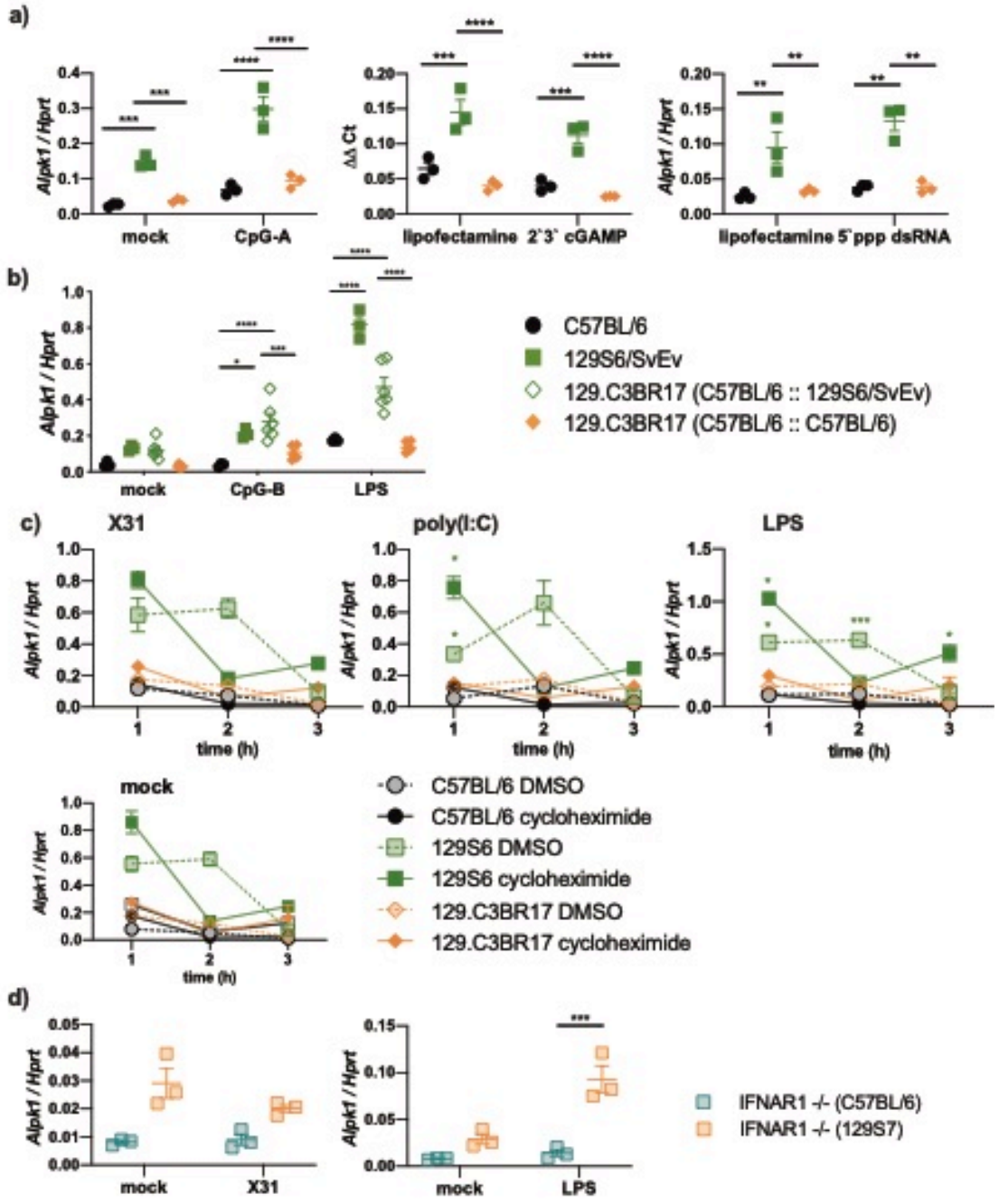

Figure 4.12 *Alpk1* mRNA expression in different stimulation conditions is modulated by the genetic origin of the R17 locus, and is dependent on de novo protein synthesis. BMDMs from BL/6, 129S6 and 129.C3BR17 mice were cultured as previously described and stimulated for 6h unless otherwise indicated. *Alpk1* mRNA was quantified by QPCR and results are represented as fold enrichment compared to the expression of the housekeeping gene HPRT. **A.** 6h-long stimulation

with CpG-A (TLR9) and lipofectamine-transfected stimuli 2'3'cGAMP (cGAS/STING) and 5'ppp dsRNA (RIG-I). Each symbol represents BMDMs from one mouse. **B.** Expression of *Alpk1* mRNA after 6h of stimulation with CpG-B or LPS, in different genotypes. BL/6, 129S6, 129.C3BR17 Het (one copy of R17 BL/6 and the other of 129S6 origin), and 129.C3BR17 (both copies of R17 of BL/6 origin, WT congenic mice). Each symbol represents BMDMs derived from one mouse. **C.** Time-course of infection with X31 (10^6 $TCID_{50}$/ml), and stimulation with poly(I:C) or LPS, for 1h, 2h, and 3h post-stimulation. *Alpk1* mRNA expression is analysed in presence of cycloheximide (full lines) or DMSO (dashed lines, controls). Cells were treated with cycloheximide or DMSO for 1h before and during stimulation. Results are represented as mean ± SEM of three biological replicates for each sample and each timepoint. **D.** *Alpk1* mRNA expression in *Ifnar1*$^{-/-}$ BMDMs (BL/6 and 129 backgrounds), 6h post-infection with X31 (10^6 $TCID_{50}$/ml) or post-stimulation with LPS. Each symbol represents one mouse. Statistical tests in all graphs 2-way ANOVA, of significance * $p<0.05$; ** $p<0.01$; *** $p<0.001$; **** $p<0.0001$, non-significant comparisons not shown. Data pooled from different independent assays (each subsection of the figure is from a different experiment).

4.3 Discussion

Experiments in this chapter aimed to verify whether the R17 locus in Chr3 was of interest in studying the causes of influenza susceptibility and high IFN production in 129 mice. Since the congenic strain 129.C3BR17 contains the R17 locus of BL/6 origin embedded into the 129S6 genome, it was possible to compare the effects of having a BL/6 or a 129 copy of the locus on IFN-α/β and cytokine production *in vivo* and *in vitro.*

4.3.1 *In vivo* susceptibility and IFN/cytokine production of 129.C3BR17 mouse strain in IAV infection

Taking into account the decreased susceptibility to influenza and lower IFN-α/β production early in infection in congenic 129.C3BR17 mice, it is possible that the R17 locus is a partial contributor to the 129 phenotype and, in part, the cause of high IFN-α/β production in mice. However, R17 origin is not sufficient to explain other data in this chapter. 129S6 susceptible mice experience a "cytokine storm", whereas in the analysed time points during infection, the production of IL-6 was not significantly reduced in 129.C3BR17 mice. Only a handful of cytokines such as MIP-1α, MIP-1β and IL-27 were significantly lower than in 129S6 controls in the early response on day 2, presented here. It is however possible that larger differences in cytokine production are to be found in later time points in the infection, as was demonstrated

in the 129 strain om days 6-10 in infection by (Davidson et al., 2014). This can be tested in future experiments by choosing a later time point. Although these molecules serve as chemoattractants to macrophages and monocytes, the recruitment of immune cells early on in infection was not in line with this finding, as it was similar between the congenic and the 129S6 backgrounds. The proportions of pDCs were reduced, indicating a possible cause of the reduction in IFN-α/β observed in the lung in congenic mice. Overall, while the susceptibility was rescued by the R17 locus, it was unclear from the *in vivo* findings why the congenic mice were surviving infection and 129S6 mice succumbing to it.

4.3.2 *In vitro* responses to IAV infection and PRR stimulation in BMDM and pDC cultures from 129.C3BR17 mice

In vitro assays in this chapter were performed to analyse if the R17 locus has an effect in any particular signaling pathway leading to IFN/cytokine synthesis. A reduction in IFN-α/β expression compared to 129S6 cells was primarily observed in pDC-enriched cultures upon influenza challenge. As IFN-α/β production in influenza infection in pDCs is mediated by the TLR7-TRAF6-IRF7 axis, it is possible that the R17 locus genes have an effect in this signaling cascade. It could be that the 129 allele of R17 is mediating a stronger activation of IFN-α/β production, although it is difficult to say by which molecular mechanism this happens. This result was in line with the *in vivo* findings. While RIG-I-mediated recognition of influenza in BMDMs was an exception, in the cGAS/STING, TLR3 and TLR4 cascades in BMDMs, a reduction in IFN-β production was observed in congenic cells compared to 129S6 controls. In all these pathways, the activation of IFNβ transcription is triggered by TBK1-mediated IRF3 activation. This could be another branch of signaling that is possibly affected by the R17 locus. On the other hand, the predominantly NFκB-mediated IL-6 production was not affected by the R17 locus in any circumstance, in p38 or p65-NFκB mediated signaling (such as TLR9/TLR4 in BMDMs).

mRNA expression of *Ifn-β1*, *Il-6* and *Stat1* was largely similar across genotypes. Given that protein quantities of IFNβ and IL-6 were variable depending on the genotype and the stimulus, it is possible that mRNA stability is increased in the 129 background regardless of the variant of the R17 locus. This hypothesis was not further pursued, although it would be of interest to compare the half-life of *Ifn-β1*

and *Il-6* mRNAs between the three genotypes in the future. Also, according to the results obtained after cycloheximide treatment, the R17 locus genotype effect (if there is any) is not mediated by newly synthetised proteins. To confirm this finding in the future, it could be interesting to try and prolong the stimulation in presence of cyloheximide beyond 3h. However, this might prove challenging due to toxicity issues: toxicity was already visible as early as 3h in this assay in poly(I:C) stimulation, as seen by the extremely high *Ifn-β1* mRNA levels.

Although some limited conclusions could be drawn from protein and mRNA data, the verification by WB of phosphorylation patterns of TBK1 and p65 yielded no confirmation to this. No reduction in TBK1 phosphorylation could be observed in stimulated 129.C3BR17 BMDMs compared to 129 controls. In line with previous results, p65 phosphorylation was similar in the 129S6 and 129.C3BR17 BMDMs. These assays were insufficiently informative about the step in signaling where the genotype of the R17 locus could have an impact.

4.3.3 Overall conclusions and intra-R17 gene functional interactions

The results in this chapter indicated that the role of the R17 locus in influenza susceptibility could be in driving IFN-α/β levels down to a level where the pathology was avoided. The possible source of this reduction could be the decrease in the recruitment of pDCs into the lung and the production of IFN-α/β by pDCs in congenic mice, compared to the 129S6 controls. Given that the weight loss of 129.C3BR17 and 129S6 mice was similar for a big part of the infection, it is possible that the high cytokine levels in the congenic mice are driving influenza sensitivity but are insufficient to cause high mortality. Alternatively, the cytokine drivers of increased mortality in 129 mice could be the result of cell recruitment in the late-stage in infection, which was not addressed here.

While this project was being carried out, a functional link between ALPK1 and TIFA was recognised by different groups in the context of bacterial infection recognition ((Zimmermann et al., 2017), (Milivojevic et al., 2017), see Introduction and next chapter of Results). Both of these genes are contained within the R17 locus. This raised concerns of possible interactions between the genes within the locus that may be affecting phenotyping efforts of the congenic 129.C3BR17 mice. Moreover, the mRNA expression of genes from the locus had revealed that *Alpk1* was the only

gene under direct transcriptional control from inside the R17 locus. Expression of *Alpk1* is significantly higher in the 129S6 background than in BL/6 at steady state, and this difference is exacerbated in stimulation, especially with LPS. With each BL/6 copy of R17 introduced into the 129S6 genome, the expression of *Alpk1* mRNA is reduced in a step-wise manner, until reaching BL/6 levels in 129.C3BR17 BMDMs.

Sequencing of R17 locus genes revealed that the coding sequence of *Alpk1* contained 17 missense mutations between BL/6 and 129S6 mice, more than any other gene from the locus (Boulard et al., 2012). This result, along with our own findings presented in this chapter, motivated a decision to analyse *Alpk1*$^{-/-}$ mice in depth and try to assess the impact of this factor on influenza susceptibility. The results from this study are detailed in the next chapter.

Chapter 5. Results 3 : Role of ALPK1 in influenza susceptibility and production of interferon in mice

5.1 Introduction

From the experiments using 129.C3BR17 mice it is clear that one or more components of the R17 locus could explain the susceptibility of 129 mice to influenza. Namely, the genetic origin of the R17 locus, regardless of the surrounding genome (BL/6 or 129S6), modulates influenza susceptibility *in vivo* and IFN-α/β production *in vitro.* Therefore, it is plausible that one or more genes from within the R17 locus could be affecting IFN and cytokine levels *in vitro* and *in vivo* in the 129 background. As a start, one of the genes from the R17 locus was chosen to pursue further experiments. Given its expression patterns, the high number of non-synonymous mutations in the 129 background that could affect its function, and no less because a KO mouse strain was readily available and easy to test, further work on the origins of high IFN production was pursued by addressing *Alpk1* as a candidate gene.

Alpk1 is a gene located on the anti-sense strand of Chr3 within the R17 locus. It encodes a protein called α-protein kinase, which belongs to a non-canonical family of protein kinases capable of phosphorylating target sites embedded in α-helices (Middelbeek et al., 2010). It is a protein of unsolved structure, localised in the

cytoplasm, with a putative disordered domain connecting an N-terminal anchoring domain to the kinase domain located in the C-terminus.

The first mouse model of *Alpk1* knockdown was generated by a PiggyBac transposon insertion into the coding sequence (Chen and Xu, 2011). The mice showed no apparent phenotype, save for slight coordination deficits. In the first studies, ALPK1 was mostly connected to gout inflammation in human cell models in *in vitro* models ((Ko et al., 2013, Wang et al., 2011), (Lee et al., 2016). However, while two SNPs of *Alpk1* were associated to gout in one GWAS study (Ko et al., 2013), a replicate study had found no association for one of the two, rs11726117 (Chiba et al., 2015). It had been demonstrated that ALPK1 participated in the MSU crystal-induced production of pro-inflammatory cytokines (Wang et al., 2011). In a more mechanistically detailed study, myosin IIA was identified as a target of Alpk1 (Lee et al., 2016). Namely, ALPK1 Nt domain, cloned and immunoprecipitated, was demonstrated to be sufficient for myosin IIA binding. Furthermore, the phosphorylation of myosin IIA was shown to be to be dependent on ALPK1 presence in THP-1 cells. Binding and phosphorylation were further shown to induce the trafficking and secretion of TNFα. The same pro-inflammatory effects on TNFα and TGFβ1 were demonstrated in a human cell model, with testosterone shown to inhibit this activity of ALPK1 (Kuo et al., 2015). Furthermore, ALPK1 had been implicated in the transport of lipid raft-associated apical vesicles and epithelial cell polarity (Heine et al., 2005), making it an interesting candidate in our system of IAV infection as well.

The most detailed role of ALPK1 was recently described in bacterial recognition. ALPK1 was shown to be a novel cytosolic receptor for a specific bacterial PAMP, ADP-heptose, which is an intermediate product of the LPS synthesis pathway (Hu et al., 2019). Namely, ALPK1 recognises ADP-heptose during infection with bacterial strains such as *H.pylori* and *S.flexneri*, activating the NFκB signaling cascade downstream and resulting in the production of pro-inflammatory cytokines IL-1β, TNF-α, IL-8 and others (Garcia-Weber et al., 2018, Zhou et al., 2018, Zimmermann et al., 2017).

A recent study by (Ryzhakov et al., 2018) has shown that *Alpk1*-deficient BL/6 mice had increased pro-inflammatory cytokine production responses in a mouse model of *H.hepaticus*-induced colitis. In this paper, they concluded that the *Alpk1*$^{-/-}$

BL/6 mice showed the same phenotype as the susceptible 129 strain, thus assuming that the *Alpk1* 129 allele is a loss-of-function. This study is somewhat in opposition with other findings concerning the role of ALPK1 in inflammation. In previous work, ALPK1 was indicated as a pro-inflammatory factor, activating NFκB-mediated responses via TIFA phosphorylation (Milivojevic et al., 2017). This was confirmed in the infection with three separate bacterial type-Infections in mice (one of which *B.cenocepacia* infection in the lung), where *Alpk1*-lacking mice had a reduced production of GM-CSF, MIP-1α/β and RANTES (Zhou et al., 2018). In the same study, the ALPK1 Nt region was crystallised in a complex with ADP-heptose confirming the binding between the two molecules and the function of ALPK1 as a PRR in bacterial infection.

In the influenza infection model presented in this thesis, ALPK1 seems more highly expressed in the 129S6 background than in C57BL/6, and its expression at least partially controlled from within the R17 locus and responsive to different stimuli. Moreover, given the numerous non-synonymous mutations identified in the ALPK1 sequence (including within its Ct kinase domain), it is conceivable that the function of the 129S6 version of ALPK1 is affected either positively or negatively. To explore this hypothesis, *Alpk1*$^{-/-}$ mice were used in this thesis to investigate the potential role of this kinase in influenza susceptibility, and IFN-α/β and cytokine production.

In this chapter, I show results of experiments on *Alpk1* double-knockout mice (*Alpk1*$^{-/-}$ or *Alpk1* KO) and derived cells. The knock-out of *Alpk1* was achieved by exon 10 deletion in the C57BL/6 background, and the *Alpk1*$^{-/-}$ mouse model identical to the one used by (Ryzhakov et al., 2018). Exon 10 is part of the kinase domain of ALPK1, therefore its deletion is thought to abolish the kinase activity of ALPK1. However, the rest of the protein, if correctly translated, could still play a role separate to the kinase one. I will show results of *in vivo* and *in vitro* experiments similar to those presented previously in this thesis, where susceptibility and cytokine and IFN-α/β production are assessed in *Alpk1*$^{-/-}$ mice and compared to the BL/6 controls. Also, since direct phosphorylation targets of ALPK1 remain relatively unknown, phospho-proteomics experiments were performed in BMDMs to compare the landscape of protein phosphorylation in presence and absence of ALPK1. These experiments have led this project in a new direction, pointing towards a new possible regulation target of ALPK1.

5.2 Results

5.2.1 Influenza susceptibility and lung phenotypes in *Alpk1*$^{-/-}$ mice

The role of ALPK1 was first assessed *in vivo* by comparing weight loss and survival in influenza infection in WT C57BL/6 mice and *Alpk1* heterozygous (+/-) and homozygous (-/-) knock-outs (Figure 5.1a). Mice that lack *Alpk1* show more severe weight loss and higher mortality (up to 75%) compared to WT mice. At the same time, *Alpk1*$^{+/-}$ mice showed similar survival as the WT BL/6 controls and intermediate weight loss, indicating that the absence of one copy of *Alpk1* was sufficient to increase morbidity of mice in influenza infection. However, reproducibility of this finding was relatively poor and the mortality of control C57BL/6 mice was higher in subsequent experiments. For this reason, the viral dose was reduced to $10*10^3$ $TCID_{50}$/mouse or $3*10^3$ $TCID_{50}$/mouse (Figure 5.1b) and the weight loss and survival of the same mouse genotypes followed up (with the clinical endpoint defined at 80% of d0 weight due to a change in standard operating procedures). Reducing the viral dose helped keep the mortality of control mice relatively low, but also resulted in a

loss of the C57BL/6$^{Alpk1-/-}$ susceptibility phenotype. Therefore, it was challenging to find a viral dose for infection that would reproduce the phenotype initially observed.

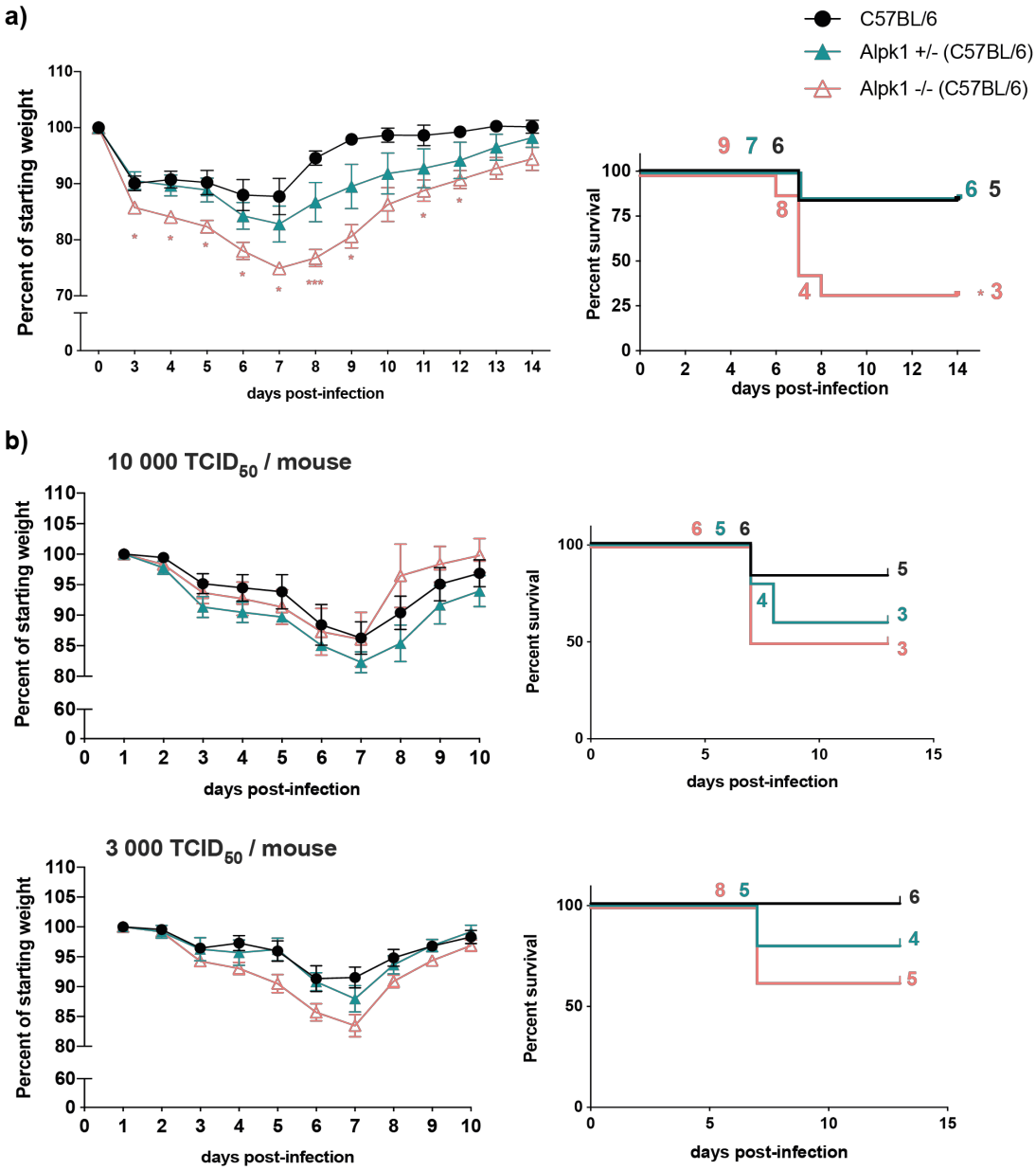

Figure 5.1 The absence of *Alpk1* in C57BL/6 mice renders them more susceptible to influenza infection, but this phenotype is highly dependent on the viral dose used. Mice of corresponding ages and gender ratios of genotypes were infected with X31 influenza virus and their weight loss and survival monitored 14 days post-infection. Mouse numbers are indicated in corresponding colours on the survival graphs, and represent the evolution of mouse numbers during the infection. Viral dose: **A.** 35000 $TCID_{50}$ / mouse and clinical endpoint at 75% of d0 weight, **B.** 10000 $TCID_{50}$ / mouse or 3000 $TCID_{50}$ / mouse and clinical endpoint at 80% of d0 weight. Results are represented as mean±SEM of the indicated number of mice per group.

Weight loss curves statistical tests 2-way ANOVA, comparing *Alpk1*$^{-/-}$ survival curve with that of C57BL/6 controls (* indicate corresponding statistical significance * $p<0.05$; ** $p<0.01$; $p<0.001$). Survival tests log-rank (Mantel-Cox) * $p<0.05$. Data is representative of one experiment, since subsequent experiments showed significant variability (see main text).

The previous infection having been carried out at a high infection dose of $35*10^3$ $TCID_{50}$/mouse, the infection dose was reduced to $10*10^3$ $TCID_{50}$/mouse for subsequent experiments (Figure 5.2b). At this viral dose, levels of type-I IFN and IL-6 were also assessed in the lung of infected *Alpk1*$^{-/-}$ mice at different infection timepoints (Figure 5.2a). Somewhat surprisingly given their increased susceptibility to influenza, *Alpk1*$^{-/-}$ mice showed no increase in either IFN-α, IFN-β or IL-6 proteins secreted in the BAL compared to WT mice. This was true at all timepoints in infection that were tested, namely day 2 (peak of IFN-α/β production in the lung), day 3, day 6 and day 7. Moreover, the activity of the mainly epithelium-driven IL-28 (IFN-λ) production was tested at days 6 and 7 and no significant difference was found between WT and *Alpk1*$^{-/-}$ lungs. Given that this viral dose was lower than the one previously used, $35*10^3$ $TCID_{50}$ of X31 virus were administered per mouse in a separate experiment (Figure 5.2b). At day 2 post-infection, there was again no difference observed in IFN-α/β or IL-6 levels between the lungs of *Alpk1*$^{-/-}$ and WT mice. Given this result and the one presented in the previous figure, it is important to mention that more experiments were then performed to compare the susceptibility of the two mouse strains when using $10*10^3$ $TCID_{50}$ as infection dose. At the same time, our experimental design had to be modified to include endpoints at 80% of d0 weight. In this experimental design, the susceptibility of *Alpk1*$^{-/-}$ mice to influenza was more variable and more mortality was recorded in the WT mice because of the 80% cut-off. Although these variations were taken into account, the experiments with *Alpk1*$^{-/-}$ mice were pursued *in vivo* and *in vitro.*

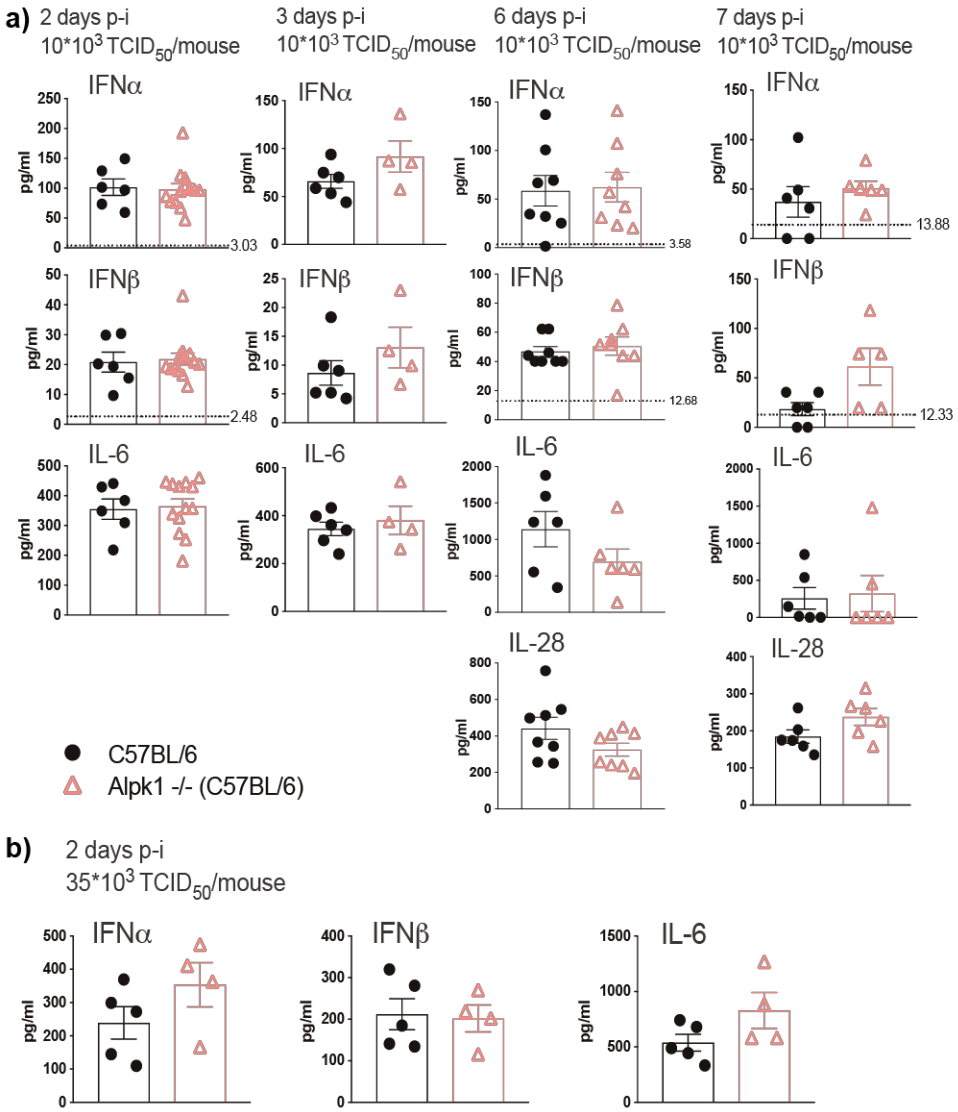

Figure 5.2 ALPK1 does not have an effect on the in vivo levels of IFN-α/β, IL-6 or IL-28 in the lung upon infection. Mice were infected with **A.** $10*10^3$ $TCID_{50}$ or **B.** $35*10^3$ $TCID_{50}$ X31 per mouse and the production of IFN-α,IFN-β, IL-6 and IL-28 in the BAL quantified by ELISA at the indicated time points post-infection. The dashed lines represent the lower detection limit in pg/ml for the ELISA assay for each target. Each symbol represents a single mouse, and results are represented as mean±SEM and compared using the Mann-Whitney t-test without assumption of normal distribution of data (* $p<0.05$; ** $p<0.01$; *** $p<0.001$; **** $p<0.0001$; non-significant comparisons are not shown). The represented results are pooled from 4 independent experiments, and representative of a total of 6 experiments.

Although no significant differences were observed in levels of IFN-α/β and cytokines in presence or absence of ALPK1 *in vivo*, recruitment of immune cells to the infected lung was tested at day 2 post-infection between WT and *Alpk1*$^{-/-}$ mice (Figure 5.3a). A reduction in proportions of alveolar macrophages and an increase

in neutrophils in *Alpk1*$^{-/-}$ mice mirror those observed in the 129S6 background compared to the BL/6 controls, which was interesting in light of the increase in susceptibility of *Alpk1* knock-outs. An increase in the proportion of inflammatory monocytes was also observed in absence of ALPK1, mimicking the tendency observed comparing BL/6 and 129 genotypes in Results Part 1. A higher proportion of PDCA-1 positive dendritic cells (Figure 5.3b) was noted in *Alpk1*$^{-/-}$ mice, but the activations of alveolar macrophages and neutrophils in these mice was less than in BL/6 controls, despite the fact that recruitment of both these cell types into the lungs was increased.

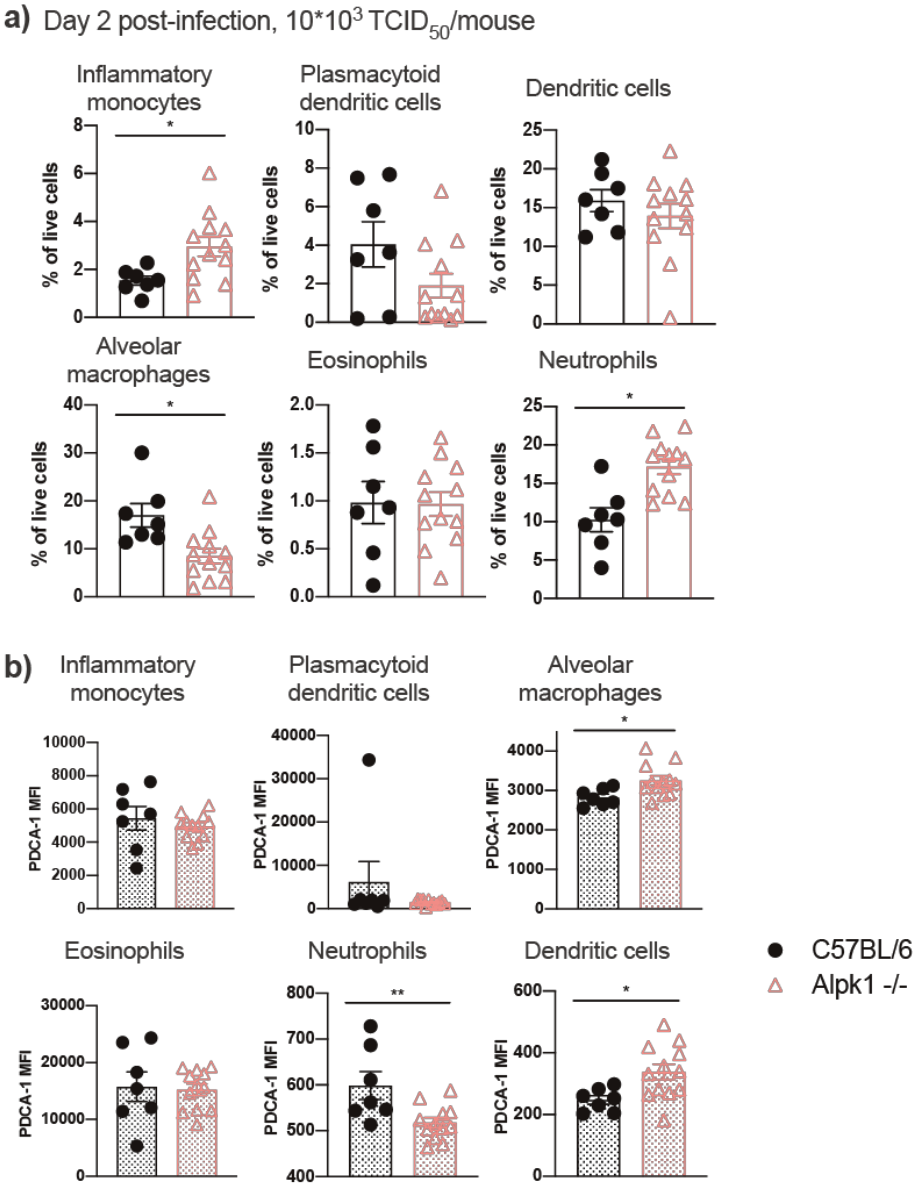

Figure 5.3 *Alpk1*$^{-/-}$ mice show increased infiltration of neutrophils and inflammatory monocytes into the lung but the expression of PDCA-1 on these cells

is not higher than in BL/6 controls. Mice were infected with $10*10^3$ $TCID_{50}$ X31 per mouse and at day 2 p.i. the composition of the whole lung was analysed by flow cytometry after BAL flushing. Immune cell proportions (for immune cell markers see Material and Methods) **A.** and PDCA-1 expression on them **B.** are represented. Each symbol represents one mouse, and results are represented as a mean±SEM. Statistical test: t-test Mann-Whitney without assumption of normal distribution of data (* p<0.05; ** p<0.01; *** p<0.001; **** p<0.0001; non-significant comparisons are not shown). Data representative of three independent experiments.

After testing an early time point of infection, the same experiment was completed to investigate immune cell infiltration into the lung 6 days post-infection (Figure 5.4a). The relative proportion of inflammatory monocytes in the lungs in *Alpk1*$^{-/-}$ mice remained higher than in controls, and a stronger infiltration of pDCs was also observed at this point of infection. Interestingly, there were also more CD4+ T-cells in the lungs of *Alpk1*$^{-/-}$ mice than in controls. However, PDCA-1 expression was only observed to be higher in the recruited eosinophils in the *Alpk1*$^{-/-}$, while SCA-1 expression (another marker of cellular activation expressed in response to IFN) was similar across the lymphocyte population in both genotypes (Figure 5.4b). Similar to before, there was little difference in activation levels of different immune cell populations between controls and *Alpk1*$^{-/-}$ mice. While the results of early points in infection were more variable, a test of immune cell infiltration at day 7 post-infection also showed an increase in pDC recruitment, thus confirming the observed result at day 6.

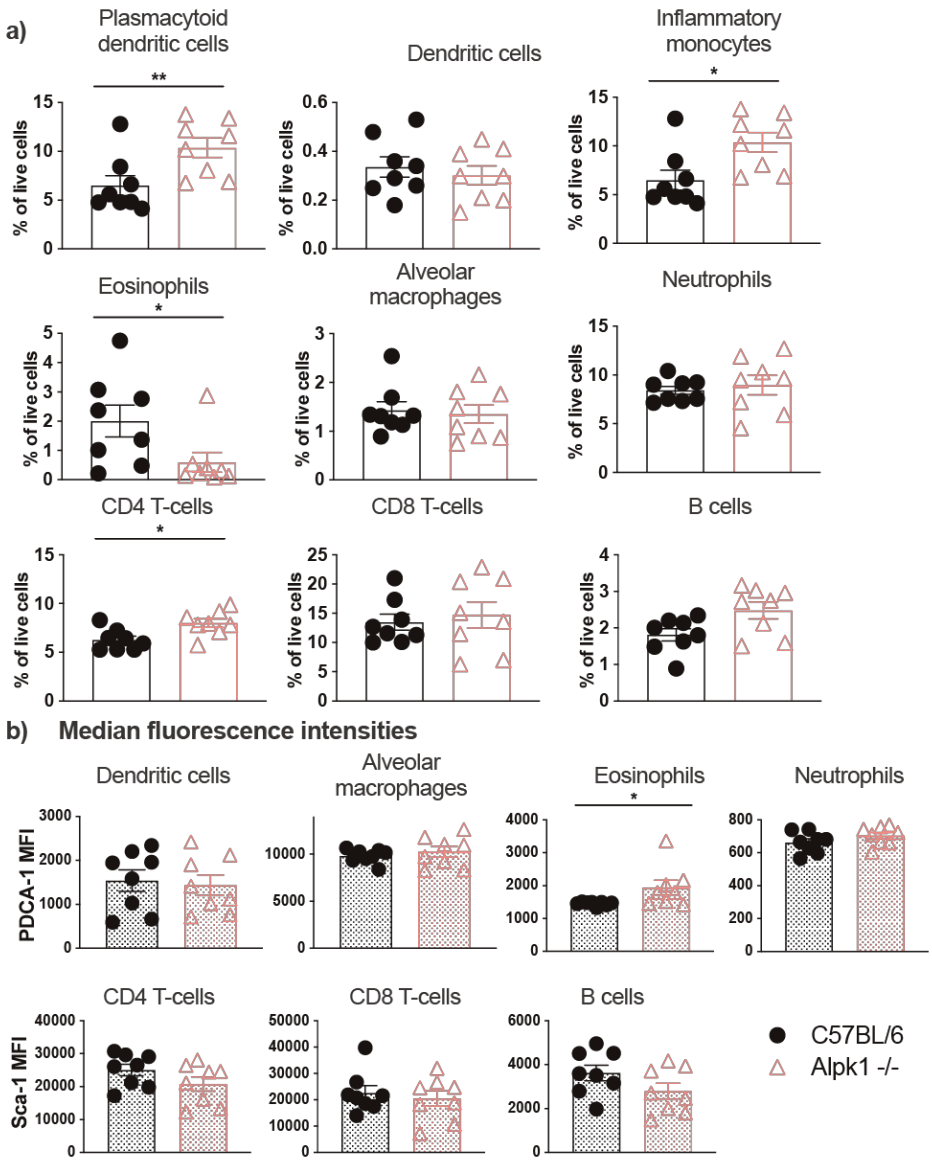

Figure 5.4 At day 6 p.i., an increase in pDC, inflammatory monocyte and CD4+ T-cell recruitment is observed in *Alpk1*$^{-/-}$ mice, but none of these cell types show an increase in activation markers PDCA-1 or SCA-1. Mice were infected with 10*10^3 $TCID_{50}$ X31 per mouse. At day 6 p.i. the whole lung after BAL flushing was analysed by flow cytometry. Immune cell proportions **A.** and PDCA-1 and SCA-1 expressions on these cells **B.** are represented. Statistical test: Mann-Whitney t-test without assumption of normal distribution of data (* $p<0.05$; ** $p<0.01$; *** $p<0.001$; **** $p<0.0001$; non-significant comparisons are not shown.). The results represented are from one performed experiment for this timepoint in infection.

5.2.2 Lung viral burden during infection in *Alpk1*$^{-/-}$ mice

In order to ensure that the observed phenotypes were not due to differences in viral burden, the X31 virus matrix RNA was quantified in the whole lung of BL/6

and *Alpk1*$^{-/-}$ mice in the early stages of infection (Figure 5.5). At days 2 and 3 p.i. there was no observable difference in the quantity of viral matrix RNA between WT and *Alpk1*$^{-/-}$ mice. Similar pattern was observed for *Ifn-β1* mRNA expression as well, confirming all the previous mRNA quantification results presented in this thesis.

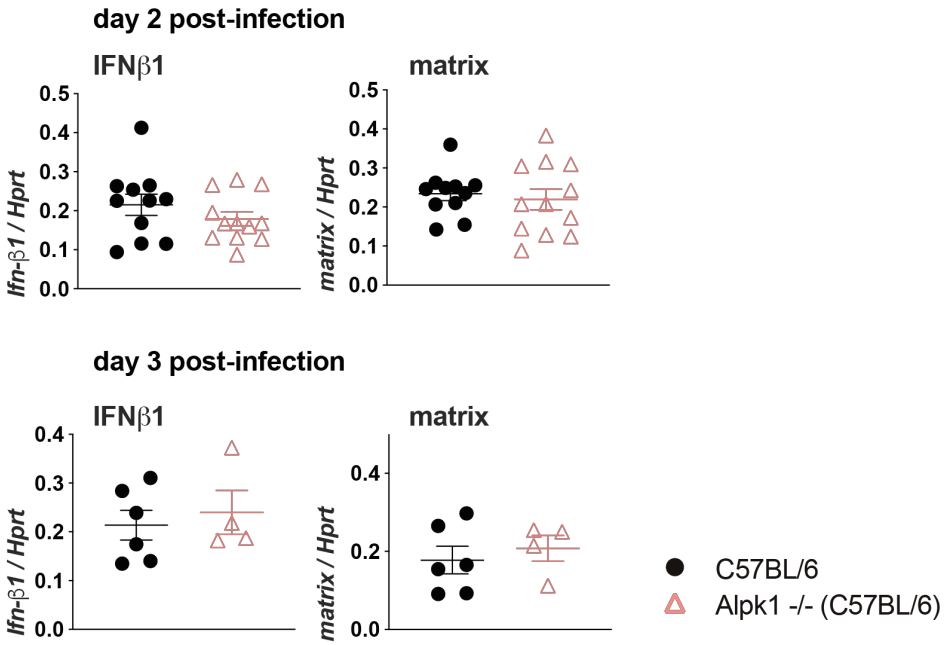

Figure 5.5 mRNA expression of *Ifn-β1* and viral RNA matrix levels in the whole lung are similar between WT and *Alpk1*$^{-/-}$ mice at day 2 and 3 post-infection. Mice were infected with 10*10^3 $TCID_{50}$ X31 and at indicated times post-infection whole lung was harvested and processed. mRNA of *Ifn-β1* and viral matrix RNA quantified by QPCR. Results from day 2 and day 3 post-infection are from two independent experiments. Each symbol is one mouse and results are represented as mean±SEM. Statistical test: Mann-Whitney t-test (significance $p<0.05$ not detected). Data is representative of one pilot experiment.

5.2.3 ALPK1-dependent *in vitro* BMDM responses to stimuli

Next, the responses to stimuli *in vitro* were compared between WT BL/6 and *Alpk1*$^{-/-}$ in bone marrow-derived macrophages (Figure 5.6). Responses were assessed by quantifying IFN-α/β and IL-6 in the supernatant of stimulated cells as described in the previous chapters. In response to TLR3 stimulation with poly(I:C) there was no significant difference in IFN responses, but IL-6 secretion by *Alpk1*$^{-/-}$ BMDMs was significantly reduced compared to WT-cells (Figure 5.6a). Inversely, TLR4 stimulation with LPS showed increased responses in cells lacking Alpk1, with higher secretion of both IFN-β and IL-6. Alpk1 seems to affect the responses to

infection to X31 virus *in vitro*, since IFN-α, IFN-β and IL-6 levels were significantly higher in *Alpk1*$^{-/-}$ BMDMs than in controls. This suggested that Alpk1 could have an impact on IRF-3 dependent IFN-β production and on NFκB activation overall. Transfection of STING activator 2'3' cGAMP, as well as RIG-I stimulant 5'ppp dsRNA was assessed in different concentrations of these stimuli in both genotypes (Figure 5.6b). Surprisingly, no difference in IFN-α, IFN-β or IL-6 production was observed in BMDMs lacking Alpk1 compared to controls.

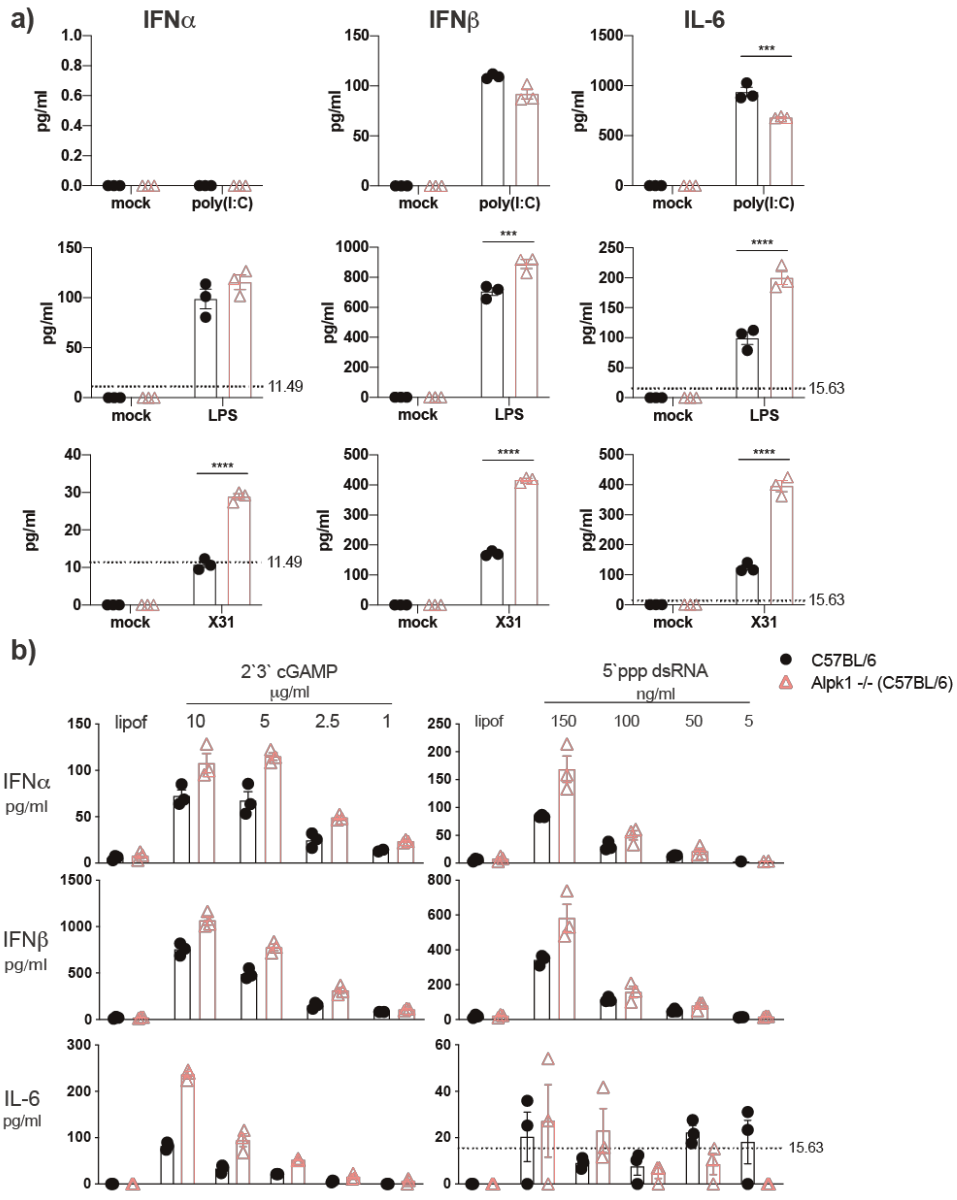

Figure 5.6 Secretion of IFN-α/β and IL-6 is significantly increased in LPS stimulation and X31 infection of *Alpk1*$^{-/-}$ BMDMs compared to WT controls in vitro. BMDMs were stimulated in vitro with as previously described and IFN-α/β and IL-6 protein concentrations assessed in the collected supernatants 24h post-stimulation

by ELISA. **A.** TLR3 stimulation with poly(I:C), TLR4 activation by LPS and influenza infection (for dosages of particular stimuli, unless indicated, refer to Material and Methods). **B.** Responses of BMDMs to transfection of cGAS/STING stimulus 2'3' cGAMP or RIG-I stimulus 5'ppp dsRNA, of indicated concentrations. Statistical testing 2-way ANOVA (* $p<0.05$; ** $p<0.01$; *** $p<0.001$; **** $p<0.0001$; non-significant comparisons are not shown.). Results are represented as mean±SEM. Dashed lines represent lower detection limit of the corresponding ELISA assay where appropriate. The represented data is from two independent experiments and representative of a total of ten independent assays.

Similar to the previous chapters of this thesis, mRNA expression levels of different targets during stimulation were also tested in *Alpk1*$^{-/-}$ BMDMs *in vitro* (Figure 5.7). Both in TLR4 and TLR9 stimulations, as well as in influenza infection (Figure 5.7a) and STING or RIG-I specific stimulations (Figure 5.7b), there was no difference in expression of any of the targets investigated. Namely, *Ifn-β1*, *Il-6* and *Stat1* expression were similar between the two genotypes 6h post-stimulation, regardless of the stimulus used. This result was indeed in line with the observed similar mRNA expression levels between congenic 129.C3BR17 and 129S6 BMDMs, as well as (in some instances) between BL/6 and 129S6 cells. The lack of discernible differences in mRNA expression could indicate that the studied locus and the Alpk1 gene product affect cytokine production post-transcriptionally. These results will be further discussed in the Discussion to this chapter and this thesis.

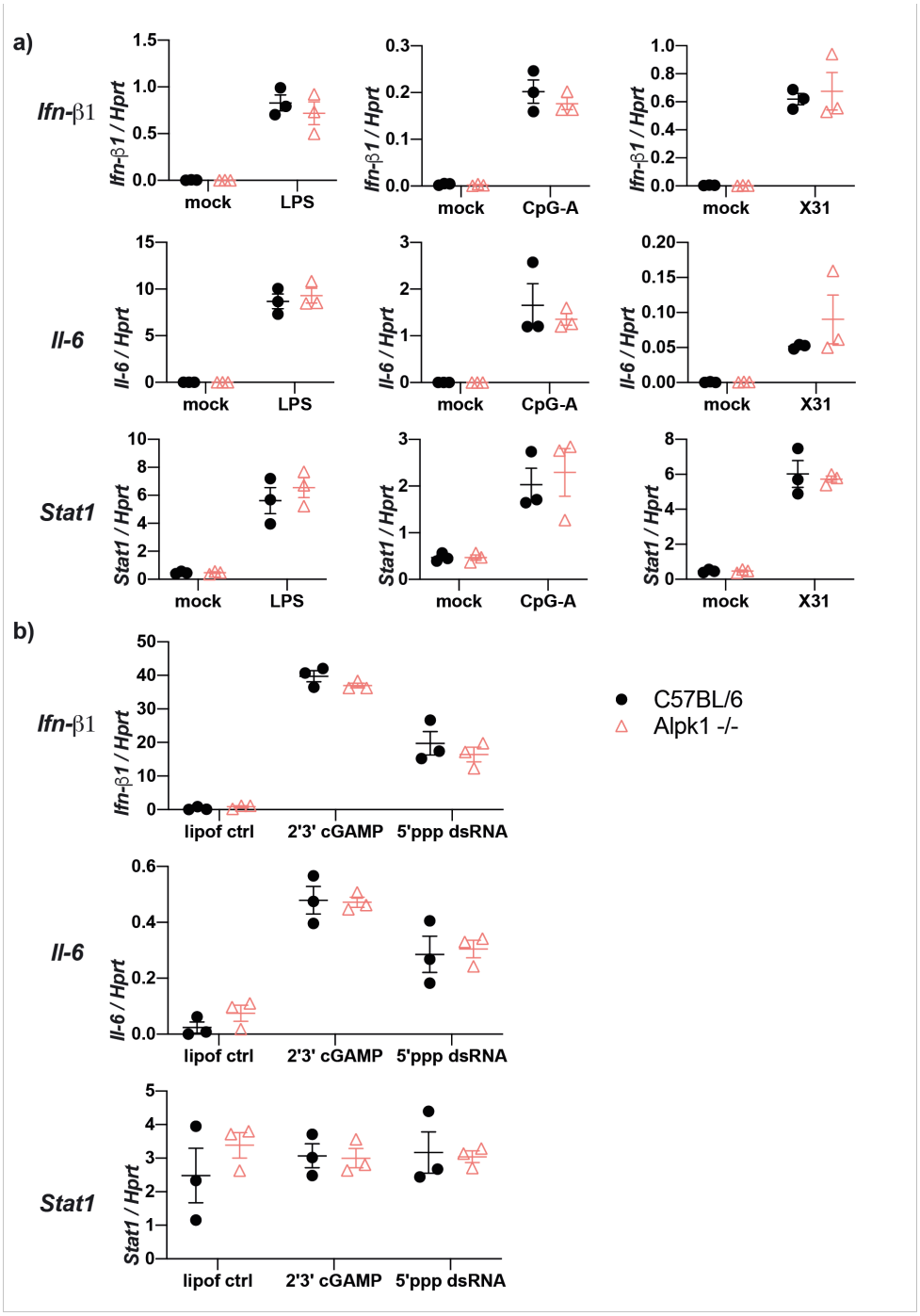

Figure 5.7 mRNA expressions levels of *Ifn-β1*, *Il-6* and *Stat1* are not affected by the absence of Alpk1 in the BL/6 genome, in different stimulation settings as well as influenza infection in vitro. BMDMs of BL/6 WT and *Alpk1*$^{-/-}$ were exposed to **A.** LPS (TLR4), CpG-A (TLR9), X31 virus or **B.** 2'3' cGAMP (cGAS/STING), 5'ppp dsRNA (RIG-I) for 6h. Cells were then processed and mRNA quantified by QPCR. The y-axis values represent fold enrichment of the target compared to the housekeeping gene HPRT. Per experiment **A.** or **B.** each symbol per genotype represents a BMDM culture from a single mouse (biological replicates). Statistical comparisons were performed using a 2-way ANOVA (* p<0.05; ** p<0.01; *** p<0.001; **** p<0.0001;

non-significant comparisons are not shown.). The represented data is from three separate experiments, and representative of 10 assays.

5.2.4 *In vitro* pDC cytokine secretion during infection and stimulations in *Alpk1*$^{-/-}$ background

In Chapter 3 of this thesis, a reduction in IFN-α/β production in 129.C3BR17 pDC-enriched cultures was observed compared to 129S6 controls. Given that the *Alpk1*$^{-/-}$ BMDMs showed cytokine production patterns similar to those of 129S6 cells *in vitro*, responses of pDC-enriched cultures to stimulation were tested as well. In response to TLR7-specific agonist poly:U, *Alpk1*-deficient cultures showed a significant increase in the production of IFN-α and IL-28, with the same trend observed for IFN-β (Figure 5.8a). A higher IFN-β and IL-28 response was also recorded in *Alpk1*$^{-/-}$ cells in response to the typical TLR9 stimuli CpG-A and CpG-B. The most striking differences in IFN production were found upon infection of pDC-enriched cultures with different influenza viruses (Figure 5.8b). Both in infection with X31 (MDCK-derived) and PR8, the pDCs lacking *Alpk1* had very strongly increased IFN-α/β production compared to WT controls. IL-28 production was also significantly increased in *Alpk1*-deficient cultures. While this result has shown that *Alpk1* might have a role to play in *in vitro* stimulation conditions, the lack of an *in vivo* phenotype remained. Also, at this point it was not possible to determine whether the effects of *Alpk1* were upstream or downstream of the IFNAR receptor and thus of the IFN-α positive amplification loop. However, the impact of newly synthetised proteins upon stimulations with TLR agonists or influenza virus could be addressed in BMDMs by cycloheximide treatment.

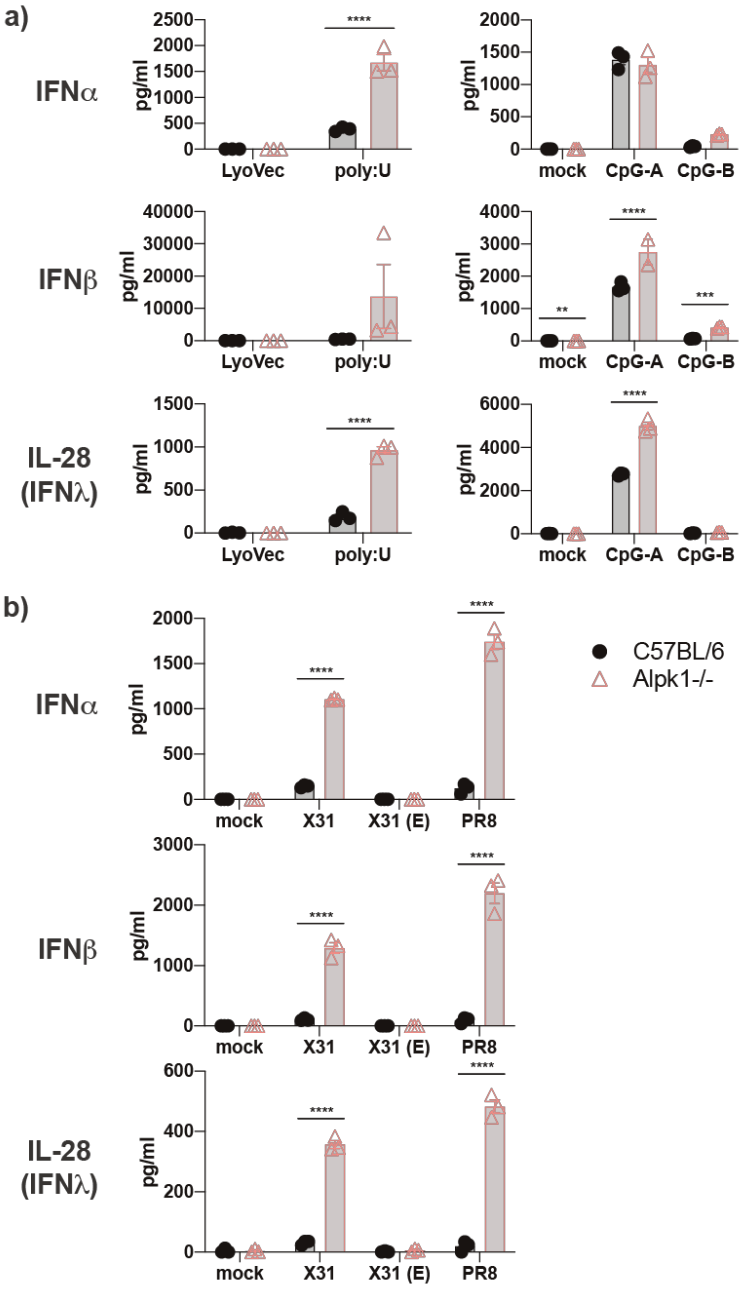

Figure 5.8 *Alpk1* deficiency in pDC-enriched cultures results in strong increases in IFN-α/β and IL-28 production in response to TLR7/9 stimulation and influenza infection. pDC-enriched cultures were generated from the bone marrow of BL/6 and *Alpk1*$^{-/-}$ mice, as previously described. Stimulated cultures were MACS-selected for B220-positivity. The cultures were exposed to **A.** TLR7 agonist poly:U or TLR9 agonists CpG-A/B or **B.** X31 virus (MDCK or (E)-egg derived) or PR8 virus for 24h hours prior to collection of supernatants for ELISA analyses. In each genotype, technical replicates were achieved by pooling bone marrow from 3 male mice and splitting the cultures into replicates post-differentiation and MACS purification. Statistical test: two-way ANOVA; significance * p<0.05; ** p<0.01; *** p<0.001; ****

p<0.0001; non-significant comparisons are not shown. The data is representative of two independent experiments.

5.2.5 Role of newly synthetised proteins in ALPK1-driven responses in BMDMs

The innate immune response effects are a result of immediate signalling pathway activation (RLR/TLR/STING), but also of the effect of *de novo* synthetised proteins (IFNAR cascade for example). Previous results did not allow to conclude at which point during the innate immune response *in vitro* ALPK1 had a role. To get an indication on the timing of ALPK1 involvement and whether it required *de novo* synthetised proteins to exercise its role, BMDMs were exposed to cycloheximide, a blocker of protein synthesis, before and during *in vitro* stimulations. Transcription of *Ifn-β1*, *Il-6* and *Stat1* mRNA in response to stimuli in presence of cycloheximide was assessed in BMDMs from WT and *Alpk1*$^{-/-}$ mice (Figure 5.9). While overall an increase in *Ifn-β1* and *Il-6* expression was observed in unstimulated and stimulated cells, there was no difference between WT and *Alpk1*$^{-/-}$ BMDMs in any of the conditions. However, it is worth noting that cycloheximide treatment did in all cases increase the expression of the two targets, and that this effect was amplified in time. Stat1 expression was reduced (but not abrogated) upon cycloheximide treatment in the context of TLR3 stimulation with poly(I:C), but was otherwise independent of *Alpk1* presence in the BL/6 genome. Overall, these results once again confirmed that the expressions of *Ifn-β1* and *Il-6* were responsive to the abrogation of *de novo* protein synthesis, but ALPK1 did not have an impact on this effect.

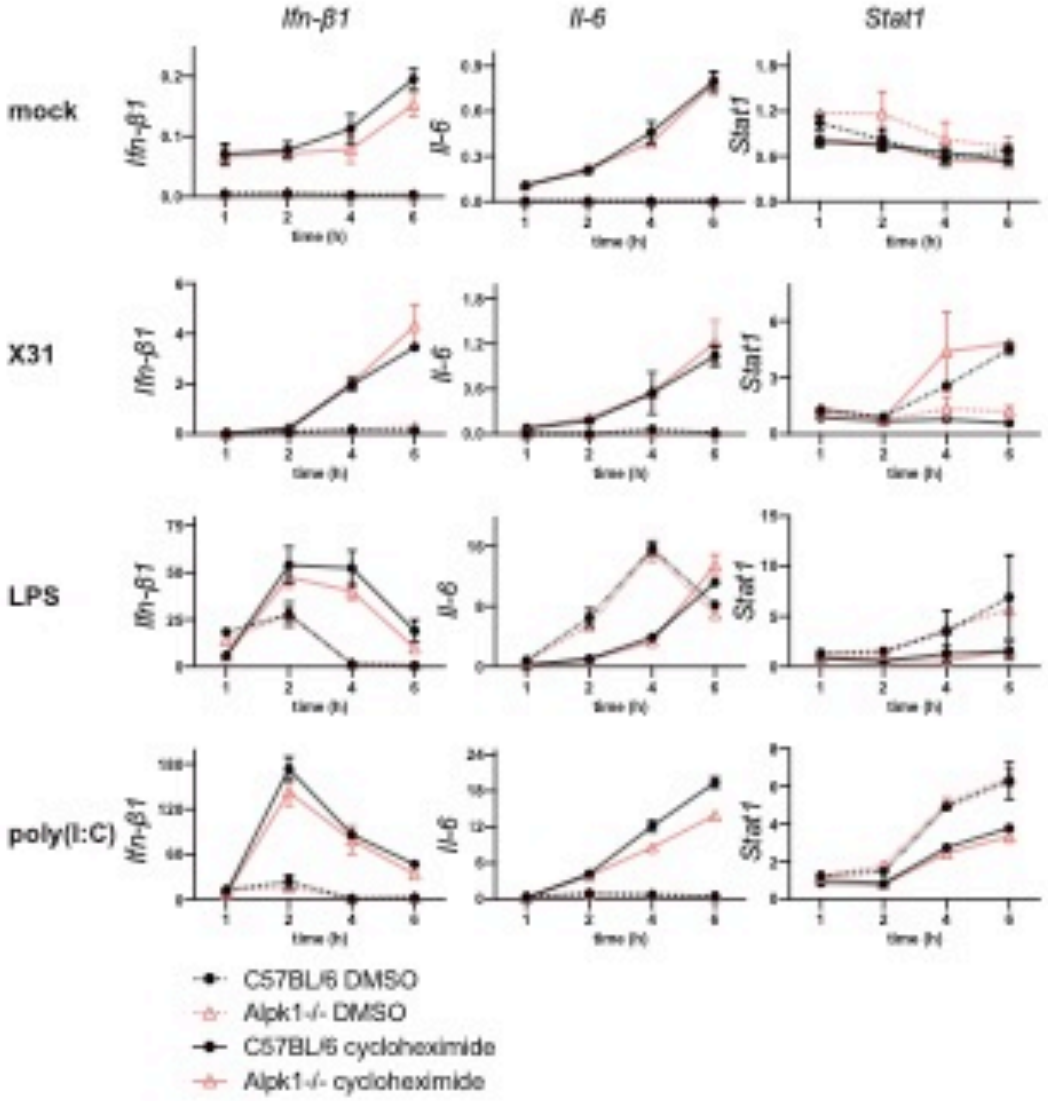

Figure 5.9 Cycloheximide treatment releases the brakes on *Ifn-β1* and *Il-6* mRNA expression in both WT and *Alpk1*$^{-/-}$, but there is no effect of Alpk1 on the impact of newly synthetised proteins on this expression pattern. BMDMs from WT and *Alpk1*$^{-/-}$ mice were incubated with cycloheximide or DMSO (cycloheximide control) for 1h prior to exposure to LPS, poly(I:C) or the X31 virus for 6h in total. At 1h, 2h, 4h and 6h post-stimulation cells were harvested, processed and mRNA levels of *Ifn-β1*, *Il-6* and *Stat1* quantified by QPCR. Represented values on the y axes are fold enrichments relative to the expression of the housekeeping gene HPRT. Expressions at different time points are represented as a mean±SEM of three biological replicates. Statistical testing two-way ANOVA compared BL/6 vs *Alpk1*$^{-/-}$ conditions within DMSO, or within cycloheximide treatment conditions. No significance defined under $p<0.05$ was found. Results from one experiment only.

5.2.6 PRR-triggered activation of signalling pathways in *Alpk1*$^{-/-}$ BMDM

As mRNA expression in the first hours post-stimulation was similar between the two genotypes, it was necessary to check the activation of cellular pathways leading to their expression. This was done by assessing the phosphorylation levels of some of the key components of the pathways activated by stimulation. Moreover, as it became clear that a more general approach was needed to identify the possible phosphorylation targets of ALPK1, it was necessary to optimise the concentrations of stimuli used and the stimulation times for this particular experiment.

Stimulations with LPS, 2'3' cGAMP and 5'ppp dsRNA were tested in WT and *Alpk1*$^{-/-}$ BMDMs at different time points (Figure 5.10). In 2'3' cGAMP stimulation, an increase in phosphorylation of both TBK1 and p65 was observed, more intense in the *Alpk1*$^{-/-}$ background than in the WT-cells (Figure 5.10a). Overall, at a higher concentration of the stimulus (15 μg/ml) there was no difference in TBK1 phosphorylation observed regardless of the time point (1h or 2h), but p65 phosphorylation was increased in the *Alpk1*$^{-/-}$. Possibly this indicated that the concentration of the stimulus was saturating and that the differences between the genotypes were only observable very early on. On the other hand, reducing the concentration to 5μg/ml yielded higher phosphorylation levels of TBK1 reproducibly, at both time points. Similarly, in the case of 5'ppp dsRNA, lowering the concentration of stimulus uncovered some differences in TBK1 and p65 phosphorylation (Figure 5.10a). In response to LPS stimulation (Figure 5.10b), an upregulation of phosphorylation of p65 and p38 was observed in the *Alpk1*$^{-/-}$ cells. TBK1 phosphorylation was only observed at short time points of stimulation. Overall, the results had pointed towards possible timepoints and stimuli concentrations to use in the future global analyses. For 2'3' cGAMP, a concentration of 5μg/ml was used, and for 5'ppp dsRNA 50ng/ml. Also, increases in phosphorylation of the analysed proteins are indicating a possible increase in activation of NFκB-mediated pathways in *Alpk1*$^{-/-}$ cells.

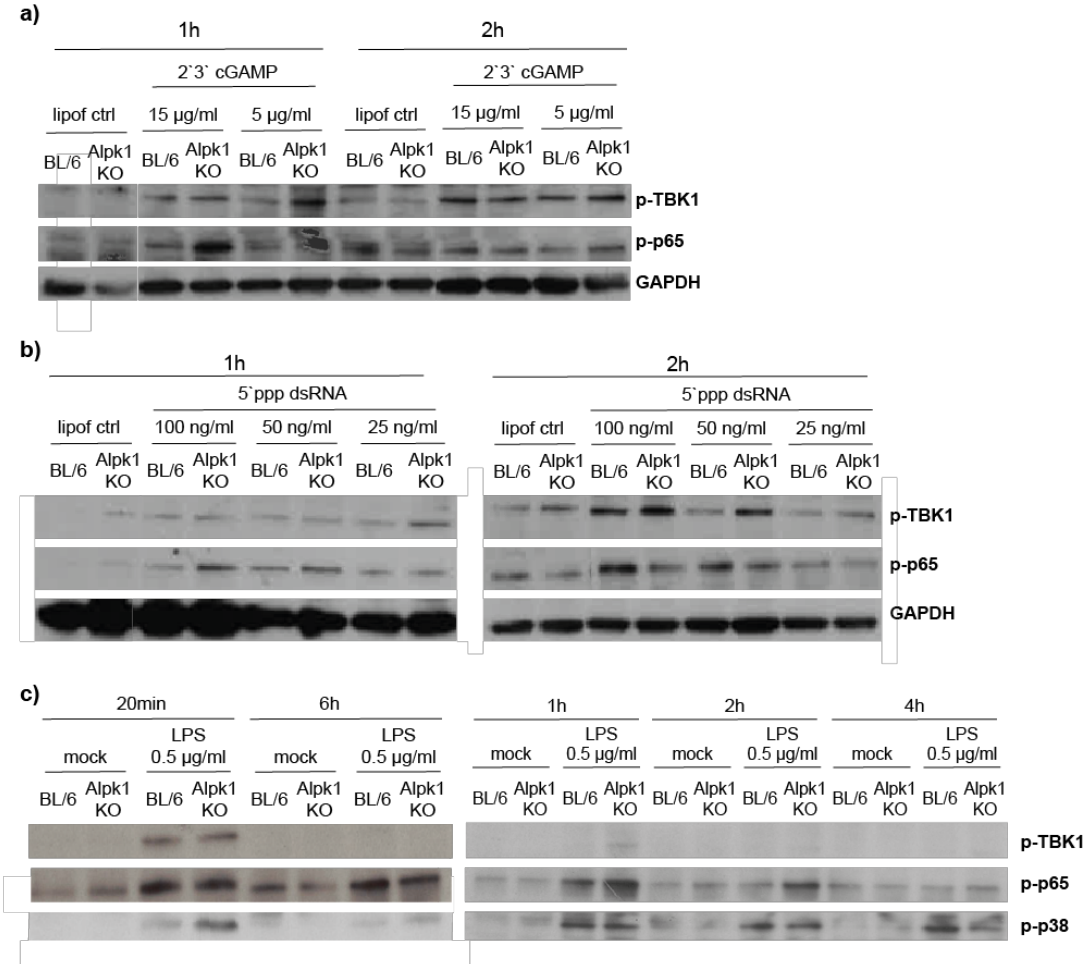

Figure 5.10 At intermediate-low concentrations of stimuli, subtle increases in phosphorylation of TBK1, p65 and p38 are detected in *Alpk1*$^{-/-}$ BMDMs compared to WT controls. C57BL/6 and *Alpk1*$^{-/-}$ BMDMs were **A.** transfected with 2'3' cGAMP, **B.** 5'ppp dsRNA or **C.** exposed to LPS, and harvested and lysed at the indicated times post-stimulation. Total protein was extracted, dosed, and equal amounts of protein loaded onto gels, separated and transferred to nitrocellulose membranes as described in Material and Methods. Membranes were incubated with antibodies directed against phosphorylated TBK1, phosphorylated p65, phosphorylated p38 and GAPDH (details in Material and Methods). Representative of six experiments testing different stimuli concentrations and timings.

Although some phosphorylation targets of ALPK1 (eg TIFA and myosin-IIA, see Introduction) were described in other systems, no target or role of Alpk1 in viral infection was known. Since lack of Alpk1 seemingly incurs a survival disadvantage in influenza infection *in vivo* and increased cytokine and IFN-α/β production during TLR/RLR/STING pathway activation *in vitro,* an attempt was made at identifying Alpk1 phosphorylation targets by phospho-proteomics.

5.2.7 Global phospho-proteomics assays to identify Alpk1 phosphorylation targets in stimulated BMDMs

In total, two phospho-proteomics experiments were carried out as a part of this PhD project. However, only the second one will be presented in detail in this chapter, as the first assay served as a pilot experiment and was performed with no biological replicates. In both, given the number of cells and protein quantity required, the cell type of choice were bone marrow derived macrophages. The concentrations of stimuli used and the timepoints of stimulations were chosen based on WB optimisation experiments for which results are shown above.

While the details of the first phospho-proteomics assay will be reported in the Appendix (in detailed text and Figure 8.4, Figure 8.5, Figure 8.6, and Figure 8.7) the experiment will be briefly described here. The main goal of this assay was to examine different conditions of stimulation and the responses of WT and *Alpk1*$^{-/-}$ BMDMs. The assessed conditions included “mock” untreated cells (30min incubation), LPS (30min) treated cells, empty lipofectamine control transfection (2h), 2’3’ cGAMP transfection (2h) and 5’ppp dsRNA (2h) transfection. These stimuli were each compared between BL/6 and *Alpk1*$^{-/-}$ cells, in a single replicate per condition. LPS stimulation induced overwhelmingly large changes in global phospho-proteome compared to untreated cells, while transfected agonists showed little difference to the negative control for transfection (empty lipofectamine). However, when the BL/6 and *Alpk1*$^{-/-}$ BMDMs were compared between them, only subtle differences in protein phosphorylation were detected, especially in the case of LPS stimulation. This prompted a change in the experimental design for the second experiment, where only transfection stimulation conditions were maintained to be tested and the stimulation time reduced to 1h.

For the second phospho-proteomics experiment, three conditions of stimulation were tested in BL/6 and *Alpk1*$^{-/-}$ BMDMs: empty lipofectamine transfection, 2’3’ cGAMP transfection and 5’ppp dsRNA transfection. Each of the stimulations was maintained for 1h before processing cells for analysis. Moreover, five biological replicates per genotype per condition were introduced for this assay.

Principal component analysis was performed on the processed data to identify the main drivers for variation in phosphorylation across conditions and replicates (Figure 5.11a). Based on Component 1 (over 80% of total variance), the

lipofectamine-control samples of both genotypes clustered away from the treated samples which were not notably different between them. While the impact of the treatment is visible, almost no variance according to the top two components was detected between genotypes. No genotype-dependent variance was detected upon comparing Components 2 and 3 (Figure 5.11a), but along Component 3 all treatment conditions clustered away from each other. Ultimately, taking into account variance based on Component 4, the genotype replicates could be segregated to some degree in the lipofectamine-treated samples but not in the stimulated ones. Thus, at a global phospho-proteome level, ALPK1 does not exert strong influence.

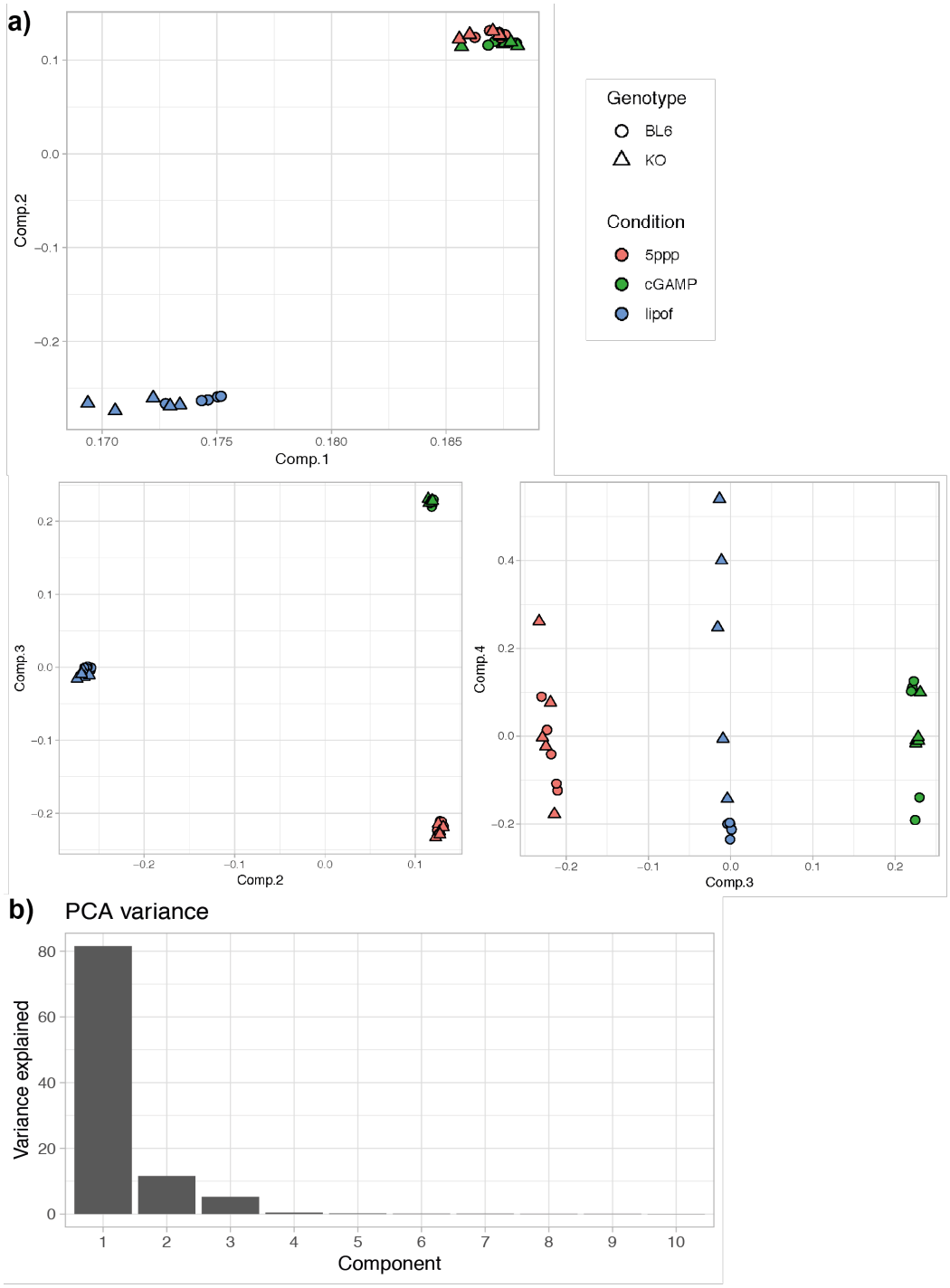

Figure 5.11 Principal component analysis based on reporter ion intensities data from lipofectamine, 2'3' cGAMP and 5'ppp dsRNA treated WT and *Alpk1*$^{-/-}$ BMDMs reveals more variation between treatments than between genotypes within the same treatment. BMDMs were seeded as previously described and stimulated for 1h with empty lipofectamine, lipofectamine+2'3' cGAMP or lipofectamine+5'ppp dsRNA. Five biological replicates were used per genotype. Principal component analysis of all the entire phospho-proteomics dataset of both genotypes was performed. The analysis was completed using normalised ion intensities from

MaxQuant and Perseus software, and PCA analysis and figure generation completed in R. **A.** PCA for three first components Squares: WT samples, triangles: *Alpk1*$^{-/-}$; blue: lipofectamine control; green: 2'3' cGAMP stimulation, salmon: 5'ppp dsRNA stimulation. **B.** Percentage of variance explained by the different components. NB: to avoid introducing a bias because lipofectamine control samples were run separately, a normalisation for median ion intensity and labelling efficiency has been applied to this dataset before the represented analyses. Data from one experiment.

To observe the effects of ALPK1, analyses that identify local perturbations of the phospho-proteome were performed. To this end, the unequal variances two-sample t-test called Welch was used to compare means of reporter ion intensities between WT vs *Alpk1*$^{-/-}$ BMDMs. The Welch test results can be represented in form of volcano plots (Figure 5.12). The fold-change in mean reporter intensity between genotypes is represented on the x axis as $\log_2$(C57BL/6 - *Alpk1*$^{-/-}$). On the y axis, the log-transformed p-value of the Welch test for each phospho-peptide is represented, and the red line indicates the threshold of statistical significance (y=-$\log_{10}$(0.05)=1.3).

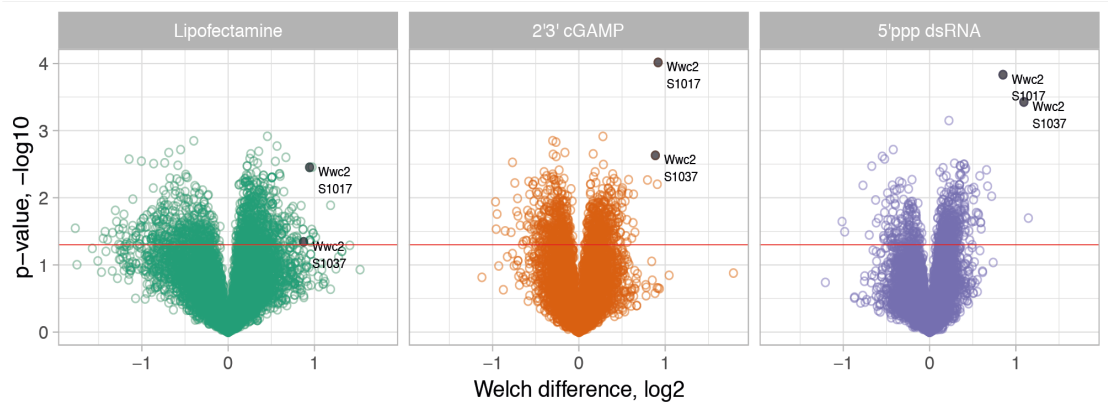

Figure 5.12 Volcano plots of all phospho-residues detected by MaxQuant analysis of phospho-proteomics data, following a Welch t-test of difference of means BL/6-*Alpk1*$^{-/-}$. Normalised mean ion intensities across 5 biological replicates in *Alpk1*$^{-/-}$ and BL/6 BMDMs were compared by a Welch t-test. The difference, represented as $\log_2$(BL6- *Alpk1*$^{-/-}$) was plotted against the p-value score of the test represented as -$\log_{10}$(p-value). The volcano plots were plotted in R using data from Perseus software. Each dot is an identified phospho-site regardless of its score or detection history. The red line indicates statistical significance at -$\log_{10}$(0.05)=1.3. The two residues of WWC2 are represented with the residue nature and position and the gene name. Data from one experiment.

WWC2 was the only protein that was common to the two stimulation conditions, with noticeable phosphorylation differences on two residues, Ser1017 and Ser1037, represented as full dots in Figure 5.12. The phosphorylation patterns can be clearly visible in the profile plots for all three conditions. Ser1017 appears

phosphorylated in a very reproducible pattern in all three stimulation conditions (though the significance of the difference is lower in the case of lipofectamine), whereas Ser1037 phosphorylation is induced by stimulation in both 2'3' cGAMP and 5'ppp dsRNA. Both of these residues have been detected previously with high throughput methods (Perseus® data information based on phosphosite.org database, not shown). Given that the phosphorylation patterns of the two residues are similar between control and stimulated conditions, it is possible that this lack of WWC2 phosphorylation in *Alpk1*$^{-/-}$ BMDMs is a baseline state. Ultimately, this experiment does not allow to conclude on the overall expression of WWC2 in BMDMs. It is possible that the lack of phosphorylation observed in the *Alpk1*$^{-/-}$ cells is in fact due to an overall reduction in protein levels.

Moreover, the volcano plot confirmed that there are only few phosphorylation sites that are more than 1.5-fold less phosphorylated in the *Alpk1*$^{-/-}$ BMDMs (corresponding to x=0.585). Of a total 11807 phospho-peptides detected, only 10% or less showed significantly different mean phosphorylation between the two genotypes: 1037 in lipofectamine control, 771 in 2'3' cGAMP, and 540 in 5'ppp dsRNA stimulation. Of those, the phospho-residues showing 1.5x less phosphorylation in *Alpk1*$^{-/-}$ cells in all three stimulations are represented in Table 5.1 (for lipofectamine only the highest differentially phosphorylated residues are represented).

Table 5.1 Phospho-residues significantly less phosphorylated in *Alpk1*$^{-/-}$ BMDMs compared to WT, in lipofectamine, 2'3' cGAMP or 5'ppp dsRNA stimulations. The gene names and names of leading proteins (according to Uniprot in Perseus® software), as well as the nature and position of the identified phosphorylated residues are represented. S- serine, T- threonine, Y – tyrosine. All of the represented residues had a significant score in the Welch test comparing the means of *Alpk1*$^{-/-}$ and BL/6 BMDMs phosphorylation scores, and had 1,5-fold or lower phosphorylation in the *Alpk1*$^{-/-}$ background. In the case of lipofectamine, where 50 residues were identified according to these criteria, only the first 15 are represented. The known site column indicates whether this phospho-residue has been identified previously, in high-throughput studies or other. NB: only the phosphoresidues belonging to identified proteins were represented in this table. Data from one experiment.

	Gene name	Protein name	Phospho-residue	AA position	Known site ?
lipofectamine	Raly	RNA-binding protein Raly	S	294	y
	Cir1	Corepressor interacting with RBPJ 1	S	202	y
	Fen1	Flap endonuclease 1	S	352	y
	Srsf7	Serine/arginine-rich splicing factor 7	S	210	y
	Cenpu	Centromere protein U	S	106	y
	Cenpu	Centromere protein U	S	111	y
	Srrm2	Serine/arginine repetitive matrix protein 2	S	251	y
	Wwc2	Protein WWC2	S	1017	y
	Wwc2	Protein WWC2	S	1037	y
	Cir1	Corepressor interacting with RBPJ 1	S	425	y
	Ndrg1	Protein NDRG1	T	335	y
	Macf1	Microtubule-actin cross-linking factor 1	S	2823	y
	Hdac2	Histone deacetylase 2	S	422	y
	Pdcd4	Programmed cell death protein 4	S	94	y
	Srrm2	Serine/arginine repetitive matrix protein 2	T	1439	y
2`3` cGAMP	Wwc2	Protein WWC2	S	1017	y
	Rabep1	Rab GTPase-binding effector protein 1	S	410	y
	Wwc2	Protein WWC2	S	1037	y
	Pdcd4	Programmed cell death protein 4	S	94	y
	Asxl2	Putative Polycomb group protein ASXL2	S	653	y
	Sort1	Sortilin	S	819	y
	Kctd12	BTB/POZ domain-containing protein KCTD12	S	178	y
5`ppp dsRNA	Safb	Scaffold attachment factor B1	S	24	n/
	Wwc2	Protein WWC2	S	1037	y
	Wwc2	Protein WWC2	S	1017	y
	Kctd12	BTB/POZ domain-containing protein KCTD12	S	178	y
	Tcp11l2	T-complex protein 11-like protein 2	S	16	y
	Pdcd4	Programmed cell death protein 4	S	94	y
	Kctd12	BTB/POZ domain-containing protein KCTD12	Y	163	n/
	Nucks1	Nuclear ubiquitous casein and cyclin-dependent kinase substrate 1	S	181	y
	Nucks1	Nuclear ubiquitous casein and cyclin-dependent kinase substrate 1	T	179	y

To address the possibility that the reduced WWC2 phosphorylation in the *Alpk1*$^{-/-}$ background was due to reduced protein quantity overall, the total proteome left after purification and phospho-peptide enrichment was analysed for the first phospho-proteomics experiment (results not shown in this thesis). However, WWC2 protein was not detected in any of the samples. This suggests either that WWC2 expression is very low in general, or that almost the totality of the protein is being phosphorylated upon stimulation in both genotypes, leaving little to none to detect in the leftover proteome. However, in spite of the total protein quantity results,

reproducible reduction in phosphorylation of WWC2 was a novel result. Its implications are addressed further in this thesis with validation experiments and are discussed more in detail in the Discussion part of this chapter and further.

For a more detailed overview of the pathways enriched in this dataset, the Reactome knowledgebase was used (Fabregat et al., 2018). Only the proteins comprising phospho-peptides with a significant Welch test p-value were analysed (in Figure 5.12 all residues above the y=1.3 line). The results represented in this and the subsequent figure show p-values attributed to each of the pathways, but not the adjusted p values (FDRs), since only one pathway showed a significant padj (FDR). This result is discussed in detail further.

Very few pathways were found to have a significant p-value, and only one showed a significant adjusted p-value (FDR). Moreover, the pathway “entity ratios” (ratio of the number of proteins assigned to a pathway vs. the total number of proteins in that pathway within the Reactome database) were extremely low in all conditions. This indicated a very low representation of pathways by their components from the dataset. Of the pathways with the highest p-values, almost all in the lipofectamine control involve mRNA synthesis and stability (Figure 5.13a). The “mRNA splicing” and “Metabolism of RNA” showed amongst the highest entity ratios (respectively around 2% and 6%). In 2’3’cGAMP stimulation (Figure 5.13b), the proteins with a lack of phosphorylation in *Alpk1*$^{-/-}$ cells were attributed to mRNA elongation and translation initiation pathways. The 5’ppp dsRNA stimulation unveiled enrichment in, amongst others, mTORC and SOS-mediated signalling and translation initiation pathways, but only the “HDM demethylate histones” pathway was found to be significantly enriched (FDR) (Figure 5.13c). Therefore, it seems like in the *Alpk1*$^{-/-}$ BMDMs, the “HDM demethylate histones” pathway components are less phosphorylated than in the BL/6 controls. The entities ratios for both 2’3’ cGAMP and 5’ppp dsRNA stimulations were around or below 1%, which indicated poor representation.

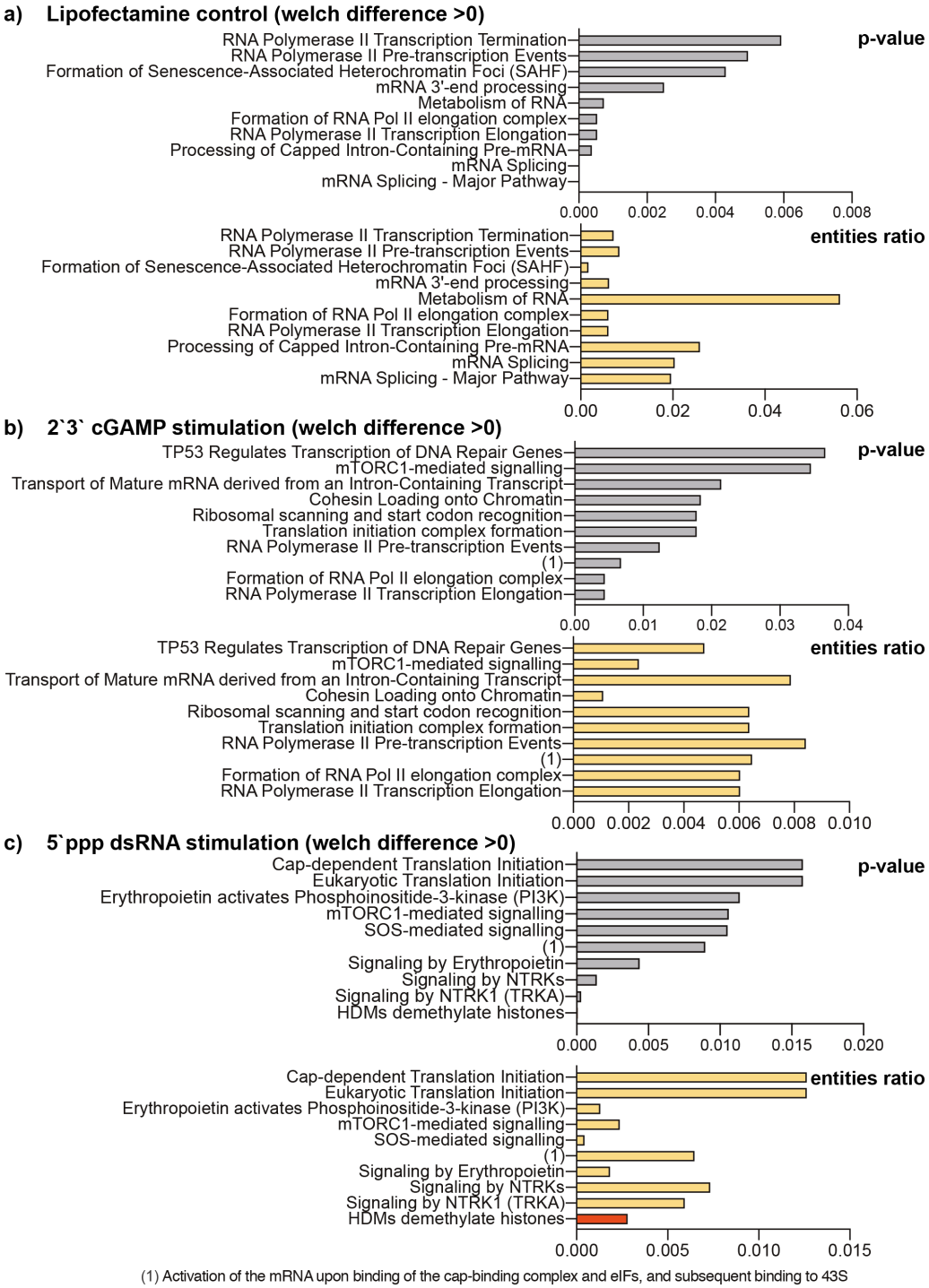

Figure 5.13 Reactome pathway database shows dysregulation in pathways related to mRNA stability and processing in *Alpk1*$^{-/-}$. The bar plots shown were generated following the Reactome database statistical test for enrichment of signalling pathways in the protein list (pathway "over-representation"), which indicates if the submitted dataset contains significantly more proteins assigned to a given pathway than would be the case by chance. The ten pathways with the lowest p-values, each containing proteins that show loss of phosphorylation in *Alpk1*$^{-/-}$ (Welch difference in means is >0) are represented for the three stimuli **A.** lipofectamine, **B.** 2'3' cGAMP

and **C.** 5'ppp dsRNA**.** The number of dataset proteins (entities) assigned to a pathway compared to the total number of proteins (entities) in that pathway, stored in the Reactome knowledgebase, yields a proportion called the "entities ratio". The FDR was also calculated for each pathway to correspond to the p-value, and the only pathway found with an FDR score inferior to 0.05 is marked in red: HDMs demethylate histones. The analysed data is from one phospho-proteomics experiment.

Further, Welch test-significant proteins with increased phosphorylation in *Alpk1*$^{-/-}$ BMDMs vs controls (negative fold-change in Figure 5.12), were also analysed using Reactome (Figure 5.14). In the lipofectamine control stimulation condition, the VEGF-dependent, autophagy and mTOR signalling pathways appeared most significant and most represented (Figure 5.14a). In 2'3' cGAMP stimulation, mTORC1 and phosphatase pathways were detected as containing proteins with increased phosphorylation in *Alpk1*$^{-/-}$ cells. Ultimately, 5'ppp dsRNA induced phosphorylation in various distinct and apparently disconnected pathways in *Alpk1*$^{-/-}$ (Figure 5.14c).

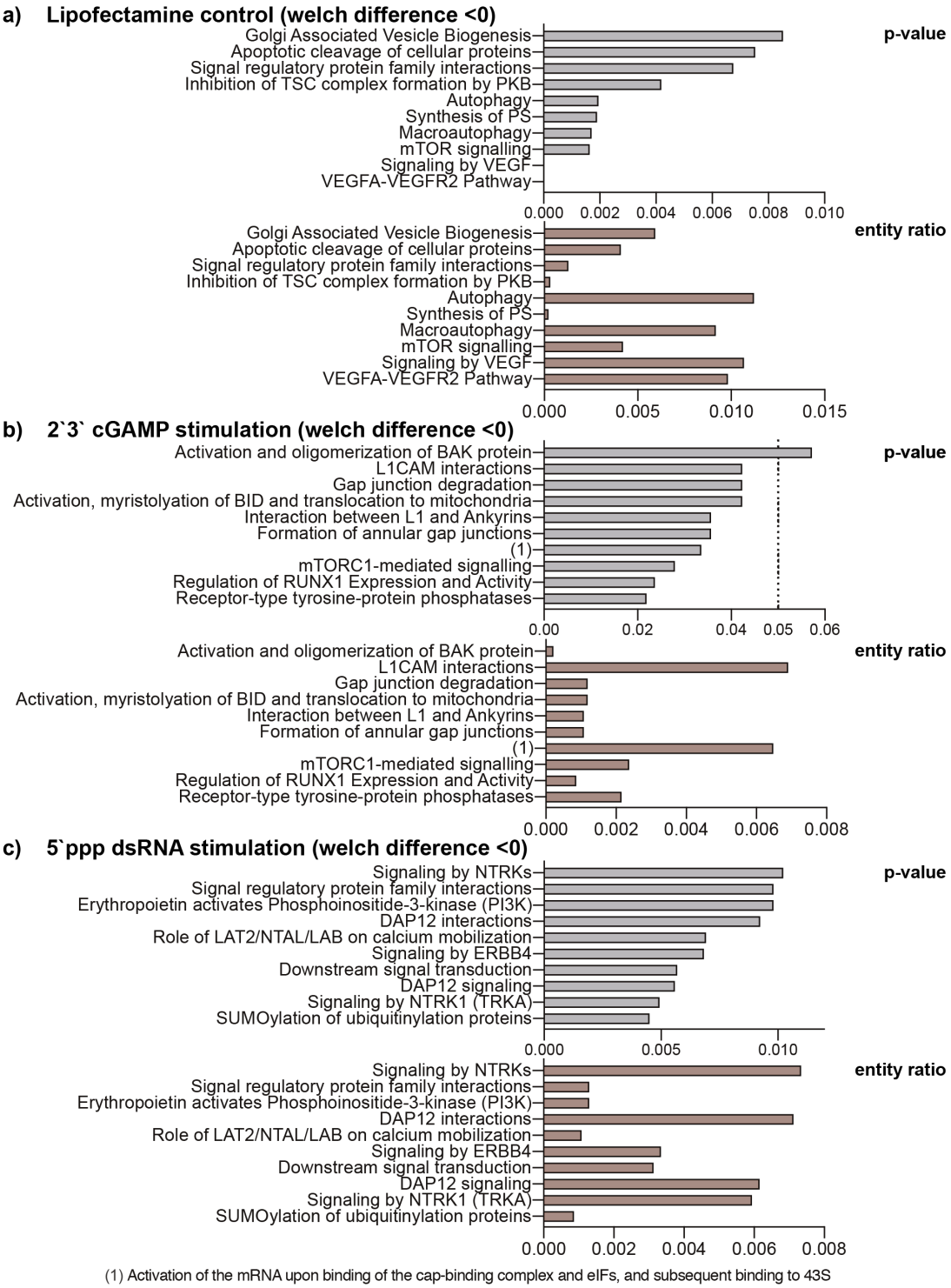

Figure 5.14 Pathways that show increased phosphorylation in *Alpk1*$^{-/-}$ (Welch difference <0) are varied and include SUMOylation of ubiquitination proteins and mTOR signalling. Phospho-residues of the experimental dataset that showed a Welch difference score <0 were assessed for pathway data in the same way as in the previous figure. None of the pathways identified by this means showed a

significant FDR score. The analysed data is from one phospho-proteomics experiment.

5.2.8 RNA-seq of WT and *Alpk1*$^{-/-}$ BMDMs in different stimulations

Results in this chapter pointed towards WWC2 as a candidate phosphorylation target of ALPK1. Validation assays to confirm these findings could not be performed due to the unavailability of a corresponding phospho-WWC2 antibody. The phospho-proteomics assay showed a lack of phosphorylation on Ser1017 and Ser1037 residues in *Alpk1*$^{-/-}$ in all conditions (including the lipofectamine negative control), suggesting that the basal expression of WWC2 is possibly different between the two genotypes. Further, the role of Alpk1 had only been reported in bacterial infection assays that do not correspond to our influenza infection model. Given these circumstances, we decided to use a non-targeted RNA-seq approach to assay the impact of Alpk1 in BMDMs upon stimulation.

In the RNA-seq experiment, a total of five conditions per genotype was probed: mock untreated control, X31 infection (10^6 $TCID_{50}$/ml), empty lipofectamine (transfection control), 2'3' cGAMP transfection and 5'ppp dsRNA transfection. Per genotype, three biological replicates were included. The length of each stimulation was 6h. The RNA-seq reads were aligned to the *M. musculus* genome known genes (more detail in Material and Methods).

To identify the main drivers for transcriptome variation, the RNA-seq results were interrogated using Principal Component Analysis (Figure 5.15). Almost 80% of total variability could be explained by one component, with all others determining 5% or less of total variance. Along Component 1, the transfected conditions (lipofectamine control, 2'3' cGAMP and 5'ppp dsRNA) were segregated from the others (mock/X31). However, little difference was detected within the mock and X31 clusters, whereas the lipofectamine negative control segregated away from the transfected stimuli. Moreover, genotype-dependent variability seemed negligible in all conditions, with all replicates of both genotypes appearing grouped in treatment-determined clusters.

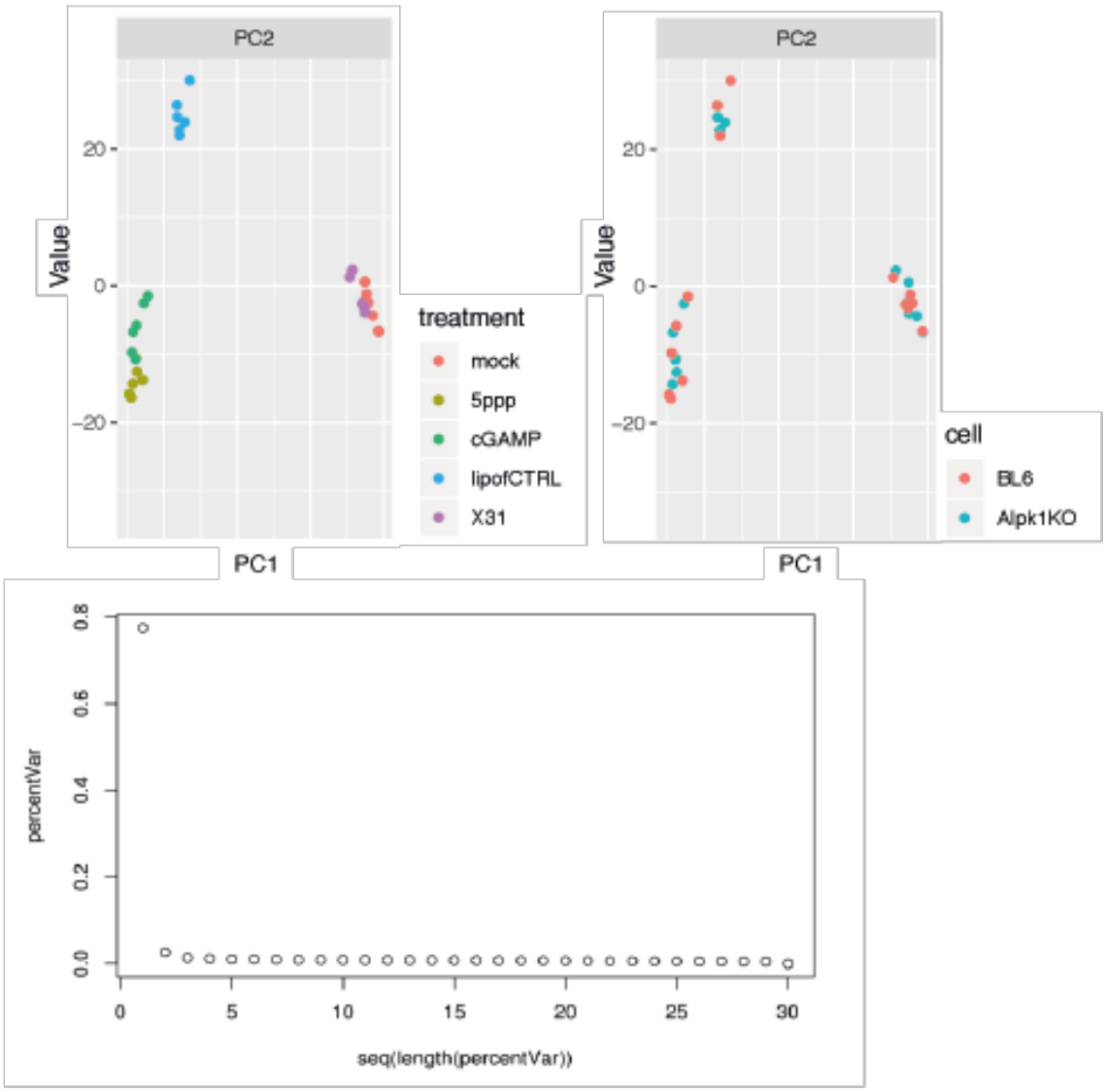

Figure 5.15 Principal component analysis of the RNA-seq dataset shows little impact of genotype on variability, but good segregation by treatment, with X31 infection showing virtually no difference to its negative control. BMDMs were seeded as previously described, at $4*10^5$ cells/condition and three biological replicates per genotype, and infected with X31 10^6 $TCID_{50}$/ml (plus mock negative control) or transfected with empty lipofectamine, 2'3' cGAMP, or 5'ppp dsRNA for 6h. Cells were harvested and processed for RNAseq analysis. All quality control checks were passed (data not shown). A principal component analysis was carried out on the entirety of the dataset obtained by RNA-seq. The proportion of variance explained by each component is represented in the lower graph. In the top two graphs, each coloured dot is a representation of either treatment or genotype, as indicated by the legend. The results represented here are from the only RNA-seq experiment that was carried out in this thesis.

In order to compare the expression of targets between BL/6 and *Alpk1*$^{-/-}$ BMDMs, the DESeq2 method (Love et al., 2014) was used. The results were

visualised in the form of heatmaps (Figure 5.16) using DESeq2 and variance stabilising transformation (VST, see Material and Methods). In Figure 5.16a, only the significantly differentially expressed genes between BL/6 and *Alpk1*$^{-/-}$ backgrounds from the statistical test are represented. It is worth noting that for these heatmaps the column clustering was enforced in order to keep the genotype replicates together for a clearer comparison. The general lack of effect of genotype on gene expression variation remained visible, confirming the findings of the PCA plots where no segregation between genotypes was observed. In addition, it is clear from this heatmap that the X31 infection did not induce significant changes in gene expression compared to the negative control. Meanwhile, the transfection of two agonists seemed to induce slight changes compared to their transfection control (lipofectamine).

Further, we assessed the expression in the two genotypes of significantly differentially expressed genes induced by stimulation. In short, significantly differentially expressed genes - within each genotype - between X31 infected and mock BMDMs, and between 2'3' cGAMP/5'ppp dsRNA and lipofectamine controls were first detected. Therefore, a total of six comparisons was performed (three for BL/6 and three for *Alpk1*$^{-/-}$ BMDMs). Then, of the union of all the significant genes detected across the six comparisons, the 200 genes with the highest log2(fold change) in expression were selected for each of the comparisons. Further, a union of those genes was visualised in the heatmap as a function of DeSeq2 VST. A total of 727 genes is represented in Figure 5.16b. In this way, the effects of the treatment were primarily addressed, for each genotype separately. However, there was no notable difference in gene expression in infection compared to mock especially in the case of viral infection. Treatment of BMDMs with 2'3' cGAMP or 5'ppp dsRNA induced very few noticeable changes compared to their corresponding control, empty lipofectamine transfection. This was the case for both BL/6 and *Alpk1*$^{-/-}$ BMDMs. Notably, the patterns of gene expression were well segregated between treatments

that did or did not include a lipofectamine vehicle, but no major effect of treatment on any side was noticed. This finding confirmed the PCA results presented earlier.

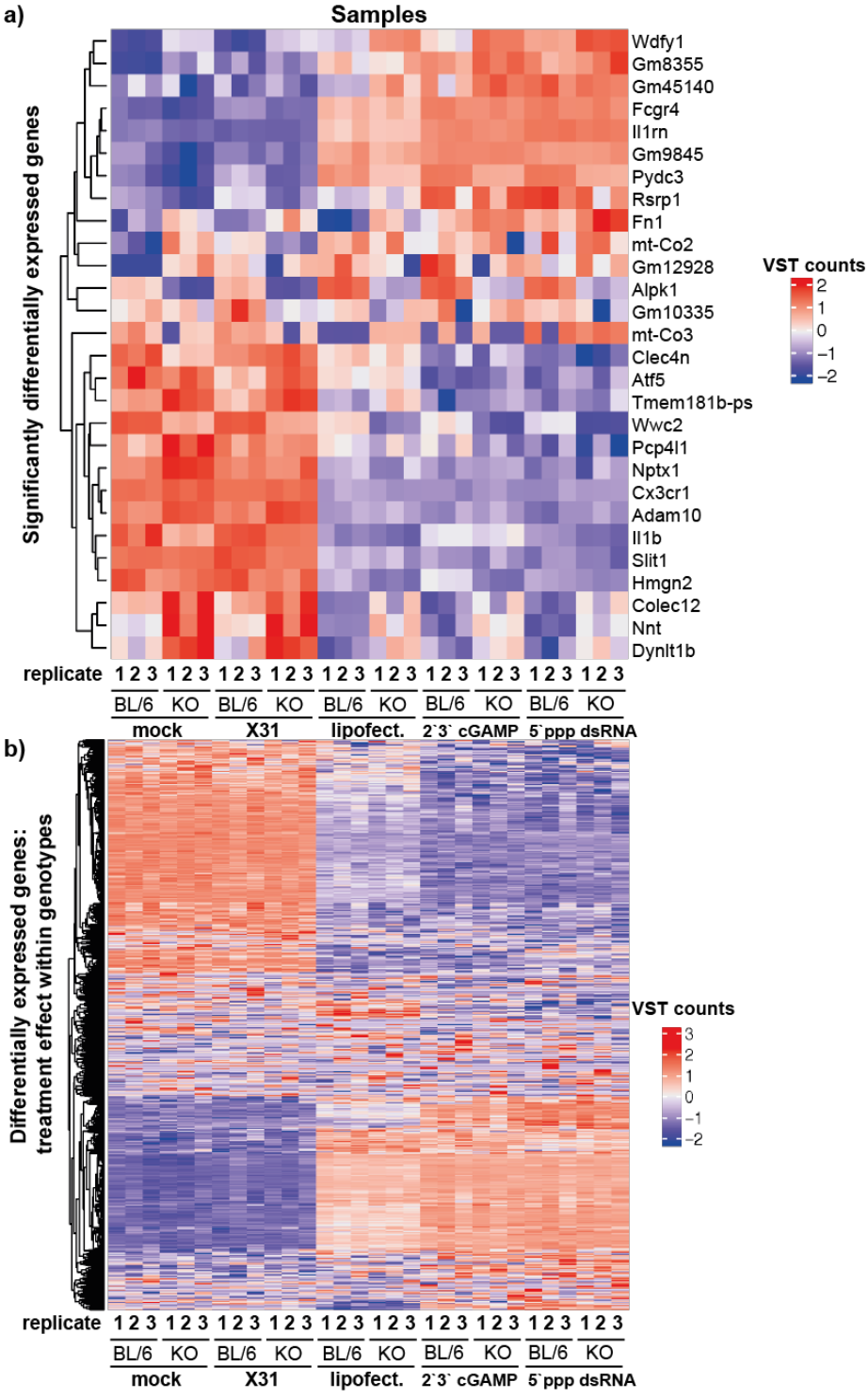

Figure 5.16 Little inter-genotype difference is detected in the RNA-seq significant mRNA dataset, and the effect of treatment per genotype-ls only marginal; stimulation conditions seem to be very similar between them. Top heatmap: analysis of differential gene expression was completed using the DeSeq2 package.

Expression of each gene identified in the dataset was compared between BL/6 and *Alpk1*$^{-/-}$ for each control and treatment condition. The significantly (padj≤0.05) differentially expressed genes are represented in a heatmap (unsupervised clustering) as a function of VST (DESeq2). The list of genes is to the right of the heatmap and their full names can be found in the Abbreviations part of this thesis. Bottom heatmap: analysis of differential gene expression was completed using the DeSeq2 package to compare expression of genes between stimulated and unstimulated conditions separately for each genotype. Namely, the comparisons were as follows: BL/6 (mock vs X31), *Alpk1*$^{-/-}$ (mock vs X31), BL/6 (lipofectamine vs 2'3' cGAMP), *Alpk1*$^{-/-}$ (lipofectamine vs 2'3' cGAMP), BL/6(lipofectamine vs 5'ppp dsRNA), and *Alpk1*$^{-/-}$ (lipofectamine vs 5'ppp dsRNA). A union of top 200 dysregulated genes amongst those considered to be significantly differentially expressed (p_{adj}≤0.05) in each of these comparisons, is represented. A total of 727 genes analysed this way are represented as a function of the VST score. The results represented here are from the only RNA-seq experiment that was carried out in this thesis.

Next, fold-changes of BL/6 – *Alpk1*$^{-/-}$ and log-transformed p-values were represented in form of volcano plots, similar to those in the phospho-proteomics experiment. The volcano plots of mock and X31-infected conditions are represented in Figure 5.17a. As expected given the PCA results, very few genes showed significantly different expression between the two genotypes (genes indicated in red dots, above the y=1.3 dashed line). The results confirmed the genotype of *Alpk1*$^{-/-}$ mice, as *Alpk1* was identified as a significantly under-represented gene in the *Alpk1*$^{-/-}$ background. It is worth noting here that the expression of Alpk1 was still detectable even in the KO cells. This finding was due to the lack of read alignment to exon 10 of this gene, as BL/6 *Alpk1*$^{-/-}$ mice from which these cells were derived were generated by exon deletion in the gene sequence. The evidence for this, in the form of Integrative Genomics Viewer® visualisation, is to be found in the Appendix Figure 8.8. All other exons are transcribed in both WT and *Alpk1*$^{-/-}$ BMDMs, with reads aligning to them, thus explaining the background expression still detected in *Alpk1*$^{-/-}$ cells. It is therefore possible that binding or scaffolding properties of ALPK1 are intact even in *Alpk1*$^{-/-}$ mice and cells (more detail in Discussion). *Alpk1* induction of transcription (position of red dot relative to x axis) was similar in mock and X31-infected conditions, possibly indicating that ALPK1 does not impact its own expression during X31 virus recognition. A new gene with a significant expression difference in this analysis was *Wdfy1*, known to be involved in TLR3/4 signaling and moreover, in negatively regulating *Ifn* gene expression (Hu et al., 2015), (Ning et al., 2019). In mock and X31-infected BMDMs alike, the expression of *Wdfy1* was higher

in the *Alpk1*$^{-/-}$ background, which, given its described roles, contradict the previously observed increase in IFN-α/β expression in absence of *Alpk1*. Furthermore, *Wwc2* gene expression was significantly lower in *Alpk1*$^{-/-}$ than in BL/6 BMDMs.

Given the little difference in mock and infected BMDMs, the dataset was interrogated for the expression of viral mRNAs and the results compared between mock and X31-infected cells (Figure 5.17b). Arguably, the stimulation (6h) would be sufficiently long to allow for viral mRNA transcription and viral replication. Since the X31 virus strain used here was propagated in mice and in MDCK cells prior to this stimulation, it is imaginable that it accumulated considerable mutations compared to the publicly available human H3N2 strain sequence used for this alignment. Nevertheless, the sequence alignment detected each of the eight genome segments in the viral genome in the case of infected cells, and none in the mock conditions. Moreover, the count number of detected aligned mRNA was similar between BL/6 and *Alpk1*$^{-/-}$ BMDMs, indicating similar rates of viral replication.

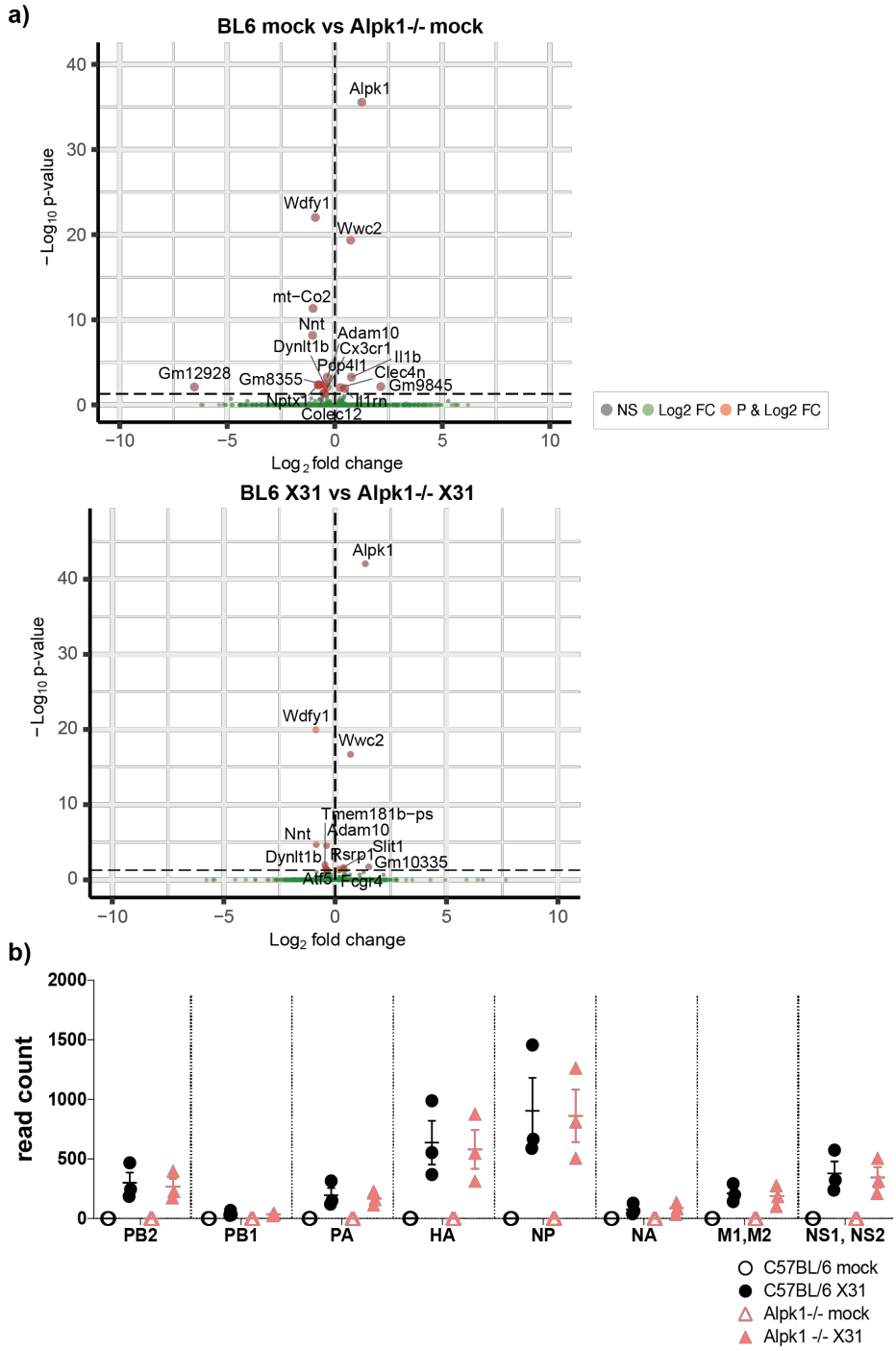

Figure 5.17 Although the X31 infection shows viral mRNA transcription activity equal between genotypes, only a small portion of mRNA targets is significantly dysregulated between Alpk1$^{-/-}$ and BL/6 BMDMs, with only one, mt-Co2, specific to infection. A. Expression of each mRNA identified in the dataset was compared by a t-test between BL/6 and *Alpk1*$^{-/-}$ BMDMs. The value of the fold change (BL/6 – *Alpk1*$^{-/-}$) is represented as a $\log_2$ value on the x-axis, and the significance of the performed test is represented as a -$\log_{10}$(p-value) on the y-axis. Each mRNA was represented as a dot and colour coded: the non-significant mRNAs as gray dots, non-significant mRNAs that showed more than 1.5x dysregulation between genotypes

(corresponding to 0.585 on the x axis) as green dots, and significantly dysregulated mRNAs with a dysregulation score of 1.5 and above as red dots (and named). Mock negative control and X31-infected cells are represented in these graphs. **B.** The same dataset was interrogated for H3N2 mRNA expression of different genomic segments by aligning the reads from the dataset to the human H3N2 Hong Kong available sequence. Results are shown per genotype and replicate as a mean ± SEM for each gene/viral genome segment. The results represented here are from the only RNA-seq experiment that was carried out in this thesis.

The same analysis was carried out on the transfected conditions, with lipofectamine negative control, 2'3' cGAMP and 5'ppp dsRNA (Figure 5.18). Overall, the transfection effect appears to trump stimulation, as most of the genes that are significantly differentially expressed between the genotypes are present in all three lipofectamine-dependent conditions. The *Pydc3* mRNA, detected in the lipofectamine and agonist transfections alike, was significantly less expressed in the *Alpk1*$^{-/-}$ background. The corresponding protein, PYDC3, was shown in one study to be involved in the prostaglandin-driven inflammasome activation and IL-1β secretion (Vijay et al., 2017). Moreover, the authors of this study have shown that Pydc3 transcription is IFNAR-dependent in BMDMs and *in vivo.* The only significantly dysregulated gene detected only in a stimulation condition, 2'3' cGAMP, is *Hmgn2*, encoding a high mobility group nucleosomal binding domain 2 protein, with a role in α5β1 integrin expression in A549 cells (Wang et al., 2016b). On the other hand, the pattern of *Wwc2* gene expression remained the same as in the mock and X31-infected cells, indicating a baseline, genotype-dependent and treatment-independent lower expression of *Wwc2* in the *Alpk1*$^{-/-}$ BMDMs. Overall, the results of the RNA-seq experiment pointed towards individual novel targets to investigate, but did not show very large differences induced by the lack of *Alpk1*. Some interpretations of these results are offered in the Discussion part of this chapter.

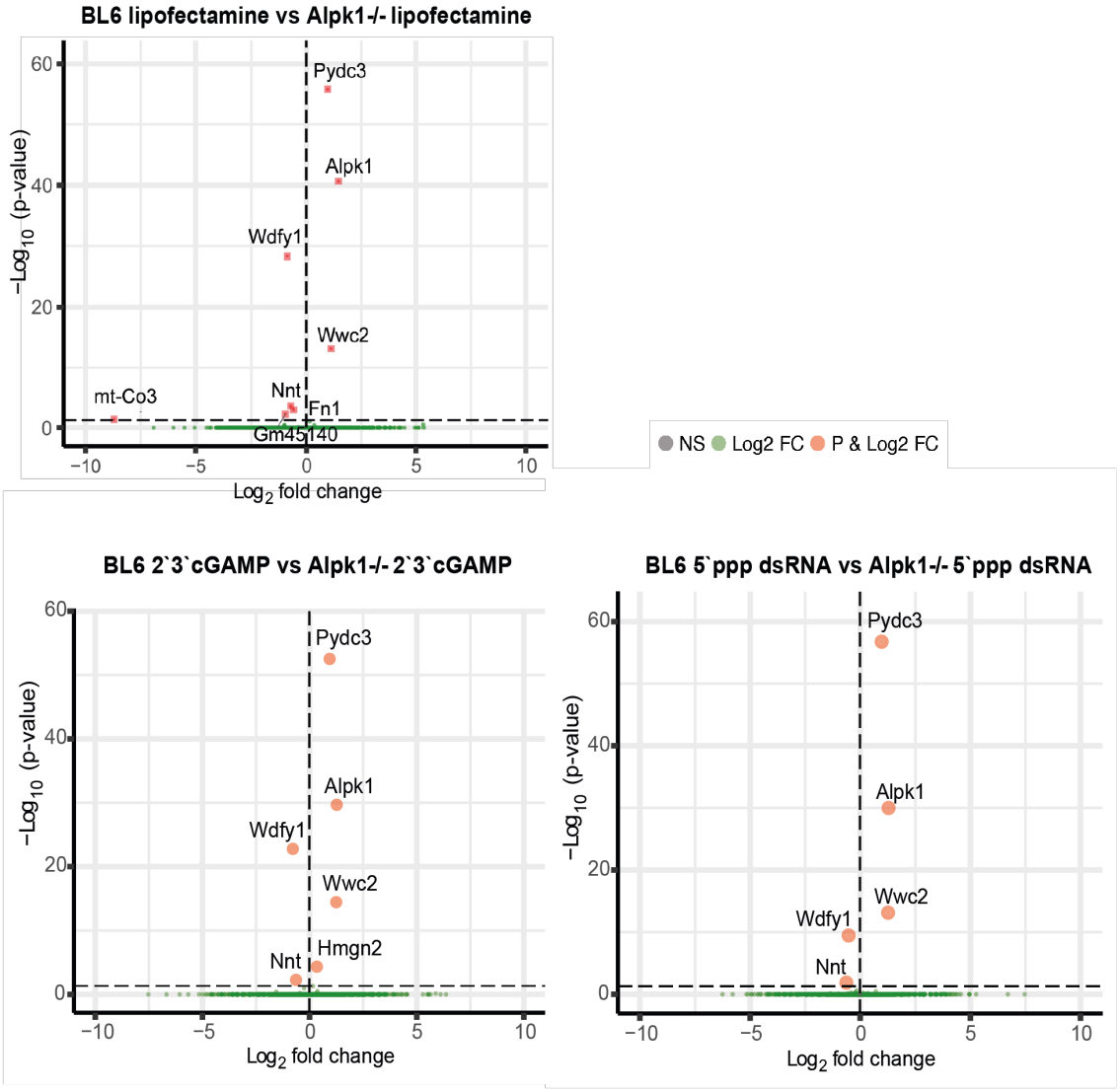

Figure 5.18 In transfection conditions, the observed inter-genotype differences seem to be baseline-detected and not stimulation-induced, and only low dysregulation is observed between genotypes. Volcano plots of the remaining three stimulation conditions (empty lipofectamine, lipofectamine+2'3' cGAMP, lipofectamine+5'ppp dsRNA) were visualised after a t-test as previously described. mRNAs are represented as colour-coded dots: the non-significant mRNAs in gray, non-significant mRNAs with >1.5x dysregulation between genotypes (corresponding to 0.585 on the x axis) in green, and significant mRNAs with >1.5x dysregulation in red (with gene names). Welch t-test was carried out as BL/6 – *Alpk1*$^{-/-}$ difference, so positive values on the x-axis indicate an induction in expression in the BL/6 background as opposed to *Alpk1*$^{-/-}$. The results represented here are from the only RNA-seq experiment that was carried out in this thesis.

5.3 Discussion

5.3.1 *Alpk1* deficiency effects *in vivo*

Results in this chapter indicate that *Alpk1* reduces mouse susceptibility to influenza *in vivo,* as the *Alpk1*$^{-/-}$ mice show increased weight loss and mortality during infection compared to BL/6 controls. However, during the testing of different viral doses, weight loss and mortality results depended on the viral dose used. The viral burden of the two mouse strains being similar, it indicated a difference between the two genotypes in pathogenic rather than antiviral pathways (more details in overall thesis Discussion chapter).

Analyses of the BAL fluid IFN-α/β and cytokines showed no difference between BL/6 and *Alpk1*$^{-/-}$ mice at any of the timepoints in infection. While infection doses used for experiments in sections 1.2.1 and 1.2.2 of this chapter were lower than the one used to demonstrate increased *Alpk1*$^{-/-}$ mice susceptibility, increasing the viral dose to $35*10^3$ $TCID_{50}$ highlighted no difference in cytokine production early on in infection. While this result indicates that Alpk1 might not be regulating IFN-α/β *in vivo*, expression of other cytokines should be addressed in the future (IL-1β, MIP-1α, MIP-1β etc). Moreover, although a reproducibly increased presence of pDCs in the lung at late stages of infection was detected in *Alpk1*$^{-/-}$ mice, no corresponding increase of IFN-α/β was observed. The IFN-driven activation levels of immune cells, mirrored by PDCA-1 and SCA-1 expression, were also relatively similar between the genotypes, thus leaving the susceptibility phenotype of *Alpk1*$^{-/-}$ mice unexplained.

5.3.2 *Alpk1* deficiency effects *in vitro*

While considerable variation was observed during *in vitro* assays of BMDMs, the represented results are indicative of a pattern of cytokine expression in BM-derived cells *in vitro.* Increased IFN-α/β and IL-6 secretion upon X31 infection or LPS challenge indicated a shared IRF3 and NFκB-driven pathway of target production. Similar patterns, although less extensive, were observed in the RIG-I agonist 5'ppp dsRNA stimulation and STING stimulation with 2'3' cGAMP.

More pronounced differences in cytokine production upon stimulation were observed in pDCs derived from WT and *Alpk1*-deficient mice. Namely, in absence of *Alpk1*, a two to three-fold increase in IFN-α/β production was observed as compared

to the WT background. However, in a pilot experiment analysing the percentage of pDCs (defined as PDCA-1+ Siglec-H+ in B220-MACS-purified cultures), it was found that the purity of the *Alpk1*-deficient cultures was higher, though not significantly (Supplementary Figure 8.3). While it is possible that this purity difference is influencing the observed differences in IFN-α/β levels between the two genotypes, further confirmation of the pDC percentage result will be necessary in the future.

Phospho-proteomics data identified ALPK1-dependent phosphorylation of Ser1017 and Ser1037 residues in WWC2 protein as the most significant changes between BL/6 and *Alpk1*$^{-/-}$ cells. However, very few significant changes were observed overall. The Reactome database that was used to assign the significantly dysregulated proteins to known signaling cascades functions by principally analysing human data. Therefore, the submitted mouse data was first referred to homologous proteins in the human genome, then assigned to pathways according to the software's algorithm. Therefore, the identified pathways may not mirror the situation in the mouse system faithfully. Overall, the association of significantly dysregulated phosphorylated proteins to pathways was modest. The only significantly recognised pathway (after multiple testing corrections) appeared to contain proteins less phosphorylated in *Alpk1*$^{-/-}$ BMDMs during 5'ppp dsRNA stimulation: the histone demethylation pathway. The identified proteins belonging to this pathway that were found in the dataset are encoded by genes *Kdm4c*, *Phf2*, *Kdm5c, Kdm2b, Kdm4b, Arid5b,* and *Phf8*. All of these factors participate in removing Lysine-bound methylation marks on different histone proteins, thus releasing epigenetic brakes on gene expression. While these demethylases have been implicated in other processes such as Wnt pathway and cancer progression, a member of the same family not found in this dataset, KDM5A, was shown to negatively regulate NFκB activity by interfering with p65 methylation (Zhao et al., 2016), (Lu et al., 2010). However, his finding is not very representative of the entire pathway, as less than 0.3% of all pathway components were identified in this dataset when submitted to the Reactome database.

Given somewhat confounding results in the immune cells, and the fact that ALPK1 was linked to lipid raft transport and polarization of epithelial cells (Heine et al., 2005), the responses of *Alpk1*$^{-/-}$ MTECs *in vitro* were assessed as well (data not shown). Both at mRNA and protein secretion level, IFN-α/β and IL-28 production were found to be similar between BL/6 and *Alpk1*$^{-/-}$ MTECs.

The parity of mRNA levels between BL/6 and *Alpk1*$^{-/-}$ BMDMs upon the same kinds of stimulation was contradictory to the increase in phosphorylation of p65 and TBK1 observed by WB assays. However, the analysis of the global transcriptome confirmed these findings and showed very few differences between BL/6 and *Alpk1*$^{-/-}$ BMDMs during stimulation (and in unstimulated conditions). It seems that most of the dysregulated transcripts between WT and *Alpk1*$^{-/-}$ BMDMs are already differentially expressed in the baseline conditions and that there is no induction of their expression upon stimulation or infection. It was interesting to note that the expression of mRNA *Wwc2* was lower in absence of *Alpk1*, as it was previously reported in this thesis that WWC2 phosphorylation is reduced in *Alpk1*$^{-/-}$ BMDMs. While this result was not informative of the overall expression of WWC2 protein, it was interesting to observe that ALPK1 effects are not limited only to direct phosphorylation to WWC2 but also to indirect control of its transcription. Overall, these results could therefore indicate that 1) the 6h timepoint was too early to detect differences or 2) the effects of ALPK1 *in vitro* affect post-transcriptional (and/or post-translational) mechanisms involved in production of IFN and cytokines.

5.3.3 A published *Alpk1*$^{-/-}$ mouse colitis model and findings

Alpk1 deficiency was demonstrated in a BL/6 background *Alpk1*$^{-/-}$ *Rag1*$^{-/-}$ mouse model to increase colitis susceptibility and IL-12 production, in a phenotype reminiscent of the 129 mice (Ryzhakov et al., 2018). The authors also report expression of *Alpk1* (by interrogation of the ImmGen database) in splenic macrophages and splenic and mesenteric lymph node pDCs, monocytes and DCs. They confirmed the ALPK1 impact in the hematopoietic compartment using a bone marrow chimera system where colitis susceptibility was driven by *Alpk1*$^{-/-}$ donor cells. A higher IL-12 production was also detected in *Alpk1*$^{-/-}$ BMDMs, but, importantly, the authors used GM-CSF to derive these cells *in vitro.* Therefore, the observed differences in IL-12 secretion could be originating from DCs or even monocytes in culture, as it was previously shown that GM-CSF-differentiated BM progenitors yield a mixed culture where macrophages are not in majority (Helft et al., 2015).

It is worth mentioning that in the (Ryzhakov et al., 2018) study all experiments were carried out in an IL-10-deficient system (systemic blocking with the α-IL-10R antibody). In these conditions, they reported a similar inflammation phenotype-In the

absence of *Alpk1* in the BL/6 background as in the WT 129 mice. While blocking the IL-10 pathway is necessary along with *H.hepaticus* infection for obtaining a colitis induction mouse model, IL-10 has important systemic anti-inflammatory effects through the induction of the Jak/STAT cascade via STAT3 (Moore et al., 2001, Ouyang et al., 2011). Without IL-10 blockade, simple *H.hepaticus* infection of WT and Alpk1-deficient mice showed little to no significant difference in colitis susceptibility. In addition, this study found a positive correlation between *Alpk1* expression and pro-inflammatory cytokine production (IL-12, CXCL10, IFN-γ) in colitis patients' ileal samples, thus directly contradicting their mouse *in vivo* findings. Therefore, the *in vivo* impact of ALPK1 on inflammation claimed by this publication is to be interpreted cautiously, as the increased inflammation could be due to the lifting of molecular brakes through abrogation of IL-10 signaling. The proposed comparison between *Alpk1*$^{-/-}$ and 129 mice, though they present similarities in their colitis susceptibility, therefore lacks conclusive evidence.

The ALPK1 study presented in this chapter of this thesis did not succeed in bringing forward a clear connection between ALPK1 and any characteristic immune inflammation pathway. However, it seems like the global signatures of protein production in absence of *Alpk1* are in concordance with the data from (Ryzhakov et al., 2018). However, one major finding in this thesis contradicts a side note from the Methods part of their study. They reported that the deletion of exon 10 in the *Alpk1* gene in the mouse model they used induced a frameshift mutation in the coding sequence (without offering any evidence). However, the RNA-seq data presented in this thesis convincingly and significantly shows that all other exons after exon 10 are transcribed in the *Alpk1*$^{-/-}$ BMDMs just as well as in the WT-cells. This is important to consider in the interpretation of the results from this thesis, but also to use as caution when interpreting the (Ryzhakov et al., 2018) data.

5.3.4 Overall conclusion

The most important result from this chapter included the identification of a possible novel phosphorylation substrate target of ALPK1: a protein called WWC2. It also indicated a possible role for ALPK1 in its transcription. Ser1017 and Ser1037 residues of WWC2 were significantly less phosphorylated in absence of *Alpk1*, indicating an effect of this kinase on the phosphorylation patterns of WWC2.

However, it is not possible to conclude from this experiment whether WWC2 is a direct or indirect target of ALPK1 activity. WWC2 and its possible connection to the innate immune response, as well as investigation of its transcription in an effort to further investigate the RNA-seq result are addressed in detail in the next chapter.

Chapter 6. Results 4 : Investigating the putative roles of Alpk1/WWC2 interaction in innate immunity

6.1 Introduction

Although phospho-proteomics showed few differences between WT and *Alpk1*$^{-/-}$ responses, a significant lack of phosphorylation of WWC2 was detected. The phosphorylation on two residues, Ser1017 and Ser1037, was increased with stimulation, but in all cases lower in absence of *Alpk1*. Moreover, *Wwc2* mRNA expression was also reduced in absence of *Alpk1*, showing a possible indirect expression regulation mechanism of the two. However, no validation of WWC2 protein expression was shown in the previous chapter.

WWC2 (WW domain-containing protein 2) is not very well studied. One study described it as a regulator of the Hippo pathway and a prognostic factor in a HEK293T human cancer cell model (Zhang et al., 2017b), but no studies demonstrating a function for WWC2 were published in mice at the time of writing this thesis. No commercially available antibodies for the identified phosphorylated residues of WWC2 were found, making a WB-based validation of the observed results difficult.

Given that this protein was not known to play a role in the mouse immune system pathways, its sequence was compared to a known member of the same protein family, WWC1. This protein (also called KIBRA), implicated in memory and Alzheimer's disease (Zhang et al., 2014), is generally known as an upstream regulator of the Hippo signaling pathway (Wennmann et al., 2014), (Xiao et al., 2011). The Hippo pathway is a well-known kinase cascade regulating cell proliferation, differentiation and death. First discovered in *Drosophila,* it was since found to be extremely well conserved in mammals as well. The Hippo pathway contributes to cell death and differentiation, limiting cancer onset and spread, and to tissue

homeostasis, organ size and development in general (Yu and Guan, 2013). The main environment cues that activate Hippo pathway are nutrient starvation, or the detection of mechanical cues via GPCR signaling. Typically, Hippo pathway is activated by increased cell density. The activation of the Hippo pathway is mediated by two hallmark kinases: MST1/2, which initiates signaling, and its phosphorylation targets, LATS1/2 kinases. Once LATS1/2 are phosphorylated and activated by MST1/2, they phosphorylate the effector of the Hippo pathway, the protein YAP(TAZ). This phosphorylation keeps YAP/TAZ in the cytoplasm by initiating its association with the 14-3-3 protein, or by directing it for proteasomal degradation. Either way, the main consequence of the prevention of nuclear translocation of YAP/TAZ is the abolishment of transcription of their target genes, including Amotl2. Amotl2 is involved in the maintenance of tight junctions and epithelial cell polarity (Yu and Guan, 2013). KIBRA was found to activate LATS kinases which phosphorylate YAP, thus preventing its nuclear translocation (Zhao et al., 2010). Also, in a publication of interest for this thesis, KIBRA was found to affect epithelial cell polarity through suppression of apical exocytosis (Yoshihama et al., 2011) by inhibiting an atypical protein kinase C - aPKCζ.

Interestingly, it was recently shown that the Hippo pathway is implicated in responses to viral infection via the regulation of TBK1 and IRF3 phosphorylation (Zhang et al., 2017a). Namely, the activation of the Hippo pathway was reported to increase RNA and DNA viral sensing via RIG-I and STING pathways, both of which are studied in detail in this thesis. Zhang and colleagues have shown through *Ifn-β1* luciferase assays that YAP can prevent TBK1 phosphorylation and thus IRF3 phosphorylation and activation downstream. They demonstrate that, upon Hippo pathway activation (in this case by serum starvation) during viral infection, YAP is phosphorylated, does not bind to TBK1 anymore, and *Ifn-β1* responses are increased. Importantly, (Wennmann et al., 2014) have shown that the LATS1/2 binding and phosphorylation capacity of human WWC1 had been conserved in WWC2 as well. This was an encouraging finding, as it indicated that the binding partners found for WWC1 could perhaps be valid for WWC2 as well.

Therefore, in this final chapter of this thesis, I recapitulate results of some validation experiments exploring the possible connection of Alpk1 with WWC proteins and the Hippo pathway in the *Alpk1*$^{-/-}$ phenotype. I also show results of an

RNA-seq experiment performed in search of novel candidate genes and pathways that could be affected by Alpk1 activity.

6.2 Results

6.2.1 WWC proteins similarity and binding partners

In order to be able to infer putative protein binding capabilities of WWC2, the sequences of WWC2 and WWC1 mouse and human proteins were aligned to compare the Ser modified residues uncovered by the phospho-proteomics analysis. The Ct region alignments of the four proteins are represented in Figure 6.1. Since Alpk1 is an α-protein kinase, coiled-coil predicted domains in WWC2 are highlighted in green. The modified residues Thr999, Ser1017 and Ser1037 identified in the phospho-proteomics experiments in previous results chapter in mouse WWC2 are highlighted in brown and red, respectively. Thr999 was present in the first phospho-proteomics experiment but did not appear in the second assay after normalisations (possibly due to the different FDR in statistically comparing the many conditions in the second phospho-proteomics assay). Generally, WWC2 and WWC1 proteins are very well conserved in mice and humans. The conservation score between mouse and human WWC2 amino-acid sequences was 86%, whereas WWC2 and WWC1 mouse similarity was 48%. The coiled-coil domain adjacent to the modified residues seems very well conserved across species and WWC proteins. Most importantly, all three residues identified in the earlier experiment appear in the human and mouse WWC2 and WWC1 sequences, in conserved peptide surrounding sequences. The aPKC binding site in human KIBRA (represented in the black rectangle) is overall well conserved between WWC1 and WWC2 sequences, and identical between corresponding mouse and human proteins. Furthermore, one of the identified modified residues, Ser1037, appears to be in the middle of the aPKC binding site. Given all the previously published data on WWC1 role in the Hippo pathway and its binding to aPKCs in epithelial cells, this was a confirmation encouraging further validation experiments.

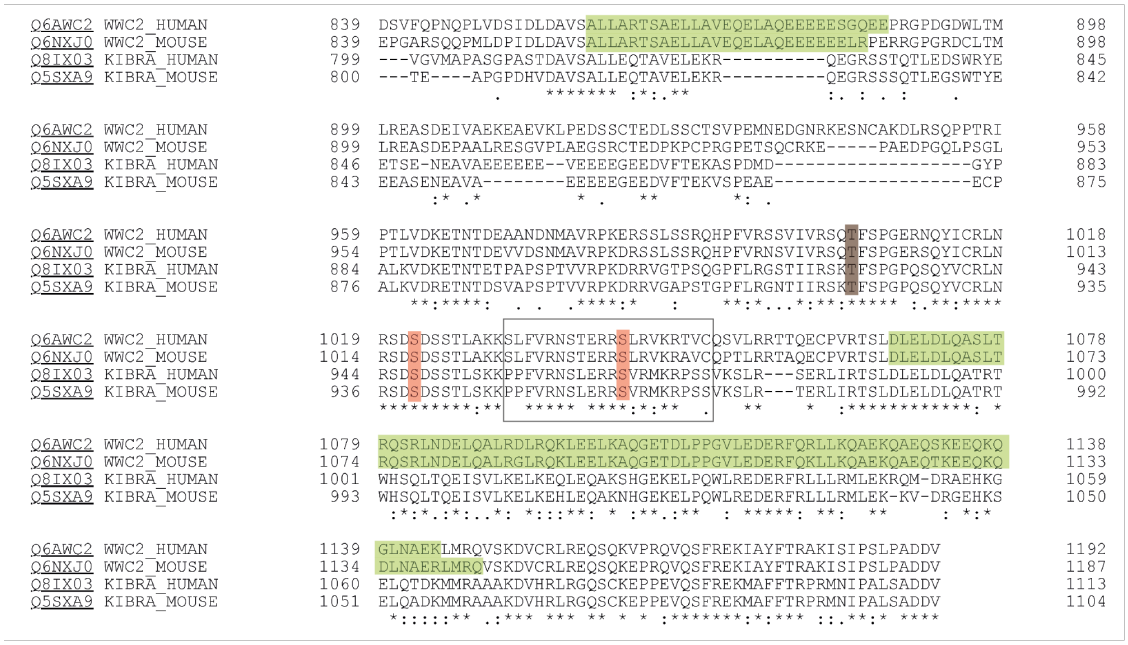

Figure 6.1 Ct domain alignments of human and mouse WWC2 and KIBRA (WWC1) show a conservation of the identified phospho-residues. UNIPROT BLAST ClustalOmega alignment was performed on the four protein sequences – in the case of WWC1, isoform 1 was used for the alignment. Green highlights indicate regions of putative coiled-coil domains in the WWC2 sequence. Black rectangle indicated the position of the aPKC binding sequence in human WWC1/WWC2 according to (Wennmann et al., 2014). Brown highlight indicates the previously detected modified Thr999 residue, and the red highlights mark Ser1017 and Ser1037 identified in the latest phospho-proteomics experiment.

In the absence of a commercially available phospho-WWC2 antibody, an attempt was made at investigating whether WWC2 can bind aPKCζ in BMDMs by co-immunoprecipitation. For this experiment, BMDMs were stimulated using 2'3' cGAMP to activate the STING cascade, or 5'ppp dsRNA, the specific agonist of the RIG-I receptor. Once again, empty lipofectamine was used as a transfection control. A polyclonal aPKCζ antibody was used to capture the total amount of this protein in the cells, and bound proteins were immunoprecipitated alongside it. IPs and total lysates were analysed for WWC2 expression (for binding analysis) and for aPKCζ expression (as a control). Results are shown in Figure 6.2 and are representative of two independent experiments. Using aPKCζ for immunoprecipitation did not show WWC2 as a binding partner (left hand-side gel, IP section) in any of the tested conditions. The presence of WWC2 in total cell lysates was tested in parallel and it revealed distinct bands of size corresponding to that of WWC2 (134kDa – left hand gel, right section). Moreover, a protein band corresponding to the expected size of

aPKCζ (68kDa) was detected both in the IP and total lysate samples, though with weak intensity in the IPs. The specificity of both the α-WWC2 and α-aPKCζ antibodies was noticeably low, as many other bands (especially in the case of aPKCζ) were recognised by these antibodies. Therefore, it is unclear whether the IP assay was successful and/or whether there is genuinely no binding of the two proteins in the studied conditions.

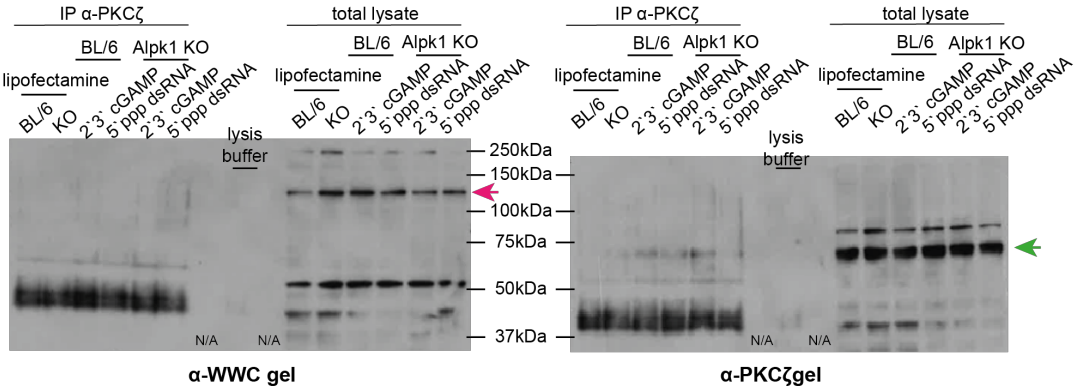

Figure 6.2 Immunoprecipitation assays show no binding of WWC2 and aPKCζ in the analysed conditions in BMDMs. 2*10^6 BMDMs were seeded per condition and per genotype and incubated overnight in 1% FCS media. They were then transfected with empty lipofectamine, 2'3' cGAMP or 5'ppp dsRNA for 1h long-incubations to mimic the phospho-proteomics stimulation conditions. Post-stimulation, cells were processed as described in Material and Methods, by using an aPKCζ polyclonal antibody to extract and purify this protein along with its binding partners. The total lysate prior to immunoprecipitaion, as well as the immunoprecipitates, were run on NU-PAGE SDS gels and the membranes probed for WWC2 detection and a-PKCζ presence as a control. A negative control for IP was the pure lysis buffer incubated with aPKCζ antibody used for purification. Magenta arrow indicates the presumed WWC2 protein band, and the green arrow the aPKCζ one. Results representative of two experiments.

6.2.2 Analysis of possible Hippo pathway activation in BMDMs

Given the literature about WWC1, WWC2 and the Hippo pathway activation, the effects of cell density on the expression of main target genes and proteins was analysed next. Cell density is known to activate Hippo pathway, whereby cells in immediate contact initiate this signaling cascade to stop proliferation (Yu and Guan, 2013). To replicate this, BMDMs were seeded at 1.2*10^6 cells/well, 4*10^5 cells/well or 2*10^5 per well, and stimulated with 2'3' cGAMP, 5'ppp dsRNA or empty

lipofectamine control. For comparison, the usual cell density for cell stimulation for QPCR is $4*10^5$ cells/well in a 24w plate, and for ELISA $2*10^5$ cells/well in a 96w plate. Therefore, to analyse the effects of cell density, all cells were plated in 24w plates, lysed for QPCR, and their supernatants collected for ELISA analyses. In the case of protein synthesis, and possibly because the supernatants were taken in a bigger volume than for the optimized conditions, no difference in IFN-α/β protein levels between genotypes were recorded in either stimulations (Figure 3.5a). However, a step-wise reduction in protein levels of IFN-α and IFN-β was observed in the more sparsely plated cells compared to the densely plated ones. As such, this result could indicate that cell density could indeed affect the IFN-α/β synthesis and export efficiency in BMDMs, but independently of Alpk1 presence. Similar patterns were observed at the transcription level (Figure 3.5b). *Ifn-β1* and *Il-6* transcription was similar between genotypes once again, but responded well to cell density. In sparsely plated cells the overall activation of transcription of both *Ifn-β1* and *Il-6* was extremely low, similar to the negative control. Interestingly, both in the case of protein and mRNA levels, the STING signaling pathway activated with 2'3' cGAMP was more responsive to cell density than was the case with the RIG-I pathway in 5'ppp dsRNA stimulation. It is important to note here that the results represented here are from a pilot experiment and that their interpretation is thus limited.

The transcription of *Amotl2* was also addressed in this experiment (Figure 3.5b), alongside those of *Ifn-β1*, *Il-6* and *Stat1*. As Hippo pathway activation negatively regulates YAP activity as a transcription factor, it was encouraging to see that in STING stimulation *Amotl2* expression was increased at $4*10^5$ cells/well compared to $1.2*10^6$ cells/well. It is worth remembering here that the $4*10^5$ cells/well density was the one used for all QPCR experiments represented in this thesis, so it is conceivable that Hippo pathway signaling was somewhat active throughout all these assays. However, as for the other targets, there was no difference recorded between the two genotypes in mRNA production. This experiment was only carried out once, as a pilot assay, and it is possible that some variation might be observed in the future repeats.

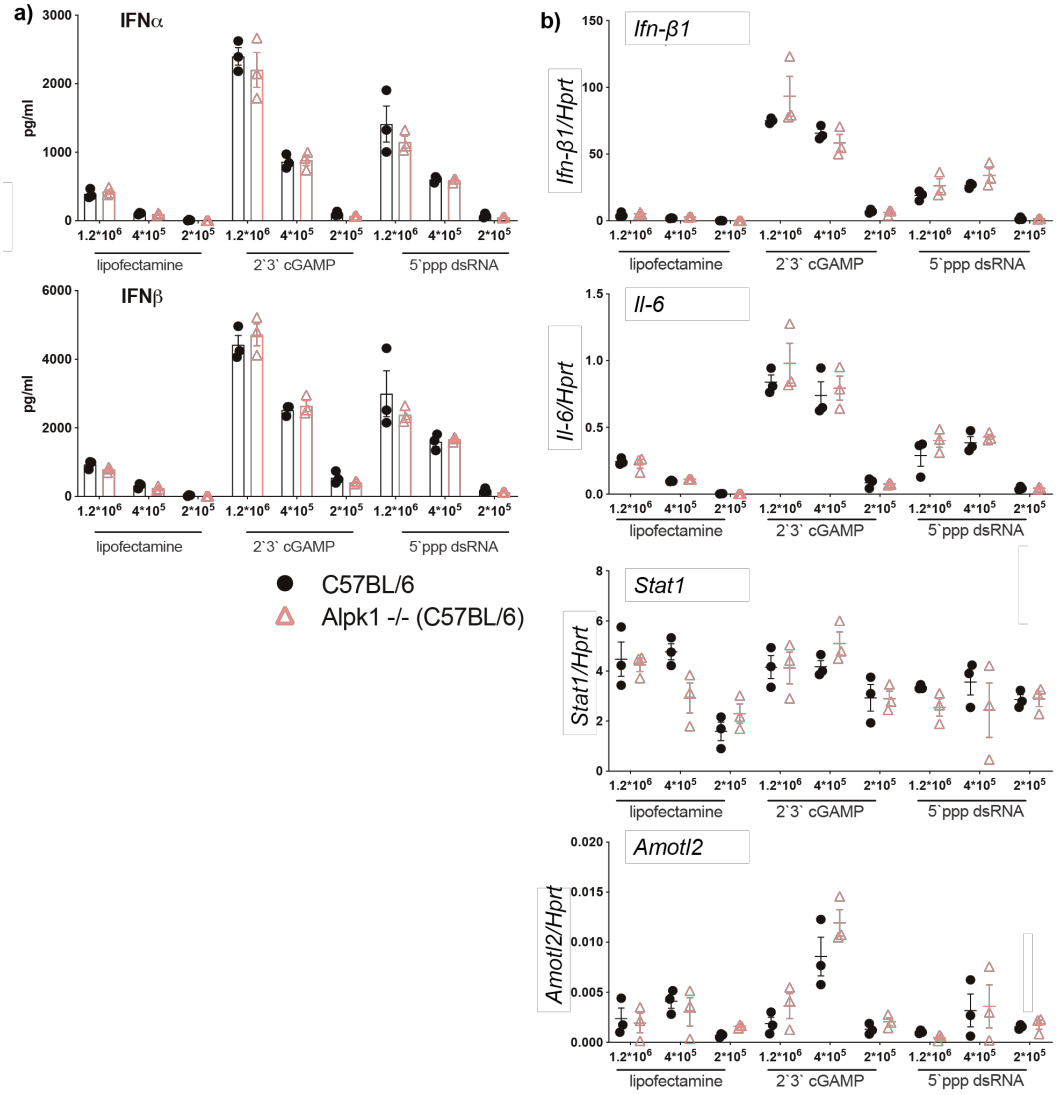

Figure 6.3 While there is a stimulating effect of Hippo pathway with cell density on IFN-α/β and IL-6 expression, no difference in expression was Alpk1-dependent. BMDMs were were seeded at indicated numbers in 24w plates for stimulation. They were stimulated by transfecting empty lipofectamine of lipofectamine+2'3' cGAMP or 5'ppp dsRNA. **A.** IFN-α and IFN-β protein quantity was assessed in the supernatant of stimulated cells 24h post-stimulation. **B.** *Ifn-β1*, *Il-6*, *Stat1* and *Amotl2* mRNA was quantified in cells after 6h of stimulation as indicated. Comparison of protein or mRNA levels between genotypes was assessed for significance by a two-way ANOVA. Each symbol is a biological replicate, and results are represented as a mean ± SEM value. Results representative of one pilot experiment.

Further, *Amotl2* transcription was addressed in the context of X31 infection and LPS and poly(I:C) stimulations in presence or absence of cycloheximide. *Amotl2* expression was analysed in these conditions in order to verify the impact of newly synthetised proteins on the readout target of Hippo pathway activity (if there was

any). Results in Figure 3.6 show no visible induction of *Amotl2* expression upon any stimulation tested, and little to no impact of *Alpk1*. However, a reproducible pattern, mostly observed in *Alpk1*$^{-/-}$ BMDMs, but also in WTs, was a peak of expression of *Amotl2* 2hrs post-stimulation in presence of cycloheximide. This was followed by a sharp decline in mRNA synthesis of *Amotl2* in both *Alpk1*$^{-/-}$ and BL/6 cells from 4h post-stimulation onwards. In stimulation of STING and RIG-I pathways with 2'3' cGAMP and 5'ppp dsRNA stimuli, respectively, there was no effect on *Amotl2* expression after 6h of incubation. Overall, these results indicate that *Amotl2* expression is possibly kept low by a constantly replenished (synthetised) protein in the background. This is visible because in the 2-3 hours post-cycloheximide exposure (corresponding to 1-2h post-stimulation), the expression of *Amotl2* is transiently increased in both unstimulated and stimulated cells. However, no stimulus amongst those tested could induce its expression in a significant way.

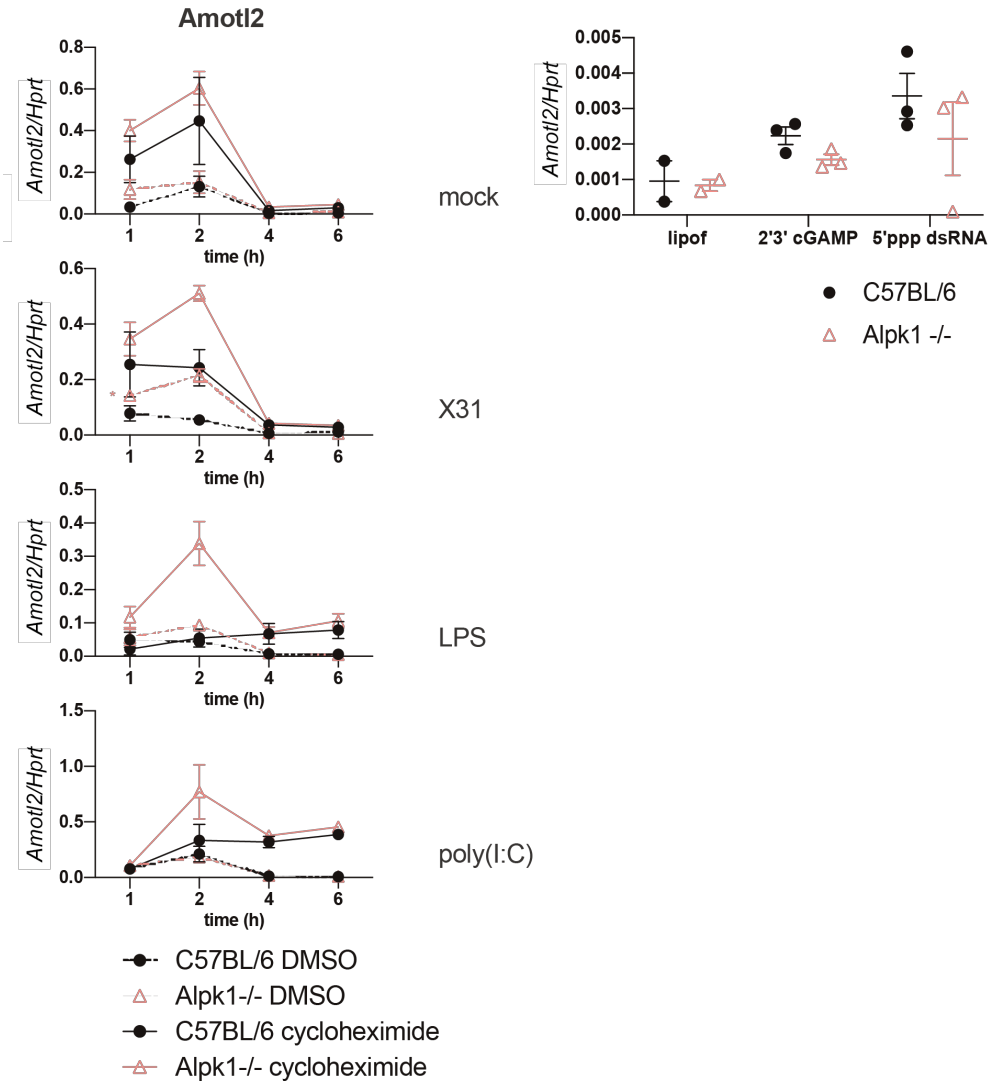

Figure 6.4 *Amotl2* expression (as a possible readout of the Hippo pathway activation) is not *Alpk1*-dependent, but is affected by cycloheximide treatment in different stimulation conditions. BMDMs were pre-incubated with cycloheximide or DMSO for 1h, then stimulated with the indicated stimuli (X31 10^6 $TCID_{50}$/ml) for the indicated amounts of time before harvesting and quantification of mRNA by QPCR. NB: the top right graph indicates a 6h-long stimulation as previously described. Results represent mean ± SEM values of three biological replicates and * indicates $p<0.05$ in a two-way ANOVA test between BL/6 and *Alpk1*$^{-/-}$ genotypes. Results from one pilot experiment.

6.2.3 *Wwc2* expression study in different stimulations

Since the RNA-seq experiment from the previous chapter had shown an unexpected negative impact of ALPK1 loss on *Wwc2* transcription, the expression of *Wwc2* was checked in different conditions in both genotypes to explore this result

further. Therefore, *Wwc2* mRNA was quantified upon presumed activation of the Hippo pathway by cell density changes. This was done for 2'3' cGAMP and 5'ppp dsRNA stimulations, but also for CpG-A induced stimulation of TLR9 (Figure 6.5a). While cell density generally does not appear to regulate *Wwc2* transcription, a pattern of lower *Wwc2* in *Alpk1*$^{-/-}$ than in WT-cells confirms the RNA-seq findings. Ultimately, it does not appear that *Wwc2* expression is induced upon any of the stimulations studied. To investigate whether *Wwc2* expression depends on newly synthetised proteins, its transcription was measured in cells exposed to cycloheximide prior to different stimulations (Figure 6.5b). Once again, in baseline conditions, as well as in stimulations with LPS or poly(I:C) or influenza virus infection, *Wwc2* expression in *Alpk1*$^{-/-}$ BMDMs was lower than in the BL/6 ones, confirming the RNA-seq findings. Interestingly, in influenza infection there seemed to be no effect of newly synthetised proteins on *Wwc2* expression in *Alpk1*$^{-/-}$, but in WT BMDMs a significant induction of *Wwc2* mRNA expression was observed. However, this induction was not higher than in the cycloheximide-treated negative controls, meaning that there is little to no induction of *Wwc2* expression upon influenza infection in any case. Upon LPS and poly(I:C) stimulation the two genotypes showed similar patterns of *Wwc2* expression with cycloheximide treatment. Overall, this result confirmed the RNA-seq findings and pointed to a marginal impact of newly synthetised proteins, but not stimulation, on the induction of *Wwc2* expression. Moreover, the significant difference in *Wwc2* mRNA 6h post-X31 infection, but lacking a significant increase compared to the mock-treated cells, confirmed the RNA-seq findings as well.

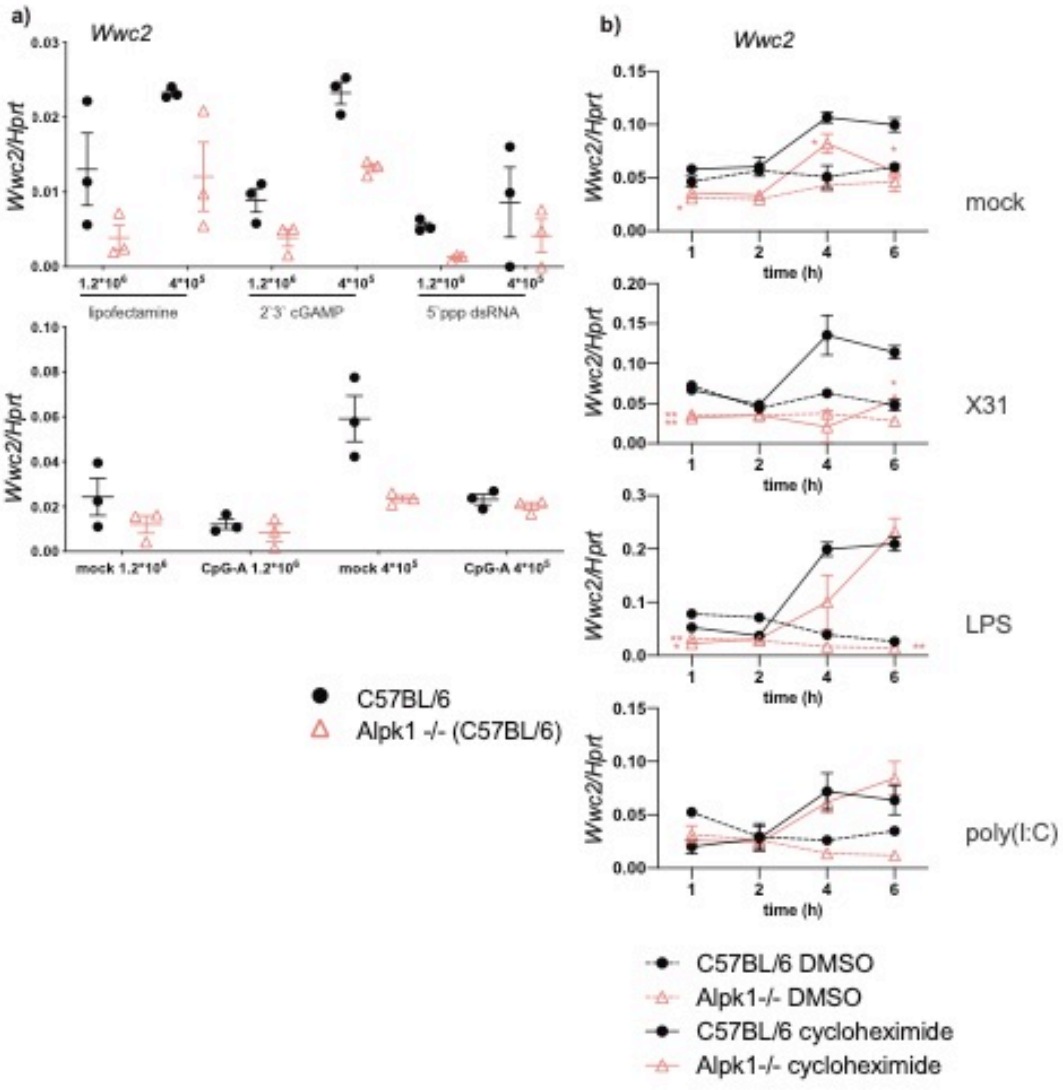

Figure 6.5 Expression of *Wwc2* mRNA in *Alpk1*$^{-/-}$ BMDMs is lower in baseline and some stimulated conditions than in BL/6 controls, an effect maintained in the presence of cycloheximide during X31 infection. BMDMs were differentiated as previously described and seeded, unless otherwise indicated, at 4*10^5 cells/well in 24w plates for stimulation. *Wwc2* mRNA expression was assessed by QPCR as previously described. **A.** Cells were transfected with empty lipofectamine, 2'3' cGAMP or 5'ppp dsRNA or stimulated with CpG-A for 6h before quantifying Wwc2 mRNA levels. **B.** 4*10^5 BMDMs per condition were pre-incubated with cycloheximide or DMSO 1h before and during stimulation (infection with X31 10^6 $TCID_{50}$/ml, LPS or poly(I:C) incubation). Cells were harvested at the indicated time points during stimulation for mRNA quantification. Results are represented as a mean ± SEM of three biological replicates per genotype. Each symbol is a biological replicate. Statistical testing two-way ANOVA compared BL/6 vs *Alpk1*$^{-/-}$ conditions within DMSO, or within cycloheximide treatment conditions (* p<0.05; ** p<0.01; *** p<0.001; **** p<0.0001; non-significant comparisons are omitted for clarity). Represented data from A. and B. are from two different experiments.

6.3 Discussion

In this final chapter, some hypotheses on the role of Alpk1 in stimulated BMDMs were investigated based on the results obtained using phospho-proteomics assays. The implications of these results in the light of the other chapter results in this thesis will be discussed in the final Discussion section.

6.3.1 The WWC-aPKCζ connection

The most noticeable result of the phospho-proteomics assay was the detection of loss of phosphorylation of WWC2 on two separate residues in a reproducible manner. Given that this protein is relatively unknown, its AA sequence comparison with KIBRA (WWC1) was encouraging for the IP validation attempts. However, the lack of detectable interaction between aPKCζ and WWC2 observed in the IP assay could be interpreted in different ways. The first one, that cannot be overlooked at this time, is that the antibody specificity for both WWC2 and aPKCζ was poor (many other bands detected), rendering the assay unsuccessful. Another probable interpretation is that WWC2 is not a binding partner for aPKCζ in these conditions. Given that the putative binding sequence is present, it is possible that the binding itself is not happening due to post-translational modifications around the site, or perhaps competitive binding to other proteins of the same family (such as aPKCλ/ι which were not analysed in this thesis). The other possibility is that the aPKC binding site proposed for KIBRA by (Wennmann et al., 2014), (Yoshihama et al., 2011) and (Buther et al., 2004) can be disrupted by the few mutations between WWC1 and WWC2, even though the sequences are well conserved. In fact, (Yoshihama et al., 2011) and (Buther et al., 2004) also identified that KIBRA is a phosphorylation target of aPKC, but it is unclear whether this activity is preserved for WWC2, or if it could potentially affect the binding as well.

6.3.2 Effects of ALPK1 and WWC2 interaction on hypothetical Hippo signaling in innate immunity

It is interesting to speculate about a possible ALPK1-Hippo pathway interaction through WWC2 in innate immune activation. While KIBRA is known to be a phosphorylation target of hallmark Hippo kinase LATS2 in *D.melanogaster*, the

consequence of which is the activation of the Hippo pathway and the suppression of YAP activity (Xiao et al., 2011), (Genevet et al., 2010), (Baumgartner et al., 2010), the effects of WWC2 are less well understood.

YAP was recently identified as an antagonist of the TBK1-mediated cytosolic nucleic acid sensing pathway during RIG-I or STING activation, preventing IRF3 phosphorylation and nuclear translocation (Zhang et al., 2017a), and as a target of IKKε for proteasomal degradation (Wang et al., 2017). The Hippo pathway was therefore proposed to enhance nucleic acid sensing in the cytoplasm by blocking YAP. WWC2 was identified as an upstream regulator of the Hippo pathway by virtue of its activation of the LATS2 kinase, which resulted in phosphorylation of YAP, the pathway effector (Zhang et al., 2017b). YAP phosphorylation, in turn, prevents its nuclear translocation and marks it for proteasomal degradation. The possible connection with Alpk1 could involve a negative regulation of WWC2 by Alpk1-driven phosphorylation (for example, by earmarking it for degradation). In the absence of Alpk1, there could therefore be an efficient inhibition of YAP by phosphorylation, allowing for IRF3 phosphorylation and nuclear translocation, and therefore an added source of transcription downstream of TBK1 (such as cytokines and possibly IFN-α/β). However, the RNA-seq data from the previous chapter is in direct opposition to this, as Alpk1 seemed to positively regulate Wwc2 expression, and it is impossible to know from the data in this thesis whether the protein levels of WWC2 are affected by Alpk1 absence. At least, given the issue with Alpk1 knock-out that we used in this thesis, it can be concluded with certainty that the kinase domain of Alpk1 affects *Wwc2* gene expression downstream via an unknown mechanism. Another caveat to this hypothesis is that no difference in Amotl2 transcription was observed between the two genotypes upon modulation of cell density, and there was no observable difference in cytokine or IFN transcription as a result.

Given that the IP experiment from this chapter indicated that the levels of WWC2 are possibly similar across genotypes and conditions (in spite of low specificity of the antibody), it is possible that the reduction of *Wwc2* transcription that was observed in the RNA-seq experiment is not relevant in the ultimate mechanism of interaction with Alpk1. However, it is possibly indicating a pathway upstream of *Wwc2* transcription that could be affected by Alpk1. More validation experiments, including WWC2 protein quantification via MS and WB and other ways of Hippo pathway activation (for example by FCS starvation) can be explored in the future to

try and address the possible connections between these factors. FCS starvation would be particularly interesting to address as an effect on Hippo activation, as WB and phospho-proteomics assays in this thesis were carried out in presence of 1% FCS only (complete media is 10%). This was done in order to reduce background phosphorylation levels, but given the WWC2 possible implications, it could mean that the activation of the Hippo pathway was inadvertently brought about.

6.3.3 Concluding remarks

Generally speaking, whatever the effects of Alpk1 on the stimulation of BMDMs in different conditions, they seem to be very discrete and difficult to pinpoint. WWC2 still remains a candidate protein of interest as a phosphorylation target of Alpk1, but this hypothesis needs to be addressed by *in vitro* binding and phosphorylation assays in the future. A general Discussion, taking into account results from previous chapters of this thesis, will address these questions more in depth.

Chapter 7. Discussion

The main goal of this work has been to contribute to the identification of the genetic causes of high IFN production in the influenza susceptible 129 mouse strain. This project was done with the idea that the findings could be applied not only to influenza susceptibility but also to other diseases where high IFN production is a burden to the host.

The phenotype of increased influenza morbidity and mortality of the 129 mice is reliably confirmed here in the 129S6 sub-strain compared to the BL/6 controls. Further, it is reported that introducing a single Chr3 locus, R17, of BL/6 origin, into the 129S6 genome (in the 129.C3BR17 congenic mouse strain) contributes to the reduction of IFN-α/β and cytokine production and to the improved survival of the infection compared to WT 129S6 mice. The reproducibility of this result was robust *in vivo* but less so *in vitro.* The R17 locus gene with the most missense mutations in the 129 sequence, Alpk1, was further explored for its role in mouse influenza susceptibility and cytokine production. While the role of Alpk1 *in vivo* was less obvious, *in vitro* loss of Alpk1 caused higher IFN-α/β and cytokine production. A

putative target for the kinase activity of ALPK1, the protein WWC2 has been identified in a phospho-proteomics assay but insofar not validated. Phosphorylation on two separate residues of WWC2 was reduced in absence of ALPK1 kinase activity. While the reported results of each chapter in this thesis were discussed separately, in this final Discussion the findings are interpreted together, in light of each other.

Globally, the data in this thesis pointed towards R17 as a candidate locus that contributes to high IFN and cytokine production in influenza susceptible 129 mice. Whether this is the result of the activity of a single gene or multiple ones within the locus remains unclear. ALPK1 and TIFA have been shown to interact in other systems, so it is possible the same interaction is at play in the tested IAV infection and stimulations represented in this thesis. Given the fact that both the susceptibility and the IFN-α/β production of the 129.C3BR17 mice remain at a level intermediate between the BL/6 and 129 extremes, another factor in the 129 genome could be contributing to the phenotype-In addition. This is in concordance with our initial hypothesis that multiple genes could be encoding host-specific influenza susceptibility due to high IFN-α/β.

7.1 Alpk1 effect on pathways leading to IFN/cytokine production

The interpretation of the findings on the role of ALPK1 in this model has an important consideration. The knock-out of *Alpk1* was obtained by targeted deletion of exon 10 (Ryzhakov et al., 2018), encoding a part of the Ct kinase domain of the protein. Meanwhile, the Nt part of ALPK1 is still transcribed in the *Alpk1*$^{-/-}$ cells, as verified in the RNA-seq dataset. The Nt domain of ALPK1 was shown to bind its phosphorylation target myosin IIA (Lee et al., 2016), and to HBP derivative from the bacterial wall that serves as a PAMP for recognition (Zhou et al., 2018). While in the absence of a functional α-ALPK1 antibody no assumption about protein expression can be made with certainty, both of the aforementioned studies clearly showed that the Nt domain of ALPK1 could bind its targets independently of the Ct portion. Therefore, it cannot be excluded that, in *Alpk1*$^{-/-}$ mice, the ALPK1 Nt exerts its scaffolding properties with binding partner proteins and affects signaling downstream similarly to WT conditions. This considerably complicates the interpretation of the

Alpk1$^{-/-}$ results, but this will nevertheless be attempted in this part of the discussion. A fully functional ALPK1 scaffolding activity could at least partly explain the observed modest differences between *Alpk1*$^{-/-}$ and WT backgrounds. However, it also means that any observed phenotypic difference in the *Alpk1*$^{-/-}$ mice is exclusively due to the Ct kinase domain activity, regardless of binding or scaffolding properties.

From the results reported in this thesis, lack of Alpk1 Ct domain kinase activity seems to increase IL-6 protein secretion in stimulations of TLR3/4 and RIG-I cascades in BMDMs. Moreover, *Ifn-β1* production was also reproducibly higher in *Alpk1*$^{-/-}$ background during X31 infection, i.e. during RIG-I pathway activation. The regulators shared by the sub-branches corresponding these pathways to yield IFN or IL-6 production could be IKK proteins or TBK1, but it remains unclear by what mechanism ALPK1 controls their activity. The increase in IFN-α/β production in TLR7-stimulated or infected pDCs also points towards an IKK-dependent mechanism controlling IRF7 activation. It is also possible that ALPK1 and TIFA indeed interact in these pathways as well, activating TRAF6 phosphorylation downstream, as was shown in previous work (Milivojevic et al., 2017). However, neither TIFA nor TRAF6 appeared in the phospho-proteomics datasets (in WT or *Alpk1*$^{-/-}$ BMDMs). While it seems unlikely from this data that *Alpk1* modulates ISG mRNA expression, it cannot be excluded that it also has an effect in the IFNAR pathway as no IFNAR-deficient mouse or cells were tested in the *Alpk1*$^{-/-}$ background.

However, all of these results indicate protein level differences, whereas mRNA expression of the same targets (and of *Stat1*) was found to be independent of ALPK1 kinase activity. This was in concordance with other mRNA data reported in this thesis, namely in comparing BL/6 controls with 129S6 and 129.C3BR17 cells. This common line of results could suggest an effect by an unidentified factor independent of ALPK1, acting on protein translation or secretion. In fact, ALPK1 has been reported to stimulate TNF-α secretion in gout by phosphorylating myosin IIA (Lee et al., 2016), and to increase vesicle transport in epithelial cells (Heine et al., 2005). It is therefore possible that a loss of ALPK1 is affecting protein translation or trafficking. In order to address this hypothesis, it would be interesting to test for IFN-α/β or cytokine levels in the stimulated cells by WB assays or by intracellular staining for flow cytometry. The results of these experiments could allow the comparison of

intracellular vs extracellular levels of these factors. *Ifn-β1* mRNA stability was previously shown to be increased upon cycloheximide treatment (reviewed in (Savan, 2014)). While this was in line with the findings of this thesis (independently of genotype), the factor affecting it remains unelucidated, and, judging by the results of this work, seems independent of ALPK1. Ultimately, it is also possible that BMDMs were not the best model for a study of phospho-protein regulation in this model, and that an assay on X31-infected or poly:U stimulated pDCs would be more informative.

7.2 ALPK1 roles in different mouse models in IFN-α/β responses

7.2.1 The IFN-influenza susceptibility correlation in mouse models

This project set out to elucidate the origins of high IFN production because it was shown to positively correlate with influenza susceptibility in a mouse model (Davidson et al., 2014). In humans, the same effect has not yet been demonstrated in the context of influenza infection. Generally, the host-determined increased susceptibility to influenza in humans was linked to dampened immune responses or a cytokine storm (Ciancanelli et al., 2016, Fukuyama and Kawaoka, 2011, Peiris et al., 2010). Increase in IFN production has been linked with the onset of autoimmune diseases like systemic lupus erythematosus or with allergies such as asthma. Therefore, the results presented in this thesis could potentially be applied to other disease models.

In fact, the positive correlation between high *in vivo* IFN and IAV susceptibility, while valid in the 129 mice and in the congenic mouse model, seem to be limited to mouse strains other than BL/6 (129s, CBA/J or DBA/2 mice for example). Conversely, the 129.C3BR17 mice, 129S6 of background save for the R17 locus of BL/6 origin, showed reduced IFN production and lowered susceptibility compared to the 129 controls.

The *Alpk1*$^{-/-}$ mice, themselves of the BL/6 background, showed more variable susceptibility to influenza. Namely, the weight loss and survival experiment result represented in this thesis originated from *Alpk1*$^{-/-}$ mice that were imported into our Institute from the team of F. Powrie in Oxford. Since then, the same virus dose given on at least three separate occasions to the BL/6 and *Alpk1*$^{-/-}$ mice produced variable results, with albeit more toxicity for BL/6 controls. Since then, our team has identified through different experimentators that the dose initially used for this experiment

caused increased mortality in BL/6 controls. When this dose ($35*10^3$ $TCID_{50}$/mouse) was reduced to $10*10^3$ $TCID_{50}$/mouse, the relative reduced susceptibility of BL/6 mice was restored, but the susceptibility of the *Alpk1*$^{-/-}$ mice from then onwards resembled that of the BL/6 controls. This was regardless of modulation of viral dose and in spite of many attempts at weight loss and survival experiments. Moreover, the BAL experiments carried out at $10*10^3$ $TCID_{50}$/mouse viral dose yielded little to no difference in IFNα/β and cytokine expression between BL/6 and *Alpk1*$^{-/-}$ mice. However, *in vitro, Alpk1*$^{-/-}$ cells were higher IFN producers that the WT controls. These results could indicate that the causes behind the *in vivo* influenza susceptibility in 129 and *Alpk1*$^{-/-}$ (BL/6) mice could be different in nature, or that systemic factors of the host are in play to regulate IFN production *in vivo* in *Alpk1*$^{-/-}$ mice. As previously mentioned, ALPK1 was identified as a novel receptor for ADP-heptose present on Gram-negative bacteria, activating a signaling cascade resulting in IFN-γ and/or pro-inflammatory cytokine production (Garcia-Weber et al., 2018), (Zhou et al., 2018). It has been proposed that ALPK1 could, through ADP-heptose recognition in their Nt domain, participate in the maintenance of the gut microbiota homeostasis. It is possible that the imported mice contained a microbiome slightly different to that of the mice bred at the Francis Crick Institute, affecting ADP-heptose binding to ALPK1. This in turn could have affected mouse susceptibility and IFN and cytokine production downstream.

Instead of being IFN-driven, the *Alpk1*$^{-/-}$ mouse susceptibility could otherwise be a result of increased inflammation, as suggested by the *in vitro* high production of IL-6 by *Alpk1*$^{-/-}$ BMDMs. This hypothesis would be in concordance with the observed survival phenotypes of C57BL/6$^{Ifnar1-/-}$ and 129S7$^{Ifnar1-/-}$ mice, namely that their survival differences were largely independent of the IFNAR cascade (see Chapter 3 Discussion). Taken together with the findings in the 129.C3BR17 mice (where inflammation was still high regardless of the lowering of IFN-α/β levels) and in the C57BL/6$^{Alpk1-/-}$ strain, these data suggest a bigger role for high cytokine production in influenza susceptibility in 129 mice than previously assumed. It would therefore be interesting to investigate the influenza susceptibility as a function of pro-inflammatory cytokine production in the congenic and Alpk1-/- backgrounds (possibly by blocking or dampening the production of IL-6, TNF-α, IL-1β or others).

To probe for cytokine production in the *Alpk1*$^{-/-}$ background in future experiments, pro-inflammatory cytokines levels could be evaluated in the BAL at different points of infection. Moreover, a demonstrated cause of morbidity in 129 mice, namely the interaction between TRAIL and DR5, is a direct consequence of intensified IFN production since both these molecules are ISGs (Davidson et al., 2014). It would be therefore interesting to examine the lung epithelium of *Alpk1*$^{-/-}$ infected mice for signs of apoptosis and overall verify the IFNAR expression *in vivo* in the lung. It is worth mentioning here that probing MTECs for responses to X31 and PR8 infections *in vitro* did not show significant dependence on ALPK1 function.

7.2.2 The 129 allele of Alpk1 and its impact on IFN production

The 129 *Alpk1* allele contains 17 non-synonymous exon mutations compared to the BL/6 sequence, the most of all genes within the R17 locus. Isolating *Alpk1* for analysis of contribution to high IFN production yielded conflicting results in this thesis.

It has been previously demonstrated that, in *H.hepaticus*-driven colitis, Alpk1-knockout BL/6 mice phenotype mimicked that of the 129 WT controls (Ryzhakov et al., 2018) . The authors therefore suggested that the *Alpk1* 129 allele encoded a non-functional protein. While this conclusion was motivated by their observations (in spite of the caveats of their colitis *in vivo* system, as detailed in the Introduction of Chapter 4), it may not be entirely applicable to the findings in this thesis, and it is generally a slight over-interpretation. *Alpk1* specific-knockout mice are entirely of BL/6 genomics background. Therefore, concluding that ALPK1 was non-functional in 129 mice would neglect the impact of the rest of the mouse genome on this phenotype. In fact, the working hypothesis of this thesis that led to the ALPK1 analysis was that the 129 phenotype of high IFN production is most probably a multi-genic trait. The data presented in this thesis supports this assumption.

Indeed, in this thesis a reduction in IFN-α/β and cytokine production, as well as IAV morbidity and mortality was observed *in vivo* and in the pDCs of the 129.C3BR17 congenic mice where the R17 locus comprising the *Alpk1* gene was of BL/6 origin. Based on the reported data, is possible that the R17 locus genotype affects TRAF6 and/or TBK1-mediated IFN transcription. The R17 locus comprises other genes as well, most notably *Tifa*. In spite of not comprising differences in the coding sequence between BL/6 and 129 backgrounds, TIFA is a binding partner to ALPK1 with effects

on TRAF6-mediated pathways (Milivojevic et al., 2017). Given that purely the binding of TIFA to ALPK1 was shown to be sufficient for the induction of TIFA/TRAF6 complexes and TRAF6 phosphorylation, there is a possibility that this binding happens via the ALPK1 Nt domain. It could be speculated that in BL/6 mice this binding could be increased or decreased compared to the 129 background, given that there are non-synonymous mutations of unknown effect in the ALPK1 Nt region sequence between the two genotypes. As the RNA-seq data indicate, the Nt domain could be still produced in the *Alpk1*$^{-/-}$ BL/6 background, which could in turn mean that the binding is happening as normal. It is therefore difficult to conclude on the similarities of the BL/6 ALPK12 Ct-/- and 129 systems in these circumstances, as there are too many unknowns and assumptions.

Based on the findings of this thesis, the 129 phenotype of high IFN production is a multi-genic phenotype. It is regulated in part by one or more factors from within the R17 locus. The effects of these factors seem limited to post-transcriptional regulation of IFN in macrophages, as mRNA levels were found to be similar independently of the R17 locus phenotype. This effect is also dependent on a factor present in the cell in steady-state, as abrogation of newly synthetised proteins did not affect mRNA transcription of *Ifn-β1*, *Il-6* or *Stat1*. It is possible that the factor(s) from the R17 locus, and/or the missing factors affecting IFN production in the 129 mice, act upstream of the IFNAR cascade.

However, the phospho-proteomics result pointed to WWC2 protein as lacking phosphorylation on two separate residues in absence of ALPK1 kinase activity. On the other hand, the RNA-seq experiment findings pointed towards a possible ALPK1-driven regulation of *Wwc2* mRNA expression altogether. Given these findings, WWC2 was studied more in detail to try and investigate its possible role in IFN production.

7.3 ALPK1 and WWC2 putative role in innate immune responses

In the *in vitro* BMDM model studied in this work, two different experiments indicated a connection between ALPK1 and *Wwc2*. Firstly, ALPK1 kinase activity was shown to correlate with the phosphorylation of Ser1017 and Ser1037 residues on WWC2. Additionally, ALPK1 kinase activity loss negatively affected *Wwc2* mRNA

transcription in stimulation and X31 infection, with a reproducible and significant reduction observed in *Alpk1*$^{-/-}$ BMDMs.

While these results were observed in RIG-I stimulation with 5'ppp dsRNA, and in STING stimulation with 2'3' cGAMP, the same effects on WWC2 protein and mRNA were observed in the control conditions (empty lipofectamine and mock, respectively). This indicates that the effects of ALPK1 on WWC2 are intrinsic and baseline, weakly affected by stimulation of TLR/RLR pathways and unaffected by newly synthetised proteins. While WWC2 could be connected to the Hippo pathway by virtue of its homology with KIBRA (see last Results chapter), it seems from the results in this work that ALPK1 or, at least its kinase activity, has no effect on the Hippo pathway activation. It is therefore difficult to implicate ALPK1 as a kinase in the Hippo pathway itself. A possibility remains that ALPK1 could play a scaffolding role via its Nt domain binding but this is purely speculative. However, it seems like ALPK1 could have a direct or indirect effect on WWC2 phosphorylation. ALPK1 kinase domain functionality could be regulating the expression of WWC2 altogether (given the RNA-seq data) or its phosphorylation, via its kinase domain. WWC2 regions containing the modified residues include α-helices, and the protein itself is a coiled-coil domain rich protein. This would place it well amongst the putative targets of the α-kinase family, of which ALPK1 is a member. The assumed hypothetical interaction with aPKCζ (or λ/ι) remains to be addressed with more detailed IP experiments, but the preliminary experiments seem to indicate that its impact is limited.

7.4 Future work

To avoid the caveats associated with using the *Alpk1*$^{-/-}$ mice reported in this thesis, a useful tool would be to rely on an *in vitro* cell model to eliminate *Alpk1* quickly and reliably in its entirety. Two attempts were made at creating immortalized cells using the Hoxb8-estradiol dependent system of bone marrow progenitors reported in other work (Rosas et al., 2011, Wang et al., 2006), with no success so far. Such an *in vitro* model could be of great use in the future studies of the ALPK1-related mechanisms affecting IFN and cytokine production. The macrophages originating from these immortalized progenitors are extremely similar to their BMDM counterparts, convenient to propagate and expand *ad libitum in vitro* and involve the

use of M-CSF for differentiation. An elegant assay could be imagined where BMDMs generated in such a way from the BL/6 and *Alpk1*$^{-/-}$ background could be compared with an *Alpk1* siRNA blockade in a BL/6 line. This would allow to compare the effects of missing only the kinase domain of ALPK1 with missing the entire mRNA. What's more, these cells could be used for validation phospho-proteomics assays, with different time points used to study the global protein phosphorylation during stimulation. Also, *Wwc2* could easily be eliminated in these cells to study its putative interaction with ALPK1. Same could be done with another proven ALPK1 partner, TIFA, which could be taking part in regulating the amplitude of IFN and cytokine responses. Ultimately, the biggest use of this kind of *in vitro* system would be to circumvent the very limiting lack of suitable monoclonal antibodies for recognition of ALPK1 and WWC2. By tagging these proteins and using the tags for immunoprecipitation or labelling for imaging, a lot can be learned of the possible roles of both proteins separately or their interaction.

Generally, it would be more prudent to approach the study of the role of ALPK1 from the *in vitro* side, as this thesis has shown a discrepancy between the *in vivo* and *in vitro* effects of a loss of *Alpk1*. *In vivo* studies in mice are necessary to prove any kind of *in vitro* finding concerning systemic responses such as IFN, but they do also bring additional complexity into the study of the role of ALPK1.

7.5 Conclusions and outlook

Influenza remains a public health burden, constant pandemic threat, and a fast-evolving pathogen which is difficult to eliminate by host-independent treatment. Host responses to influenza in both humans and mice have been linked to disease outcome, and their major mediators, type-I IFNs, are known contributors to the severity and the efficiency of the immune response.

The results presented in this work have helped contribute, albeit to a small extent, towards identifying novel candidates in the regulation of IFN expression in mice. In the 129 mouse model of influenza disease, the extent of IFN production can make the difference between overcoming or succumbing to the infection. It seems like a candidate gene locus on Chromosome 3, namely R17, contributes to the modulation of IFN-α and IFN-β production *in vivo* and *in vitro.* The genes within this locus have insofar been linked to colitis disease and epithelial cell polarisation, but

not with IAV infection, so the work in this thesis represents a step in a new direction for their study.

Alpk1, an R17 locus gene, represents a plausible candidate contributor to the extent of IFN responses *in vitro*. It can affect the outcome of infection in mice, but the mechanisms behind this remain unclear. ALPK1 has been connected to gout susceptibility, cancer prognosis, and bacterial colitis in humans and mice. This work has laid the ground for further in-depth studies of ALPK1 and its putative phosphorylation target WWC2 and their roles in type-I IFN production in mice and humans. If successful, ALPK1 could mark the identification of a novel pathway implicated in IAV disease recognition in mice, and possibly humans.

Chapter 8. Appendix

8.1 Flow cytometry gating strategy for myeloid cells: neutrophils, eosinophils, alveolar macrophages, pDCs and cDCs

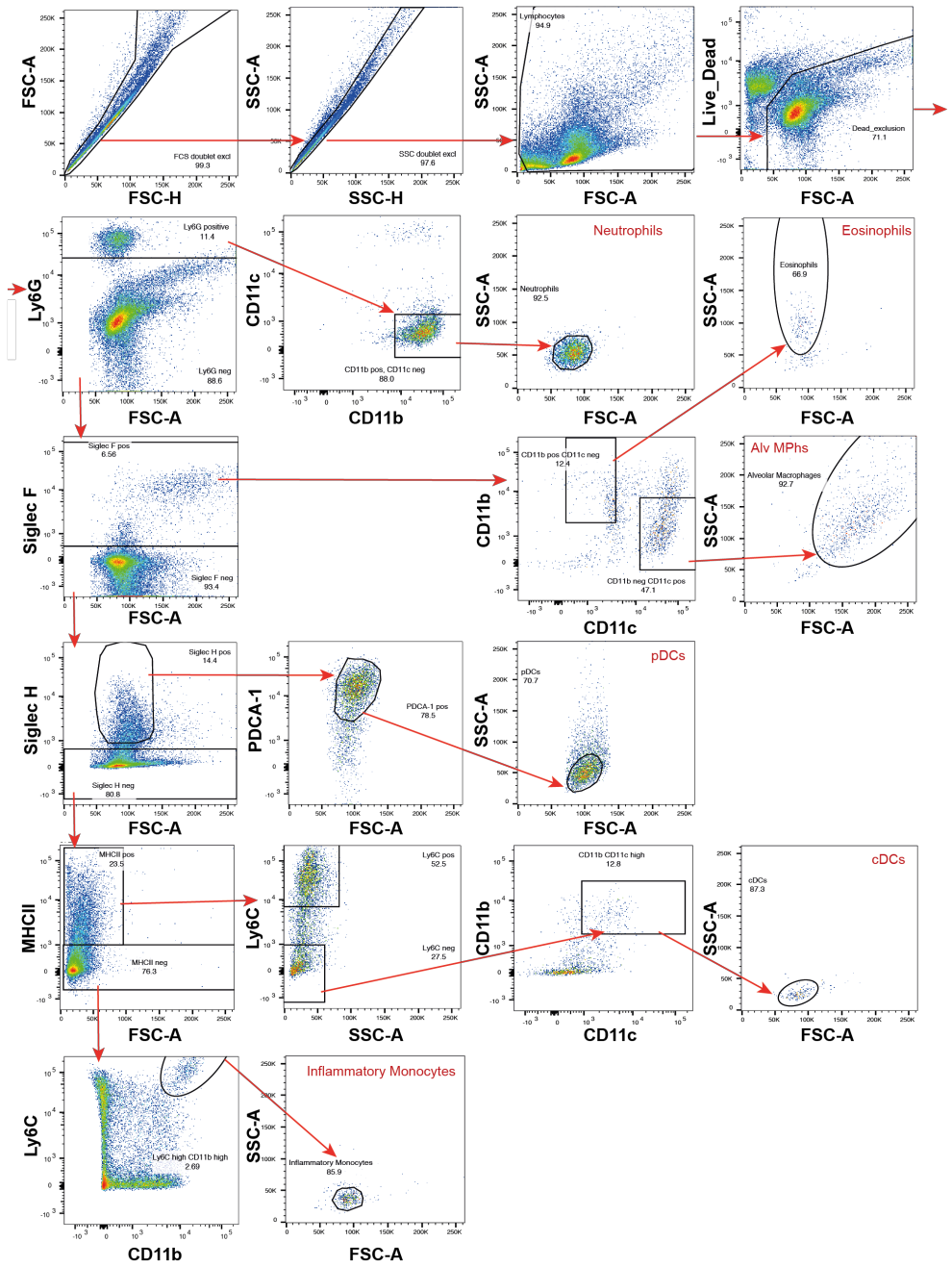

Figure 8.1 Flow cytometry gating strategy using surface markers. Whole lungs from BL/6 and *Alpk1*$^{-/-}$ mice after infection were prepared as described in Material and Methods section and cells stained for flow cytometry for surface markers. First,

the doublets were eliminated by FSC and SSC criteria, lymphocytes identified by size and live cells identified using the Zombie Live/Dead stain. Neutrophils were identified using Ly6G marker and isolated, and all Ly6G-negative cells further split into Siglec-F-positive (CD11b-positive eosinophils and CD11c-positive alveolar macrophages) and Siglec-F negative cells. From the latter population, pDCs were identified as Siglec-H-positive cells and confirmed by PDCA-1 positivity. Siglec-H negative populations were further split into MHCII-positive and -negative cells. In the MHCII-positive population, Ly6C-negative, CD11b and CD11c-positive cells were identified as conventional dendritic cells. Meanwhile, MHCII-negative cell population was tested for Ly6C expression and all Ly6C-high cells identified as inflammatory monocytes. This gating is representative of all *in vivo* lung flow cytometry experiments performed in this work.

8.2 Flow cytometry gating strategy for lymphoid cells: NK cells, CD4 T-cells, CD8 T-cells and B-cells

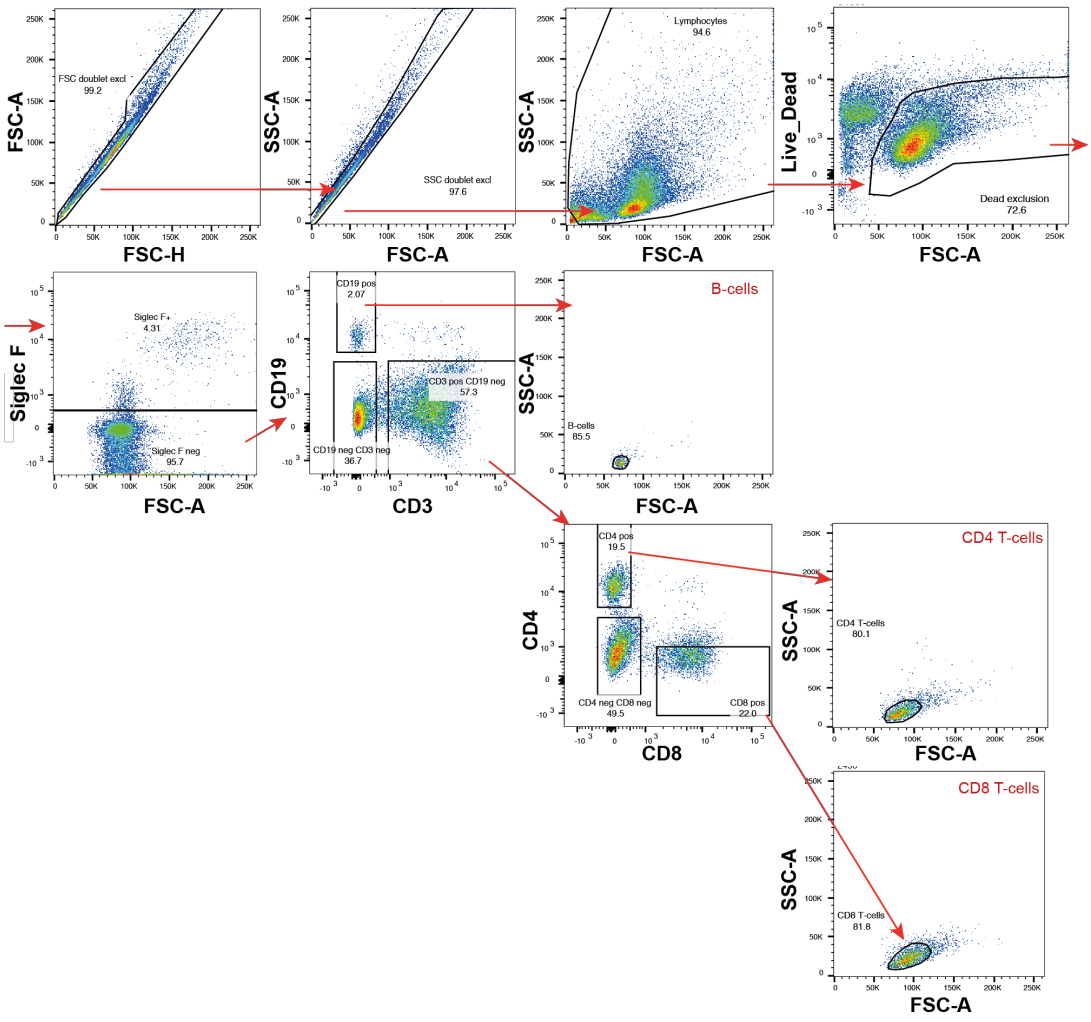

Figure 8.2 Flow cytometry gating strategy for lymphoid cells. Whole lungs from BL/6 and *Alpk1*$^{-/-}$ mice-post-infection were prepared and stained as described in

Material and Methods. Of the whole population, doublets were excluded based on FSC and SSC criteria, then lymphocites selected by size and live cells by their Live/Dead Zombie stain negativity. Further, a Siglec-F exclusion gate was used to exclude Siglec-F positive cells (AMs, eosinophils). In the Siglec-F negative population, CD3 and CD19 markers were used to separate T anc B-cell populations, respectively. The CD3 positive cell population was split into CD4-positive and CD8-positive T-cells. This gating is representative of all *in vivo* lung flow cytometry experiments performed in this work.

8.3 BMDM and pDC proportions in cell cultures of different genotypes

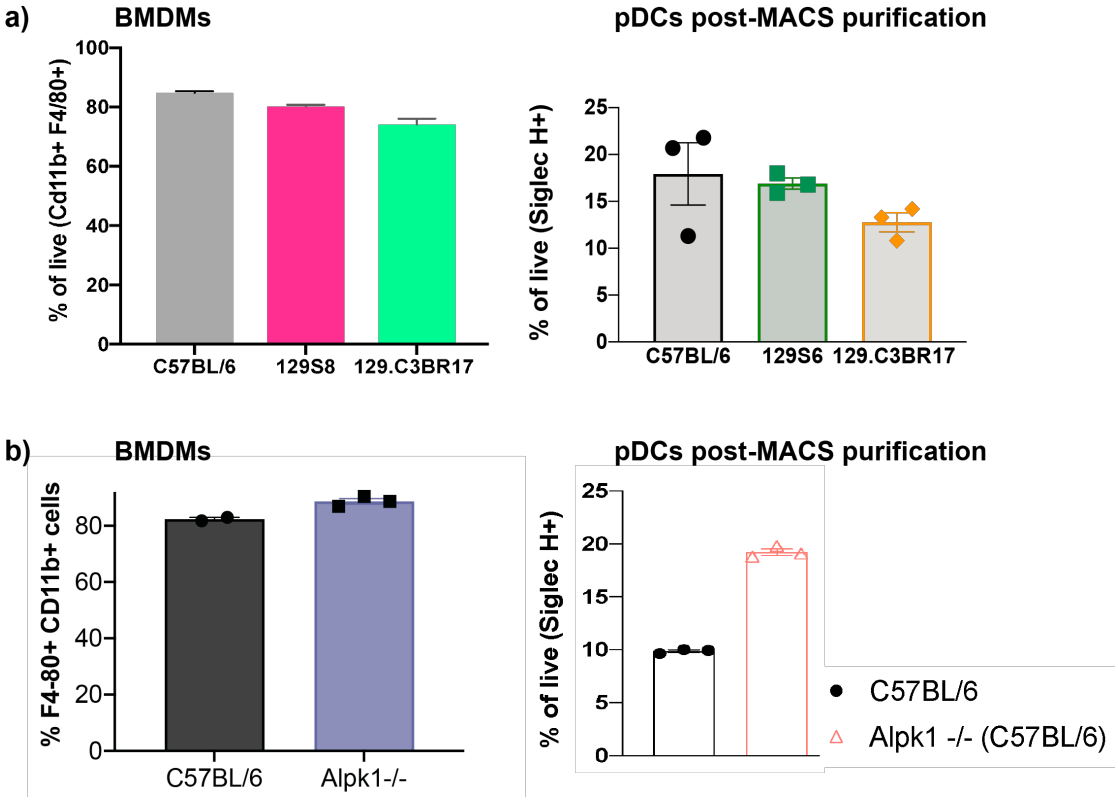

Figure 8.3 Percentage of BMDMs (F4/80+ CD11b+) and pDCs (Siglec H+) amongst live cells in bone marrow cultures in different genotypes.

Bone marrow cultures were prepared as previously described and cultured for 7 days in media enriched with M-CSF (BMDMs) or Flt3L (pDC). Percentages of cells, defined as BMDMs when CD11b+ F4/80+ or pDCs when Siglec H+, amongst live cells, are represented for **A.** BL/6, 129 and 129.C3BR17 or **B.** BL/6 and BL6$^{Alpk1-/-}$ genotype-derived cultures. For pDC-enriched cultures, results represent suspensions after a MACS-purification step to isolate B220-positive cells. After 7 days, BMDMs cultures or purified pDC-enriched cultures were probed by flow cytometry for expression of surface markers. The results represent proportions of marker-positive cells as a percentage of live cells in each culture. In BMDM cultures, each dot represents an individual culture issued from a single mouse

bone marrow and in pDC-enriched cultures each dot is a technical replicate from a culture of pooled bone marrows.

8.4 The first phospho-proteomics assay to identify Alpk1 phosphorylation targets in stimulated BMDMs

This first phospho-proteomics experiment was designed to examine different conditions of stimulation and the responses of WT and *Alpk1*$^{-/-}$ BMDMs. There were no biological replicates in this experiment because of the design of the TMT-labelling kits that all processing and comparison of only 10 samples at a time. The mock condition was included as a control for LPS stimulation, and empty lipofectamine was a transfection control for 2'3' cGAMP and 5'ppp dsRNA transfection conditions.

The raw dataset was processed and the normalised reporter ion intensities analysed in the figures that follow (for details see Material and Methods). Firstly, a PCA analysis was conducted on the entire sample set (Figure 8.4a). First of all, it was visible that the biggest source of variation amongst samples was not to be attributed to the genotype, as WT and *Alpk1*$^{-/-}$ BMDMs cluster together in every treatment type. The biggest proportion of the variation (67.7%) seems to coincide with the treatment undergone by the cells. LPS-treated samples are clearly separated from their corresponding mock control according to the two highest variation components (x and y axes in the graph). This was expected to an extent, as it is known that LPS treatment of macrophages induces global and intense changes in the proteome and the phosphorylation landscape. All transfected conditions were different to untreated controls and presented great similarity between each other according to either of the two variation components. This indicated that transfection as such has a great effect on the cells, and only subtle (if any) changes in the captured phospho-proteomic landscape were induced by 2'3' cGAMP and 5'ppp dsRNA stimulation in comparison to the empty lipofectamine control. The reporter ion intensities for each phosphorylated residue identified in the dataset, in different stimulation conditions, are also represented in the form of profile plots (Figure 8.4b). For each residue, a horizontal grey line connects the $\log_2$(intensity value) of the corresponding reporter ion intensity in different conditions. The ion intensities are at their highest in the LPS stimulation condition, which stands

out from other controls and stimulations in this experiment. This shows the intensity of the phospho-proteomic changes in BMDMs upon LPS stimulation. Also, the profile plots did not show a marked difference between genotypes, confirming the PCA finding.

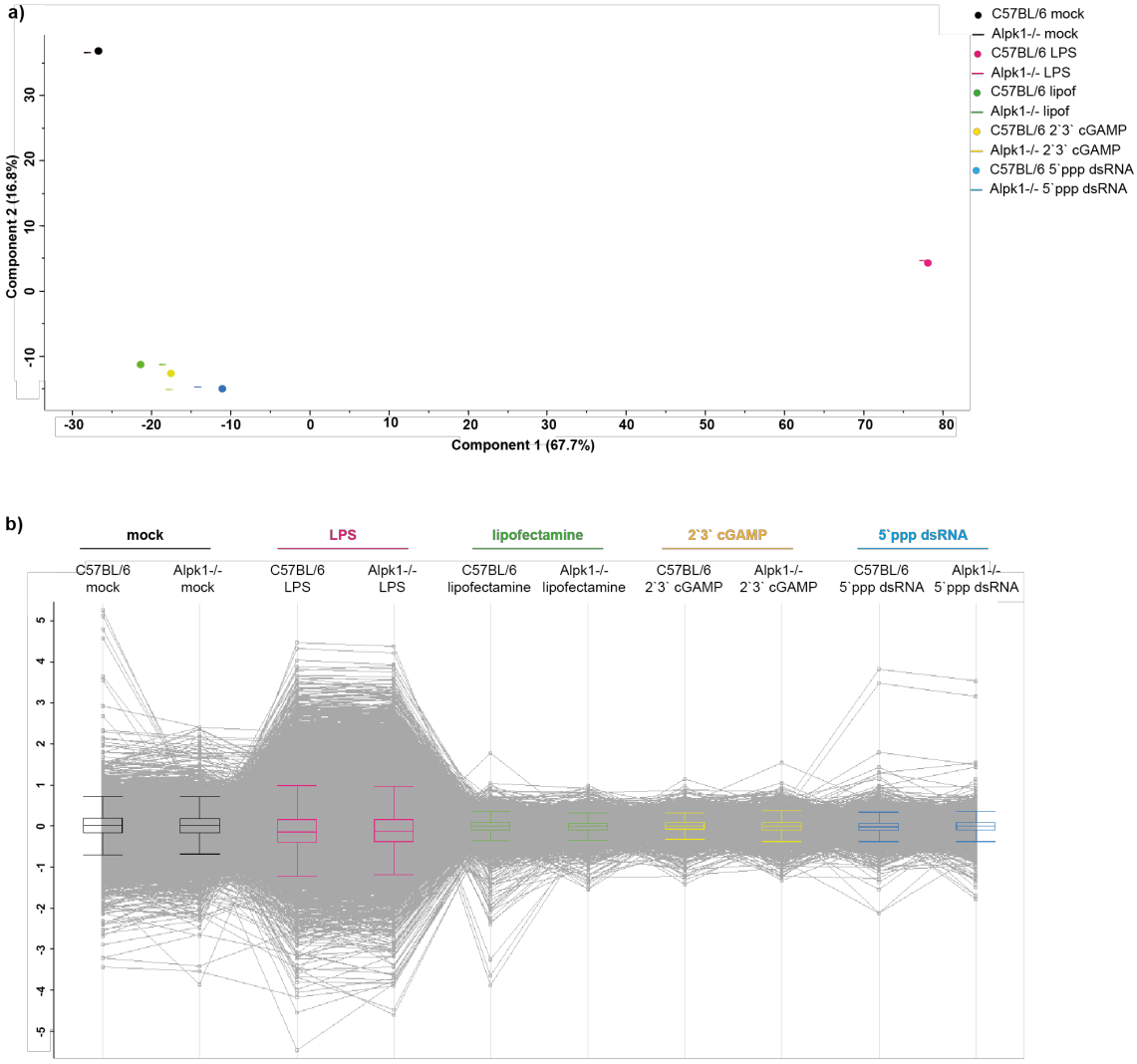

Figure 8.4 LPS induces significant changes in the phospho-proteome landscape of BMDMs; 2'3' cGAMP and 5'ppp dsRNA transfections have a comparably smaller effect. BMDMs were differentiated from one C57BL/6 and one *Alpk1*$^{-/-}$ mouse. 9 million BMDMs per condition and per genotype were stimulated with LPS for 30min, 2'3' cGAMP for 2h or 5'ppp dsRNA for 2h (respective controls were untreated cells and 2h-long incubation with empty lipofectamine). 200μg of total protein per sample underwent two-fold peptide digestion, peptide TMT-labelling and two-fold phospho-residue purification before LC-MS analysis (details of protocols in Material and Methods). Represented figures were generated using the software Perseus. **A.** principal component analysis to include each sample in the dataset (sample key on the right), with the first two components explaining 84.5% total sample variation between them. **B.** Ion intensities associated with each detected phospho-peptide were normalised to the mean ion intensity of the dataset (y axis) and plotted for each

condition (x axis). The connecting lines aid the visualisation of each residue's associated perceived ion intensity in different samples. Boxplots used, with SD whiskers, contain 95% of the total number of phosphorylated residues within that genotype and that stimulation condition.

These results were indicative of the subtlety in differences between BL/6 and *Alpk1*$^{-/-}$ in all conditions tested. Using Perseus, it was possible to visualise and compare the reporter ion intensities of phospho-peptides in both genotypes directly (Figure 8.5). C57BL/6 BMDM reporter ion intensities are represented on the x axis, and the *Alpk1*$^{-/-}$ ones on the y axis. The lines x=y were drawn for clarity of comparison of the ion intensity between genotypes. It is immediately visible that in LPS-treated cells the intensity of cell responses is in fact very similar between the two genotypes. The only peptides that are comparatively further away from the x=y line, are in fact centred around 0. Their reporter ion intensities are therefore not highly increased or decreased compared to the median phosphorylation patterns across samples. A similar pattern is found in the untreated condition, although the global ion intensity signature is in fact centred around zero, as expected in non-challenged cells. It is worth noting that both axes are expressed as log2(corrected reporter ion intensity). In comparison, all transfected conditions show extremely low enrichment in phospho-peptides and almost no difference between WT and *Alpk1*$^{-/-}$ cells.

In these scatterplots, the entire phospho-peptide dataset is represented. However, it is worth noting that amongst these peptides, a significant number was not reliably assigned to a protein and thus scored as contaminants. Moreover, the obvious limits of this particular experiment, namely the lack of any replicates in genotypes, is to be kept in mind when considering the represented results.

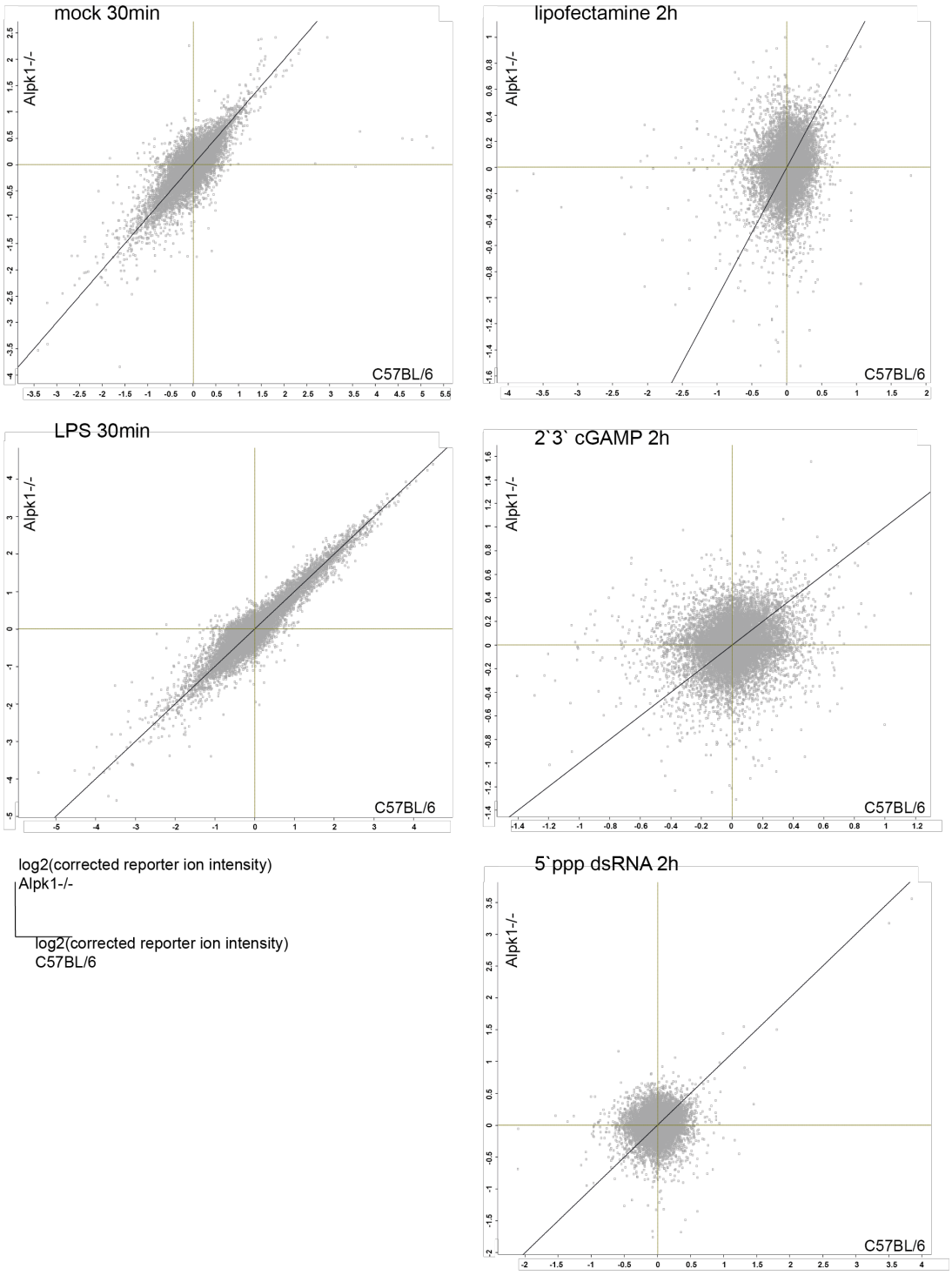

Figure 8.5 Within the same treatment (LPS, 2'3' cGAMP or 5'ppp dsRNA), the genotype effect is extremely limited. Reporter ion intensities normalised to mean of the sample set are represented as log2() values on x axis (C57BL/6) and y axis (*Alpk1*$^{-/-}$) to compare the phosphorylation patterns between the two genotypes. Each grey dot represents an identified phospho-peptide of the dataset. Black line: x=y; x=0 and y=0 are also represented. Figures were generated using the Perseus software.

The phospho-peptide dataset obtained in this way was cross-referenced with the KEGG pathway database in an attempt to look at patterns of pathway activation in different stimulations and genotypes. Using Perseus, it was possible to highlight each phospho-peptide assigned to a protein that, according to the KEGG database entries, belongs to this pathway. A few relevant examples of these pathways, with their respective phospho-residues highlighted in red, are cited in Figure 8.6. LPS is a stimulus of the TLR4 pathway, whose components can be found assigned to the Toll-like receptor pathway in the KEGG database. Highlighting the phospho-peptides of proteins belonging to this pathway unveiled changes in phosphorylation patterns in LPS treatment as expected. However, no striking difference was observed in these patterns between the two genotypes (Figure 8.6a), given that all the highlighted peptides line the x=y axis. Peptides in the “Cytosolic DNA-detection signaling” (corresponding to cGAS/STING activation by 2’3’ cGAMP) or “RIG-I like receptor signaling” (corresponding to 5’ppp dsRNA stimulation) pathways showed little change in patterns of phosphorylation. However, in testing for “Jak/STAT signaling” pathway activation (Figure 8.6b) it was encouraging to see very little phosphorylation changes across different conditions of stimulation. The timepoints of stimulation for this experiment were chosen so as to preclude the IFNAR1-cascade activation and seemingly this was achieved to some degree.

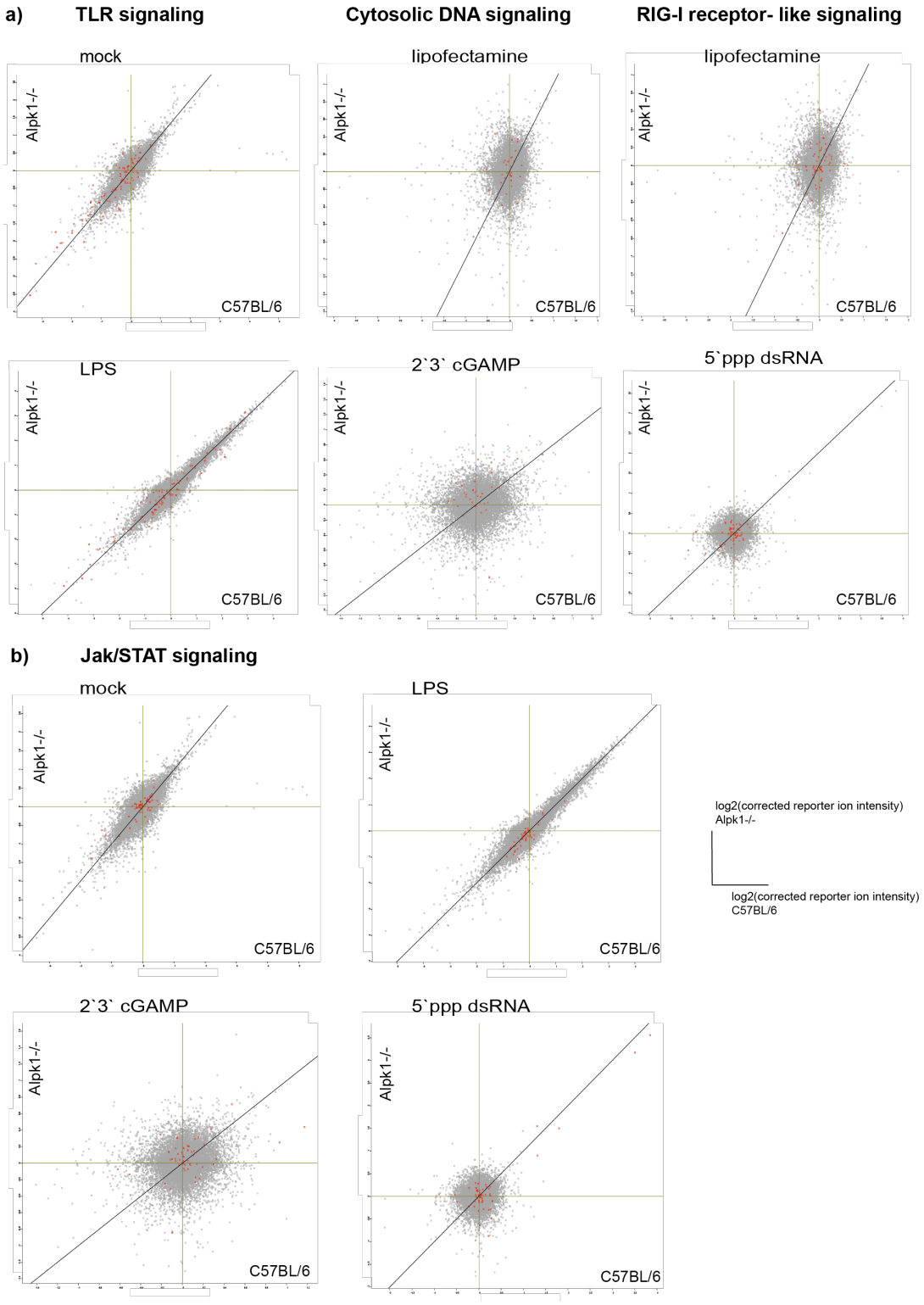

Figure 8.6 Changes in phosphorylation of proteins belonging to different pathways defined by the KEGG database. Phospho-peptide residues in proteins belonging to KEGG pathways that correspond to the used stimuli were highlighted in red in the scatterplot datasets. **A.** “Toll-like receptor signaling” peptides visualised in mock and LPS conditions; “Cytosolic DNA sensing” in lipofectamine and 2’3’ cGAMP; “RIG-I receptor-like signalling” in lipofectamine and 5’ppp dsRNA. The assignment

of the peptides to KEGG signalling pathways was achieved by cross-referencing this dataset to the KEGG database in Perseus. **B. "**Jak-Stat signalling" pathway visualised for all stimulation conditions a means to verify the activation of IFNAR1-induced cascade at these timepoints of stimulation.

To try and single out individual peptides that could be of interest in these stimulation conditions, differences in reporter ion intensities between C57BL/6 and *Alpk1*$^{-/-}$ genotypes were visualised in scatterplots (Figure 8.7a). All peptides exhibiting a loss of phosphorylation in the *Alpk1*$^{-/-}$ background higher than 1.5 fold ($\log_2(1.5)=0.585$) were highlighted and the lists compared between LPS, 2'3' cGAMP and 5'ppp dsRNA stimulations in the effort to find a common denominator. This would possibly indicate a peptide whose phosphorylation is at least partly dependent on the presence of *Alpk1*. A Venn diagram (Figure 8.7b) was then used to compare the peptides that appear in different stimulations. Partly as expected, and because of the difference in nature of LPS stimulation compared to the transfected stimuli, no common phospho-peptides were detected for all three stimulation conditions. However, in the more similar 2'3' cGAMP and 5'ppp dsRNA, peptides belonging to proteins encoded by *Nes*, *Rasal3* and *Nucks1* genes were detected as less phosphorylated in *Alpk1*$^{-/-}$ cells. Although this result could be of interest, it was not addressed further as there was no statistical credibility in this experiment. Moreover, it seemed useful to change the timepoints used for transfected stimuli as obviously they were not reflecting the cellular activation in the best way.

For these reasons, a new phospho-proteomics experiment was performed, keeping only the lipofectamine, 2'3' cGAMP transfection and 5'ppp dsRNA transfection conditions, and the length of stimulation to 1h only. The motivations for the choice of these stimuli and this timepoint were a combination of the WB optimisation results shown previously, and the ambiguous result of the first phospho-proteomics assay. A report on the results of this experiment follows.

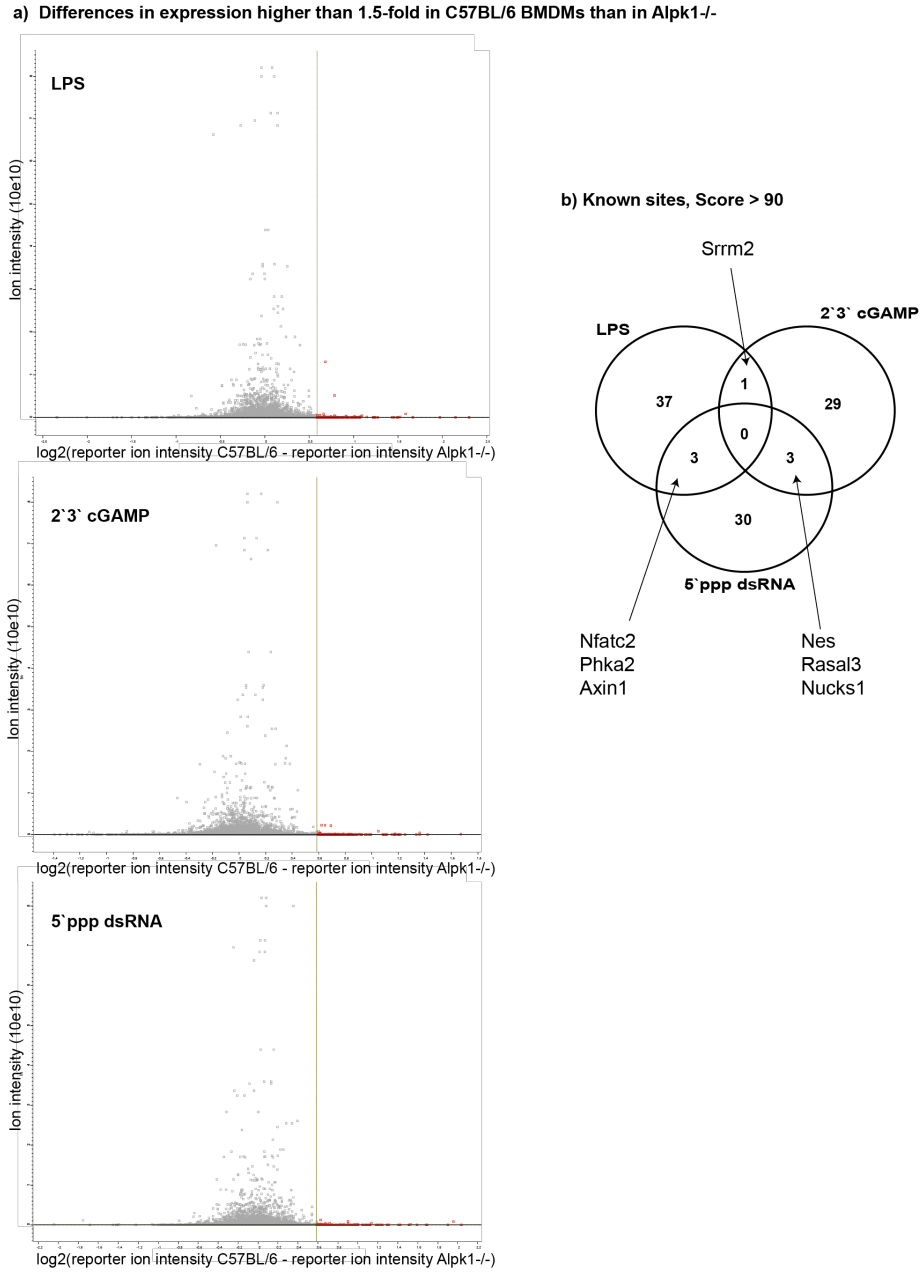

Figure 8.7 Detection of phospho-peptides 1.5-fold less phosphorylated in *Alpk1*$^{-/-}$ than in WT-cells unveils three common proteins in transfected stimulation conditions. A. The graphs were made using Perseus, with on y-axis the ion intensity and on x axis the logarithmic difference in enrichment of phospho-peptides in BL/6 vs *Alpk1*$^{-/-}$ backgrounds. A 1.5-fold enrichment cut-off is represented on the x-axis at the 0.585 point (log_2). **B.** Manually drawn Venn diagram based on the gene names appearing in the three stimulation conditions as 1.5-fold less phosphorylated in *Alpk1*$^{-/-}$ cells. The common denominators are indicated and their lists cited. Nes- Nestin; Rasal3 – Ras protein activator-like 3; Nucks1 – Nuclear ubiquitous casein and cyclin-dependent kinase substrate 1; Srrm2 – Serine/Arginine repetitive matrix protein 2; Nfatc2 – Nuclear Factor of Activated T-cells; Phka2 – phosphorylase b kinase regulatory subunit alpha.

8.5 *Alpk1* gene reads alignment (Integrative Genomics Viewer)

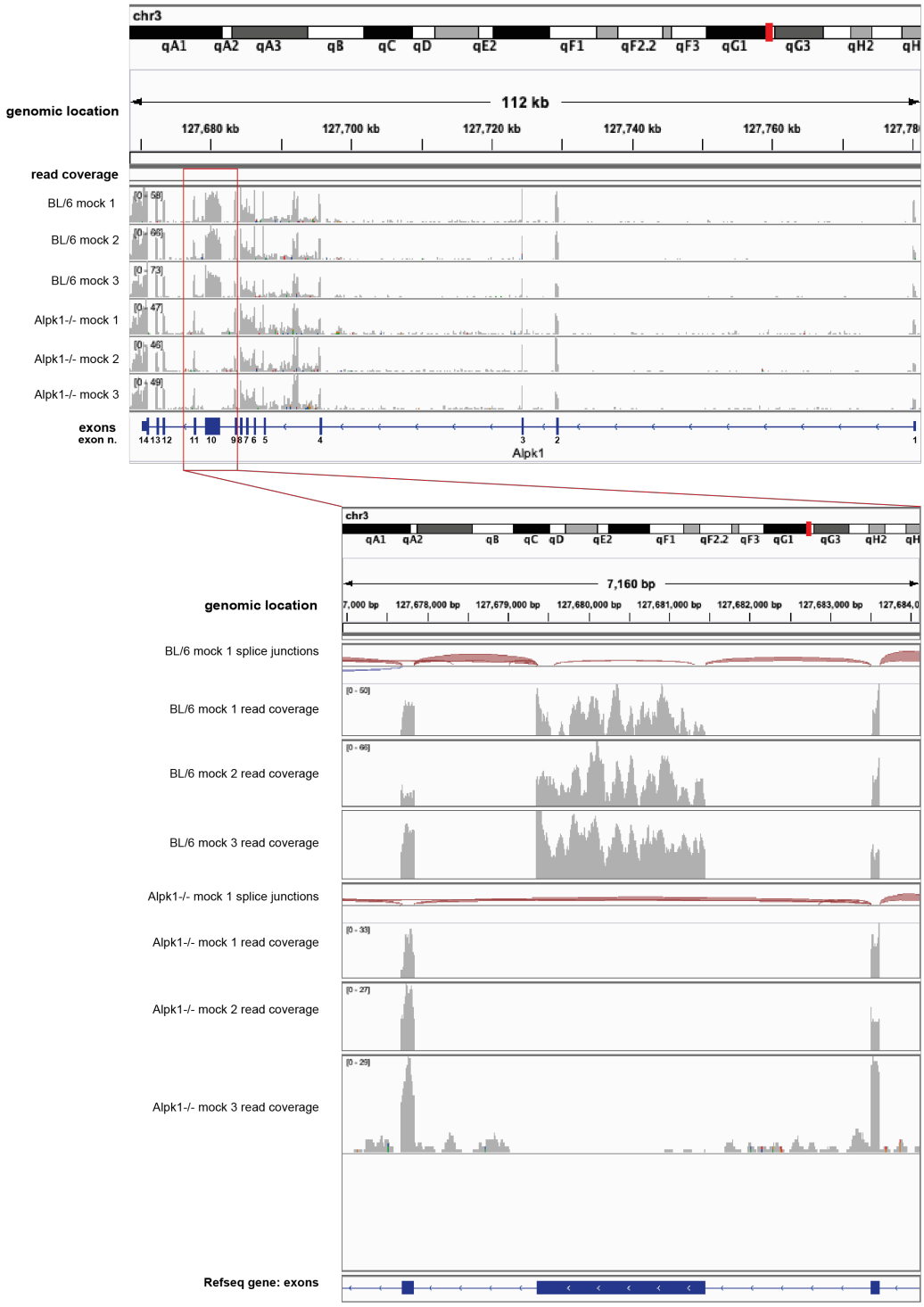

Figure 8.8 The RNA-seq read alignment on the *Alpk1* gene shows the deletion of exon 10 in *Alpk1*$^{-/-}$ BMDMs. Integrative Genomics Viewer (IGV) visualisation of RNA-seq read alignment on the *Alpk1* gene (overview panel, blue boxes). The top panel shows the chromosomal location of the gene and its entire length, and the bottom panel is a zoom onto the area marked in red, around exon 10. *Alpk1* is a gene

transcribed on the reverse strand, and each blue box in the top panel represents one exon (marked 1-14 in order, with the poly:A tail represented as an additional rectangle at the end of the last exon). Above the exon lane are represented the read coverage lanes for three replicates of BL/6 and *Alpk1*$^{-/-}$ mock conditions. It is clearly visible, especially from the bottom zoomed-in panel, that there is no read alignment on exon 10 in the *Alpk1*$^{-/-}$ conditions. The same result was observed for all the cells in stimulated conditions. Importantly, the alignment is similar between BL/6 and *Alpk1*$^{-/-}$ reads on the remaining exons 11-14, indicating that the rest of the gene following exon 10 is transcribed as usual. This is in direct contradiction with the claim (with no evidence provided) made by (Ryzhakov et al., 2018) that the *Alpk1* exon 10 deletion induces a frameshift mutation.

Reference List

A. W. S. HO, N. P., R. JOHN BETTS, M.Q. GE, X. DAI, P. E. HUTCHINSON, F.C. LEW, K.L. WONG, B.J. HANSON, P. A. MACARY AND D.M. KEMENY 2011. Lung CD103+ Dendritic Cells Efficiently Transport Influenza Virus to the Lymph Node and Load Viral Antigen onto MHC Class I for Presentation to CD8 T Cells. *J Immunol,* 187 6011-6021.

AKASHI, K., TRAVER, D., MIYAMOTO, T. & WEISSMAN, I. L. 2000. A clonogenic common myeloid progenitor that gives rise to all myeloid lineages. *Nature,* 404**,** 193-7.

AKIRA, S., UEMATSU, S. & TAKEUCHI, O. 2006. Pathogen recognition and innate immunity. *Cell,* 124**,** 783-801.

AL-MUHSEN, S. & CASANOVA, J. L. 2008. The genetic heterogeneity of mendelian susceptibility to mycobacterial diseases. *J Allergy Clin Immunol,* 122**,** 1043-51; quiz 1052-3.

ALEXANDER, W. S. 2002. Suppressors of cytokine signalling (SOCS) in the immune system. *Nat Rev Immunol,* 2**,** 410-6.

AMULIC, B., CAZALET, C., HAYES, G. L., METZLER, K. D. & ZYCHLINSKY, A. 2012. Neutrophil function: from mechanisms to disease. *Annu Rev Immunol,* 30**,** 459-89.

ARULANANDAM, B. P., RAEDER, R. H., NEDRUD, J. G., BUCHER, D. J., LE, J. & METZGER, D. W. 2001. IgA immunodeficiency leads to inadequate Th cell priming and increased susceptibility to influenza virus infection. *J Immunol,* 166**,** 226-31.

ASSELIN-PATUREL, C., BOONSTRA, A., DALOD, M., DURAND, I., YESSAAD, N., DEZUTTER-DAMBUYANT, C., VICARI, A., O'GARRA, A., BIRON, C., BRIERE, F. & TRINCHIERI, G. 2001. Mouse type I IFN-producing cells are immature APCs with plasmacytoid morphology. *Nat Immunol,* 2**,** 1144-50.

ASSIL, S., WEBSTER, B. & DREUX, M. 2015. Regulation of the Host Antiviral State by Intercellular Communications. *Viruses,* 7**,** 4707-33.

BAHAROM, F., THOMAS, O. S., LEPZIEN, R., MELLMAN, I., CHALOUNI, C. & SMED-SORENSEN, A. 2017. Visualization of early influenza A virus trafficking in human dendritic cells using STED microscopy. *PLoS One,* 12**,** e0177920.

BALACHANDRAN, S., ROBERTS, P. C., BROWN, L. E., TRUONG, H., PATTNAIK, A. K., ARCHER, D. R. & BARBER, G. N. 2000. Essential Role for the dsRNA-Dependent Protein Kinase PKR in Innate Immunity to Viral Infection. *Immunity,* 13**,** 129-141.

BARBALAT, R., LAU, L., LOCKSLEY, R. M. & BARTON, G. M. 2009. Toll-like receptor 2 on inflammatory monocytes induces type I interferon in response to viral but not bacterial ligands. *Nat Immunol,* 10**,** 1200-7.

BASAGOUDANAVAR, S. H., THAPA, R. J., NOGUSA, S., WANG, J., BEG, A. A. & BALACHANDRAN, S. 2011. Distinct roles for the NF-kappa B RelA subunit during antiviral innate immune responses. *J Virol,* 85**,** 2599-610.

BAUM, A., SACHIDANANDAM, R. & GARCIA-SASTRE, A. 2010. Preference of RIG-I for short viral RNA molecules in infected cells revealed by next-generation sequencing. *Proc Natl Acad Sci U S A,* 107**,** 16303-8.

BAUMGARTNER, R., POERNBACHER, I., BUSER, N., HAFEN, E. & STOCKER, H. 2010. The WW domain protein Kibra acts upstream of Hippo in Drosophila. *Dev Cell,* 18**,** 309-16.

BEDI, S., NODA, T., KAWAOKA, Y. & ONO, A. 2018. A Defect in Influenza A Virus Particle Assembly Specific to Primary Human Macrophages. *MBio,* 9.

BEL, M., OCANA-MACCHI, M., LINIGER, M., MCCULLOUGH, K. C., MATROSOVICH, M. & SUMMERFIELD, A. 2011. Efficient sensing of avian influenza viruses by porcine plasmacytoid dendritic cells. *Viruses,* 3**,** 312-30.

BELL, L. C. K. & NOURSADEGHI, M. 2018. Pathogenesis of HIV-1 and Mycobacterium tuberculosis co-infection. *Nat Rev Microbiol,* 16**,** 80-90.

BELSER, J. A., KATZ, J. M. & TUMPEY, T. M. 2011. The ferret as a model organism to study influenza A virus infection. *Dis Model Mech,* 4**,** 575-9.

BJORCK, P. 2001. Isolation and characterization of plasmacytoid dendritic cells from Flt3 ligand and granulocyte-macrophage colony-stimulating factor-treated mice. *Blood,* 98**,** 3520-6.

BLAZEK, K., EAMES, H. L., WEISS, M., BYRNE, A. J., PEROCHEAU, D., PEASE, J. E., DOYLE, S., MCCANN, F., WILLIAMS, R. O. & UDALOVA, I. A. 2015. IFN-lambda resolves inflammation via suppression of neutrophil infiltration and IL-1beta production. *J Exp Med,* 212**,** 845-53.

BOIVIN, G. A., POTHLICHET, J., SKAMENE, E., BROWN, E. G., LOREDO-OSTI, J. C., SLADEK, R. & VIDAL, S. M. 2012. Mapping of clinical and expression quantitative trait loci in a sex-dependent effect of host susceptibility to mouse-adapted influenza H3N2/HK/1/68. *J Immunol,* 188**,** 3949-60.

BOON, A. C., DEBEAUCHAMP, J., HOLLMANN, A., LUKE, J., KOTB, M., ROWE, S., FINKELSTEIN, D., NEALE, G., LU, L., WILLIAMS, R. W. & WEBBY, R. J. 2009. Host genetic variation affects resistance to infection with a highly pathogenic H5N1 influenza A virus in mice. *J Virol,* 83**,** 10417-26.

BOON, A. C., FINKELSTEIN, D., ZHENG, M., LIAO, G., ALLARD, J., KLUMPP, K., WEBSTER, R., PELTZ, G. & WEBBY, R. J. 2011. H5N1 influenza virus pathogenesis in genetically diverse mice is mediated at the level of viral load. *MBio,* 2.

BOON, A. C., WILLIAMS, R. W., SINASAC, D. S. & WEBBY, R. J. 2014. A novel genetic locus linked to pro-inflammatory cytokines after virulent H5N1 virus infection in mice. *BMC Genomics,* 15**,** 1017.

BORGHINI, L., LU, J., HIBBERD, M. & DAVILA, S. 2018. Variation in Genome-Wide NF-kappaB RELA Binding Sites upon Microbial Stimuli and Identification of a Virus Response Profile. *J Immunol,* 201**,** 1295-1305.

BOTTOMLY, D., FERRIS, M. T., AICHER, L. D., ROSENZWEIG, E., WHITMORE, A., AYLOR, D. L., HAAGMANS, B. L., GRALINSKI, L. E., BRADEL-TRETHEWAY, B. G., BRYAN, J. T., THREADGILL, D. W., DE VILLENA, F. P., BARIC, R. S., KATZE, M. G., HEISE, M. & MCWEENEY, S. K. 2012. Expression quantitative trait Loci for extreme host response to influenza a in pre-collaborative cross mice. *G3 (Bethesda),* 2**,** 213-21.

BOULARD, O., KIRCHBERGER, S., ROYSTON, D. J., MALOY, K. J. & POWRIE, F. M. 2012. Identification of a genetic locus controlling bacteria-driven colitis and associated cancer through effects on innate inflammation. *J Exp Med,* 209**,** 1309-24.

BOUVIER, N. M. & LOWEN, A. C. 2010. Animal Models for Influenza Virus Pathogenesis and Transmission. *Viruses,* 2**,** 1530-1563.

BOUVIER, N. M. & PALESE, P. 2008. The biology of influenza viruses. *Vaccine,* 26 Suppl 4**,** D49-53.

BRAAM, J., ULMANEN, I. & KRUG, R. M. 1983. Molecular model of a eucaryotic transcription complex: Functions and movements of influenza P proteins during capped RNA-primed transcription. *Cell,* 34**,** 611-618.

BRASEL, K., DE SMEDT, T., SMITH, J. L. & MALISZEWSKI, C. R. 2000. Generation of murine dendritic cells from flt3-ligand-supplemented bone marrow cultures. *Blood,* 96**,** 3029-39.

BRASS, A. L., HUANG, I. C., BENITA, Y., JOHN, S. P., KRISHNAN, M. N., FEELEY, E. M., RYAN, B. J., WEYER, J. L., VAN DER WEYDEN, L., FIKRIG, E., ADAMS, D. J., XAVIER, R. J., FARZAN, M. & ELLEDGE, S. J. 2009. The IFITM proteins mediate cellular resistance to influenza A H1N1 virus, West Nile virus, and dengue virus. *Cell,* 139**,** 1243-54.

BROWN, D. A. & ROSE, J. K. 1992. Sorting of GPI-anchored proteins to glycolipid-enriched membrane subdomains during transport to the apical cell surface. *Cell,* 68**,** 533-544.

BUTHER, K., PLAAS, C., BARNEKOW, A. & KREMERSKOTHEN, J. 2004. KIBRA is a novel substrate for protein kinase Czeta. *Biochem Biophys Res Commun,* 317**,** 703-7.

CAI, X., CHIU, Y. H. & CHEN, Z. J. 2014. The cGAS-cGAMP-STING pathway of cytosolic DNA sensing and signaling. *Mol Cell,* 54**,** 289-96.

CAMP, J. V. & JONSSON, C. B. 2017. A Role for Neutrophils in Viral Respiratory Disease. *Front Immunol,* 8**,** 550.

CAO, W., TAYLOR, A. K., BIBER, R. E., DAVIS, W. G., KIM, J. H., REBER, A. J., CHIRKOVA, T., DE LA CRUZ, J. A., PANDEY, A., RANJAN, P., KATZ, J. M., GANGAPPA, S. & SAMBHARA, S. 2012. Rapid differentiation of monocytes into type I IFN-producing myeloid dendritic cells as an antiviral strategy against influenza virus infection. *J Immunol,* 189**,** 2257-65.

CARRASCO, M., AMORIM, M. J. & DIGARD, P. 2004. Lipid raft-dependent targeting of the influenza A virus nucleoprotein to the apical plasma membrane. *Traffic,* 5**,** 979-92.

CHEN, B. J., LESER, G. P., MORITA, E. & LAMB, R. A. 2007. Influenza virus hemagglutinin and neuraminidase, but not the matrix protein, are required for assembly and budding of plasmid-derived virus-like particles. *J Virol,* 81**,** 7111-23.

CHEN, K., LIU, J. & CAO, X. 2017. Regulation of type I interferon signaling in immunity and inflammation: A comprehensive review. *J Autoimmun,* 83**,** 1-11.

CHEN, M. & XU, R. 2011. Motor coordination deficits in Alpk1 mutant mice with the inserted piggyBac transposon. *BMC Neurosci,* 12**,** 1.

CHEN, Q., SUN, L. & CHEN, Z. J. 2016. Regulation and function of the cGAS-STING pathway of cytosolic DNA sensing. *Nat Immunol,* 17**,** 1142-9.

CHEN, X., LIU, S., GORAYA, M. U., MAAROUF, M., HUANG, S. & CHEN, J. L. 2018. Host Immune Response to Influenza A Virus Infection. *Front Immunol,* 9**,** 320.

CHEN, Y. L., CHEN, T. T., PAI, L. M., WESOLY, J., BLUYSSEN, H. A. & LEE, C. K. 2013. A type I IFN-Flt3 ligand axis augments plasmacytoid dendritic cell development from common lymphoid progenitors. *J Exp Med,* 210**,** 2515-22.

CHIBA, T., MATSUO, H., SAKIYAMA, M., NAKAYAMA, A., SHIMIZU, S., WAKAI, K., SUMA, S., NAKASHIMA, H., SAKURAI, Y., SHIMIZU, T., ICHIDA, K. & SHINOMIYA, N. 2015. Common variant of ALPK1 is not associated with gout: a replication study. *Hum Cell,* 28**,** 1-4.

CIANCANELLI, M. J., ABEL, L., ZHANG, S. Y. & CASANOVA, J. L. 2016. Host genetics of severe influenza: from mouse Mx1 to human IRF7. *Curr Opin Immunol,* 38**,** 109-20.

CIANCANELLI, M. J., HUANG, S. X., LUTHRA, P., GARNER, H., ITAN, Y., VOLPI, S., LAFAILLE, F. G., TROUILLET, C., SCHMOLKE, M., ALBRECHT, R. A., ISRAELSSON, E., LIM, H. K., CASADIO, M., HERMESH, T., LORENZO, L., LEUNG, L. W., PEDERGNANA, V., BOISSON, B., OKADA, S., PICARD, C., RINGUIER, B., TROUSSIER, F., CHAUSSABEL, D., ABEL, L., PELLIER, I., NOTARANGELO, L. D., GARCIA-SASTRE, A., BASLER, C. F., GEISSMANN, F., ZHANG, S. Y., SNOECK, H. W. & CASANOVA, J. L. 2015. Infectious disease.

Life-threatening influenza and impaired interferon amplification in human IRF7 deficiency. *Science,* 348**,** 448-53.

CLINE, T. D., KARLSSON, E. A., SEUFZER, B. J. & SCHULTZ-CHERRY, S. 2013. The hemagglutinin protein of highly pathogenic H5N1 influenza viruses overcomes an early block in the replication cycle to promote productive replication in macrophages. *J Virol,* 87**,** 1411-9.

COATES, B. M., STARICHA, K. L., KOCH, C. M., CHENG, Y., SHUMAKER, D. K., BUDINGER, G. R. S., PERLMAN, H., MISHARIN, A. V. & RIDGE, K. M. 2018. Inflammatory Monocytes Drive Influenza A Virus-Mediated Lung Injury in Juvenile Mice. *J Immunol,* 200**,** 2391-2404.

COCCIA, E. M., SEVERA, M., GIACOMINI, E., MONNERON, D., REMOLI, M. E., JULKUNEN, I., CELLA, M., LANDE, R. & UZE, G. 2004. Viral infection and Toll-like receptor agonists induce a differential expression of type I and lambda interferons in human plasmacytoid and monocyte-derived dendritic cells. *Eur J Immunol,* 34**,** 796-805.

COLLABORATIVE CROSS, C. 2012. The genome architecture of the Collaborative Cross mouse genetic reference population. *Genetics,* 190**,** 389-401.

COLLINS, S. E., NOYCE, R. S. & MOSSMAN, K. L. 2004. Innate cellular response to virus particle entry requires IRF3 but not virus replication. *J Virol,* 78**,** 1706-17.

CROTTA, S., DAVIDSON, S., MAHLAKOIV, T., DESMET, C. J., BUCKWALTER, M. R., ALBERT, M. L., STAEHELI, P. & WACK, A. 2013. Type I and type III interferons drive redundant amplification loops to induce a transcriptional signature in influenza-infected airway epithelia. *PLoS Pathog,* 9**,** e1003773.

DALEY, J. M., THOMAY, A. A., CONNOLLY, M. D., REICHNER, J. S. & ALBINA, J. E. 2008. Use of Ly6G-specific monoclonal antibody to deplete neutrophils in mice. *Journal of Leukocyte Biology,* 83**,** 64-70.

DAVIDSON, S., CROTTA, S., MCCABE, T. M. & WACK, A. 2014. Pathogenic potential of interferon alphabeta in acute influenza infection. *Nat Commun,* 5**,** 3864.

DAVIDSON, S., MAINI, M. K. & WACK, A. 2015. Disease-promoting effects of type I interferons in viral, bacterial, and coinfections. *J Interferon Cytokine Res,* 35**,** 252-64.

DAVIDSON, S., MCCABE, T. M., CROTTA, S., GAD, H. H., HESSEL, E. M., BEINKE, S., HARTMANN, R. & WACK, A. 2016. IFNlambda is a potent anti-influenza therapeutic without the inflammatory side effects of IFNalpha treatment. *EMBO Mol Med,* 8**,** 1099-112.

DE WEERD, N. A., VIVIAN, J. P., NGUYEN, T. K., MANGAN, N. E., GOULD, J. A., BRANIFF, S. J., ZAKER-TABRIZI, L., FUNG, K. Y., FORSTER, S. C., BEDDOE, T., REID, H. H., ROSSJOHN, J. & HERTZOG, P. J. 2013. Structural basis of a unique interferon-beta signaling axis mediated via the receptor IFNAR1. *Nat Immunol,* 14**,** 901-7.

DEL RIO, M. L., RODRIGUEZ-BARBOSA, J. I., KREMMER, E. & FORSTER, R. 2007. CD103- and CD103+ bronchial lymph node dendritic cells are specialized in presenting and cross-presenting innocuous antigen to CD4+ and CD8+ T cells. *J Immunol,* 178**,** 6861-6.

DENNEY, L. & HO, L. P. 2018. The role of respiratory epithelium in host defence against influenza virus infection. *Biomed J,* 41**,** 218-233.

DI PIETRO, A., KAJASTE-RUDNITSKI, A., OTEIZA, A., NICORA, L., TOWERS, G. J., MECHTI, N. & VICENZI, E. 2013. TRIM22 inhibits influenza A virus infection by targeting the viral nucleoprotein for degradation. *J Virol,* 87**,** 4523-33.

DIEBOLD, S. S., KAISHO, T., HEMMI, H., AKIRA, S. & REIS E SOUSA, C. 2004. Innate antiviral responses by means of TLR7-mediated recognition of single-stranded RNA. *Science,* 303**,** 1529-31.

DIEBOLD, S. S., MASSACRIER, C., AKIRA, S., PATUREL, C., MOREL, Y. & REIS E SOUSA, C. 2006. Nucleic acid agonists for Toll-like receptor 7 are defined by the presence of uridine ribonucleotides. *Eur J Immunol,* 36**,** 3256-67.

DIENZ, O., RUD, J. G., EATON, S. M., LANTHIER, P. A., BURG, E., DREW, A., BUNN, J., SURATT, B. T., HAYNES, L. & RINCON, M. 2012. Essential role of IL-6 in protection against H1N1 influenza virus by promoting neutrophil survival in the lung. *Mucosal Immunol,* 5**,** 258-66.

DIVANGAHI, M., KING, I. L. & PERNET, E. 2015. Alveolar macrophages and type I IFN in airway homeostasis and immunity. *Trends Immunol,* 36**,** 307-14.

DOYLE, S. E., VAIDYA, S. A., O'CONNELL, R., DADGOSTAR, H., DEMPSEY, P. W., WU, T.-T., RAO, G., SUN, R., HABERLAND, M. E., MODLIN, R. L. & CHENG, G. 2002. IRF3 Mediates a TLR3/TLR4-Specific Antiviral Gene Program. *Immunity,* 17**,** 251-263.

DREUX, M., GARAIGORTA, U., BOYD, B., DECEMBRE, E., CHUNG, J., WHITTEN-BAUER, C., WIELAND, S. & CHISARI, F. V. 2012. Short-range exosomal transfer of viral RNA from infected cells to plasmacytoid dendritic cells triggers innate immunity. *Cell Host Microbe,* 12**,** 558-70.

EDINGER, T. O., POHL, M. O. & STERTZ, S. 2014. Entry of influenza A virus: host factors and antiviral targets. *J Gen Virol,* 95**,** 263-77.

ELLIS, G. T., DAVIDSON, S., CROTTA, S., BRANZK, N., PAPAYANNOPOULOS, V. & WACK, A. 2015. TRAIL+ monocytes and monocyte-related cells cause lung damage and thereby increase susceptibility to influenza-Streptococcus pneumoniae coinfection. *EMBO Rep,* 16**,** 1203-18.

ENGEL, A. & BARTON, G. M. 2010. Compartment-specific control of signaling from a DNA-sensing immune receptor. *Sci Signal,* 3**,** pe45.

EVERITT, A. R., CLARE, S., PERTEL, T., JOHN, S. P., WASH, R. S., SMITH, S. E., CHIN, C. R., FEELEY, E. M., SIMS, J. S., ADAMS, D. J., WISE, H. M., KANE, L., GOULDING, D., DIGARD, P., ANTTILA, V., BAILLIE, J. K., WALSH, T. S., HUME, D. A., PALOTIE, A., XUE, Y., COLONNA, V., TYLER-SMITH, C., DUNNING, J., GORDON, S. B., GEN, I. I., INVESTIGATORS, M., SMYTH, R. L., OPENSHAW, P. J., DOUGAN, G., BRASS, A. L. & KELLAM, P. 2012. IFITM3 restricts the morbidity and mortality associated with influenza. *Nature,* 484**,** 519-23.

FABREGAT, A., JUPE, S., MATTHEWS, L., SIDIROPOULOS, K., GILLESPIE, M., GARAPATI, P., HAW, R., JASSAL, B., KORNINGER, F., MAY, B., MILACIC, M., ROCA, C. D., ROTHFELS, K., SEVILLA, C., SHAMOVSKY, V., SHORSER, S., VARUSAI, T., VITERI, G., WEISER, J., WU, G., STEIN, L., HERMJAKOB, H. & D'EUSTACHIO, P. 2018. The Reactome Pathway Knowledgebase. *Nucleic Acids Res,* 46**,** D649-D655.

FAIRFAX, B. P., HUMBURG, P., MAKINO, S., NARANBHAI, V., WONG, D., LAU, E., JOSTINS, L., PLANT, K., ANDREWS, R., MCGEE, C. & KNIGHT, J. C. 2014. Innate immune activity conditions the effect of regulatory variants upon monocyte gene expression. *Science,* 343**,** 1246949.

FANG, R., WANG, C., JIANG, Q., LV, M., GAO, P., YU, X., MU, P., ZHANG, R., BI, S., FENG, J. M. & JIANG, Z. 2017. NEMO-IKKbeta Are Essential for IRF3 and NF-kappaB Activation in the cGAS-STING Pathway. *J Immunol,* 199**,** 3222-3233.

FERRIS, M. T., AYLOR, D. L., BOTTOMLY, D., WHITMORE, A. C., AICHER, L. D., BELL, T. A., BRADEL-TRETHEWAY, B., BRYAN, J. T., BUUS, R. J., GRALINSKI, L. E., HAAGMANS, B. L., MCMILLAN, L., MILLER, D. R., ROSENZWEIG, E., VALDAR, W., WANG, J., CHURCHILL, G. A., THREADGILL, D. W., MCWEENEY, S. K., KATZE, M. G., PARDO-MANUEL DE VILLENA, F., BARIC, R. S. & HEISE, M. T. 2013. Modeling host genetic regulation of influenza pathogenesis in the collaborative cross. *PLoS Pathog,* 9**,** e1003196.

FISCHER, H. G., FROSCH, S., RESKE, K. & RESKE-KUNZ, A. B. 1988. Granulocyte-macrophage colony-stimulating factor activates macrophages derived from bone marrow cultures to synthesis of MHC class II molecules and to augmented antigen presentation function. *J Immunol,* 141**,** 3882-8.

FLEETWOOD, A. J., LAWRENCE, T., HAMILTON, J. A. & COOK, A. D. 2007. Granulocyte-macrophage colony-stimulating factor (CSF) and macrophage CSF-dependent macrophage phenotypes display differences in cytokine profiles and transcription factor activities: implications for CSF blockade in inflammation. *J Immunol,* 178**,** 5245-52.

FONTENEAU, J. F., GILLIET, M., LARSSON, M., DASILVA, I., MUNZ, C., LIU, Y. J. & BHARDWAJ, N. 2003. Activation of influenza virus-specific CD4+ and CD8+ T cells: a new role for plasmacytoid dendritic cells in adaptive immunity. *Blood,* 101**,** 3520-6.

FOUCHIER, R. A., MUNSTER, V., WALLENSTEN, A., BESTEBROER, T. M., HERFST, S., SMITH, D., RIMMELZWAAN, G. F., OLSEN, B. & OSTERHAUS, A. D. 2005. Characterization of a novel influenza A virus hemagglutinin subtype (H16) obtained from black-headed gulls. *J Virol,* 79**,** 2814-22.

FUKUYAMA, S. & KAWAOKA, Y. 2011. The pathogenesis of influenza virus infections: the contributions of virus and host factors. *Curr Opin Immunol,* 23**,** 481-6.

GAO, D., WU, J., WU, Y. T., DU, F., AROH, C., YAN, N., SUN, L. & CHEN, Z. J. 2013. Cyclic GMP-AMP synthase is an innate immune sensor of HIV and other retroviruses. *Science,* 341**,** 903-6.

GARCIA-RAMIREZ, R. A., RAMIREZ-VENEGAS, A., QUINTANA-CARRILLO, R., CAMARENA, A. E., FALFAN-VALENCIA, R. & MEJIA-ARANGURE, J. M. 2015. TNF, IL6, and IL1B Polymorphisms Are Associated with Severe Influenza A (H1N1) Virus Infection in the Mexican Population. *PLoS One,* 10**,** e0144832.

GARCIA-SASTRE, A. 2011. Induction and evasion of type I interferon responses by influenza viruses. *Virus Res,* 162**,** 12-8.

GARCIA-SASTRE, A., EGOROV, A., MATASSOV, D., BRANDT, S., LEVY, D. E., DURBIN, J. E., PALESE, P. & MUSTER, T. 1998. Influenza A virus lacking the NS1 gene replicates in interferon-deficient systems. *Virology,* 252**,** 324-30.

GARCIA-WEBER, D., DANGEARD, A. S., CORNIL, J., THAI, L., RYTTER, H., ZAMYATINA, A., MULARD, L. A. & ARRIEUMERLOU, C. 2018. ADP-heptose is a newly identified pathogen-associated molecular pattern of Shigella flexneri. *EMBO Rep,* 19.

GAUTIER, G., HUMBERT, M., DEAUVIEAU, F., SCUILLER, M., HISCOTT, J., BATES, E. E., TRINCHIERI, G., CAUX, C. & GARRONE, P. 2005. A type I interferon autocrine-paracrine loop is involved in Toll-like receptor-induced interleukin-12p70 secretion by dendritic cells. *J Exp Med,* 201**,** 1435-46.

GEISSMANN, F., MANZ, M. G., JUNG, S., SIEWEKE, M. H., MERAD, M. & LEY, K. 2010. Development of monocytes, macrophages, and dendritic cells. *Science,* 327**,** 656-61.

GENEVET, A., WEHR, M. C., BRAIN, R., THOMPSON, B. J. & TAPON, N. 2010. Kibra is a regulator of the Salvador/Warts/Hippo signaling network. *Dev Cell,* 18**,** 300-8.

GIBBERT, K., SCHLAAK, J. F., YANG, D. & DITTMER, U. 2013. IFN-alpha subtypes: distinct biological activities in anti-viral therapy. *Br J Pharmacol,* 168**,** 1048-58.

GILLIET, M., CAO, W. & LIU, Y. J. 2008. Plasmacytoid dendritic cells: sensing nucleic acids in viral infection and autoimmune diseases. *Nat Rev Immunol,* 8**,** 594-606.

GORAYA, M. U., WANG, S., MUNIR, M. & CHEN, J. L. 2015. Induction of innate immunity and its perturbation by influenza viruses. *Protein Cell,* 6**,** 712-21.

GORITZKA, M., DURANT, L. R., PEREIRA, C., SALEK-ARDAKANI, S., OPENSHAW, P. J. & JOHANSSON, C. 2014. Alpha/beta interferon receptor signaling amplifies

early proinflammatory cytokine production in the lung during respiratory syncytial virus infection. *J Virol,* 88**,** 6128-36.

GORITZKA, M., MAKRIS, S., KAUSAR, F., DURANT, L. R., PEREIRA, C., KUMAGAI, Y., CULLEY, F. J., MACK, M., AKIRA, S. & JOHANSSON, C. 2015. Alveolar macrophage-derived type I interferons orchestrate innate immunity to RSV through recruitment of antiviral monocytes. *J Exp Med,* 212**,** 699-714.

GOUBAU, D., DEDDOUCHE, S. & REIS E SOUSA, C. 2013. Cytosolic sensing of viruses. *Immunity,* 38**,** 855-69.

GOUBAU, D., SCHLEE, M., DEDDOUCHE, S., PRUIJSSERS, A. J., ZILLINGER, T., GOLDECK, M., SCHUBERTH, C., VAN DER VEEN, A. G., FUJIMURA, T., REHWINKEL, J., ISKARPATYOTI, J. A., BARCHET, W., LUDWIG, J., DERMODY, T. S., HARTMANN, G. & REIS E SOUSA, C. 2014. Antiviral immunity via RIG-I-mediated recognition of RNA bearing 5'-diphosphates. *Nature,* 514**,** 372-375.

GRANT, E. J., QUINONES-PARRA, S. M., CLEMENS, E. B. & KEDZIERSKA, K. 2016. Human influenza viruses and CD8(+) T cell responses. *Curr Opin Virol,* 16**,** 132-142.

GUILLIAMS, M., LAMBRECHT, B. N. & HAMMAD, H. 2013. Division of labor between lung dendritic cells and macrophages in the defense against pulmonary infections. *Mucosal Immunol,* 6**,** 464-73.

HASHIMOTO, Y., MOKI, T., TAKIZAWA, T., SHIRATSUCHI, A. & NAKANISHI, Y. 2007. Evidence for phagocytosis of influenza virus-infected, apoptotic cells by neutrophils and macrophages in mice. *J Immunol,* 178**,** 2448-57.

HEINE, M., CRAMM-BEHRENS, C. I., ANSARI, A., CHU, H. P., RYAZANOV, A. G., NAIM, H. Y. & JACOB, R. 2005. Alpha-kinase 1, a new component in apical protein transport. *J Biol Chem,* 280**,** 25637-43.

HELFT, J., BOTTCHER, J., CHAKRAVARTY, P., ZELENAY, S., HUOTARI, J., SCHRAML, B. U., GOUBAU, D. & REIS E SOUSA, C. 2015. GM-CSF Mouse Bone Marrow Cultures Comprise a Heterogeneous Population of CD11c(+)MHCII(+) Macrophages and Dendritic Cells. *Immunity,* 42**,** 1197-211.

HEROLD, S., STEINMUELLER, M., VON WULFFEN, W., CAKAROVA, L., PINTO, R., PLESCHKA, S., MACK, M., KUZIEL, W. A., CORAZZA, N., BRUNNER, T., SEEGER, W. & LOHMEYER, J. 2008. Lung epithelial apoptosis in influenza virus pneumonia: the role of macrophage-expressed TNF-related apoptosis-inducing ligand. *J Exp Med,* 205**,** 3065-77.

HERVAS-STUBBS, S., PEREZ-GRACIA, J. L., ROUZAUT, A., SANMAMED, M. F., LE BON, A. & MELERO, I. 2011. Direct effects of type I interferons on cells of the immune system. *Clin Cancer Res,* 17**,** 2619-27.

HETTINGER, J., RICHARDS, D. M., HANSSON, J., BARRA, M. M., JOSCHKO, A. C., KRIJGSVELD, J. & FEUERER, M. 2013. Origin of monocytes and macrophages in a committed progenitor. *Nat Immunol,* 14**,** 821-30.

HOCHREIN, H., O'KEEFFE, M. & WAGNER, H. 2002. Human and mouse plasmacytoid dendritic cells. *Human Immunology,* 63**,** 1103-1110.

HOEVE, M. A., NASH, A. A., JACKSON, D., RANDALL, R. E. & DRANSFIELD, I. 2012. Influenza virus A infection of human monocyte and macrophage subpopulations reveals increased susceptibility associated with cell differentiation. *PLoS One,* 7**,** e29443.

HOFFMANN, A., LEVCHENKO, A., SCOTT, M. L. & BALTIMORE, D. 2002. The IkappaB-NF-kappaB signaling module: temporal control and selective gene activation. *Science,* 298**,** 1241-5.

HOLOHAN, B., KIM, W., LAI, T. P., HOSHIYAMA, H., ZHANG, N., ALAZAMI, A. M., WRIGHT, W. E., MEYN, M. S., ALKURAYA, F. S. & SHAY, J. W. 2016. Impaired

telomere maintenance in Alazami syndrome patients with LARP7 deficiency. *BMC Genomics,* 17**,** 749.

HONDA, K., OHBA, Y., YANAI, H., NEGISHI, H., MIZUTANI, T., TAKAOKA, A., TAYA, C. & TANIGUCHI, T. 2005. Spatiotemporal regulation of MyD88-IRF-7 signalling for robust type-I interferon induction. *Nature,* 434**,** 1035-40.

HONDA, K., TAKAOKA, A. & TANIGUCHI, T. 2006. Type I interferon [corrected] gene induction by the interferon regulatory factor family of transcription factors. *Immunity,* 25**,** 349-60.

HORBY, P., NGUYEN, N. Y., DUNSTAN, S. J. & BAILLIE, J. K. 2013. An updated systematic review of the role of host genetics in susceptibility to influenza. *Influenza Other Respir Viruses,* 7 Suppl 2**,** 37-41.

HORNUNG, V., ELLEGAST, J., KIM, S., BRZOZKA, K., JUNG, A., KATO, H., POECK, H., AKIRA, S., CONZELMANN, K. K., SCHLEE, M., ENDRES, S. & HARTMANN, G. 2006. 5'-Triphosphate RNA is the ligand for RIG-I. *Science,* 314**,** 994-7.

HORNUNG, V., GUENTHNER-BILLER, M., BOURQUIN, C., ABLASSER, A., SCHLEE, M., UEMATSU, S., NORONHA, A., MANOHARAN, M., AKIRA, S., DE FOUGEROLLES, A., ENDRES, S. & HARTMANN, G. 2005. Sequence-specific potent induction of IFN-alpha by short interfering RNA in plasmacytoid dendritic cells through TLR7. *Nat Med,* 11**,** 263-70.

HOSHINO, K., SUGIYAMA, T., MATSUMOTO, M., TANAKA, T., SAITO, M., HEMMI, H., OHARA, O., AKIRA, S. & KAISHO, T. 2006. IkappaB kinase-alpha is critical for interferon-alpha production induced by Toll-like receptors 7 and 9. *Nature,* 440**,** 949-53.

HU, X., YANG, C., WANG, P. G. & ZHANG, G. L. 2019. ADP-heptose: A new innate immune modulator. *Carbohydr Res,* 473**,** 123-128.

HU, Y. H., ZHANG, Y., JIANG, L. Q., WANG, S., LEI, C. Q., SUN, M. S., SHU, H. B. & LIU, Y. 2015. WDFY1 mediates TLR3/4 signaling by recruiting TRIF. *EMBO Rep,* 16**,** 447-55.

HUGHES, R., TOWERS, G. & NOURSADEGHI, M. 2012. Innate immune interferon responses to human immunodeficiency virus-1 infection. *Rev Med Virol,* 22**,** 257-66.

HUNTER, K. W. & CRAWFORD, N. P. S. 2008. The Future of Mouse QTL Mapping to Diagnose Disease in Mice in the Age of Whole-Genome Association Studies. *Annual Review of Genetics,* 42**,** 131-141.

HUSSAIN, M., GALVIN, H. D., HAW, T. Y., NUTSFORD, A. N. & HUSAIN, M. 2017. Drug resistance in influenza A virus: the epidemiology and management. *Infect Drug Resist,* 10**,** 121-134.

IMAI, M., WATANABE, T., KISO, M., NAKAJIMA, N., YAMAYOSHI, S., IWATSUKI-HORIMOTO, K., HATTA, M., YAMADA, S., ITO, M., SAKAI-TAGAWA, Y., SHIRAKURA, M., TAKASHITA, E., FUJISAKI, S., MCBRIDE, R., THOMPSON, A. J., TAKAHASHI, K., MAEMURA, T., MITAKE, H., CHIBA, S., ZHONG, G., FAN, S., OISHI, K., YASUHARA, A., TAKADA, K., NAKAO, T., FUKUYAMA, S., YAMASHITA, M., LOPES, T. J. S., NEUMANN, G., ODAGIRI, T., WATANABE, S., SHU, Y., PAULSON, J. C., HASEGAWA, H. & KAWAOKA, Y. 2017. A Highly Pathogenic Avian H7N9 Influenza Virus Isolated from A Human Is Lethal in Some Ferrets Infected via Respiratory Droplets. *Cell Host Microbe,* 22**,** 615-626 e8.

INABA, K., INABA, M., ROMANI, N., AYA, H., DEGUCHI, M., IKEHARA, S., MURAMATSU, S. & STEINMAN, R. M. 1992. Generation of large numbers of dendritic cells from mouse bone marrow cultures supplemented with granulocyte/macrophage colony-stimulating factor. *J Exp Med,* 176**,** 1693-702.

ISAACS, A., LINDENMANN, J. 1957a. Virus interference. I. The interferon. *Proceedings of the Royal Society of London. Series B - Biological Sciences,* 147**,** 258-267.

ISAACS, A., LINDENMANN, J., VALENTINE, R.C. 1957b. Virus interference. II. Some properties of interferon. *Proceedings of the Royal Society of London. Series B - Biological Sciences,* 147**,** 268-273.

ISHIKAWA, A. 2017. A Strategy for Identifying Quantitative Trait Genes Using Gene Expression Analysis and Causal Analysis. *Genes (Basel),* 8.

ISHIKAWA, H. & BARBER, G. N. 2008. STING is an endoplasmic reticulum adaptor that facilitates innate immune signalling. *Nature,* 455**,** 674-8.

IWASAKI, A. & PILLAI, P. S. 2014. Innate immunity to influenza virus infection. *Nat Rev Immunol,* 14**,** 315-28.

JAKS, E., GAVUTIS, M., UZE, G., MARTAL, J. & PIEHLER, J. 2007. Differential receptor subunit affinities of type I interferons govern differential signal activation. *J Mol Biol,* 366**,** 525-39.

JAMES, C. M., ABDAD, M. Y., MANSFIELD, J. P., JACOBSEN, H. K., VIND, A. R., STUMBLES, P. A. & BARTLETT, E. J. 2007. Differential activities of alpha/beta IFN subtypes against influenza virus in vivo and enhancement of specific immune responses in DNA vaccinated mice expressing haemagglutinin and nucleoprotein. *Vaccine,* 25**,** 1856-67.

JANEWAY, C. A., JR. 1989. Approaching the asymptote? Evolution and revolution in immunology. *Cold Spring Harb Symp Quant Biol,* 54 Pt 1**,** 1-13.

JOHNSON, N. P. A. S. & MUELLER, J. 2002. Updating the Accounts: Global Mortality of the 1918-1920 "Spanish" Influenza Pandemic. *Bulletin of the History of Medicine,* 76**,** 105-115.

KAGAN, J. C., SU, T., HORNG, T., CHOW, A., AKIRA, S. & MEDZHITOV, R. 2008. TRAM couples endocytosis of Toll-like receptor 4 to the induction of interferon-beta. *Nat Immunol,* 9**,** 361-8.

KANAREK, N. & BEN-NERIAH, Y. 2012. Regulation of NF-kappaB by ubiquitination and degradation of the IkappaBs. *Immunol Rev,* 246**,** 77-94.

KARSUNKY, H., MERAD, M., COZZIO, A., WEISSMAN, I. L. & MANZ, M. G. 2003. Flt3 ligand regulates dendritic cell development from Flt3+ lymphoid and myeloid-committed progenitors to Flt3+ dendritic cells in vivo. *J Exp Med,* 198**,** 305-13.

KAUR, S. & PLATANIAS, L. C. 2013. IFN-beta-specific signaling via a unique IFNAR1 interaction. *Nat Immunol,* 14**,** 884-5.

KAWAI, T. & AKIRA, S. 2007. Signaling to NF-kappaB by Toll-like receptors. *Trends Mol Med,* 13**,** 460-9.

KAWAI, T. & AKIRA, S. 2011. Toll-like receptors and their crosstalk with other innate receptors in infection and immunity. *Immunity,* 34**,** 637-50.

KAWAI, T., SATO, S., ISHII, K. J., COBAN, C., HEMMI, H., YAMAMOTO, M., TERAI, K., MATSUDA, M., INOUE, J., UEMATSU, S., TAKEUCHI, O. & AKIRA, S. 2004. Interferon-alpha induction through Toll-like receptors involves a direct interaction of IRF7 with MyD88 and TRAF6. *Nat Immunol,* 5**,** 1061-8.

KAWAI, T., TAKEUCHI, O., FUJITA, T., INOUE, J. I., MUHLRADT, P. F., SATO, S., HOSHINO, K. & AKIRA, S. 2001. Lipopolysaccharide Stimulates the MyD88-Independent Pathway and Results in Activation of IFN-Regulatory Factor 3 and the Expression of a Subset of Lipopolysaccharide-Inducible Genes. *The Journal of Immunology,* 167**,** 5887-5894.

KELL, A. M. & GALE, M., JR. 2015. RIG-I in RNA virus recognition. *Virology,* 479-480**,** 110-21.

KERKMANN, M., ROTHENFUSSER, S., HORNUNG, V., TOWAROWSKI, A., WAGNER, M., SARRIS, A., GIESE, T., ENDRES, S. & HARTMANN, G. 2003. Activation with CpG-A and CpG-B oligonucleotides reveals two distinct regulatory pathways of type I IFN synthesis in human plasmacytoid dendritic cells. *J Immunol,* 170**,** 4465-74.

KILLIP, M. J., SMITH, M., JACKSON, D. & RANDALL, R. E. 2014. Activation of the interferon induction cascade by influenza a viruses requires viral RNA synthesis and nuclear export. *J Virol,* 88**,** 3942-52.

KIM, T. S. & BRACIALE, T. J. 2009. Respiratory dendritic cell subsets differ in their capacity to support the induction of virus-specific cytotoxic CD8+ T cell responses. *PLoS One,* 4**,** e4204.

KO, A. M., TU, H. P., LIU, T. T., CHANG, J. G., YUO, C. Y., CHIANG, S. L., CHANG, S. J., LIU, Y. F., KO, A. M., LEE, C. H., LEE, C. P., CHANG, C. M., TSAI, S. F. & KO, Y. C. 2013. ALPK1 genetic regulation and risk in relation to gout. *Int J Epidemiol,* 42**,** 466-74.

KONDO, M., WAGERS, A. J., MANZ, M. G., PROHASKA, S. S., SCHERER, D. C., BEILHACK, G. F., SHIZURU, J. A. & WEISSMAN, I. L. 2003. Biology of hematopoietic stem cells and progenitors: implications for clinical application. *Annu Rev Immunol,* 21**,** 759-806.

KONDO, M., WEISSMAN, I. L. & AKASHI, K. 1997. Identification of Clonogenic Common Lymphoid Progenitors in Mouse Bone Marrow. *Cell,* 91**,** 661-672.

KOTENKO, S. V., GALLAGHER, G., BAURIN, V. V., LEWIS-ANTES, A., SHEN, M., SHAH, N. K., LANGER, J. A., SHEIKH, F., DICKENSHEETS, H. & DONNELLY, R. P. 2003. IFN-lambdas mediate antiviral protection through a distinct class II cytokine receptor complex. *Nat Immunol,* 4**,** 69-77.

KOTEY, E., LUKOSAITYTE, D., QUAYE, O., AMPOFO, W., AWANDARE, G. & IQBAL, M. 2019. Current and Novel Approaches in Influenza Management. *Vaccines (Basel),* 7.

KREIJTZ JH, F. R., RIMMELZWAAN GF 2011. Immune responses to influenza virus infection. *Virus Research,* 162**,** 19-30.

KUMAGAI, Y., TAKEUCHI, O., KATO, H., KUMAR, H., MATSUI, K., MORII, E., AOZASA, K., KAWAI, T. & AKIRA, S. 2007. Alveolar macrophages are the primary interferon-alpha producer in pulmonary infection with RNA viruses. *Immunity,* 27**,** 240-52.

KUO, T. M., YEH, K. T., HSU, H. T., CHIANG, S. L., CHANG, J. G., HUANG, C. M., TU, H. P., LIU, C. S. & KO, Y. C. 2015. ALPK1 affects testosterone mediated regulation of proinflammatory cytokines production. *J Steroid Biochem Mol Biol,* 154**,** 150-8.

LAM, J. H. & BAUMGARTH, N. 2019. The Multifaceted B Cell Response to Influenza Virus. *J Immunol,* 202**,** 351-359.

LANDOLT, G. A. & OLSEN, C. W. 2007. Up to new tricks - a review of cross-species transmission of influenza A viruses. *Anim Health Res Rev,* 8**,** 1-21.

LAUVAU, G., CHORRO, L., SPAULDING, E. & SOUDJA, S. M. 2014. Inflammatory monocyte effector mechanisms. *Cell Immunol,* 291**,** 32-40.

LAVOIE, T. B., KALIE, E., CRISAFULLI-CABATU, S., ABRAMOVICH, R., DIGIOIA, G., MOOLCHAN, K., PESTKA, S. & SCHREIBER, G. 2011. Binding and activity of all human alpha interferon subtypes. *Cytokine,* 56**,** 282-9.

LE GOFFIC, R., BALLOY, V., LAGRANDERIE, M., ALEXOPOULOU, L., ESCRIOU, N., FLAVELL, R., CHIGNARD, M. & SI-TAHAR, M. 2006. Detrimental contribution of the Toll-like receptor (TLR)3 to influenza A virus-induced acute pneumonia. *PLoS Pathog,* 2**,** e53.

LE GOFFIC, R., POTHLICHET, J., VITOUR, D., FUJITA, T., MEURS, E., CHIGNARD, M. & SI-TAHAR, M. 2007. Cutting Edge: Influenza A Virus Activates TLR3-Dependent Inflammatory and RIG-I-Dependent Antiviral Responses in Human Lung Epithelial Cells. *The Journal of Immunology,* 178**,** 3368-3372.

LEE, C. P., CHIANG, S. L., KO, A. M., LIU, Y. F., MA, C., LU, C. Y., HUANG, C. M., CHANG, J. G., KUO, T. M., CHEN, C. L., TSAI, E. M. & KO, Y. C. 2016. ALPK1

phosphorylates myosin IIA modulating TNF-alpha trafficking in gout flares. *Sci Rep,* 6**,** 25740.

LEE, J., CHUANG, T. H., REDECKE, V., SHE, L., PITHA, P. M., CARSON, D. A., RAZ, E. & COTTAM, H. B. 2003. Molecular basis for the immunostimulatory activity of guanine nucleoside analogs: activation of Toll-like receptor 7. *Proc Natl Acad Sci U S A,* 100**,** 6646-51.

LEE, M. N., YE, C., VILLANI, A. C., RAJ, T., LI, W., EISENHAURE, T. M., IMBOYWA, S. H., CHIPENDO, P. I., RAN, F. A., SLOWIKOWSKI, K., WARD, L. D., RADDASSI, K., MCCABE, C., LEE, M. H., FROHLICH, I. Y., HAFLER, D. A., KELLIS, M., RAYCHAUDHURI, S., ZHANG, F., STRANGER, B. E., BENOIST, C. O., DE JAGER, P. L., REGEV, A. & HACOHEN, N. 2014. Common genetic variants modulate pathogen-sensing responses in human dendritic cells. *Science,* 343**,** 1246980.

LESER, G. P. & LAMB, R. A. 2005. Influenza virus assembly and budding in raft-derived microdomains: a quantitative analysis of the surface distribution of HA, NA and M2 proteins. *Virology,* 342**,** 215-27.

LI, H., BRADLEY, K. C., LONG, J. S., FRISE, R., ASHCROFT, J. W., HARTGROVES, L. C., SHELTON, H., MAKRIS, S., JOHANSSON, C., CAO, B. & BARCLAY, W. S. 2018. Internal genes of a highly pathogenic H5N1 influenza virus determine high viral replication in myeloid cells and severe outcome of infection in mice. *PLoS Pathog,* 14**,** e1006821.

LI, Q. & VERMA, I. M. 2002. NF-kappaB regulation in the immune system. *Nat Rev Immunol,* 2**,** 725-34.

LIN, K. L., SUZUKI, Y., NAKANO, H., RAMSBURG, E. & GUNN, M. D. 2008. CCR2+ monocyte-derived dendritic cells and exudate macrophages produce influenza-induced pulmonary immune pathology and mortality. *J Immunol,* 180**,** 2562-72.

LIN, S. J., LO, M., KUO, R. L., SHIH, S. R., OJCIUS, D. M., LU, J., LEE, C. K., CHEN, H. C., LIN, M. Y., LEU, C. M., LIN, C. N. & TSAI, C. H. 2014. The pathological effects of CCR2+ inflammatory monocytes are amplified by an IFNAR1-triggered chemokine feedback loop in highly pathogenic influenza infection. *J Biomed Sci,* 21**,** 99.

LIU, G., PARK, H. S., PYO, H. M., LIU, Q. & ZHOU, Y. 2015. Influenza A Virus Panhandle Structure Is Directly Involved in RIG-I Activation and Interferon Induction. *J Virol,* 89**,** 6067-79.

LIU, Q., ZHOU, Y. H. & YANG, Z. Q. 2016. The cytokine storm of severe influenza and development of immunomodulatory therapy. *Cell Mol Immunol,* 13**,** 3-10.

LONDRIGAN, S. L., SHORT, K. R., MA, J., GILLESPIE, L., ROCKMAN, S. P., BROOKS, A. G. & READING, P. C. 2015. Infection of Mouse Macrophages by Seasonal Influenza Viruses Can Be Restricted at the Level of Virus Entry and at a Late Stage in the Virus Life Cycle. *J Virol,* 89**,** 12319-29.

LONG, J. S., MISTRY, B., HASLAM, S. M. & BARCLAY, W. S. 2019. Host and viral determinants of influenza A virus species specificity. *Nat Rev Microbiol,* 17**,** 67-81.

LOVE, M. I., HUBER, W. & ANDERS, S. 2014. Moderated estimation of fold change and dispersion for RNA-seq data with DESeq2. *Genome Biol,* 15**,** 550.

LU, T., JACKSON, M. W., WANG, B., YANG, M., CHANCE, M. R., MIYAGI, M., GUDKOV, A. V. & STARK, G. R. 2010. Regulation of NF-kappaB by NSD1/FBXL11-dependent reversible lysine methylation of p65. *Proc Natl Acad Sci U S A,* 107**,** 46-51.

LUI, G., MANCHES, O., ANGEL, J., MOLENS, J. P., CHAPEROT, L. & PLUMAS, J. 2009. Plasmacytoid dendritic cells capture and cross-present viral antigens from influenza-virus exposed cells. *PLoS One,* 4**,** e7111.

MAELFAIT, J., ROOSE, K., BOGAERT, P., SZE, M., SAELENS, X., PASPARAKIS, M., CARPENTIER, I., VAN LOO, G. & BEYAERT, R. 2012. A20 (Tnfaip3) deficiency in myeloid cells protects against influenza A virus infection. *PLoS Pathog,* 8**,** e1002570.

MAKRIS, S., PAULSEN, M. & JOHANSSON, C. 2017. Type I Interferons as Regulators of Lung Inflammation. *Front Immunol,* 8**,** 259.

MARASKOVSKY, E., BRASEL, K., TEEPE, M., ROUX, E. R., LYMAN, S. D., SHORTMAN, K. & MCKENNA, H. J. 1996. Dramatic increase in the numbers of functionally mature dendritic cells in Flt3 ligand-treated mice: multiple dendritic cell subpopulations identified. *J Exp Med,* 184**,** 1953-62.

MARIE, I., DURBIN, J. E. & LEVY, D. E. 1998. Differential viral induction of distinct interferon-alpha genes by positive feedback through interferon regulatory factor-7. *EMBO J,* 17**,** 6660-9.

MARTIN K., H. A. 1991. Transport of incoming influenza virus nucleocapsids into the nucleus. *Journal of Virology,* 65**,** 232-244.

MARVIN, S. A., RUSSIER, M., HUERTA, C. T., RUSSELL, C. J. & SCHULTZ-CHERRY, S. 2017. Influenza Virus Overcomes Cellular Blocks To Productively Replicate, Impacting Macrophage Function. *J Virol,* 91.

MATROSOVICH, M. N., MATROSOVICH, T. Y., GRAY, T., ROBERTS, N. A. & KLENK, H. D. 2004. Neuraminidase is important for the initiation of influenza virus infection in human airway epithelium. *J Virol,* 78**,** 12665-7.

MCKIMM-BRESCHKIN, J. L. 2013. Influenza neuraminidase inhibitors: antiviral action and mechanisms of resistance. *Influenza Other Respir Viruses,* 7 Suppl 1**,** 25-36.

MCNAB, F., MAYER-BARBER, K., SHER, A., WACK, A. & O'GARRA, A. 2015. Type I interferons in infectious disease. *Nat Rev Immunol,* 15**,** 87-103.

MEDINA, K. L., TANGEN, S. N., SEABURG, L. M., THAPA, P., GWIN, K. A. & SHAPIRO, V. S. 2013. Separation of plasmacytoid dendritic cells from B-cell-biased lymphoid progenitor (BLP) and Pre-pro B cells using PDCA-1. *PLoS One,* 8**,** e78408.

MEDZHITOV, R. 2001. Toll-like receptors and innate immunity. *Nat Rev Immunol,* 1**,** 135-45.

MERTINS, P., PRZYBYLSKI, D., YOSEF, N., QIAO, J., CLAUSER, K., RAYCHOWDHURY, R., EISENHAURE, T. M., MARITZEN, T., HAUCKE, V., SATOH, T., AKIRA, S., CARR, S. A., REGEV, A., HACOHEN, N. & CHEVRIER, N. 2017. An Integrative Framework Reveals Signaling-to-Transcription Events in Toll-like Receptor Signaling. *Cell Rep,* 19**,** 2853-2866.

MIDDELBEEK, J., CLARK, K., VENSELAAR, H., HUYNEN, M. A. & VAN LEEUWEN, F. N. 2010. The alpha-kinase family: an exceptional branch on the protein kinase tree. *Cell Mol Life Sci,* 67**,** 875-90.

MILIVOJEVIC, M., DANGEARD, A. S., KASPER, C. A., TSCHON, T., EMMENLAUER, M., PIQUE, C., SCHNUPF, P., GUIGNOT, J. & ARRIEUMERLOU, C. 2017. ALPK1 controls TIFA/TRAF6-dependent innate immunity against heptose-1,7-bisphosphate of gram-negative bacteria. *PLoS Pathog,* 13**,** e1006224.

MILLS, T. C., RAUTANEN, A., ELLIOTT, K. S., PARKS, T., NARANBHAI, V., IEVEN, M. M., BUTLER, C. C., LITTLE, P., VERHEIJ, T., GARRARD, C. S., HINDS, C., GOOSSENS, H., CHAPMAN, S. & HILL, A. V. 2014. IFITM3 and susceptibility to respiratory viral infections in the community. *J Infect Dis,* 209**,** 1028-31.

MONTEIRO, J. M., HARVEY, C. & TRINCHIERI, G. 1998. Role of interleukin-12 in primary influenza virus infection. *J Virol,* 72**,** 4825-31.

MOORE, K. W., DE WAAL MALEFYT, R., COFFMAN, R. L. & O'GARRA, A. 2001. Interleukin-10 and the interleukin-10 receptor. *Annu Rev Immunol,* 19**,** 683-765.

MORDSTEIN, M., KOCHS, G., DUMOUTIER, L., RENAULD, J. C., PALUDAN, S. R., KLUCHER, K. & STAEHELI, P. 2008. Interferon-lambda contributes to innate

immunity of mice against influenza A virus but not against hepatotropic viruses. *PLoS Pathog,* 4**,** e1000151.

MUIR, A. J., ARORA, S., EVERSON, G., FLISIAK, R., GEORGE, J., GHALIB, R., GORDON, S. C., GRAY, T., GREENBLOOM, S., HASSANEIN, T., HILLSON, J., HORGA, M. A., JACOBSON, I. M., JEFFERS, L., KOWDLEY, K. V., LAWITZ, E., LUETH, S., RODRIGUEZ-TORRES, M., RUSTGI, V., SHEMANSKI, L., SHIFFMAN, M. L., SRINIVASAN, S., VARGAS, H. E., VIERLING, J. M., XU, D., LOPEZ-TALAVERA, J. C., ZEUZEM, S. & GROUP, E. S. 2014. A randomized phase 2b study of peginterferon lambda-1a for the treatment of chronic HCV infection. *J Hepatol,* 61**,** 1238-46.

MUNIR, M. 2010. TRIM proteins: another class of viral victims. *Sci Signal,* 3**,** jc2.

MURPHY, K. P. 2012. *Janeway's Immunobiology*, Garland Science, Taylor & Francis Group, LLC.

MURRAY, P. J., ALLEN, J. E., BISWAS, S. K., FISHER, E. A., GILROY, D. W., GOERDT, S., GORDON, S., HAMILTON, J. A., IVASHKIV, L. B., LAWRENCE, T., LOCATI, M., MANTOVANI, A., MARTINEZ, F. O., MEGE, J. L., MOSSER, D. M., NATOLI, G., SAEIJ, J. P., SCHULTZE, J. L., SHIREY, K. A., SICA, A., SUTTLES, J., UDALOVA, I., VAN GINDERACHTER, J. A., VOGEL, S. N. & WYNN, T. A. 2014. Macrophage activation and polarization: nomenclature and experimental guidelines. *Immunity,* 41**,** 14-20.

NAIK, S. H., SATHE, P., PARK, H. Y., METCALF, D., PROIETTO, A. I., DAKIC, A., CAROTTA, S., O'KEEFFE, M., BAHLO, M., PAPENFUSS, A., KWAK, J. Y., WU, L. & SHORTMAN, K. 2007. Development of plasmacytoid and conventional dendritic cell subtypes from single precursor cells derived in vitro and in vivo. *Nat Immunol,* 8**,** 1217-26.

NAKANO, H., YANAGITA, M. & GUNN, M. D. 2001. CD11c(+)B220(+)Gr-1(+) cells in mouse lymph nodes and spleen display characteristics of plasmacytoid dendritic cells. *J Exp Med,* 194**,** 1171-8.

NEIL, S. J., ZANG, T. & BIENIASZ, P. D. 2008. Tetherin inhibits retrovirus release and is antagonized by HIV-1 Vpu. *Nature,* 451**,** 425-30.

NING, F., LI, X., YU, L., ZHANG, B., ZHAO, Y., LIU, Y., ZHAO, B., SHANG, Y. & HU, X. 2019. Hes1 attenuates type I IFN responses via VEGF-C and WDFY1. *J Exp Med,* 216**,** 1396-1410.

NOURSADEGHI, M., TSANG, J., HAUSTEIN, T., MILLER, R. F., CHAIN, B. M. & KATZ, D. R. 2008. Quantitative imaging assay for NF-kappaB nuclear translocation in primary human macrophages. *J Immunol Methods,* 329**,** 194-200.

NUNEZ, I. A. & ROSS, T. M. 2019. A review of H5Nx avian influenza viruses. *Ther Adv Vaccines Immunother,* 7**,** 2515135518821625.

OHKURA, T., MOMOSE, F., ICHIKAWA, R., TAKEUCHI, K. & MORIKAWA, Y. 2014. Influenza A virus hemagglutinin and neuraminidase mutually accelerate their apical targeting through clustering of lipid rafts. *J Virol,* 88**,** 10039-55.

ONAI, N., OBATA-ONAI, A., SCHMID, M. A., OHTEKI, T., JARROSSAY, D. & MANZ, M. G. 2007. Identification of clonogenic common Flt3+M-CSFR+ plasmacytoid and conventional dendritic cell progenitors in mouse bone marrow. *Nat Immunol,* 8**,** 1207-16.

ONAI, N., OBATA-ONAI, A., TUSSIWAND, R., LANZAVECCHIA, A. & MANZ, M. G. 2006. Activation of the Flt3 signal transduction cascade rescues and enhances type I interferon-producing and dendritic cell development. *J Exp Med,* 203**,** 227-38.

ONG, A. K. & HAYDEN, F. G. 2007. John F. Enders lecture 2006: antivirals for influenza. *J Infect Dis,* 196**,** 181-90.

OSTERLUND, P. I., PIETILA, T. E., VECKMAN, V., KOTENKO, S. V. & JULKUNEN, I. 2007. IFN regulatory factor family members differentially regulate the expression of type III IFN (IFN-lambda) genes. *J Immunol,* 179**,** 3434-42.

OUYANG, W., RUTZ, S., CRELLIN, N. K., VALDEZ, P. A. & HYMOWITZ, S. G. 2011. Regulation and functions of the IL-10 family of cytokines in inflammation and disease. *Annu Rev Immunol,* 29**,** 71-109.

PALESE P, S. M. 2013. Orthomyxoviridae: The viruses and their replication. *In:* KNIPE DM, H. P. (ed.) *Fields VIROLOGY 6th edition.* 6 ed. Philadelphia: Lippincott Williams & Wilkins

PALESE, P., TOBITA, K., UEDA, M. & COMPANS, R. W. 1974. Characterization of temperature sensitive influenza virus mutants defective in neuraminidase. *Virology,* 61**,** 397-410.

PANNE, D., MANIATIS, T. & HARRISON, S. C. 2007. An atomic model of the interferon-beta enhanceosome. *Cell,* 129**,** 1111-23.

PATTISON, M. J., MACKENZIE, K. F., ELCOMBE, S. E. & ARTHUR, J. S. 2013. IFNbeta autocrine feedback is required to sustain TLR induced production of MCP-1 in macrophages. *FEBS Lett,* 587**,** 1496-503.

PAVLOVIC, J., ARZET, H. A., HEFTI, H. P., FRESE, M., ROST, D., ERNST, B., KOLB, E., STAEHELI, P. & HALLER, O. 1995. Enhanced virus resistance of transgenic mice expressing the human MxA protein. *J Virol,* 69**,** 4506-10.

PAVLOVIC, J., HALLER, O. & STAEHELI, P. 1992. Human and mouse Mx proteins inhibit different steps of the influenza virus multiplication cycle. *J Virol,* 66**,** 2564-9.

PEIRIS, J. S., HUI, K. P. & YEN, H. L. 2010. Host response to influenza virus: protection versus immunopathology. *Curr Opin Immunol,* 22**,** 475-81.

PELLETIER, A. N., GUIMONT-DESROCHERS, F., ASHTON, M. P., BRODNICKI, T. C. & LESAGE, S. 2012. The size of the plasmacytoid dendritic cell compartment is a multigenic trait dominated by a locus on mouse chromosome 7. *J Immunol,* 188**,** 5561-70.

PERRONE, L. A., PLOWDEN, J. K., GARCIA-SASTRE, A., KATZ, J. M. & TUMPEY, T. M. 2008. H5N1 and 1918 pandemic influenza virus infection results in early and excessive infiltration of macrophages and neutrophils in the lungs of mice. *PLoS Pathog,* 4**,** e1000115.

PICHLMAIR, A., SCHULZ, O., TAN, C. P., NASLUND, T. I., LILJESTROM, P., WEBER, F. & REIS E SOUSA, C. 2006. RIG-I-mediated antiviral responses to single-stranded RNA bearing 5'-phosphates. *Science,* 314**,** 997-1001.

PLATANIAS, L. C. 2005. Mechanisms of type-I- and type-II-interferon-mediated signalling. *Nat Rev Immunol,* 5**,** 375-86.

PRAKASH, A. & LEVY, D. E. 2006. Regulation of IRF7 through cell type-specific protein stability. *Biochem Biophys Res Commun,* 342**,** 50-6.

PRAKASH, A., SMITH, E., LEE, C. K. & LEVY, D. E. 2005. Tissue-specific positive feedback requirements for production of type I interferon following virus infection. *J Biol Chem,* 280**,** 18651-7.

RAJASURIAR, R., KHOURY, G., KAMARULZAMAN, A., FRENCH, M. A., CAMERON, P. U. & LEWIN, S. R. 2013. Persistent immune activation in chronic HIV infection: do any interventions work? *AIDS,* 27**,** 1199-208.

RANGEL-MORENO, J., CARRAGHER, D. M., MISRA, R. S., KUSSER, K., HARTSON, L., MOQUIN, A., LUND, F. E. & RANDALL, T. D. 2008. B cells promote resistance to heterosubtypic strains of influenza via multiple mechanisms. *J Immunol,* 180**,** 454-63.

REHWINKEL, J., TAN, C. P., GOUBAU, D., SCHULZ, O., PICHLMAIR, A., BIER, K., ROBB, N., VREEDE, F., BARCLAY, W., FODOR, E. & REIS E SOUSA, C. 2010.

RIG-I detects viral genomic RNA during negative-strand RNA virus infection. *Cell,* 140**,** 397-408.
REIZIS, B. 2019. Plasmacytoid Dendritic Cells: Development, Regulation, and Function. *Immunity,* 50**,** 37-50.
REIZIS, B., BUNIN, A., GHOSH, H. S., LEWIS, K. L. & SISIRAK, V. 2011. Plasmacytoid dendritic cells: recent progress and open questions. *Annu Rev Immunol,* 29**,** 163-83.
ROBERTS, K. K., HILL, T. E., DAVIS, M. N., HOLBROOK, M. R. & FREIBERG, A. N. 2015. Cytokine response in mouse bone marrow derived macrophages after infection with pathogenic and non-pathogenic Rift Valley fever virus. *J Gen Virol,* 96**,** 1651-1663.
RODGERS, B. & MIMS, C. A. 1981. Interaction of influenza virus with mouse macrophages. *Infect Immun,* 31**,** 751-7.
RODGERS, B. C. & MIMS, C. A. 1982. Influenza virus replication in human alveolar macrophages. *Journal of Medical Virology,* 9**,** 177-184.
RODRIGUEZ BOULAN, E. & SABATINI, D. D. 1978. Asymmetric budding of viruses in epithelial monlayers: a model system for study of epithelial polarity. *Proc Natl Acad Sci U S A,* 75**,** 5071-5.
ROSAS, M., OSORIO, F., ROBINSON, M. J., DAVIES, L. C., DIERKES, N., JONES, S. A., REIS E SOUSA, C. & TAYLOR, P. R. 2011. Hoxb8 conditionally immortalised macrophage lines model inflammatory monocytic cells with important similarity to dendritic cells. *Eur J Immunol,* 41**,** 356-65.
ROSSMAN, J. S. & LAMB, R. A. 2011. Influenza virus assembly and budding. *Virology,* 411**,** 229-36.
RUSSIER, M., YANG, G., REHG, J. E., WONG, S. S., MOSTAFA, H. H., FABRIZIO, T. P., BARMAN, S., KRAUSS, S., WEBSTER, R. G., WEBBY, R. J. & RUSSELL, C. J. 2016. Molecular requirements for a pandemic influenza virus: An acid-stable hemagglutinin protein. *Proc Natl Acad Sci U S A,* 113**,** 1636-41.
RYZHAKOV, G., WEST, N. R., FRANCHINI, F., CLARE, S., ILOTT, N. E., SANSOM, S. N., BULLERS, S. J., PEARSON, C., COSTAIN, A., VAUGHAN-JACKSON, A., GOETTEL, J. A., ERMANN, J., HORWITZ, B. H., BUTI, L., LU, X., MUKHOPADHYAY, S., SNAPPER, S. B. & POWRIE, F. 2018. Alpha kinase 1 controls intestinal inflammation by suppressing the IL-12/Th1 axis. *Nat Commun,* 9**,** 3797.
SAHA, B., JYOTHI PRASANNA, S., CHANDRASEKAR, B. & NANDI, D. 2010. Gene modulation and immunoregulatory roles of interferon gamma. *Cytokine,* 50**,** 1-14.
SAMARASINGHE, A. E., MELO, R. C., DUAN, S., LEMESSURIER, K. S., LIEDMANN, S., SURMAN, S. L., LEE, J. J., HURWITZ, J. L., THOMAS, P. G. & MCCULLERS, J. A. 2017. Eosinophils Promote Antiviral Immunity in Mice Infected with Influenza A Virus. *J Immunol,* 198**,** 3214-3226.
SAMET, S. J. & TOMPKINS, S. M. 2017. Influenza Pathogenesis in Genetically Defined Resistant and Susceptible Murine Strains. *Yale J Biol Med,* 90**,** 471-479.
SASAI, M., LINEHAN, M. M. & IWASAKI, A. 2010. Bifurcation of Toll-like receptor 9 signaling by adaptor protein 3. *Science,* 329**,** 1530-4.
SATO, M., HATA, N., ASAGIRI, M., NAKAYA, T., TANIGUCHI, T. & TANAKA, N. 1998. Positive feedback regulation of type I IFN
genes by the IFN-inducible transcription factor IRF-7. *FEBS Letters,* 441**,** 106-110.
SATO, M., SUEMORI, H., HATA, N., ASAGIRI, M., OGASAWARA, K., NAKAO, K., NAKAYA, T., KATSUKI, M., NOGUCHI, S., TANAKA, N. & TANIGUCHI, T. 2000. Distinct and Essential Roles of Transcription Factors IRF-3 and IRF-7 in Response to Viruses for IFN-α/β Gene Induction. *Immunity,* 13**,** 539-548.
SAVAN, R. 2014. Post-transcriptional regulation of interferons and their signaling pathways. *J Interferon Cytokine Res,* 34**,** 318-29.

SCHEIFFELE, P., RIETVELD, A., WILK, T. & SIMONS, K. 1999. Influenza viruses select ordered lipid domains during budding from the plasma membrane. *J Biol Chem,* 274**,** 2038-44.

SCHLEE, M., ROTH, A., HORNUNG, V., HAGMANN, C. A., WIMMENAUER, V., BARCHET, W., COCH, C., JANKE, M., MIHAILOVIC, A., WARDLE, G., JURANEK, S., KATO, H., KAWAI, T., POECK, H., FITZGERALD, K. A., TAKEUCHI, O., AKIRA, S., TUSCHL, T., LATZ, E., LUDWIG, J. & HARTMANN, G. 2009. Recognition of 5' triphosphate by RIG-I helicase requires short blunt double-stranded RNA as contained in panhandle of negative-strand virus. *Immunity,* 31**,** 25-34.

SCHMIDT, A., SCHWERD, T., HAMM, W., HELLMUTH, J. C., CUI, S., WENZEL, M., HOFFMANN, F. S., MICHALLET, M. C., BESCH, R., HOPFNER, K. P., ENDRES, S. & ROTHENFUSSER, S. 2009. 5'-triphosphate RNA requires base-paired structures to activate antiviral signaling via RIG-I. *Proc Natl Acad Sci U S A,* 106**,** 12067-72.

SCHMITZ, M. L., KRACHT, M. & SAUL, V. V. 2014. The intricate interplay between RNA viruses and NF-kappaB. *Biochim Biophys Acta,* 1843**,** 2754-2764.

SCHOENBORN, J. R. & WILSON, C. B. 2007. Regulation of interferon-gamma during innate and adaptive immune responses. *Adv Immunol,* 96**,** 41-101.

SCHOGGINS, J. W., MACDUFF, D. A., IMANAKA, N., GAINEY, M. D., SHRESTHA, B., EITSON, J. L., MAR, K. B., RICHARDSON, R. B., RATUSHNY, A. V., LITVAK, V., DABELIC, R., MANICASSAMY, B., AITCHISON, J. D., ADEREM, A., ELLIOTT, R. M., GARCIA-SASTRE, A., RACANIELLO, V., SNIJDER, E. J., YOKOYAMA, W. M., DIAMOND, M. S., VIRGIN, H. W. & RICE, C. M. 2014. Pan-viral specificity of IFN-induced genes reveals new roles for cGAS in innate immunity. *Nature,* 505**,** 691-5.

SCHOGGINS, J. W. & RICE, C. M. 2011. Interferon-stimulated genes and their antiviral effector functions. *Curr Opin Virol,* 1**,** 519-25.

SCHRAML, B. U. & REIS E SOUSA, C. 2015. Defining dendritic cells. *Curr Opin Immunol,* 32**,** 13-20.

SCHRAUWEN, E. J. & FOUCHIER, R. A. 2014. Host adaptation and transmission of influenza A viruses in mammals. *Emerg Microbes Infect,* 3**,** e9.

SEO, S. U., KWON, H. J., KO, H. J., BYUN, Y. H., SEONG, B. L., UEMATSU, S., AKIRA, S. & KWEON, M. N. 2011. Type I interferon signaling regulates Ly6C(hi) monocytes and neutrophils during acute viral pneumonia in mice. *PLoS Pathog,* 7**,** e1001304.

SERBINA, N. V. & PAMER, E. G. 2006. Monocyte emigration from bone marrow during bacterial infection requires signals mediated by chemokine receptor CCR2. *Nat Immunol,* 7**,** 311-7.

SHELTON, H., ROBERTS, K. L., MOLESTI, E., TEMPERTON, N. & BARCLAY, W. S. 2013. Mutations in haemagglutinin that affect receptor binding and pH stability increase replication of a PR8 influenza virus with H5 HA in the upper respiratory tract of ferrets and may contribute to transmissibility. *J Gen Virol,* 94**,** 1220-9.

SHORT, K. R., BROOKS, A. G., READING, P. C. & LONDRIGAN, S. L. 2012. The fate of influenza A virus after infection of human macrophages and dendritic cells. *J Gen Virol,* 93**,** 2315-25.

SIMONS, K. & IKONEN, E. 1997. Functional rafts in cell membranes. *Nature,* 387**,** 569-72.

SIMPSON, E. M., LINDER, C. C., SARGENT, E. E., DAVISSON, M. T., MOBRAATEN, L. E. & SHARP, J. J. 1997. Genetic variation among 129 substrains and its importance for targeted mutagenesis in mice. *Nat Genet,* 16**,** 19-27.

SKEHEL, J. J. & WILEY, D. C. 2000. Receptor binding and membrane fusion in virus entry: the influenza hemagglutinin. *Annu Rev Biochem,* 69**,** 531-69.

SMITH, D. J., LAPEDES, A. S., DE JONG, J. C., BESTEBROER, T. M., RIMMELZWAAN, G. F., OSTERHAUS, A. D. & FOUCHIER, R. A. 2004. Mapping the antigenic and genetic evolution of influenza virus. *Science,* 305**,** 371-6.

SMITH, D. K., YANG, J., LIU, M. L. & ZHANG, C. L. 2016. Small Molecules Modulate Chromatin Accessibility to Promote NEUROG2-Mediated Fibroblast-to-Neuron Reprogramming. *Stem Cell Reports,* 7**,** 955-969.

SOGHOIAN D.Z., S. H. 2010. Cytolytic CD4+ T cells in viral immunity. *Expert Review of Vaccines,* 9**,** 1453-1463.

STAEHELI, P., GROB, R., MEIER, E., SUTCLIFFE, J. G. & HALLER, O. 1988. Influenza virus-susceptible mice carry Mx genes with a large deletion or a nonsense mutation. *Mol Cell Biol,* 8**,** 4518-23.

STARY, G., KLEIN, I., KOHLHOFER, S., KOSZIK, F., SCHERZER, T., MULLAUER, L., QUENDLER, H., KOHRGRUBER, N. & STINGL, G. 2009. Plasmacytoid dendritic cells express TRAIL and induce CD4+ T-cell apoptosis in HIV-1 viremic patients. *Blood,* 114**,** 3854-63.

STETSON, D. B. & MEDZHITOV, R. 2006. Recognition of cytosolic DNA activates an IRF3-dependent innate immune response. *Immunity,* 24**,** 93-103.

SUN, J., MADAN, R., KARP, C. L. & BRACIALE, T. J. 2009. Effector T cells control lung inflammation during acute influenza virus infection by producing IL-10. *Nat Med,* 15**,** 277-84.

SUN, L., WU, J., DU, F., CHEN, X. & CHEN, Z. J. 2013. Cyclic GMP-AMP synthase is a cytosolic DNA sensor that activates the type I interferon pathway. *Science,* 339**,** 786-91.

SUZUKI, T., TAKAHASHI, T., GUO, C. T., HIDARI, K. I., MIYAMOTO, D., GOTO, H., KAWAOKA, Y. & SUZUKI, Y. 2005. Sialidase activity of influenza A virus in an endocytic pathway enhances viral replication. *J Virol,* 79**,** 11705-15.

SWIECKI, M. & COLONNA, M. 2011. Type I interferons: diversity of sources, production pathways and effects on immune responses. *Curr Opin Virol,* 1**,** 463-75.

TAKAHASHI, T. & SUZUKI, T. 2015. Low-pH Stability of Influenza A Virus Sialidase Contributing to Virus Replication and Pandemic. *Biol Pharm Bull,* 38**,** 817-26.

TAKATSUNA, H., KATO, H., GOHDA, J., AKIYAMA, T., MORIYA, A., OKAMOTO, Y., YAMAGATA, Y., OTSUKA, M., UMEZAWA, K., SEMBA, K. & INOUE, J. 2003. Identification of TIFA as an adapter protein that links tumor necrosis factor receptor-associated factor 6 (TRAF6) to interleukin-1 (IL-1) receptor-associated kinase-1 (IRAK-1) in IL-1 receptor signaling. *J Biol Chem,* 278**,** 12144-50.

TAKEDA, M., LESER, G. P., RUSSELL, C. J. & LAMB, R. A. 2003. Influenza virus hemagglutinin concentrates in lipid raft microdomains for efficient viral fusion. *Proc Natl Acad Sci U S A,* 100**,** 14610-7.

TAKEUCHI, O. & AKIRA, S. 2010. Pattern recognition receptors and inflammation. *Cell,* 140**,** 805-20.

TANIGUCHI, T. & TAKAOKA, A. 2002. The interferon-α/β system in antiviral responses: a multimodal machinery of gene regulation by the IRF family of transcription factors. *Current Opinion in Immunology,* 14**,** 111-116.

TATE, M. D., BROOKS, A. G. & READING, P. C. 2008. The role of neutrophils in the upper and lower respiratory tract during influenza virus infection of mice. *Respir Res,* 9**,** 57.

TATE, M. D., DENG, Y. M., JONES, J. E., ANDERSON, G. P., BROOKS, A. G. & READING, P. C. 2009. Neutrophils ameliorate lung injury and the development of severe disease during influenza infection. *J Immunol,* 183**,** 7441-50.

TATE, M. D., IOANNIDIS, L. J., CROKER, B., BROWN, L. E., BROOKS, A. G. & READING, P. C. 2011. The role of neutrophils during mild and severe influenza virus infections of mice. *PLoS One,* 6**,** e17618.

TATE, M. D., PICKETT, D. L., VAN ROOIJEN, N., BROOKS, A. G. & READING, P. C. 2010. Critical role of airway macrophages in modulating disease severity during influenza virus infection of mice. *J Virol,* 84**,** 7569-80.

TAUBENBERGER, J. K. & MORENS, D. M. 2008. The pathology of influenza virus infections. *Annu Rev Pathol,* 3**,** 499-522.

TEIJARO, J. R., NG, C., LEE, A. M., SULLIVAN, B. M., SHEEHAN, K. C., WELCH, M., SCHREIBER, R. D., DE LA TORRE, J. C. & OLDSTONE, M. B. 2013. Persistent LCMV infection is controlled by blockade of type I interferon signaling. *Science,* 340**,** 207-11.

THITITHANYANONT, A., ENGERING, A., EKCHARIYAWAT, P., WIBOON-UT, S., LIMSALAKPETCH, A., YONGVANITCHIT, K., KUM-ARB, U., KANCHONGKITTIPHON, W., UTAISINCHAROEN, P., SIRISINHA, S., PUTHAVATHANA, P., FUKUDA, M. M. & PICHYANGKUL, S. 2007. High susceptibility of human dendritic cells to avian influenza H5N1 virus infection and protection by IFN-alpha and TLR ligands. *J Immunol,* 179**,** 5220-7.

THOMPSON, W. W., WEINTRAUB, E., DHANKHAR, P., CHENG, P. Y., BRAMMER, L., MELTZER, M. I., BRESEE, J. S. & SHAY, D. K. 2009. Estimates of US influenza-associated deaths made using four different methods. *Influenza Other Respir Viruses,* 3**,** 37-49.

TONG, S., ZHU, X., LI, Y., SHI, M., ZHANG, J., BOURGEOIS, M., YANG, H., CHEN, X., RECUENCO, S., GOMEZ, J., CHEN, L. M., JOHNSON, A., TAO, Y., DREYFUS, C., YU, W., MCBRIDE, R., CARNEY, P. J., GILBERT, A. T., CHANG, J., GUO, Z., DAVIS, C. T., PAULSON, J. C., STEVENS, J., RUPPRECHT, C. E., HOLMES, E. C., WILSON, I. A. & DONIS, R. O. 2013. New world bats harbor diverse influenza A viruses. *PLoS Pathog,* 9**,** e1003657.

TUMPEY, T. M., SZRETTER, K. J., VAN HOEVEN, N., KATZ, J. M., KOCHS, G., HALLER, O., GARCIA-SASTRE, A. & STAEHELI, P. 2007. The Mx1 gene protects mice against the pandemic 1918 and highly lethal human H5N1 influenza viruses. *J Virol,* 81**,** 10818-21.

UCCELLINI, M. B. & GARCIA-SASTRE, A. 2018. ISRE-Reporter Mouse Reveals High Basal and Induced Type I IFN Responses in Inflammatory Monocytes. *Cell Rep,* 25**,** 2784-2796 e3.

UEMATSU, S., SATO, S., YAMAMOTO, M., HIROTANI, T., KATO, H., TAKESHITA, F., MATSUDA, M., COBAN, C., ISHII, K. J., KAWAI, T., TAKEUCHI, O. & AKIRA, S. 2005. Interleukin-1 receptor-associated kinase-1 plays an essential role for Toll-like receptor (TLR)7- and TLR9-mediated interferon-{alpha} induction. *J Exp Med,* 201**,** 915-23.

VAN RIEL, D., MUNSTER, V. J., DE WIT, E., RIMMELZWAAN, G. F., FOUCHIER, R. A., OSTERHAUS, A. D. & KUIKEN, T. 2006. H5N1 Virus Attachment to Lower Respiratory Tract. *Science,* 312**,** 399.

VANGETI, S., YU, M. & SMED-SORENSEN, A. 2018. Respiratory Mononuclear Phagocytes in Human Influenza A Virus Infection: Their Role in Immune Protection and As Targets of the Virus. *Front Immunol,* 9**,** 1521.

VELA, A., FEDOROVA, O., DING, S. C. & PYLE, A. M. 2012. The thermodynamic basis for viral RNA detection by the RIG-I innate immune sensor. *J Biol Chem,* 287**,** 42564-73.

VIJAY, R., FEHR, A. R., JANOWSKI, A. M., ATHMER, J., WHEELER, D. L., GRUNEWALD, M., SOMPALLAE, R., KURUP, S. P., MEYERHOLZ, D. K., SUTTERWALA, F. S., NARUMIYA, S. & PERLMAN, S. 2017. Virus-induced inflammasome activation is suppressed by prostaglandin D2/DP1 signaling. *Proc Natl Acad Sci U S A,* 114**,** E5444-E5453.

WACK, A., TERCZYNSKA-DYLA, E. & HARTMANN, R. 2015. Guarding the frontiers: the biology of type III interferons. *Nat Immunol,* 16**,** 802-9.

WANG, F., ALAIN, T., SZRETTER, K. J., STEPHENSON, K., POL, J. G., ATHERTON, M. J., HOANG, H. D., FONSECA, B. D., ZAKARIA, C., CHEN, L., RANGWALA, Z., HESCH, A., CHAN, E. S. Y., TUINMAN, C., SUTHAR, M. S., JIANG, Z., ASHKAR, A. A., THOMAS, G., KOZMA, S. C., GALE, M., JR., FITZGERALD, K. A., DIAMOND, M. S., MOSSMAN, K., SONENBERG, N., WAN, Y. & LICHTY, B. D. 2016a. S6K-STING interaction regulates cytosolic DNA-mediated activation of the transcription factor IRF3. *Nat Immunol,* 17**,** 514-522.

WANG, G. G., CALVO, K. R., PASILLAS, M. P., SYKES, D. B., HACKER, H. & KAMPS, M. P. 2006. Quantitative production of macrophages or neutrophils ex vivo using conditional Hoxb8. *Nat Methods,* 3**,** 287-93.

WANG, S., XIE, F., CHU, F., ZHANG, Z., YANG, B., DAI, T., GAO, L., WANG, L., LING, L., JIA, J., VAN DAM, H., JIN, J., ZHANG, L. & ZHOU, F. 2017. YAP antagonizes innate antiviral immunity and is targeted for lysosomal degradation through IKKvarepsilon-mediated phosphorylation. *Nat Immunol,* 18**,** 733-743.

WANG, S. J., TU, H. P., KO, A. M., CHIANG, S. L., CHIOU, S. J., LEE, S. S., TSAI, Y. S., LEE, C. P. & KO, Y. C. 2011. Lymphocyte alpha-kinase is a gout-susceptible gene involved in monosodium urate monohydrate-induced inflammatory responses. *J Mol Med (Berl),* 89**,** 1241-51.

WANG, X., HINSON, E. R. & CRESSWELL, P. 2007. The interferon-inducible protein viperin inhibits influenza virus release by perturbing lipid rafts. *Cell Host Microbe,* 2**,** 96-105.

WANG, X., LI, J., CHEN, S., SHEN, X., YANG, X., TENG, Y., DENG, L., WANG, Y., CHEN, J., WANG, X. & HUANG, N. 2016b. Knockdown of HMGN2 increases the internalization of Klebsiella pneumoniae by respiratory epithelial cells through the regulation of alpha5beta1 integrin expression. *Int J Mol Med,* 38**,** 737-46.

WARREN, M. K. & VOGEL, S. N. 1985. Bone marrow-derived macrophages: development and regulation of differentiation markers by colony-stimulating factor and interferons. *J Immunol,* 134**,** 982-9.

WATHELET, M. G., LIN, C. H., PAREKH, B. S., RONCO, L. V., HOWLEY, P. M. & MANIATIS, T. 1998. Virus Infection Induces the Assembly of Coordinately Activated Transcription Factors on the IFN-β Enhancer In Vivo. *Molecular Cell,* 1**,** 507-518.

WEBER, M., GAWANBACHT, A., HABJAN, M., RANG, A., BORNER, C., SCHMIDT, A. M., VEITINGER, S., JACOB, R., DEVIGNOT, S., KOCHS, G., GARCIA-SASTRE, A. & WEBER, F. 2013. Incoming RNA virus nucleocapsids containing a 5'-triphosphorylated genome activate RIG-I and antiviral signaling. *Cell Host Microbe,* 13**,** 336-46.

WEBSTER, B., ASSIL, S. & DREUX, M. 2016. Cell-Cell Sensing of Viral Infection by Plasmacytoid Dendritic Cells. *J Virol,* 90**,** 10050-10053.

WENNMANN, D. O., SCHMITZ, J., WEHR, M. C., KRAHN, M. P., KOSCHMAL, N., GROMNITZA, S., SCHULZE, U., WEIDE, T., CHEKURI, A., SKRYABIN, B. V., GERKE, V., PAVENSTADT, H., DUNING, K. & KREMERSKOTHEN, J. 2014. Evolutionary and molecular facts link the WWC protein family to Hippo signaling. *Mol Biol Evol,* 31**,** 1710-23.

WERNER, S. L., BARKEN, D. & HOFFMANN, A. 2005. Stimulus specificity of gene expression programs determined by temporal control of IKK activity. *Science,* 309**,** 1857-61.

WILEY, D. C. & SKEHEL, J. J. 1987. The structure and function of the hemagglutinin membrane glycoprotein of influenza virus. *Annu Rev Biochem,* 56**,** 365-94.

WILSON, E. B., YAMADA, D. H., ELSAESSER, H., HERSKOVITZ, J., DENG, J., CHENG, G., ARONOW, B. J., KARP, C. L. & BROOKS, D. G. 2013. Blockade of chronic type I interferon signaling to control persistent LCMV infection. *Science,* 340**,** 202-7.

WOLF, A. I., BUEHLER, D., HENSLEY, S. E., CAVANAGH, L. L., WHERRY, E. J., KASTNER, P., CHAN, S. & WENINGER, W. 2009. Plasmacytoid dendritic cells are dispensable during primary influenza virus infection. *J Immunol,* 182**,** 871-9.

WU, S., WANG, Y., ZHANG, M., WANG, M. & HE, J. Q. 2019. Genetic variants in IFNG and IFNGR1 and tuberculosis susceptibility. *Cytokine,* 123**,** 154775.

WU, W., ZHANG, W., DUGGAN, E. S., BOOTH, J. L., ZOU, M. H. & METCALF, J. P. 2015. RIG-I and TLR3 are both required for maximum interferon induction by influenza virus in human lung alveolar epithelial cells. *Virology,* 482**,** 181-8.

XIAO, L., CHEN, Y., JI, M. & DONG, J. 2011. KIBRA regulates Hippo signaling activity via interactions with large tumor suppressor kinases. *J Biol Chem,* 286**,** 7788-96.

YANG, X., TAN, B., ZHOU, X., XUE, J., ZHANG, X., WANG, P., SHAO, C., LI, Y., LI, C., XIA, H. & QIU, J. 2015. Interferon-Inducible Transmembrane Protein 3 Genetic Variant rs12252 and Influenza Susceptibility and Severity: A Meta-Analysis. *PLoS One,* 10**,** e0124985.

YI, C., ZHAO, Z., WANG, S., SUN, X., ZHANG, D., SUN, X., ZHANG, A. & JIN, M. 2017. Influenza A Virus PA Antagonizes Interferon-beta by Interacting with Interferon Regulatory Factor 3. *Front Immunol,* 8**,** 1051.

YIE, J., SENGER, K. & THANOS, D. 1999. Mechanism by which the IFN-beta enhanceosome activates transcription. *Proc Natl Acad Sci U S A,* 96**,** 13108-13.

YIP, T. F., SELIM, A. S. M., LIAN, I. & LEE, S. M. 2018. Advancements in Host-Based Interventions for Influenza Treatment. *Front Immunol,* 9**,** 1547.

YOSHIHAMA, Y., SASAKI, K., HORIKOSHI, Y., SUZUKI, A., OHTSUKA, T., HAKUNO, F., TAKAHASHI, S., OHNO, S. & CHIDA, K. 2011. KIBRA suppresses apical exocytosis through inhibition of aPKC kinase activity in epithelial cells. *Curr Biol,* 21**,** 705-11.

YU, F. X. & GUAN, K. L. 2013. The Hippo pathway: regulators and regulations. *Genes Dev,* 27**,** 355-71.

YU, W. C., CHAN, R. W., WANG, J., TRAVANTY, E. A., NICHOLLS, J. M., PEIRIS, J. S., MASON, R. J. & CHAN, M. C. 2011. Viral replication and innate host responses in primary human alveolar epithelial cells and alveolar macrophages infected with influenza H5N1 and H1N1 viruses. *J Virol,* 85**,** 6844-55.

ZENG, W., SUN, L., JIANG, X., CHEN, X., HOU, F., ADHIKARI, A., XU, M. & CHEN, Z. J. 2010. Reconstitution of the RIG-I pathway reveals a signaling role of unanchored polyubiquitin chains in innate immunity. *Cell,* 141**,** 315-30.

ZHANG, J., RAPER, A., SUGITA, N., HINGORANI, R., SALIO, M., PALMOWSKI, M. J., CERUNDOLO, V. & CROCKER, P. R. 2006. Characterization of Siglec-H as a novel endocytic receptor expressed on murine plasmacytoid dendritic cell precursors. *Blood,* 107**,** 3600-8.

ZHANG, L., YANG, S., WENNMANN, D. O., CHEN, Y., KREMERSKOTHEN, J. & DONG, J. 2014. KIBRA: In the brain and beyond. *Cell Signal,* 26**,** 1392-9.

ZHANG, Q., MENG, F., CHEN, S., PLOUFFE, S. W., WU, S., LIU, S., LI, X., ZHOU, R., WANG, J., ZHAO, B., LIU, J., QIN, J., ZOU, J., FENG, X. H., GUAN, K. L. & XU, P. 2017a. Hippo signalling governs cytosolic nucleic acid sensing through YAP/TAZ-mediated TBK1 blockade. *Nat Cell Biol,* 19**,** 362-374.

ZHANG, Y., YAN, S., CHEN, J., GAN, C., CHEN, D., LI, Y., WEN, J., KREMERSKOTHEN, J., CHEN, S., ZHANG, J. & CAO, Y. 2017b. WWC2 is an independent prognostic factor and prevents invasion via Hippo signalling in hepatocellular carcinoma. *J Cell Mol Med,* 21**,** 3718-3729.

ZHANG, Y. H., ZHAO, Y., LI, N., PENG, Y. C., GIANNOULATOU, E., JIN, R. H., YAN, H. P., WU, H., LIU, J. H., LIU, N., WANG, D. Y., SHU, Y. L., HO, L. P., KELLAM, P., MCMICHAEL, A. & DONG, T. 2013. Interferon-induced transmembrane protein-3 genetic variant rs12252-C is associated with severe influenza in Chinese individuals. *Nat Commun,* 4**,** 1418.

ZHAO, B., LI, L., TUMANENG, K., WANG, C. Y. & GUAN, K. L. 2010. A coordinated phosphorylation by Lats and CK1 regulates YAP stability through SCF(beta-TRCP). *Genes Dev,* 24**,** 72-85.

ZHAO, D., ZHANG, Q., LIU, Y., LI, X., ZHAO, K., DING, Y., LI, Z., SHEN, Q., WANG, C., LI, N. & CAO, X. 2016. H3K4me3 Demethylase Kdm5a Is Required for NK Cell Activation by Associating with p50 to Suppress SOCS1. *Cell Rep,* 15**,** 288-99.

ZHOU, P., SHE, Y., DONG, N., LI, P., HE, H., BORIO, A., WU, Q., LU, S., DING, X., CAO, Y., XU, Y., GAO, W., DONG, M., DING, J., WANG, D. C., ZAMYATINA, A. & SHAO, F. 2018. Alpha-kinase 1 is a cytosolic innate immune receptor for bacterial ADP-heptose. *Nature,* 561**,** 122-126.

ZHOU, Y., GUO, M., WANG, X., LI, J., WANG, Y., YE, L., DAI, M., ZHOU, L., PERSIDSKY, Y. & HO, W. 2013. TLR3 activation efficiency by high or low molecular mass poly I:C. *Innate Immun,* 19**,** 184-92.

ZIMMERMANN, S., PFANNKUCH, L., AL-ZEER, M. A., BARTFELD, S., KOCH, M., LIU, J., RECHNER, C., SOERENSEN, M., SOKOLOVA, O., ZAMYATINA, A., KOSMA, P., MAURER, A. P., GLOWINSKI, F., PLEISSNER, K. P., SCHMID, M., BRINKMANN, V., KARLAS, A., NAUMANN, M., ROTHER, M., MACHUY, N. & MEYER, T. F. 2017. ALPK1- and TIFA-Dependent Innate Immune Response Triggered by the Helicobacter pylori Type IV Secretion System. *Cell Rep,* 20**,** 2384-2395.